TU Delft

Delft University of Technology

Physico-chemical characterization of the extracellular polymer matrix of biofilms in membrane filtration systems

Dietrich (Pfaff), N.M.

DOI
10.4233/uuid:a6c6ee3d-55a0-4a2a-8ac9-b6e837e4862e

Publication date
2020

Document Version
Final published version

Citation (APA)
Dietrich (Pfaff), N. M. (2020). *Physico-chemical characterization of the extracellular polymer matrix of biofilms in membrane filtration systems*. [Dissertation (TU Delft), Delft University of Technology]. https://doi.org/10.4233/uuid:a6c6ee3d-55a0-4a2a-8ac9-b6e837e4862e

Important note
To cite this publication, please use the final published version (if applicable).
Please check the document version above.

Copyright
Other than for strictly personal use, it is not permitted to download, forward or distribute the text or part of it, without the consent of the author(s) and/or copyright holder(s), unless the work is under an open content license such as Creative Commons.

Takedown policy
Please contact us and provide details if you believe this document breaches copyrights.
We will remove access to the work immediately and investigate your claim.

This work is downloaded from Delft University of Technology.
For technical reasons the number of authors shown on this cover page is limited to a maximum of 10.

Natascha-Monique Dietrich

Physico-chemical characterization of the extracellular polymer matrix of biofilms on membrane filtration systems

Physico-chemical characterization of the extracellular polymer matrix of biofilms in membrane filtration systems

Dissertation

for the purpose of obtaining the degree of doctor
at Delft University of Technology,
by the authority of the Rector Magnificus prof. dr. ir. T.H.J.J. van der Hagen,
chair of the Board for Doctorates,
to be defended publicly on Tuesday, 20 October 2020 at 12:30h.

by

Natascha-Monique DIETRICH

Master of Science in Molecular Life Sciences, Wageningen University, the Netherlands,
born in Hann Münden, Germany.

The dissertation has been approved by the promoters.

Composition of the doctoral committee:

Rector magnificus	chairperson
Prof. dr. ir. M.C.M. van Loosdrecht	Delft University of Technology, promotor
Dr. ir. J.M. Kleijn	Wageningen University, copromotor
Dr. ir. A.J.B. Kemperman	University of Twente, copromotor

Independent members:

Prof. dr. H.C. van der Mei	University of Groningen
Prof. dr. ir. J. van der Gucht	Wageningen University
Prof. dr. S.J. Picken	Delft University of Technology
Dr. Y. Lin	Delft University of Technology
Dr. ir. C. Picioreanu	Delft University of Technology, reserve member

This research was financially supported by Wetsus – European Center of Excellence for Sustainable Water Technology, Oostergoweg 9, 8911 MA Leeuwarden, the Netherlands.

ISBN: 978-94-6366-319-9

Printed by: IPSKAMP printing

Cover: Picture of a fouled membrane module from the DeCo waste water treatment plant in Terneuzen, taken during a membrane autopsy in February 2015

Content

	Summary	iv
	Samenvatting	vii
Chapter 1	Introduction	1
Chapter 2	On the correlation between composition, cake layer resistance and mechanical properties of model biofilms	11
Chapter 3	Formation and ripening of alginate-like exopolymer cake layers during and after membrane filtration	41
Chapter 4	Rheological characterization of alginate-like exopolymer gels crosslinked with calcium	73
Chapter 5	Biofilms as composite materials: the effect of bacterial-sized micro-beads on the viscoelastic properties of alginate hydrogels	101
Chapter 6	Conclusions and Outlook	121
	References	127
	Acknowledgements	142
	Curriculum Vitae	145
	List of publications	146

Summary

Biofilms are the prevalent form of bacterial life on earth. Bacteria aggregate and embed themselves in a hydrogel matrix of extracellular polymeric substances (EPS), often spread over surfaces in thin films. The EPS matrix of biofilms is getting more and more attention from scientists for several reasons. On the one hand, it has been identified as the component of biofilms that is responsible for many of the adverse technological impacts of biofouling, for example for the increase of hydraulic resistance in membrane filtration systems. It has also been shown to provide structural integrity to biofilms and shield the embedded bacteria from chemicals, hampering removal in technological as well as medical environments. On the other hand, the same properties are interesting features for application as a biomaterial.
Properties like water retention or the resilience against mechanical and chemical interference are defined by the molecular interactions between the different components of the EPS matrix. Therefore, a targeted biofouling cleaning strategy needs to start with understanding those molecular interactions. Owed to the high complexity and the to date still widely undisclosed molecular composition of biofilm EPS, research on these properties requires the use of models. In this work, several experimental and physical models were applied in order to unravel correlations between chemical composition, structure and mechanical properties of biofilm EPS in membrane filtration systems.

Different types of models and levels of abstraction for biofilm EPS are presented in *Chapter 1*. The utility of different model materials for EPS, experimental setups and mathematical models is discussed based on a general introduction into the current state of research on EPS.

In *Chapter 2,* the production and analysis of thin gel layers deposited on ultrafiltration membranes by pressure-driven dead-end filtration are described and assessed as biofilm models. Both alginate and alginate-like exopolymers (ALE), a structural component of bacterial EPS, formed crosslinked hydrogel layers in combination with $CaCl_2$, the density of which were positively correlated with the $CaCl_2$ concentration. Analysis of the composition revealed, however, that the preference of Ca^{2+} over other cations was much stronger pronounced in the case of alginate. Comparison of the filtration behaviour of alginate gel layers with different amounts of $CaCl_2$ revealed that not only the density but also the porosity of the layers are crucial parameters concerning specific cake layer resistances of such crosslinked polymer networks. In the light of a significantly higher resistance compared to biofilms, the extension of the model towards a more heterogeneous composition appears attractive. With the help of nano-indentation and compression measurements, it was detected that the porosity was caused by calcium alginate aggregates forming before the filtration. The smaller those aggregates, the more continuous appeared the network. For alginate gel layers with 0.2 mM $CaCl_2$, the viscoelastic behaviour was comparable to biofilms. ALE gel layers behaved elastically similar in nano-indentation experiments, but were not stable enough for thorough analysis.

They also showed continuous swelling and eventually the development of a fibrous network structure, which were decided to investigate further.

The methods for gel layer production and analysis developed in Chapter 2 were further applied to investigate the composition and ripening behaviour of gel layers of ALE crosslinked with $CaCl_2$ in the presence of KCl. In a study with systematically variant salt combinations, presented in *Chapter 3*, it was shown that the cation accumulation within the gel layers could be described with a Donnan equilibrium model based on fixed negative charges in ALE. The latter were consequently determined around 1 mmol/g organic material. It was concluded that in contrast to the specific and long-lasting Ca^{2+}-binding behaviour of alginate, all ions could move freely over the ALE gel layers and the surrounding solutions (the supernatant). While the interactions were hence mainly electrostatic, Ca^{2+} still proved to be essential for the crosslinking process. More $CaCl_2$ in the supernatant enabled higher densities and slowed down the swelling, that was observed in all investigated Ca-ALE gel layers over 10 d and more. It was also correlated with bearing higher osmotic pressure of the gel layers. The mechanism of the again observed transition into a fibrous network remained unclear. It is assumed that the reversible binding of Ca^{2+} also plays a role here.

Stepping one level forward in abstraction, the experiments discussed in *Chapter 4* were performed on Ca-ALE gels produced under control of the solid composition by internal gelation with $CaCO_3$. The targets of those experiments were the cohesive molecular interactions in form of the viscoelastic properties of Ca-ALE gels with different Ca^{2+} contents, determined by rheology. Ca-ALE gels with relatively low $CaCO_3$ concentrations showed elastic shear moduli similar to real biofilms and were thus considered as a representative model for biofilm EPS. The observation of strain hardening before collapse and a dependency of the elastic moduli on the strain history raised the question of adequate sample treatment and representativeness of scratched biofilm samples. Even after shear strain induced collapse, the gels recovered 65 % to 90 % of their original shear modulus within less than 30 s. Underlining the need for chemical intervention before physical cleaning, the fast recovery was interpreted as another feature of the reversible, electrostatic crosslinking of ALE with Ca^{2+}. Three different molecular interactions could be distinguished, but not yet clearly assigned. Identification of the interacting groups will provide a starting point for the development of targeted chemical weakening strategies. Continuous improvement of the chemical characterization of the biofilm EPS will be essential parts of this development. Increase of the $CaCO_3$ concentration caused an increase in the elastic modulus in combination with an increase in brittleness. With further increase of $CaCO_3$, the solubility product of some calcium salts was exceeded, resulting in precipitates inside the gels that prevented the further increase of the elastic modulus and apparently caused inhomogeneity. Also the recovery was slightly less for gels with high $CaCO_3$ content. Therefore, high calcium dosing causing salt precipitation inside biofilms is considered as a potential strategy for biofouling removal.

While in Chapter 2, an effect of bacteria on the porosity and hence on the hydraulic resistance of biofilms had been proposed, in *Chapter 5,* their impact on the viscoelastic properties was addressed. For this purpose, Ca-alginate gels with spherical styrene particles functionalized with carboxyl-, amino- or sulfate groups (2.3×10^{10} particles/mL) were prepared and examined in analogy to Chapter 4. The impact was too small to be detected in case of the carboxylic particles, slightly increasing the elastic shear modulus with sulfate and slightly decreasing the elastic shear modulus with amino groups. The results were analysed assuming that the hydrogel systems (as well as biofilms) can be considered as composites of particle (/bacteria) reinforced hydrogels. Based on different composite models, it was concluded that the chosen volume fraction and aspect ratio of the utilized particles were unfavourable for the observation of an effect. A more visible impact is already expected with tenfold increase of the particle number in combination with a rod-like geometry with an aspect ratio of 5:1, both not uncommon for bacterial biofilms. In the analysis of the strength and stiffness of biofilms, the contribution of bacteria should, therefore, not be forgotten.

In *Chapter 6*, eventually, the whole thesis is wrapped up. With a short discussion on what has been learned about the binding behaviour of ALE vs alginate, about the molecular interactions in ALE as a model for biofilms, and about the non-biological impact of bacteria, perpetuating knowledge gaps and possible solutions are presented. Also the use and usefulness of the different applied models are critically discussed.

Samenvatting

Biofilms zijn de meest voorkomende vorm van bacterieel leven op aarde. Bacteriën verzamelen en bevestigen zich in een hydrogelmatrix van extracellulaire polymere stoffen (EPS), vaak in dunne vliezen verspreid over oppervlakken. De EPS-matrix van biofilms krijgt om verschillende redenen steeds meer aandacht van wetenschappers. Enerzijds wordt dit onderdeel van biofilms verantwoordelijk gehouden voor veel van de negatieve technologische effecten van biofouling, zoals de verhoging van de hydraulische weerstand in membraanfiltratiesystemen. Ook is aangetoond dat het structurele integriteit biedt aan biofilms en de ingebedde bacteriën beschermt tegen chemicaliën, wat verwijdering in zowel technologische als medische omgeving belemmert. Anderzijds zijn dezelfde eigenschappen interessant voor toepassing als biomateriaal.

Eigenschappen zoals waterretentie of de veerkracht tegen mechanische en chemische verstoring worden bepaald door de moleculaire interacties tussen de verschillende componenten van de EPS-matrix. Daarom moet een gerichte strategie voor het verwijderen van biofouling beginnen met het begrijpen van die moleculaire interacties. Vanwege de complexiteit en de nog steeds grotendeels onbekende moleculaire samenstelling van biofilm-EPS, vereist onderzoek naar deze eigenschappen het gebruik van modellen. In dit werk zijn verschillende experimentele modelsystemen en natuurkundige modellen toegepast om correlaties tussen chemische samenstelling, structuur en mechanische eigenschappen van biofilm-EPS in membraanfiltratiesystemen op te helderen.

Verschillende typen modellen en abstractieniveaus voor onderzoek aan biofilm-EPS worden gepresenteerd in *Hoofdstuk 1*. Het nut van verschillende materialen als modelsysteem voor EPS, experimentele methoden en natuurkundige modellen wordt besproken als algemene introductie op het onderzoek naar EPS zoals beschreven in dit proefschrift.

In *Hoofdstuk 2* worden de productie en analyse van dunne gellagen, afgezet op ultrafiltratiemembranen door drukgestuurde dead-end filtratie, beschreven en wordt beoordeeld in hoeverre deze lagen voldoen als modellen voor biofilms. Zowel alginaat als alginaatachtige exopolymeren (ALE) vormden in combinatie met $CaCl_2$ gecrosslinkte hydrogellagen, waarvan de dichtheid een positieve correlatie had met de $CaCl_2$-concentratie. Analyse van de samenstelling toonde echter aan dat alginaat een aanzienlijk sterkere voorkeur had dan ALE voor het binden van Ca^{2+} boven andere kationen. Vergelijking van het filtratiegedrag van alginaatgellagen met verschillende hoeveelheden $CaCl_2$, onthulde dat niet alleen de dichtheid, maar ook de porositeit (heterogeniteit) van de lagen een cruciale parameter is voor de specifieke stromingsweerstand van dergelijke gecrosslinkte polymeernetwerken. Omdat dit relatief simpele modelsysteem een significant hogere weerstand heeft vergeleken met biofilms, lijkt uitbreiding naar een meer heterogene samenstelling aan te raden. Met behulp van nano-indentatie- en compressiemetingen werd

ontdekt dat de porositeit werd veroorzaakt door calciumalginaataggregaten die zich in de oplossing vormden vóór de filtratie. Hoe kleiner die aggregaten, hoe homogener het netwerk leek. Voor alginaatgellagen met 0.2 mM $CaCl_2$ was het visco-elastische gedrag vergelijkbaar met dat van biofilms. Ook ALE-gellagen vertoonden elastisch vergelijkbaar gedrag in nano-indentatie-experimenten, maar deze films waren niet stabiel tijdens de metingen. Ze vertoonden ook voortdurende zwelling en uiteindelijk de ontwikkeling van een vezelige netwerkstructuur; besloten werd om ALE-gels verder te onderzoeken.

De in Hoofdstuk 2 ontwikkelde methoden voor de productie en analyse van gellagen werden verder toegepast om de samenstelling en het rijpingsgedrag van gellagen van ALE, gecrosslinkt met $CaCl_2$ in aanwezigheid van KCl, te onderzoeken. In een studie waarin de concentraties $CaCl_2$ en KCl systematisch gevarieerd werden, gepresenteerd in *Hoofdstuk 3*, werd aangetoond dat de accumulatie van kationen in de gellagen kon worden beschreven met een Donnan-evenwichtsmodel op basis van vaste negatieve ladingen in het ALE-netwerk. Gevonden werd dat gehalte van deze negatieve ladingen ongeveer 1 mmol per gram organisch materiaal bedroeg. De conclusie was dat in tegenstelling tot het tamelijk irreversibele en specifieke Ca^{2+}-bindende gedrag van alginaat, alle ionen vrij konden bewegen tussen de ALE-gellagen en de omringende vloeistof (het 'supernatant'). Hoewel de interacties dus voornamelijk elektrostatisch waren, bleek Ca^{2+} echter nog steeds essentieel te zijn voor het crosslinkproces. Meer $CaCl_2$ in het supernatant verhoogde de dichtheid en vertraagde de zwelling, hetgeen in alle onderzochte Ca-ALE-gellagen werd waargenomen gedurende tien dagen en langer. Dat het netwerk steviger werd door meer $CaCl_2$ in het supernatant bleek ook uit de hogere osmotische druk in de gellagen. Het mechanisme van de opnieuw waargenomen overgang naar een vezelnetwerk bleef onduidelijk. Aangenomen wordt dat ook hier het reversibele karakter van de binding van Ca^{2+} een rol speelt.

De aanpak van de experimenten besproken in *Hoofdstuk 4* bevond zich op een hoger niveau in abstractie. Deze werden uitgevoerd op Ca-ALE-gels geproduceerd door interne gelering met behulp van verschillende concentraties geleidelijk vrijkomend $CaCO_3$. Het doel was inzicht te krijgen in de complexe cohesieve moleculaire interacties die het zo moeilijk maken om biofilms te verwijderen. De visco-elastische eigenschappen van de gels werden bepaald bij verschillende Ca^{2+}-gehalten en met behulp van diverse reologische technieken. Ca-ALE-gels met relatief lage $CaCO_3$-concentraties vertoonden visco-elastisch gedrag vergelijkbaar met dat van echte biofilms en werden daarom beschouwd als een representatief model voor biofilm-EPS. De waarneming van een verharding van de structuur onder sterke (oscillerende) schuifspanning, vlak vóór het breken van de gels, en de afhankelijkheid van de elastische moduli van de deformatiegeschiedenis, riepen de vraag op of het prepareren van biofilmmonsters door afschrapen wel representatieve monsters oplevert. Zelfs na het breken van de gels door sterke schuifspanning herstelden de schuifmoduli van de gels binnen 30 s tot

65 % tot 90 % van hun oorspronkelijke waarde. Het snelle herstel, dat de noodzaak van chemische interventie vóór mechanische verwijdering van biofilms onderstreepte, werd geïnterpreteerd als een ander kenmerk van de reversibele elektrostatische crosslinking van ALE met Ca^{2+}. Analyse van de reologische resultaten aan de hand van een fysisch model leidde tot de conclusie dat er drie typen crosslinks met verschillende retardatietijden te onderscheiden zijn. De bevindingen bieden een startpunt voor de ontwikkeling van gerichte strategieën voor chemische verzwakking van biofilms. Verdere identificatie van de individuele interacties, in combinatie met het continu verbeteren van de chemische karakterisering van de biofilm-EPS, zullen essentiële onderdelen zijn van deze ontwikkeling. Verhoging van de $CaCO_3$-concentratie veroorzaakte een toename van de elastische modulus in combinatie met een toename van de brosheid. Met een verdere toename van de $CaCO_3$ concentratie werd het oplosbaarheidsproduct van sommige calciumzouten overschreden, wat resulteerde in neerslag van zout in de gels die de verdere toename van de elastische modulus verhinderden en blijkbaar inhomogeniteiten veroorzaakten. Ook was het herstel iets minder voor gels met een hoog $CaCO_3$-gehalte. Daarom wordt een hoge calciumdosering, die zoutneerslag in biofilms veroorzaakt, beschouwd als een mogelijke strategie voor het verwijderen van biofouling.

In Hoofdstuk 2 werd een effect van bacteriën op de porositeit en dus op de hydraulische weerstand van biofilms voorgesteld. In *Hoofdstuk 5* wordt de impact van de aanwezigheid van bacteriën als fysieke deeltjes op de visco-elastische eigenschappen behandeld. Voor dit doel werden Ca-alginaatgels met bolvormige styreendeeltjes met functionele carboxyl-, amino- of sulfonaatgroepen (2.3×10^{10} deeltjes/mL) bereid en onderzocht op een manier zoals beschreven in hoofdstuk 4. In het geval van de carboxyldeeltjes was de impact te klein om te worden gedetecteerd. De elastische modulus wordt iets verhoogd door sulfaatgroepen en met aminogroepen wordt deze iets verlaagd. De resultaten werden geanalyseerd in de veronderstelling dat de hydrogel-systemen (evenals biofilms) kunnen worden beschouwd als een mengsel van met deeltjes (bacteriën) versterkte hydrogels. Op basis van verschillende mengselmodellen werd geconcludeerd dat de gekozen volumefractie en aspectverhouding van de gebruikte deeltjes ongunstig waren voor het waarnemen van een effect. Een meer zichtbare impact wordt al verwacht bij een vertienvoudiging van het deeltjesaantal in combinatie met een staafachtige geometrie met een aspectverhouding van 5:1, beide niet ongebruikelijk voor bacteriële biofilms. Bij de analyse van de sterkte en stijfheid van biofilms mag daarom de bijdrage van bacteriën niet worden vergeten.

In *Hoofdstuk 6* tenslotte wordt een algemene discussie gegeven over wat er is geleerd over het bindingsgedrag van ALE versus alginaat, over de moleculaire interacties in ALE als een model voor biofilms, en over de niet-biologische impact van bacteriën, en worden ontbrekende kennis en mogelijke oplossingen daarvoor gepresenteerd. Ook het gebruik en het nut van de verschillende toegepaste modellen worden kritisch besproken.

Chapter 1

Introduction

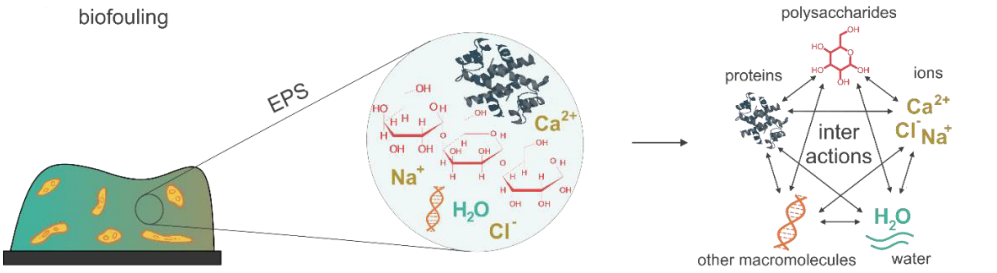

Figure 1-1: Schematic representation of the architecture of a biofilm. Bacteria are embedded in a hydrogel network that is stable because of the interaction between its constituents.

1.1 Biofilms and biofouling

Bacteria have been acknowledged as the dominant form of life on earth (Ikuma, Decho and Lau, 2013) and are found everywhere on this planet (Whitman, Coleman and Wiebe, 1998). Their most common and successful appearance are biofilms (Donlan, 2002; Hall-Stoodley, Costerton and Stoodley, 2004; Branda *et al.*, 2005; Flemming *et al.*, 2016). Biofilms are the accumulation and attachment of bacteria to surfaces or in agglomerates with the aid of a polymeric matrix.

While a success story from a bacterial point of view, biofilms have been interfering with humans and their technologies for ages. When those interferences cause significant issues, the term 'biofouling' is commonly used to refer to such biofilms. The motivation for this work originates from the 'love at first sight' (Flemming, 2000) of bacteria for membranes, as they are often used in filtration systems for water treatment (Shannon *et al.*, 2008; Singh, 2015; Krzeminski *et al.*, 2017; Rezakazemi, Khajeh and Mesbah, 2018). Adverse impact in this case mainly arises from an increase of hydraulic resistance or damage of the membrane material (Flemming *et al.*, 1997; Dreszer *et al.*, 2013; Desmond, Morgenroth and Derlon, 2018; Jafari *et al.*, 2018). As a result, the energy consumption is increased, and the necessity for regular cleaning reduces the membrane lifetime, requires high amounts of cleaning agents, and causes downtime of the installations (Shannon *et al.*, 2008). In total, biofouling has been found to increase the operational costs of such membrane filtration systems for more than 40 % (Flemming, 2020). Similarly, ship hulls (Callow and Callow, 2002; Schultz *et al.*, 2011), and heat exchange systems (Rao *et al.*, 2009; Müller-Steinhagen, Malayeri and Watkinson, 2011) can be impaired by biofilms. A recent, extensive discussion of the effects and measures against biofouling in an economic context is published by Flemming, 2020.

Beyond the economic issues, biofouling can also exert a severe impact on public health. Examples start from life-threatening infections caused by biofilms growing on implanted medical devices (Donlan, 2001; Bryers, 2008; Arciola, Campoccia and Montanaro, 2018) or otherwise causing infections of the human body (Malone *et al.*, 2017; Jamal *et al.*, 2018). Combination of the spreading of multi-resistant genes with generally enhanced antibiotic resistance of bacteria in biofilms as compared to planktonic bacteria (Høiby *et al.*, 2010; Koo *et al.*, 2017) makes surgical implants like an artificial hip joint a potentially lethal adventure (Ashton and Williams, 2019). Another potential risk for public health is posed by accumulation, growth and distribution of pathogenic bacteria in drinking water systems (Stoodley *et al.*, 2001; Bachmann and Edyvean, 2005; Wingender and Flemming, 2011; Gomes, Simões and Simões, 2014). It is not surprising that, when it comes to biofouling, the focus of research is usually on prevention or removal of biofilms.

To show the whole picture, however, it needs to be mentioned that biofilms can also be beneficial. The most popular examples for such biofilms include the human and animal digestion systems or water treatment facilities. Associated with increasing knowledge, useful applications of natural and artificial biofilms increasingly become the focus of attention (Böl *et*

al., 2013; More *et al.*, 2014). Making use either of the bacterial metabolism or the biofilms as a physical barrier, the possibilities seem stunning. The interested reader is referred to the extensive overview provided by Rittman (Rittmann, 2018).

No matter whether for the cause of prevention/removal or utilisation, the interest in characterising every aspect of biofilms keeps rising. As mentioned before, biofilms are composed of a polymeric matrix and bacteria embedded within. While the bacteria and their metabolism are of utmost importance when it comes to health threats or specific useful applications (like, for example, the cultivation of denitrifying bacteria in the denitrification step of water treatment), the majority of interferences with technology are of physical nature. Biofilms increase the pressure drop in membrane filtration systems (Dreszer *et al.*, 2013; Desmond, Morgenroth and Derlon, 2018; Jafari *et al.*, 2018) or the hydraulic resistance of ship hulls and water pipes (Christensen, 1989; Callow and Callow, 2002). Moreover, it was found that in comparison to planktonic bacteria, those living in biofilms were harder to oppose with chemicals and medicines (Davies, 2003; Aslam, 2008). Even if bacteria were successfully killed, biofilms were found remaining intact (Chen and Stewart, 2000; Bereschenko *et al.*, 2011; Zrelli *et al.*, 2013). So, technical performance could only partly be recovered, and regrowth was fast. Therefore, a critical area of biofilm research is the investigation of the extracellular polymeric substances (EPS) that constitute the biofilm matrix (Geesey, 1982; Flemming, 2016).

1.2 Extracellular polymeric substances: the powerful biofilm matrix

In addition to providing mechanical stability (which will be discussed in detail below) and protection from chemical influences (as mentioned above), the EPS supplies more advantages for the bacteria embedded in it. It prevents desiccation (Wingender, Neu and Flemming, 1999; Decho, 2016) and acts as nutrient storage and source (Zhang and Bishop, 2003; Wang, Liu and Tay, 2007; Liu, Huang and Qin, 2018). Furthermore, through the immobilisation of different types of bacteria, it promotes inter-species collaboration, communication and gene transfer (Flemming and Wingender, 2010; Chimileski, Franklin and Papke, 2014; Ma *et al.*, 2016; Decho and Gutierrez, 2017).

In the past decade great progress has been made in understanding EPS, from being entitled as the 'dark matter of biofilms' (Flemming and Wingender, 2010), the recognition as a complex but defined, although not yet determined, mixture of polymers (McCrate *et al.*, 2013), to the characterisation of particular polymers as its constituents (Zhu *et al.*, 2012; Yue *et al.*, 2015; Gagliano *et al.*, 2018; de Graaff *et al.*, 2019; Felz, Neu, *et al.*, 2020). There is agreement on the presence of carbohydrate-like, protein-like and lipid-like components, complemented by uronic acids, nucleic acids and humic substances (Lin *et al.*, 2014; Hobley *et al.*, 2015; Flemming, 2016). The EPS molecules physically interact with each other through attractive or repulsive electrostatic forces, hydrophobic forces, H-bonding, and entanglement (illustrated in Fig. 1-1). This results in reversibly crosslinked hydrogels that provide a lasting network

structure, which can incorporate up to 99 % water (Mayer *et al.*, 1999; Wingender and Flemming, 2004; Seviour *et al.*, 2009; Wilking *et al.*, 2011; Galy *et al.*, 2012; Dreszer *et al.*, 2013; Lin, Sharma and van Loosdrecht, 2013).

The interactions between the EPS molecules define the mechanical properties of biofilms: their adhesion to surfaces as well as their cohesion and mechanical response to external stress. Like other physically crosslinked hydrogels, biofilms are viscoelastic: depending on the applied stress and timescale, they behave more viscous (liquid-like) or more elastic (solid-like) (Stoodley *et al.*, 2001; Klapper *et al.*, 2002; Laspidou and Aravas, 2007; Lau *et al.*, 2009; Seviour *et al.*, 2009; Wilking *et al.*, 2011; Ehret and Böl, 2013; Safari *et al.*, 2015). These mechanical characteristics have been identified as crucial parameters for fouling potential (Li and Elimelech, 2004; Lee and Elimelech, 2006; Villacorte *et al.*, 2017) and for biofilm removal (Ang, Lee and Elimelech, 2006; Möhle *et al.*, 2007; Powell *et al.*, 2013; Peterson *et al.*, 2015; Safari *et al.*, 2015; Gloag *et al.*, 2020). They enable biofilms to mechanically respond adequately to various external mechanical conditions so that they can, to some degree, withstand physical cleaning attempts such as coughing or flushing. Therefore, it was proposed some time ago already that removal of biofilms requires a two-step approach, i.e. chemical weakening of the structure followed by physical removal (Flemming *et al.*, 1997). The targeted weakening of a structure that is still not fully understood is a challenge, though.

Cleaning studies targeting the EPS are often arbitrarily based on the chelating, oxidising or reducing, chaotropic, enzymatic, interfacial tension lowering or pH manipulating properties of the cleaning agents (Chen and Stewart, 2000; Li and Elimelech, 2004; Simões, Pereira and Vieira, 2005; Ang, Lee and Elimelech, 2006; Bereschenko *et al.*, 2011; Brindle, Miller and Stewart, 2011; Jones *et al.*, 2011; Guan *et al.*, 2018; Huang *et al.*, 2018). It turns out that due to the enormous variation in biofilm composition and population, successful cleaning strategies for one system do not necessarily work for others. The physical structure of biofilms is very heterogeneous (Massol-Deyá *et al.*, 1995; van Loosdrecht *et al.*, 1995; Wimpenny, Manz and Szewzyk, 2000; Sutherland, 2001) and depending on external influences like shear and nutrient availability (van Loosdrecht, 1997; Rochex *et al.*, 2008; Pellicer-Nàcher and Smets, 2014; Desmond, Morgenroth and Derlon, 2018). Resulting are substantial local variations in biofilm strength and elastic modulus at the microscale, up to three orders of magnitude (Galy *et al.*, 2012; Safari *et al.*, 2015). Since the mechanical properties stem from the interactions between the EPS components, which in turn are the target of chemical cleaning/weakening, it appears likely that even on a single biofilm a cleaning agent locally will have different effects. Therefore, cleaning studies or measurements of mechanical properties on distinct systems may be very useful from a practical point of view. Still, they are yet a step too far for comprehending the molecular interactions within biofilm EPS – which is necessary for the development of targeted cleaning strategies. To enable a beginning of understanding, models are needed containing the essential properties of EPS, leaving aside for the moment its full complexity.

1.3 Biofilm models: finding the balance between over-simplified and overwhelming

The aim of a model in general is simplification, a representation of something undefined by something defined (Strogatz, 2018). In the biofilm context, this means dismantling the complexity and partially undetermined composition of full biofilms into smaller portions of functional entities. Once those portions are understood, they can be extended or recombined to reach (close to) full complexity again eventually. One example for such an approach is to consider bacteria and the EPS separately, another one could be the separate investigation of cohesive and adhesive properties of EPS. In an additional step, further looking into the EPS, it could be decided that the original composition of the EPS is still too complex to investigate the molecular interactions, so hydrogels with a defined and homogeneous composition are investigated instead as a physical model. A typical example for a polymer used in this context is alginic acid extracted from brown algae (Wloka *et al.*, 2004; Ang, Lee and Elimelech, 2006; Katsoufidou, Yiantsios and Karabelas, 2007; Li, Xu and Pinnau, 2007; van den Brink *et al.*, 2009; Meng, Winters and Liu, 2015). Consisting of block copolymers of (1,4)-linked β-D-mannuronic and α-L-guluronic acid (Lee and Mooney, 2012) (see Fig. 1-2), it is well known for its specific interaction with Ca^{2+} ions, forming stable, crosslinked hydrogels.

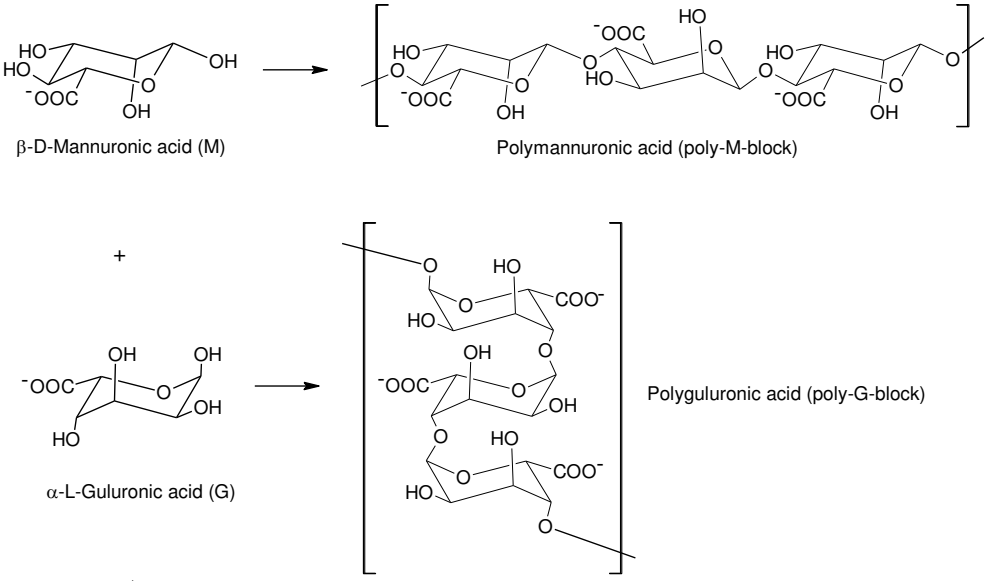

Figure 1-2: The monomers that compose alginic acid and their natural occurrence: the two homopolymers and an alternating copolymer.

The crosslinking is usually attributed to the poly-G-blocks, which form a zigzag shape. Combination of two parallel G-blocks has been found to provide vacancies in the shape and size of Ca^{2+} ions, which crosslink the two molecules (Grant *et al.*, 1973). This so-called egg-box model is illustrated in Figure 1-3.

Despite its apparent oversimplification of the biofilm system, alginate provides two benefits for biofilm researchers. Firstly, since it is a common material to produce hydrogels, e.g., in medicine (Augst, Kong and Mooney, 2006; Lee and Mooney, 2012), it is readily available and well-characterized (Davidovich-Pinhas and Bianco-Peled, 2010; Fu *et al.*, 2011; Hermansson *et al.*, 2016). Additionally, it shares several properties with the bacterial EPS. 'Bacterial alginate' has been identified, containing β-D-mannuronic and α-L-guluronic acid as well (Skjk-Bræk, Grasdalen and Larsen, 1986; Remminghorst and Rehm, 2006). Another crucial structural EPS-component (Lin, Sharma and van Loosdrecht, 2013) has been designated as 'alginate-like exopolymers' (ALE) for its alginate-resembling properties like gel-formation with Ca^{2+} ions (Lin *et al.*, 2008; Felz *et al.*, 2016).

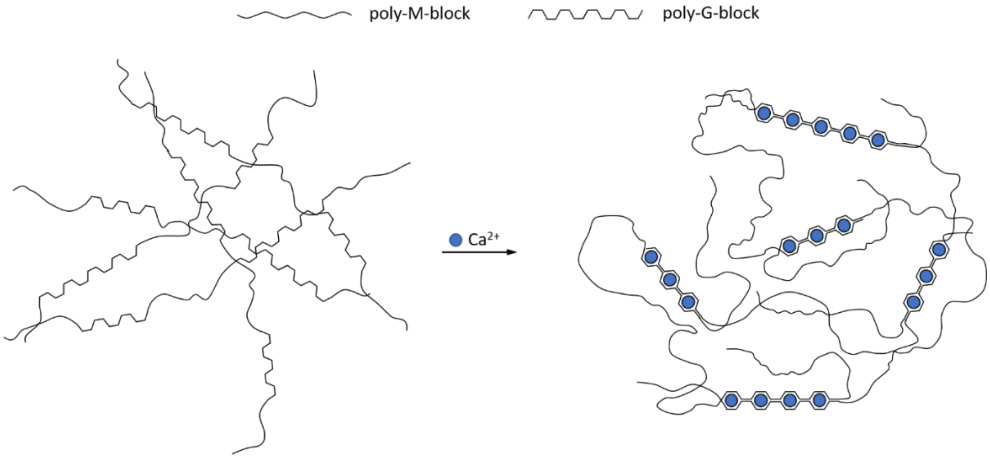

Figure 1-3: Egg-box crosslinking of alginate by Ca^{2+}.

Another physical model, one step closer to 'real' EPS but less defined in composition, is the analysis of the gelling or fouling behaviour of homogenised EPS extracts (Mayer *et al.*, 1999; Gorret *et al.*, 2003; Moresi, Bruno and Parente, 2004; Wloka *et al.*, 2004; Wang *et al.*, 2012; Lin, Sharma and van Loosdrecht, 2013; Feng *et al.*, 2014; Felz, Kleikamp, *et al.*, 2020). One example of such extracts is the above-mentioned ALE. This approach has been used mainly when the interaction with certain additives, e.g. metal ions, was the focus of interest. In such cases, the EPS extracts appear to reasonably represent the EPS. A further increase in the complexity of the models is rather straightforward. The effect of the addition of other components (molecules or particles) on the structure and mechanical properties can be investigated, or the interaction with and effects of cleaning agents. Insights into the molecular

interactions will, however, always requires sufficient knowledge and awareness of the molecular composition of the used model concerning real biofilms.

Last but not least, regardless of whether the tested materials are real biofilms or simple hydrogels, mathematical models are applied for interpretation of the results, especially from mechanical measurements. In contrast to the physical models described above, mathematical models are abstract models: the actual, indefinite processes (interactions between molecules) are represented by processes (elements) for which mathematical formulas exist. The viscoelastic behaviour of biofilms and other hydrogels is, for example, often represented by serial or parallel combinations of springs and dashpots. The most commonly used combinations are depicted in Figure 1-4.

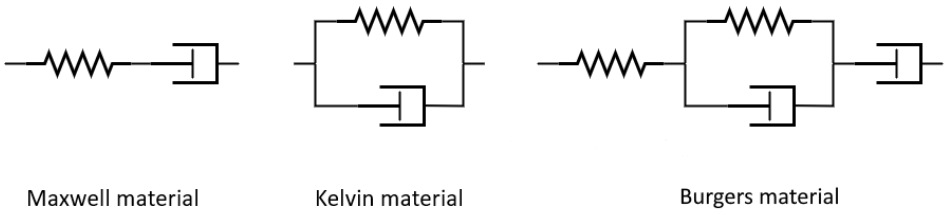

Figure 1-4: Mechanical models commonly used to describe the viscoelastic properties of hydrogels.

An underlying assumption of this modelling approach is that the gels can be treated as a continuous, homogeneous system. Alternatively, but much more complex, one could decide to start modelling with the intermolecular forces between the different components of the analysed material (Zhang *et al.*, 2018).

The decision, which mathematical model is to be used, depends on the kind of experiment and the intended insights to be gained. While strain-controlled tests are mostly interpreted with the Maxwell model (Wloka *et al.*, 2004; Ehret and Böl, 2013; Lin, Sharma and van Loosdrecht, 2013; Peterson *et al.*, 2013; Safari *et al.*, 2015; Jafari *et al.*, 2018), for stress-controlled experiments such as creep preferably the Kelvin model (Safari *et al.*, 2015) or the more complex Burgers model (Vinogradov *et al.*, 2004; Jones *et al.*, 2011; Galy *et al.*, 2012; Zrelli *et al.*, 2013; Gloag *et al.*, 2020) are used. All of those can be extended/generalised to cover higher complexity. Caution should be exercised, though, in extending to avoid overinterpretation. The identification of different processes during shear or relaxation and their attribution to molecular interactions inside the tested material seems appealing for the intended further unravelling of what holds biofilms together. However, the springs and dashpots are an abstraction and cannot always be related to real physical interactions in the biofilm (model) system under study. Numerical simulation of behaviour observed from (model) biofilms, coupling fluid dynamics with solid elastic mechanics in a finite element analysis, promises to overcome such limitations in the future (Picioreanu *et al.*, 2018).

It can be concluded that the selection of appropriate physical as well as abstract models is an essential step in research targeting to understand the properties and behaviour of biofilm EPS. Especially when the focus is on molecular interactions, which are diverse even between few different molecules, it is sensible to keep the physical model simple. Well-chosen models can hopefully help 'perceiving whatever holds biofilms together in their inmost folds'[1].

1.4 Objective and outline of this thesis

The target of this work is the correlation between composition, structure and mechanical properties of biofilm EPS in membrane filtration systems on a molecular level. Since the composition of EPS is, as mentioned, complex and still insufficiently determined, appropriate physical models have to be chosen/developed for this purpose. Requirements for these models are a good balance between defined composition and representativeness for biofilm EPS, shape-wise similarity to membrane biofilms, as well as the feasibility for structural and mechanical analyses. Focusing on the cohesion of the model films as an indication for the intermolecular forces between the components, it is furthermore essential to render the effect of adhesive forces negligible in the mechanical measurements.
As basic model components, alginate and alginate-like exopolymers (ALE) are chosen. Alginate is selected for the reasons that are described above. ALE, on the other hand, as a structural EPS component, promises higher representativity for biofilm EPS while being known for the gelation into a hydrogel (Lin *et al.*, 2010), which is necessary for the intended experiments.
Chapter 2 describes the production of hydrogel films on membranes using pressure-driven dead-end filtration, with the produced gel layers being readily available for structural and mechanical analysis on micro- and macroscale. For the analyses optical coherence tomography (OCT), atomic force spectroscopy (AFM) and low-load compression testing (LLCT) are selected, complemented by composition analysis concerning total suspended solids and volatile suspended solids (TSS/VSS) and ion content. Gel layer production of alginate and ALE under addition of $CaCl_2$ is described, as well as a study into the mechanical properties of the alginate gel layers as a function of different $CaCl_2$ concentrations.

The swelling behaviour and maturing of gel layers of alginate-like exopolymers (ALE) produced in dead-end filtration are illustrated in **Chapter 3**. The specific hydraulic resistance at the end of filtration as well as the composition after filtration and after 12 d of maturing with regards to TSS/VSS and ions are presented as a function of Ca^{2+} availability. The accumulation of ions inside the gel films is successfully described as a Donnan equilibrium, underlining the reversibility of the interactions of Ca^{2+} with the fixed negative charges in ALE. From the osmotic pressure related to the Donnan equilibrium, the strength of the films is estimated.

[1] Freely adapted from: Johann Wolfgang von Goethe, Faust. Der Tragödie erster Teil, 1808. Szene: Nacht, Faust allein in seinem gotischen Zimmer

In **Chapter 4,** the focus is switched to the molecular forces within ALE gels, which are considered representative for the interactions in biofilms and their persistence against cleaning attempts. Using different rheological methods, including amplitude sweeps, creep tests and amplitude steps, the gels' responses to long-lasting, low stress and short-lasting, high stress are displayed. Particular focus is on the recoverability of mechanical properties after application of high stress. Specific interactions are approached by fitting creep test results with a Burgers model with two Kelvin elements.

The contribution of bacterial cells to the mechanical properties of biofilms is addressed in **Chapter 5**. As a model, the bacteria are represented by polystyrene beads covered with different functional groups, embedded in Ca-alginate hydrogels. The impact of these particles on the gels' mechanical properties is illustrated by reference to the elastic shear modulus, determined in dynamic and static rheological experiments, as well as by reference to their creep behaviour, which is analysed using the Burgers model. The results are interpreted under application of theories used for composite materials.

Chapter 6 combines and concludes the results from the former chapters and shows how, based on the current findings and experiences, the goal of targeted strategies against biofouling can become a reality in the future.

Chapter 2

On the correlation between composition, cake layer resistance and mechanical properties of model biofilms

To successfully cope with biofouling, a thorough understanding of the interactions between extracellular polymeric substances (EPS) and their environment is essential. In this work, alginate and alginate-like exopolymers (ALE) were used as model polymers for the EPS matrix of biofilms, to develop an experimental setup allowing investigating the correlation between composition, structure and mechanical strength of gel layers. By deposition on ultrafiltration membranes by dead-end filtration, gel layers with thicknesses between 100 µm and 400 µm were produced. Their densities and calcium content increased with $CaCl_2$ concentration in the feed solutions. Depending on this concentration, alginate gel layers were found to contain structures of Ca-alginate aggregates that were presumably already formed in solution and showed decreasing specific resistances with increasing $CaCl_2$ content. This, at first sight, contra-intuitive behaviour is an illustration of the importance of the porosity of gel layers. For 0.2 mM $CaCl_2$ alginate gel layers, the relaxation behaviour showed an elastic response similar to that of biofilms. Gel layers made from ALE differed substantially from the alginate gel layers. From analyses of the ionic distributions over gel and solution, it was found that Ca^{2+} binding to ALE was not nearly as specific as for alginate. Still, both systems required $CaCl_2$ for crosslinking. Ca-ALE gel layers exhibited similar specific resistances as alginate gel layers with 1 mM $CaCl_2$, which were hardly dependent on $CaCl_2$ concentration. Over time, they slowly swelled, which was accompanied by the development of a fibrous network structure. Further determination of the molecular interactions within ALE gel layers and the effect of adding more biofilm components are considered important future research directions, in which the developed experimental approach can play a key role.

2.1 Introduction

Biofilms, resulting from the accumulation and growth of bacteria on surfaces or in aggregates while developing a protective polymer matrix, are a universal phenomenon. If such films cause adverse effects, for example by increasing the costs by the need for cleaning and shortening the lifetime of membranes in membrane filtration systems (Flemming *et al.*, 1997; Vrouwenvelder *et al.*, 2008), or by threatening human health on medical devices (Donlan, 2001), they are referred to as biofouling. The prevention and removal of biofouling have been a research topic for the past three decades. Since it was found that killing the bacteria hardly had a positive effect on removal of the biofilm (Flemming *et al.*, 1997; Chen and Stewart, 2000; Davison, Pitts and Stewart, 2010; Bereschenko *et al.*, 2011; Zrelli *et al.*, 2013), interest in the polymeric matrix itself increased. Often referred to as extracellular polymeric substances (EPS), this 'perfect slime' (Flemming, 2011) was found to account for up to 90 % of the organic matter of biofilms (Wingender, Neu and Flemming, 1999) and to provide the mechanical strength and integrity of biofilms (Flemming and Wingender, 2010; Lin *et al.*, 2014).
There is an agreement that EPS is in general composed of biopolymers such as polysaccharides and proteins, complemented by lipids, humic substances and eDNA (Lin *et al.*, 2014; Flemming, Neu and Wingender, 2016). A growing number of specific components of the EPS layer has been identified and characterised (Hobley *et al.*, 2015). Still, the bigger picture of the chemical components and their interactions remains in large part unfold. The sum of the molecular interactions of the EPS components and their environment defines the mechanical behaviour of biofilms. As such the EPS matrix can be described as a complex hydrogel (Mayer *et al.*, 1999; Körstgens *et al.*, 2001; Lin *et al.*, 2010; Galy *et al.*, 2012): a three dimensional, crosslinked network of polymers that can bind high amounts of water (Ahmed, 2015).

Properties of biofilms that are interesting from a membrane (bio)fouling point of view are the hydrodynamic resistance ('how much negative impact does it have?') and its resilience against cleaning ('how can it be removed?'). The resistance is dependent on the biofilm structure (Desmond *et al.*, 2018; Jafari *et al.*, 2018). As an indication for mechanical stability, the viscoelastic behaviour is a commonly used measure (Galy *et al.*, 2012; Safari *et al.*, 2015). Ultimately, the interactions between the different components of the biofilm matrix in combination with the environment (water composition, pH, shear stress, etc.) determine its structure and mechanical behaviour, and therefore eventually its resistance towards cleaning attempts. The aim of this work was the development of an experimental method to investigate the interactions between the different components of EPS and how these interactions define the structure and the mechanical properties. The main point of this approach was finding a balance between simplification and representativeness. Ideally, the system to be developed should allow strict control or at least identification of the composition. At the same time, it was intended to be comparable to real biofilms, so that a stepwise increase of complexity will eventually allow an approximation towards interactions in real biofilms. Alginate has been used

as a model polymer for biofilms before (Wloka *et al.*, 2004; Katsoufidou, Yiantsios and Karabelas, 2007; van de Ven *et al.*, 2008; van den Brink, 2014) because of its easy availability and structural similarity to polysaccharides in EPS. Alginate-like exopolymers, an extract of structural EPS also referred to as ALE, have been found in bacterial EPS and show physical-chemical similarities to alginate, i.e. gelling with calcium (Lin *et al.*, 2008). ALE is used in this work as an interim step between the fully characterised algal alginate and the complex full EPS.

2.2 Materials and Methods

2.2.1 ALE extraction

'Alginate-like exopolymers' (ALEs) are one representative group of bacterial exopolymers, which have been associated with supplying structural integrity to granular sludge (Lin *et al.*, 2008). Due to their accumulation in granular sludge, they were extracted from Nereda® sludge obtained from the wastewater treatment plant in Garmerwolde, the Netherlands following the protocol from Felz et al. (Felz *et al.*, 2016).

After collection of the granules by decantation, about 150 g of the wet granules (20 g dry weight) was mixed with 1 L demineralised water and 10 g sodium carbonate (VWR, the Netherlands). The mixture was homogenised using pulsed sonication (Branson Sonifier 250, 5 min at 70 %, max output 200 W), while cooled down on ice to prevent overheating. Subsequently, the mixture was heated to 80 °C for 30 min under vigorous stirring. After centrifugation (Allegra X-12R Centrifuge, Beckman Coulter, 20 min, 3750 rpm), the supernatant was acidified with 1 M hydrochloric acid (Merck Millipore, Germany) to pH 2 - 2.5 and centrifuged again. The pellet was kept and stored at -80 °C until further use and is henceforth referred to as ALE.

As a simple quality control, the ALE extract was directly tested for its gel-forming ability with calcium. The frozen pellet was dissolved and neutralised with 1 M NaOH (Merck Millipore, Germany) and subsequently dripped into a 2.5 wt% $CaCl_2$ solution. Gelling was considered successful if the droplets visually formed beads in the solution rather than dissolving.

Liquid chromatography coupled with organic carbon detection (LC-OCD) (Agilent 1260 Infinity with Toyopearl HW-50S, 30 µm, 250 mm, coupled with Siemens Ultramat 6E) was used to determine the molecular mass distribution of carbon compounds in the ALE.

2.2.2 Procedure for model layer production

Alginic acid sodium salt (80-120 kDa, Sigma Aldrich, henceforth referred to as alginate) was dissolved in 3/5 of the total intended volume of demineralised water by stirring and slight heating up to ca. 40 °C for 1 h. The required quantities of $CaCl_2$ (VWR, the Netherlands) and KCl (VWR, Belgium) were dissolved in the remaining volume, which was then slowly added to the polysaccharide solution.

For proof of principle, a series of Ca-alginate gel layers was produced and analysed. The ionic strength provided by the addition of salts was fixed to 15 mM. The $CaCl_2$ and KCl concentrations were varied, as shown in Table 2-1. To allow the fast formation of gel layers, a relatively high concentration of 60 mg/L alginate was used. Based on the molecular formula for sodium alginate, $(C_6H_7NaO_6)_n$, the sodium contained in the alginate powder contributed another 0.3 mM to the total ionic strength. Four gel layers were analysed per composition.

Table 2-1: Ionic concentrations for feed solutions with 60 mg/L alginate.

	$CaCl_2$ [mM]	**KCl [mM]**	**ionic strength [mM]**
combination 1	0	15	15.3
combination 2	0.2	14.4	15.3
combination 3	1	12	15.3
combination 4	3	6	15.3

After the alginate gel layers, production of Ca-ALE gel layers was tested with several ALE concentrations. The solution composition used for alginate was taken as a starting point for the ALE experiments. The first series of ALE gel layers was produced with 60 mg/L (dry mass) ALE, and the ionic strength provided by the addition of KCl and $CaCl_2$ was fixed to 45 mM, allowing a variation of the $CaCl_2$ concentration up to 15 mM. In the course of the experiments, the feed solution composition was optimised towards 120 mg/L ALE and 24 mM added ionic strength. Unless stated otherwise, results are given as an average of two samples per composition.

2.2.2.1 Dead-end filtration

Model gel layers were prepared using dead-end filtration across an ultrafiltration membrane (UP150, polyethersulfone (PES), 150 kDa, Microdyn Nadir, Wiesbaden, Germany) at room temperature (23.9 ± 0.7 °C). In order to produce uniform cake layers, the filtration was done without stirring.

From the membrane, a circle was cut with a diameter of 7.5 cm. The membrane was mounted at the bottom of a 450 mL stainless steel dead-end filtration cell with an effective diameter of 7 cm. To increase the volume capacity, the cell was connected to a 10 L pressure vessel. During filtration, a transmembrane pressure of 1 bar was applied.

Ca-alginate layers were initially detaching from the membranes as soon as the filtration pressure was released, likely because of repulsion between negative charges on the membrane surface and the alginate gel layers. To prevent this, an adhesive layer was applied by immersing the membranes in 1.8 mL of a 0.01 % sterile-filtered solution of poly-L-lysine in water (50-150 kDa, Sigma-Aldrich) for 5 min, based on a cell attachment protocol from the provider of the reagent (Sitterly, 2008). Residues were removed by thorough rinsing, and the layers were allowed to dry for 5 min. The coated membranes were stored in water until further

analysis (within 60-90 min after application of the poly-L-lysine). Ca-ALE gel layers showed steady attachment to the membrane, also without this extra layer.

During filtration, the pressure and the filtered volume were recorded. Initially, for all membranes, the clean water flux was determined by filtration of 750 mL demineralized water. Then, 1.5 L of the feed solution was added to the pressure vessel and filtered through the membrane until 600 - 1000 mL of filtered volume was reached. The membrane with the model gel layer was then removed from the filtration cell and stored in salt solutions of the same ionic composition as the feed solution until further analysis.

2.2.3 Analysis

2.2.3.1 Filtration/gel layer formation

The density of the aqueous solutions was approximated as the density of water ρ_{H2O} = 1 g/mL, in order to translate the logged data of filtered mass of solution m_f to filtered volume V_f as a function of time t.

$$V_f(t) = \frac{m_f(t)}{\rho_{H2O}} \qquad (2\text{-}1)$$

The flux $J(t)$ through the membrane area A_m was determined using Equation 2-2.

$$J(t) = \frac{V_f(t + \Delta t) - V_f(t)}{A_m \cdot \Delta t} \qquad (2\text{-}2)$$

The considered time interval Δt was depending on the flux. For the clean water flux, it was usually set to 10 s, for the later stages of the filtration it was increased to up to 10 min. In comparison to the applied pressure of 1 ± 0.1 bar, the additional hydrostatic pressure in the filtration cells of max. 1 kPa was neglected. Therefore, the transmembrane pressure (TMP) was approximated with the logged applied pressure p_a. The total filtration resistance R_f was then calculated according to Equation 2-3.

$$R_f(t) = \frac{p_a}{\eta_{H2O} \cdot J(t)} \qquad (2\text{-}3)$$

The dynamic viscosity of the solutions η_{H2O} was approximated with the value for water at 24 °C, 0.91 mPa·s (Paar, 2008). Before each experiment, the membrane resistance R_m was determined by filtration of 750 mL of demineralised water. Subtraction of the so-obtained membrane resistance from the total resistance resulted in the cake layer resistance, R_{cl}.

$$R_{cl} = R_f - R_m \qquad (2\text{-}4)$$

To characterise the final gel layers, the average resistance over the last hour before termination of the filtration was considered. In combination with the organic mass of the gel

layers per membrane area (VSS/A_m) determined later, the specific cake resistance α_m (Ripperger *et al.*, 2013) was calculated as

$$\alpha_m = \frac{R_{cl}\, A_m}{VSS}. \qquad (2\text{-}5)$$

2.2.3.2 Composition

Samples of the frozen ALE pellet were weighed into dry porcelain crucibles and heated to 105 °C for 24 h to determine the dry mass (total suspended solids, TSS). After each experiment, the alginate and ALE gel layers were scratched from the membranes and treated the same. In a second step, the samples were burnt at 550 °C for 2 h to remove the organic matter (volatile suspended solids, VSS). The water content and the organic mass were calculated according to

$$m_{water} = m_{sample} - TSS \qquad (2\text{-}6)$$

$$VSS = TSS - m_{ash} \qquad (2\text{-}7)$$

where m_{sample} was the mass before heating, TSS was the mass after heating to 105 °C, and m_{ash} was the mass after heating to 550 °C. The VSS amount was interpreted as alginate or ALE, while the ash was interpreted as the inorganic content of the materials.

Samples of the ALE pellet were diluted to a concentration below 100 mg/L carbon, after which they were analysed with a TOC analyser (Shimadzu TOC-L) on total carbon and total organic carbon content. The same analysis was exerted on the ALE solutions used for filtration.

Samples of the frozen ALE pellet were dissolved and acidified to a total of 2 wt% HNO_3 with 69 % HNO_3 (VWR, France). In case of the alginate and ALE gels produced in the experiments, the ash left after TSS/VSS determination was dissolved in 69 % HNO_3, in a microwave oven (Milestone Ethos Easy). With 1500 mW the suspensions were heated to 200 °C within 15 min and then kept at 200 °C for another 15 min. After cooling down, also these solutions were diluted to a total HNO_3 content of 2 %. The salt concentrations were subsequently determined by inductively coupled plasma-optical emission spectroscopy (ICP-OES, Perkin Elmer, type Optima 5300 DV). For determination of the ion concentrations in the filtration solutions, ion chromatography (IC, Metrohm Compact IC 761) was used.

The interactions between alginate/ALE and the added ions Ca^{2+} and K^+ were characterized regarding the Donnan potential (Sperelakis, 2012). A Donnan potential is established when charges are fixed in one part of an otherwise balancing system, for example by a semi-permeable membrane. In the present systems, the fixed charges were the negatively charged functional groups of the alginate and ALE. As a consequence, counterions accumulated inside the gels. Without specific interactions between the functional groups and counterions, the

following balance applied between ions j and k of valences z_j and z_k, respectively, in the gels (index g) and the supernatant (index s):

$$\left(\frac{c_{j,s}}{c_{j,g}}\right)^{\frac{1}{z_j}} = \left(\frac{c_{k,s}}{c_{k,g}}\right)^{\frac{1}{z_k}} \qquad (2\text{-}8)$$

For a first characterization, the quotient of the left- and right-hand sides of this equation (LHS/RHS) was calculated for Ca^{2+} (j) and K^+ (k). While a result of 1 indicated that a Donnan equilibrium was established, lower or higher values illustrated preference for Ca^{2+} or K^+, respectively.

2.2.3.3 Structure

A Ganymede SD-OCT (ThorLabs, Dachau, Germany) was used in combination with the ThorImage® Software to get insight into the smoothness of the surface and to measure the thickness of each model gel layer. During the measurements, the samples were submerged in aqueous solutions. The optical density was approximated with the value for water (refractive index = 1.33).

To determine the dry mass and organic fraction of the gel layers, they were scratched from the membranes after the experiments and treated according to the description above for TSS/VSS determination. The organic mass (VSS content) was used to calculate the density according to Equation 2-9.

$$\rho_{VSS} = \frac{VSS}{h_{cl} \cdot A_m} \qquad (2\text{-}9)$$

h_{cl} was the cake layer thickness observed with the OCT, and A_m the effective membrane area (0.0038 m^2). In the same way, also the density for the contained ions was calculated.

2.2.3.4 Mechanical properties of the model gel layers

The bulk (visco)elastic properties of the model gel layers were investigated on two different length scales, on the microscale with a contact area of maximal 5 µm diameter, and on the macroscale with 2.5 mm diameter. In this way, potential heterogeneities on the microscale and their effects on the macro scale were expected to be identified. For both methods, a requirement was that the samples stayed fully wettened over the whole measurement range.

Atomic force spectroscopy

In atomic force spectroscopy (AFM) the local interactions of a sample with a micro indenter, typically available in the range from a few nm to several µm, were investigated. In a cycle of approach, contact, indentation and retraction, the attractive and repulsive forces between indenter and sample were recorded in a force-distance curve.

For spherical indenters a correlation between the force (F) and the 'negative' distance beyond the contact point, also referred to as indentation (δ), has been described by Hertz (Hertz, 1882) as

$$F = \frac{4\,Y}{3 \cdot (1 - \nu^2)} \cdot r^{\frac{1}{2}} \cdot \delta^{\frac{3}{2}}. \qquad (2\text{-}10)$$

r is the radius of the sphere, and ν is the Poisson's ratio of the sample, describing its expansion perpendicular to the indentation. The latter is for biofilms usually estimated between 0.4 and 0.5 (Laspidou and Aravas, 2007; Safari *et al.*, 2015; Jafari *et al.*, 2018). For the analysis, 0.45 was chosen. Y in this equation stands for the Young's Modulus, also called the elastic modulus, an intrinsic parameter for the sample's stiffness. It has the unit of [Pa] and describes the relation between the applied force and deformation of the sample.

The Hertz model has been successfully applied to biofilms (Lau *et al.*, 2009; Powell *et al.*, 2013; Safari *et al.*, 2015) and on other hydrogel films with similar dimensions (Dimitriadis *et al.*, 2002; Kaklamani *et al.*, 2014) to extract Young's moduli from force-distance data taken with colloidal probes. The main assumptions made by Hertz, linear elasticity and infinite sample thickness, are sufficiently met as long as the indentation and the contact diameter are significantly smaller than the sample thickness and the indenter. The indentation depth δ and contact radius a of an indenter with radius r are geometrically connected as follows:

$$\delta = \frac{a}{2} \cdot \ln\frac{r + a}{r - a} \qquad (2\text{-}11)$$

The elasticity of the gel layers in this work was investigated using a ForceRobot® 300 (JPK Instruments, Berlin, Germany) in combination with a fluid cell and a colloidal SiO_2 probe of 5 µm diameter connected to a cantilever with a nominal spring constant of 0.36 N/m (Novascan, Milwaukee, WI, USA). For analysis, the complementary software was used.
The sensitivity of the cantilever and the instrument was calibrated by measuring a force curve on a microscope glass slide and the spring constant of the cantilever by measuring the thermal noise in solution. Before every new experiment, the status of the probe was checked by repetition of the calibration. In case the calibration force curves showed considerable divergence (e.g., there was much more adhesion, or the curve became much flatter), or the resonance frequency of the cantilever changed significantly, it was assumed that material was sticking to the probe. In this case, the cantilever was carefully rinsed with demineralised water and dried in the air for 30 min before repeating the procedure.
All tubing and the cell were rinsed with demineralized water, and the imminent salt solution before every new sample was measured. Samples were kept hydrated with the corresponding storage solution all the time. Membrane coupons with attached sample gel layers of roughly 1 × 1 cm were glued to microscope slides with thin double-sided tape. The microscope slides

were then mounted in the ForceRobot®. After positioning and filling the fluid cell, the samples were approached by the probe using the built-in function of the ForceRobot®.
Data were obtained in single-tapping mode at a velocity of 10 µm/s. The desired maximal indentation depth was 2.5 µm, assuming that at this point the indenter reached the maximal possible contact area. Measurements were done at three different positions per sample. Per location, 20-25 curves were taken using the built-in grid pattern, resulting in a total of 60 force curves per sample. To assure that the indenter detached from the surface in between measurements, the total distance moved by the indenter during a measurement was set to the relatively high value of 15 µm.
Data analysis was done with the JPK ForceRobot® software. The raw data (deflection of the cantilever as a function of the piezo position) was converted to force vs distance curves using the initial calibration data. The resulting curves subsequently were adjusted according to their contact point. Applying the Hertz model on the resulting curves revealed the Young's modulus for each curve.

Low-load compression testing

A low load compression tester (LLCT) (Körstgens *et al.*, 2001; Sharma *et al.*, 2011) was used for further macroscopic investigation of the viscoelastic properties of the gel layers. A 2.5 mm diameter plunger connected to a moving stage was used to uniaxially compress the samples for 20 % while measuring and recording the force exerted on the sample with a load-cell with automated lifting-force compensation. Subsequently, the relaxation of the samples was observed for 200 s.

The preparation and treatment of the samples were similar to the procedure described for the force spectroscopy. Ca. 1 × 1 cm pieces of the membrane with attached gel layers were stuck on microscope glass slides using thin double-sided tape. Over the whole contact area, the samples were kept hydrated using solutions of the same ionic composition as the storage solutions. The glass slide with the sample was put on the load cell, where it could be approached by the plunger. During the measurements, the position of the plunger, as well as the load on the load cell (in kg), were recorded as a function of time, $h(t)$ and $m(t)$, respectively. For the two investigated compositions, four gel layers were produced by filtration for each, and three measurements were conducted on different areas of each gel.
At the start of each measurement, the plunger position was calibrated to a zero height, determined on a spot where the gel layer had been removed from the membrane. With an approaching speed of 5 µm/s, the plunger was closed in on the membrane until detecting the surface, defined as the position where the load first exceeded 0.009 g. After retracting the plunger and moving the sample to a spot with the attached gel layer, another time the plunger was allowed to approach with the same settings. As soon as the gel layer's surface was detected with the same method as the zero height, the sample thickness h_s was determined,

and the sample was subsequently compressed for 20 % within 1 s. For the last part of the measurement, the plunger stayed in the position of 20 % compression, and the load was monitored for 200 s. The strain at any time during the measurement, $\varepsilon(t)$, was calculated as

$$\varepsilon(t) = \frac{d(t)}{h_s} \qquad (2\text{-}12)$$

with the recorded sample thickness h_s and the deformation $d(t)$, calculated as

$$d(t) = h_s - h(t). \qquad (2\text{-}13)$$

The corresponding stress $\sigma(t)$ in the sample was derived from the load $m(t)$ by

$$\sigma(t) = \frac{m(t) \cdot g}{A}. \qquad (2\text{-}14)$$

g stands for the gravitational acceleration of 9.81 m·s^{-2} and A for the plunger area of 4.91 mm^2. Plots of stress vs strain over the compression period were used for a first characterisation of the gel layers' elasticity at the macro range. From the combination of stress and strain the compressive relaxation modulus $E(t)$ was calculated as

$$E(t) = \frac{\sigma(t)}{\varepsilon(t)}. \qquad (2\text{-}15)$$

At t = 0 and if the deformation was within the linear elastic region of the material, $E(t)$ was equal to the Young's modulus Y. The obtained data for $E(t)$ was plotted and subsequently fitted with a Prony series according to the generalised Maxwell model (Sharma *et al.*, 2011). In this approach, the total modulus was split into i parallel Maxwell elements, each representing a serially connected pair of an elastic spring and a dashpot. The modulus derived from the Maxwell model was denoted as $E_M(t)$.

$$E_M(t) = E_1 \cdot e^{-\frac{t}{\tau_1}} + E_2 \cdot e^{-\frac{t}{\tau_2}} + \cdots + E_N \cdot e^{-\frac{t}{\tau_N}} \qquad (2\text{-}16)$$

As can be seen from Equation 2-16, each Maxwell element was characterised by its spring constant E_i and its relaxation time τ_i. The latter was defined as the ratio between the viscosity η_i and the spring constant E_i of each element.

For the fitting, the 'Solver' function of Microsoft Excel was used for minimising a Chi-square function by optimising the values for increasing numbers of pairs of E_i and τ_i:

$$\chi^2 = \sum_{i=1}^{N} \left(\frac{E(t) - E_M(t, \tau_1 \ldots \tau_N)}{SD} \right)^2 \qquad (2\text{-}17)$$

SD is the standard error for the device, which was found to be 2.76 × 10^{-5} N. When the addition of more elements did not cause a significant decrease of χ^2, the number of elements N was accepted as sufficient.

The relative importance E_t of each element was calculated as its spring constant's share in the sum over all spring constants.

$$E_t = 100 \cdot \frac{E_i}{\sum_{i=1}^{N} E_i} = 100 \cdot \frac{E_i}{E_M(0)} \qquad (2\text{-}18)$$

2.3 Results and Discussion

Gel layers were produced overnight in filtration experiments lasting between 16 h (alginate) and 22 h (ALE). The original setup was designed according to previous gel layer formation experiments with alginate (van de Ven *et al.*, 2009; van den Brink *et al.*, 2009), but with the condition that mechanical analyses could be performed on intact gel layers afterwards.

2.3.1 Alginate gel layers

Dry mass analysis of the sodium alginate powder showed a water content of 11.8 ± 0.1 wt%. Of the dry mass, 74.0 ± 0.1 wt% was classified as volatile organic compounds, the remaining mass after burning was considered as the inorganic part.

After dissolving, 304.5 ± 0.2 mg carbon and 97.7 ± 0.7 mg sodium were detected per g of sodium alginate powder. This ratio agreed with the molecular formula $(C_6H_7NaO_6)_n$. Further analysis with LC-OCD revealed that the carbon fraction was mainly present as polymer molecules (88 wt%) with a number average molecular weight of 240 kDa. The remaining 12 wt% was found to have a much lower molecular weight.

2.3.1.1 Filtration and gel layer formation

The filtration behaviour of the different alginate solutions is illustrated in Figure 2-1 as overall resistance as a function of filtered volume. According to cake filtration theory, for cake layers evolving from the rejection of particulate matter onto a membrane, the reverse flux shows a linear relation to the filtered volume V_f (Schippers and Verdouw, 1980; Ripperger *et al.*, 2013) if the pressure drop over the layer (TMP) is assumed constant.

$$\frac{dt}{dV_f} = \frac{\alpha_p \cdot \eta \cdot K_p}{2 \cdot A_m^2 \cdot TMP} \cdot V_f + \frac{\eta \cdot R_m}{A_m \cdot TMP} \qquad (2\text{-}19)$$

A_m and R_m stand for the area and resistance of the membrane, while η represents the dynamic viscosity of the filtered liquid. Since those terms could be considered constant over filtration, the second term could be viewed as a constant membrane contribution. α_p and K_p represented the specific resistance and the mass of the cake layer. Equation 2-19 was derived from the assumption of homogeneous mixing of the filtration solution, which allowed estimating that the amount of matter per membrane area m was proportional to the filtered volume (Ripperger *et al.*, 2013); $K_p = m/V_f$ was the proportionality factor for this. It is apparent from the equation

that linearity only held if the specific resistance α_p and the amount of matter deposited on the membrane per filtered volume were independent of the filtered volume. The theory has been found to accurately describe the fouling behaviour of alginate in the presence of Ca^{2+} (Katsoufidou, Yiantsios and Karabelas, 2007). It has also been applied to organic foulants (Roorda and van der Graaf, 2001).

Following from Equations 2-2 and 2-3, the reverse flux described in Equation 2-19 could be substituted by the resistance without changing more than a few constants. From the shape of the resulting curves, shown in Figure 2-1, it can be seen that the filtrations with 0.2 mM $CaCl_2$ and 1 mM $CaCl_2$ obeyed the cake filtration theory. There was a linear relationship between reverse flux and the filtered volume. For 3 mM $CaCl_2$, it was not easy to recognise, but after an initial phase with hardly any slope, it also showed a linear relation. Only the curve without $CaCl_2$ addition showed flattening of the slope with increasing filtered volume for V_f larger than ± 400 mL. This flattening behaviour of the resistance was associated with the compression of a cake layer while being built up during the experiment (Listiarini *et al.*, 2009), or with concentration polarisation of colloidal matter in a non-stirred environment (Katsoufidou, Yiantsios and Karabelas, 2007). Comparison of the slopes showed a decrease in slope with increasing $CaCl_2$ concentration, meaning that the higher the $CaCl_2$ concentration, the lower was the fouling potential.

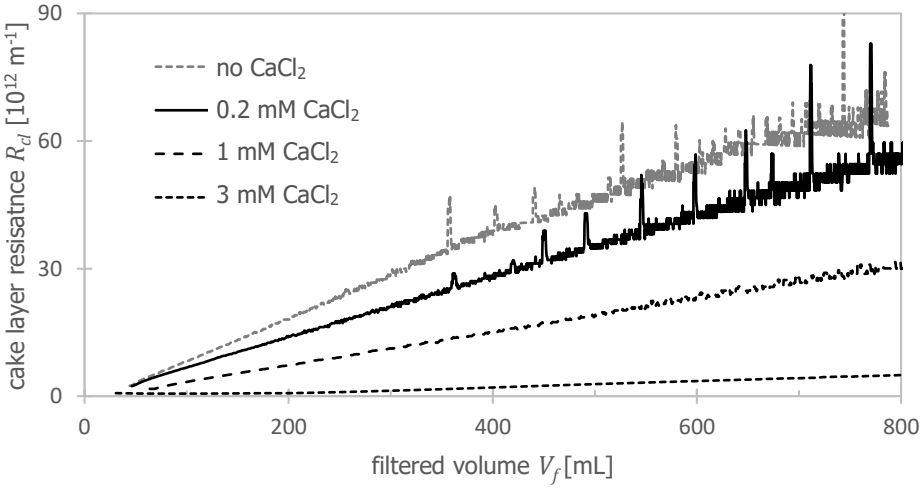

Figure 2-1: Filtration curves for alginate solutions with different ionic compositions as a function of filtered volume at 1 bar pressure difference.

The spread in slope within the quadruplets was in the range of 2-4 %, so the differences were considered significant. The same trend has been observed in fouling of hollow fibre membranes with alginate (Katsoufidou, Yiantsios and Karabelas, 2007). It was explained by the formation of alginate particles in solution at higher $CaCl_2$ concentrations, leading to less dense packing and higher porosity of the resulting cake layers. Such behaviour was therefore considered

likely also in the current case. Only for the medium $CaCl_2$ concentrations of 0.2 and 1 mM, it was possible to obtain thicknesses and masses of the cake layers (see below). With these data, specific resistances of 1.81 ± 0.04 × 10^{16} m/kg and 0.88 ± 0.02 × 10^{16} m/kg were calculated for 0.2 mM $CaCl_2$ and 1 mM $CaCl_2$, respectively. These were rather high values compared to biofilms, which have been found in the range of 10^{12} m/kg (Derlon *et al.*, 2016), but agreed well with similar experiments of alginate filtration (Sioutopoulos and Karabelas, 2012).

2.3.1.2 Gel layers' appearance and composition

In Figure 2-2, OCT pictures of three kinds of alginate gel layers after filtration are shown. Without $CaCl_2$ (only 15 mM KCl in solution), very thin gel layers were deposited on the membrane (shown in Fig. 2-2A). Even with the application of an adhesive poly-L-lysine layer, these gel layers did not adhere well to the membrane and started detaching as soon as the filtration was finished. At high $CaCl_2$ content (3 mM $CaCl_2$, 6 mM KCl), pieces of Ca-alginate could already be detected in the feed solution with the naked eye. The resulting cake-layers appeared highly inhomogeneous and porous (Fig. 2-2C), supporting the assumption that the reason for lower cake layer resistances of alginate gels with more Ca^{2+} could be the higher porosity due to alginate particle formation. These layers started disintegrating as soon as the filtration pressure was relieved. Both compositions were excluded from further analysis, leaving samples with concentrations of 0.2 mM $CaCl_2$ (with 14.4 mM KCl) and 1 mM $CaCl_2$ (with 12 mM KCl). An example of such a gel layer is presented in Figure 2-2B, showing that the two considered gel layers with 0.2 mM $CaCl_2$/14.4 mM KCl and 1 mM $CaCl_2$/12 mM KCl were homogenous with a defined surface.

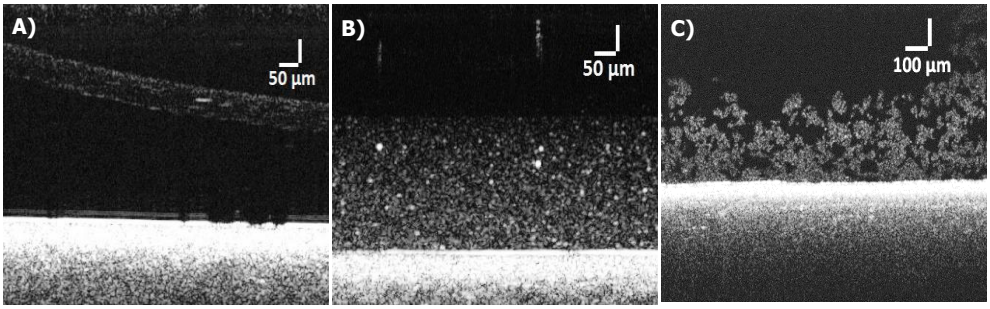

Figure 2-2: OCT pictures of alginate (60 mg/L) gel layers made without $CaCl_2$ (A), 1 mM $CaCl_2$ (B) and 3 mM $CaCl_2$ (C).

After filtration, the thickness of the gel layers initially increased over time (cf. Fig. 2-4). This is an elastic property and has been related to the porosity of polymer gels (Cai *et al.*, 2010; Hu and Suo, 2012) and biofilms (Laspidou and Aravas, 2007; Jafari *et al.*, 2018), regarding them as poroelastic materials. In this model, it is assumed that compression during filtration leads to closing of pores in the material and squeezing out of the solvent. The observed relaxation after filtration could thus be interpreted as the reflow of the water inside the gel layers. Around

2 h after termination of the filtration, stable thicknesses were recorded. Within 3 min after removal of the filtration pressure, the 0.2 mM $CaCl_2$ gel layers increased 19.6 ± 3.0 %, and those with 1 mM $CaCl_2$ 15.3 ± 1.6 % in thickness. On average, the equilibrium thicknesses (after 2 h) under the applied conditions were determined as 361 ± 3 µm for 0.2 mM $CaCl_2$-gel layers and 274 ± 5 µm for 1 mM $CaCl_2$-gel layers.

2.3.1.3 Composition

The ratios between water, volatile suspended solids and ash content for the gel layers produced with different $CaCl_2$ concentrations are shown in Figure 2-3. With 97.8 ± 0.2 wt%, the water content of the 0.2 mM $CaCl_2$ gel layers was significantly higher than that of the 1 mM $CaCl_2$ gel layers (95.0 ± 0.1 wt%). The ash:VSS ratio appeared very similar for both samples. By combining the observed gel layer thicknesses with the dry mass data, the VSS densities of the gel layers were calculated (examples are shown in Fig. 2-4). The results were 19.0 ± 0.8 mg/cm^3 and 39.6 ± 1.8 mg/cm^3 for the 0.2 mM and 1 mM $CaCl_2$ gel layers, respectively. With the molecular formula $(C_6H_7O_6^-)_n$ this could be estimated as total organic carbon (TOC) content of 8 – 17 mg/cm^3.

In the range where stable alginate gel layers were formed, an increase of $CaCl_2$ concentration caused denser gels. Such correlation has been studied intensively before (Wang and Spencer, 1998; Kuo and Ma, 2001; Davidovich-Pinhas and Bianco-Peled, 2010), and has been explained with a higher number of crosslinks. Similar behaviour has also been observed in biofilms (Körstgens *et al.*, 2001; Goode and Allen, 2011; Safari *et al.*, 2014).

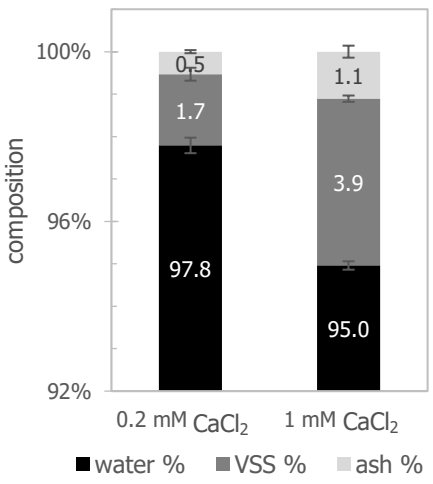

Figure 2-3: Composition (wt%) of the Ca-alginate gel layers in terms of water, VSS and ash. Error bars indicate standard deviations of four samples.

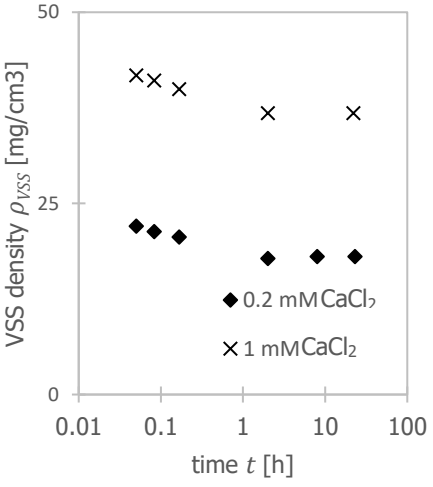

Figure 2-4: Change in densities of the Ca-alginate gel layers' densities after filtration.

In biofilms, also the bacteria are influenced by changing Ca^{2+} availability, and as a result, the composition of EPS can change (Huang and Pinder, 1995; Goode and Allen, 2011; Safari *et al.*, 2014; Gagliano *et al.*, 2020). It is, therefore, more complex to identify the underlying mechanisms of how the biofilms change density. That despite the higher density the layers with more Ca^{2+} exhibited lower cake layer resistance was interpreted as another indication for higher porosity of these samples.

The chosen setup also allowed insight into the binding capacity and specificity of the investigated biomolecules for Ca^{2+} and K^+. Analysis of the ash revealed differences in the ionic composition between the two kinds of gel layers (shown in Table 2-2). Both showed accumulation of Ca^{2+} and K^+ compared to the feed solution. For Ca^{2+}, this phenomenon was stronger developed. Using Equation 2-8, it was found that a simple Donnan equilibrium did not hold for both types of ions. The quotient of the two sides of this equation between Ca^{2+} (LHS) and K^+ (RHS) was calculated as 0.20 ± 0.01 for the gel layers with 1 mM Ca^{2+}, and 0.22 ± 0.01 for those with 0.2 mM Ca^{2+}, indicating a strong specific binding of Ca^{2+} to alginate (or disfavour of K^+). This was in accordance with the known preference of alginate for Ca^{2+}, which is usually explained by the 'egg-box' model (Grant *et al.*, 1973a; Blandino, Macias and Cantero, 1999, see also Figure 1-3). Following this model, the theoretical maximal binding capacity is one Ca^{2+} ion per two alginate monomers (Mancini, Moresi and Rancini, 1999), which corresponds to ca. 2.86 mmol Ca^{2+} per g of alginate. In dialysis experiments, up to 95 % of this theoretical value can be reached (Wang and Spencer, 1998). Assuming that all organic mass detected in the current experiments was present as alginate, the ratio could be calculated by dividing the Ca^{2+} content by the VSS density. The values found for gel layers produced with 0.2 mM and 1 mM Ca^{2+} were 2.00 ± 0.07 mmol/g and 2.98 ± 0.18 mmol/g, respectively. For 1 mM Ca^{2+}, the maximum binding capacity was apparently already reached.

Table 2-2: Inorganic composition of Ca-alginate gel layers, incl. standard deviation over four samples.

feed **elements in layers**	0.2 mM $CaCl_2$ 14.4 mM KCl	1 mM $CaCl_2$ 12 mM KCl
[Ca^{2+}] (µmol/cm^3)	75.5 ± 2.1	234 ± 4
[K^+] (µmol/cm^3)	73.6 ± 2.5	49.1 ± 3.6
ratio Ca^{2+}:K^+ (mol/mol)	1.05 ± 0.04	4.88 ± 0.31
feed ratio Ca^{2+}:K^+	$1.4 \cdot 10^{-2}$	$8.5 \cdot 10^{-2}$

2.3.1.4 Mechanical analyses

Atomic Force Spectroscopy

Atomic force spectroscopy revealed mechanical and structural differences between the gel layers with 0.2 mM $CaCl_2$ and 1 mM $CaCl_2$. Both samples appeared very soft, so that setpoints of 2 nN in case of the softer samples with 0.2 mM $CaCl_2$, and up to 3 nN for those with 1 mM

$CaCl_2$ were applied. The maximum indentation was set to 2.5 µm. Figure 2-5 shows a comparison between representative force-distance curves of two samples. The eventually steeper slope indicated that the samples with 1 mM $CaCl_2$ were overall stiffer than the ones with only 0.2 mM $CaCl_2$ (cf. Eq. 2-9).

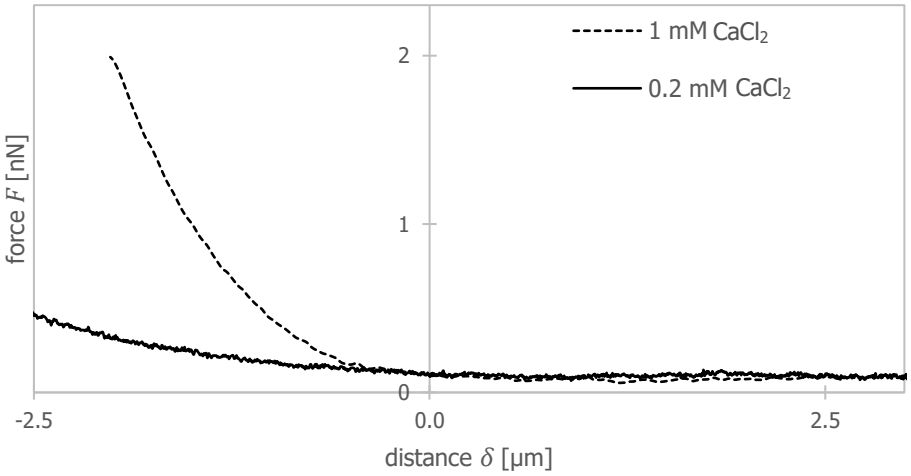

Figure 2-5: Comparison of representative force-distance curves on alginate gel layers for 0.2 mM and 1 mM $CaCl_2$ samples. The x-axis shows the distance between indenter and sample, with 0 representing the contact point.

To obtain mechanical properties of the gel layers from the force-distance curves, one of the models that are commonly used for spherical indenters is the Hertz model. A requirement for application of the Hertz model is that the radius of the contact area should be small in comparison to the indenter's radius, which was in this case 2.5 µm. Therefore, only the data between -1 µm and 1.5 µm distance was considered. The results were Young's moduli of 15.5 ± 5.2 Pa for the gel layers with 0.2 mM $CaCl_2$, and up to 1.2 kPa for those with 1 mM $CaCl_2$ (cf. also Fig. 2-6).

At small indentation depths, the curves in Figure 2-5 did not show big differences, indicating similar elastic moduli. At deeper indentation, especially for the 1 mM gel layers, an increase of the elastic modulus with deeper indentation depth was observed. With indentations in the range of 1 % of the gel layers' total thicknesses, it was assumed that the experiments were performed in the linearly elastic range. An increase in elastic modulus with deeper indentation was therefore interpreted as an indication that the Ca-alginate gel layers were not only laterally, but also in depth inhomogeneous. Inhomogeneity concerning elasticity may be representative for biofilms (Laspidou *et al.*, 2014; Safari *et al.*, 2015) but complicated the identification of molecular interactions.

For the 1 mM $CaCl_2$ samples, a high scattering in Young's moduli was found. The distributions are shown in Figure 2-6. The lowest values were in the same range as the 0.2 mM $CaCl_2$ samples; the majority was found below 200 Pa.

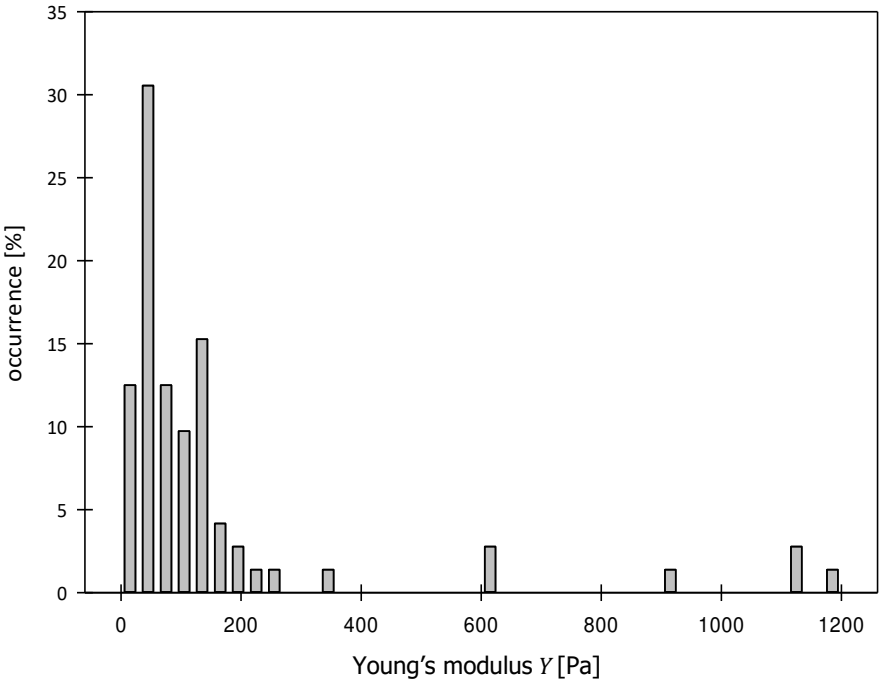

Figure 2-6: Occurrence of Young's moduli (segments of 30 Pa) measured on gel layers prepared from 1 mM $CaCl_2$ alginate solutions at intender's depths between 1 and 1.5 µm. The total number of measurements was 72.

A significant amount of measurements showed maximum values for the Young's modulus up to 1.2 kPa. These maximum values agreed well with measurements on a similar system of alginate gel layers produced with external gelation (Candiello *et al.*, 2013). Spatially, the higher values occurred as clusters on the gel layers, pointing towards lateral inhomogeneity of the gel. This could be caused by a structure of more or less densely packed particles, as already speculated from the filtration data. The relatively high porosity of the 1 mM $CaCl_2$ gel layers caused the indenter to hit one of these particles only seldom directly, which resulted in the measurement of the high Young's moduli. More often, the indenter hit the particles only partially, or even the 'gap' in between, resulting in the relatively high amount of very low Young's moduli determined. It was concluded that despite the apparent macroscopic homogeneity of the gel layers (Fig. 2-2B), the structures were microscopically inhomogeneous. For the purpose of this study, identification of molecular interactions, more homogeneous gel layers would be preferential.

Low-Load Compression Testing (LLCT)

The thicknesses identified by approaching the sample with LLCT were in overall good agreement with the corresponding values determined with the OCT (Tables 2-3 and 2-4). Both methods appeared suitable for this kind of measurements. Representative stress-strain curves recorded during the compression of both kinds of alginate gel layers are shown in Fig. 2-7.

Table 2-3: Comparison of thicknesses from OCT and LLCT measurements for the gel layers prepared with 0.2 mM $CaCl_2$. Standard deviations are for three areas per sample.

	Gel I	Gel II	Gel III	Gel IV
Thickness OCT (µm)	360 ± 4	365 ± 6	357 ± 2	361 ± 3
Thickness LLCT (µm)	363 ± 14	361 ± 6	357 ± 7	361 ± 6

Table 2-4: Comparison of thicknesses from OCT and LLCT measurements for the gels prepared with 1 mM $CaCl_2$. Standard deviations are for three areas per sample.

	Gel I	Gel II	Gel III	Gel IV
Thickness OCT (µm)	278 ± 1	280 ± 2	268 ± 1	272 ± 2
Thickness LLCT (µm)	286 ± 4	279 ± 3	252 ± 6	272 ± 8

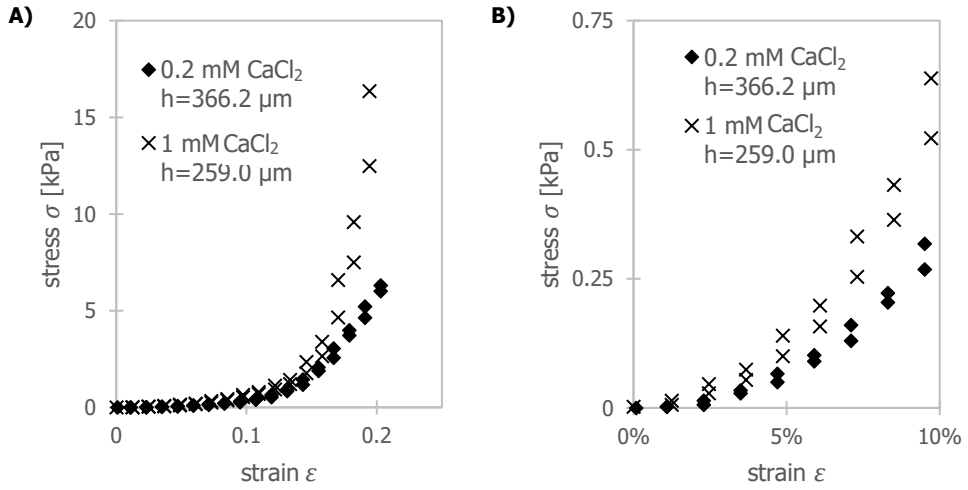

Figure 2-7: Representative compression curves for alginate gel layers with 0.2 mM and 1 mM $CaCl_2$ (A: over the entire range of 20 % strain, B: zoom into the first 10 %).

For biofilms, within the first 10 – 15 % strain a linear correlation between stress and strain has been described by Kühn *et al.*, 2017 and Paramonova *et al.*, 2009. In contrast to that and similar to the force spectroscopy experiments, upward curvature of the curves was observed during compression. As can be seen in Figure 2-7B, the curvature was also pronounced in the small deformation range. In the broad deformation range, the upward curvature could also be an indicator for strain hardening. A possible explanation for such behaviour is that the gel layers were, as explained above, poroelastic. Squeezing of the solvent containing pores

required more force, the higher the compression. Poroelasticity and strain hardening are known for alginate gel layers (Mancini, Moresi and Rancini, 1999), which linear elastic range has been found to be limited to around 6 % strain (Siviello, Greco and Larobina, 2015). The stress-strain curves of this work did not show a linear elastic range. Direct comparison of the curves revealed that for samples with 1 mM $CaCl_2$, the curves showed more stress for a given strain, indicating a higher elastic modulus (cf. Eq. 2-15).

Relaxation behaviour

The relaxation behaviour of the gels under 20 % strain showed apparent differences between different $CaCl_2$ concentrations (Fig. 2-8). The initially high modulus of the 1 mM $CaCl_2$ gel layers dropped very fast; the relaxation reached 59 ± 6 % after 1.0 s. After 100 s, the relaxation could be considered as complete. Gel layers with 0.2 mM $CaCl_2$, on the other hand, relaxed slower and still showed elastic behaviour after 200 s, with 89 ± 2 % relaxation (see Table 2-5). The latter elastic responses were comparable to biofilms after 20 % deformation (Peterson *et al.*, 2012).

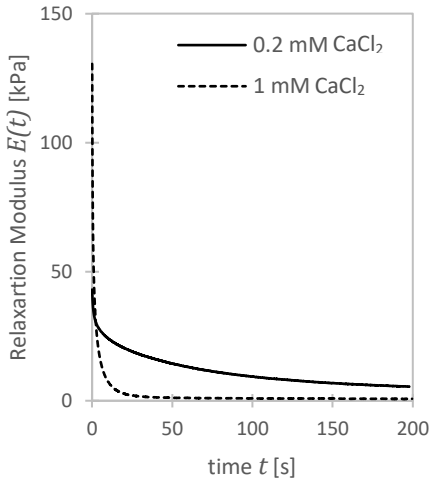

(left:) Figure 2-8: The relaxation modulus of alginate gel layers at 20 % strain as a function of time.

(down:) Table 2-5: The state of relaxation of alginate gel layers at 20 % strain over time. Standard deviation over four samples each.

	Relaxation [%]	
	0.2 mM $CaCl_2$ 14.4 mM KCl	1 mM $CaCl_2$ 12 mM KCl
1 s	22 ± 2	59 ± 6
10 s	45 ± 3	92 ± 3
100 s	80 ± 2	98 ± 1
200 s	89 ± 2	99 ± 1

The behaviour during compression was reflected by the characteristic relaxation times determined with Maxwell fits, which were grouped according to Peterson *et al.*, 2013, and are illustrated in Figure 2-9. For the 1 mM $CaCl_2$ gel layers, fast relaxation processes played a significant role, while there was hardly any longer-lasting elastic behaviour. The 0.2 mM $CaCl_2$ gel layers, in contrast, showed less contribution of fast relaxation processes.

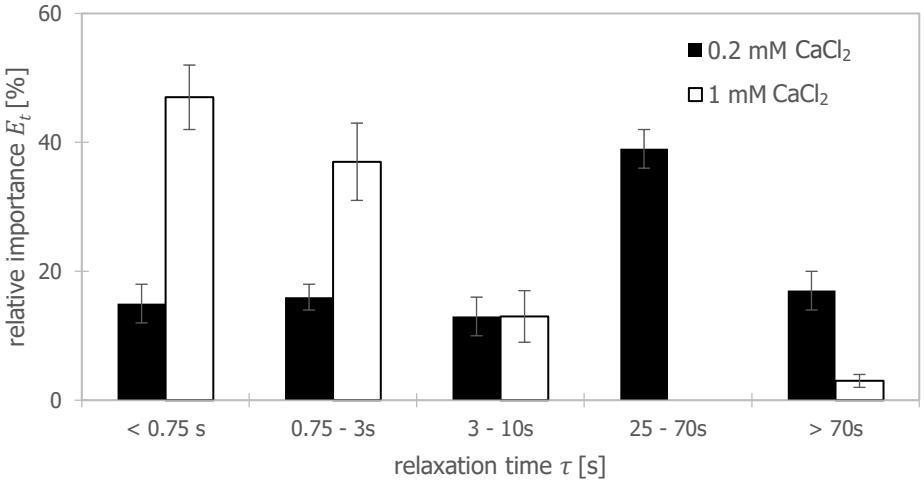

Figure 2-9: Illustration of the relative importance of the different relaxation processes in the two different samples. The error bars indicate the standard deviation obtained from the 12 measurements per concentration.

For the gel layers with 1 mM $CaCl_2$, four elements were enough to describe the relaxation. For the 0.2 mM $CaCl_2$ gel layers, five elements were necessary for satisfying fits. Four of the observed characteristic relaxation times were in the same time ranges for both gel layers, while the fifth one in the range of 1 min relaxation time was unique to the gel layers with 0.2 mM $CaCl_2$. The first three time ranges could be assigned to characteristic relaxation processes identified by Peterson *et al.* (2013) in biofilms, as will be explained later. The most extended time frame was considered as the 'stable' elastic response, exerted by the permanent network of the gel layers.

Since the starting materials for both kinds of gel layers were the same, this left the question open for the nature of the process happening solely in the 0.2 mM Ca gel layers at a relaxation time between 25 and 70 s. One possible explanation was that the network with 1 mM Ca^{2+} was not only stiffer but also more brittle than that with 0.2 mM Ca^{2+}. This observation was also made by Davidovich-Pinhas and Bianco Peled (2010) and would imply that the network structure was already damaged during the 20 % compression. The compression curves (Fig. 2-7) showed, however, no signs for network damage (like a specific change in stress caused by breaking of the structure). A more likely explanation was the assumed formation of Ca-alginate aggregates already in the solutions (see 3.3.1) giving rise to a gel layer structure involving pre-formed particles, which appeared larger and more densely packed for the 1 mM $CaCl_2$ gel layers. The observed relaxation behaviour could indicate that in the case of the 1 mM $CaCl_2$, only a few connections existed between the alginate aggregates so that no lasting continuous network was formed. Reasons for that could be that either the alginate molecules were already bound so densely in the aggregate particles, that there were hardly free binding

spots left, or that because of their shape, there were only a few and small contact points where they could get close enough to interact. Both these limitations for network formation were probably far less pronounced for alginate molecules in smaller, less densely packed 0.2 mM $CaCl_2$ colloids. The exhibition of a longer-term elastic response of the latter (Fig. 2-9), was interpreted as an indication for a continuous alginate network.

Based on the work of Peterson *et al.*, 2013, the five characteristic time ranges observed for both samples in this work were interpreted as resulting from the following relaxation processes:

- < 0.75 s: the flux of free water through/out of the gel layers
- 0.75 – 3 s: the flux of water that was associated with polymer molecules
- 3 – 10 s: unbound alginate molecules moving through the gel layer
- 25 – 70 s: the elastic response of the crosslinked alginate network, inter-particle
- > 70 s: the elastic response of the crosslinked alginate network, intra-particle

Containing microbes, EPS networks, channels and pores, biofilms have been described as a very heterogeneous structure (van Loosdrecht *et al.*, 1995). Their density can vary up to an order of magnitude between the shallower top-layers and denser bases (Zhang and Bishop, 1994; Laspidou and Rittmann, 2004), but also in the lateral direction vast differences have been described (Galy *et al.*, 2012). These lateral fluctuations in the structure are not necessarily caused by the EPS matrix, though. In this respect, it should be noted that the packed aggregates of Ca-alginate that were apparently present in the 1 mM $CaCl_2$ alginate gel layers were less representative for the biofilm matrix and not favourable for the identification of molecular interactions. To obtain more continuous networks, development of such big and dense aggregates of Ca-alginate should be prevented. This worked apparently to a reasonable degree for the lower $CaCl_2$ concentration of 0.2 mM. To completely avoid it, a reduced gelling speed is favourable, for example by controlled release of Ca^{2+} as applied in internal gelation techniques, or by a two-step procedure with initial deposition of alginate on a membrane and subsequent diffusion of Ca^{2+}.

2.3.2 ALE gel layers

2.3.2.1 ALE characterisation

The formation of weak but stable Ca-ALE aggregates was observed when a pH-neutral ALE solution was dripped into a 2.5 % $CaCl_2$ solution. An example is shown in Figure 2-10. It was therefore expected that the gel layers prepared by filtration also contain Ca-ALE.

Analysis of the composition of the ALE extract showed that the frozen starting material contained 90.6 ± 0.6 % water. Organic mass (*VSS*) accounted for 89.3 ± 1.0 % of the dry mass; the remaining part was found to be ash. An overview of the ions found in the ash by ICP-OES is shown in Table 2-6. Except for sodium, which had been provided during the extraction, also significant amounts of potassium, cobalt and sulphur were identified, as well as traces of boron. Since chloride and carbonate were added during the extraction process, also substantial quantities of these ions could be expected.

Figure 2-10: Aggregates of Ca-ALE, after ALE was dropwise added to a $CaCl_2$-containing solution.

Table 2-6: Ionic composition of the ash of the ALE extract, incl. standard deviation over two measurements

Ion	**mg/g VSS**
Sodium	54.5 ± 3.4
Potassium	27.6 ± 16.0
Cobalt	27.9 ± 4.0
Sulphur	11.9 ± 0.7
Boron	4.2 ± 0.1

The ratio of organic carbon (detected with TOC) to organic matter (as determined with TSS/VSS measurements) was 1.01 ± 0.05 mg C/mg VSS. Further differentiation of the TOC revealed that only about 34 % of the total organic carbon could be classified as non-purgeable (NPOC), indicating that the remainder contained volatile organics such as volatile fatty acids (VFAs), short hydrocarbons or carbonate. The poor compliance between the results for TOC and VSS was explained by evaporation of a part of the volatile fractions during VSS/TSS determination. It was assumed that these fractions slowly evaporated during the measurements as well, and thus did not play a crucial role in the remaining ALE layers. For the analysis of the experiments, only the measured VSS was therefore considered as ALE. A mass balance of the filtrations based on TOC measurements was not possible.

Analysis with LC-OCD showed that 28.5 ± 0.7 % of the carbon was composed of polymers with a broad mass distribution between 50 and 1,300 kDa. ALE has often been compared to alginate because of its gelling behaviour with metal ions (Lin *et al.*, 2008). However, the presence of organic nitrogen and sulphur in the ALE extract in combination with the extensive range of molecular masses and the accumulation of low molecular mass components allowed for a distinctive difference with alginates in chemical binding behaviour.

2.3.2.2 Properties of ALE gel layers

ALE deposition was observed in all experiments. The fouling potential of the tested solutions was found to be in the same range as that of the alginate solutions (cf. Fig. 2-1). The differences between the different $CaCl_2$ concentrations were less pronounced than for alginate, but the cake layer resistance increased with $CaCl_2$ (Fig. 2-11). The rather linear relationship between reverse flux and the filtered volume indicated that also the ALE gel layers with $CaCl_2$ obeyed the cake filtration theory (Eq. 2-19).

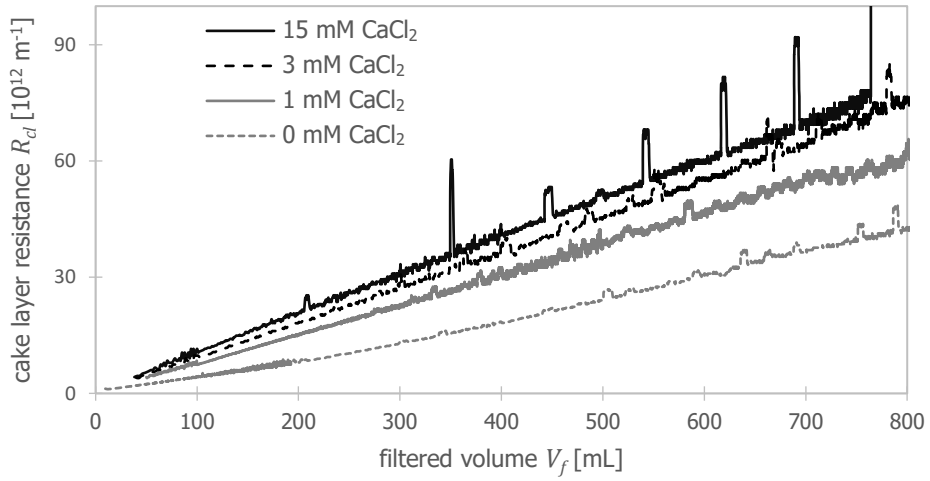

Figure 2-11: Progression of the filtration resistance during filtration of 60 mg/L ALE solutions containing different amounts of $CaCl_2$ and KCl, at a fixed ionic strength of 45 mM.

The specific cake layer resistances, shown in Table 2-7, revealed little variance between the different compositions and were in the same range as the Ca-alginate layers with 1 mM $CaCl_2$. Only in the experiment without addition of $CaCl_2$, the specific and total cake layer resistance was lower than for the rest, which could indicate less crosslinking. The values were still significantly higher than reported for biofilms that were grown on membranes (Derlon *et al.*, 2016). Reasons for those differences could be the higher density of the present gel layers (cf. discussion below), or the lack of heterogenising elements like bacterial cells or other aggregates. It has been found that the presence of inorganic particles in biofilms enhances permeability, the bigger the particles, the lower the resistance (Chomiak *et al.*, 2014). A similar impact of bacterial cells seemed possible.

Table 2-7: Specific cake layer resistances α_m calculated for gel layers after filtration of 750 ml feed solution with 60 mg/L ALE and 45 mM ionic strength. Errors indicate the standard deviation of two runs.

$CaCl_2$ in feed [mM]	0 mM	1 mM	3 mM	15 mM
α_m [10^{16} m/kg VSS]	0.82 ± 0.03	1.00 ± 0.04	1.00 ± 0.01	1.07 ± 0.11

Directly after the filtration, OCT revealed smooth, well-defined layers between 100 µm and 150 µm height. In contrast to alginate, the ALE gel layers adhered to the membrane without the need for an extra adhesive layer, as long as $CaCl_2$ was added. This was the first indication of the differences between alginate and ALE. For biofilms grown on membranes in the lab-scale units, the heights were in the lower range but could be considered as representative (Dreszer *et al.*, 2013; Desmond *et al.*, 2018). While with the current setup the possibilities for increasing the gel layers' thickness might be limited by the flux decline, it could be easily decreased to reach also the lower values between 10 µm and 100 µm, as reported for nanofiltration and reverse osmosis membranes in real installations (Vrouwenvelder *et al.*, 2008). The systems chosen thus allowed the preparation of gel layers of the dimension of biofilms, so that (mechanical) analyses can be performed in the same manner and results can be compared.

Similar to the alginate gel layers, $CaCl_2$ was necessary for the formation of stable gel layers with ALE, which was in accordance with the literature (Lin *et al.*, 2010; Lin, Sharma and van Loosdrecht, 2013). A crucial effect that the presence and concentration of Ca^{2+} can have on the structure of biofilms, like for example from *P. aeruginosa*, has been shown before as well (Körstgens *et al.*, 2001; Safari *et al.*, 2014). Without $CaCl_2$, cake layers were initially formed, though they started disconnecting from the membrane as soon as the filtration was finished. Subsequently, the gel layers disintegrated quickly into small pieces. This disintegration process of ALE gel layers without $CaCl_2$ appeared to be independent of ALE concentration and ionic strength. This supported the former assumption of missing crosslinks due to lack of Ca^{2+}. An example is shown in Figure 2-12.

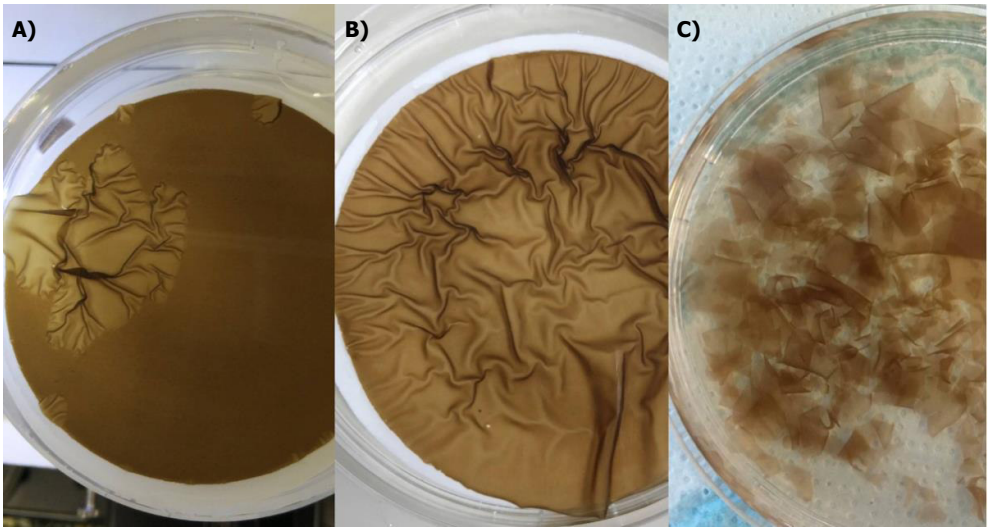

Figure 2-12: ALE gel layer on an ultrafiltration membrane, prepared with 120 mg/L ALE and 24 mM KCl but no $CaCl_2$ in the feed solutions. (A) 2 min after filtration has finished and pressure has been relieved; (B) 20 min after filtration; (C) 24 h after filtration.

The structure of the ALE gel layers appeared less constant over time than that of alginate. Figure 2-13 shows the structure recorded by OCT of 30 min, 3 d old and 5 d old gel layers with 60 mg/L ALE, 45 mM ionic strength and 1, 3 and 15 mM $CaCl_2$. While initially, all layers appeared very similar under the OCT, after 5 d of storage in the respective solutions, they showed obvious differences in structure. The gel layer without any added $CaCl_2$ had disappeared at this time (cf. Figure 2-12), the other three gel layers showed different stages of filamentation.

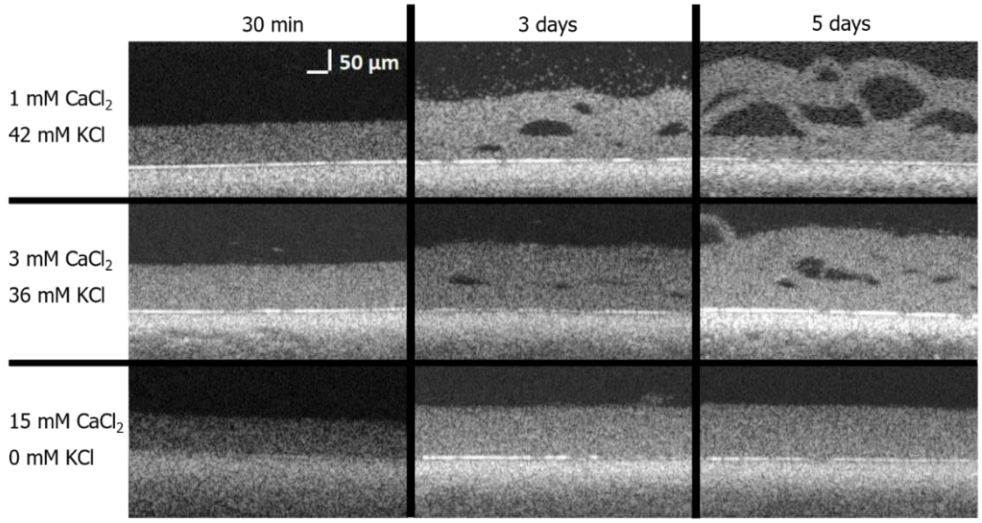

Figure 2-13: OCT images of gel layers with 60 mg/L ALE and (A) 1 mM $CaCl_2$, (B) 3 mM $CaCl_2$ and (C) 15 mM $CaCl_2$ after 5 d of storage.

The used OCT system had a resolution in the range of 10 µm (Dreszer *et al.*, 2014), meaning that pores could only be detected as soon as they reached this size in both dimensions. Based on the progression that could be observed over time, it was concluded that the development of microscopic voids happened before they became first apparent in OCT imaging. As a result, like the alginate gel layers also the ALE gel layers were probably microscopically not as homogeneous as suggested by OCT. Obviously, in the fibres, there was a higher VSS density than in the pores in between. Increasing the resolution, for example, by taking SEM pictures on stabilised samples, may reveal such changes on the microstructure level.
The macroscopic fibres that developed over time hinted towards a slow rearrangement of the ALE molecules. Fibrous structures have also been observed in biofilm matrices (Romero *et al.*, 2010; McCrate *et al.*, 2013; Song *et al.*, 2014; Lin *et al.*, 2015), and are usually attributed to amyloids. In accordance with previous work (Lin *et al.*, 2018) this finding suggested that also ALE can form some kind of fibres.

Within 3 d, the thickness of the layers increased between 30 % and 60 %, depending on the ion composition of the feed solution. The resulting densities and their change over time are

illustrated in Figure 2-14, as determined from the VSS content and the thickness measured by OCT. While there were only little differences between 1 mM $CaCl_2$ and 3 mM $CaCl_2$, the higher concentration of 15 mM led to denser gels and appeared to diminish the swelling. Nevertheless, for all observed films, the swelling continued over more than two weeks (data not shown). It was therefore considered unlikely that this behaviour was caused by simple uptake of water in the poroelastic gel network after relieving the filtration pressure (cf. Fig. 2-4). The filamentation (see Fig. 2-13), observed primarily in samples with low $CaCl_2$ concentration, pointed instead to slow internal rearrangements of the polymer network.

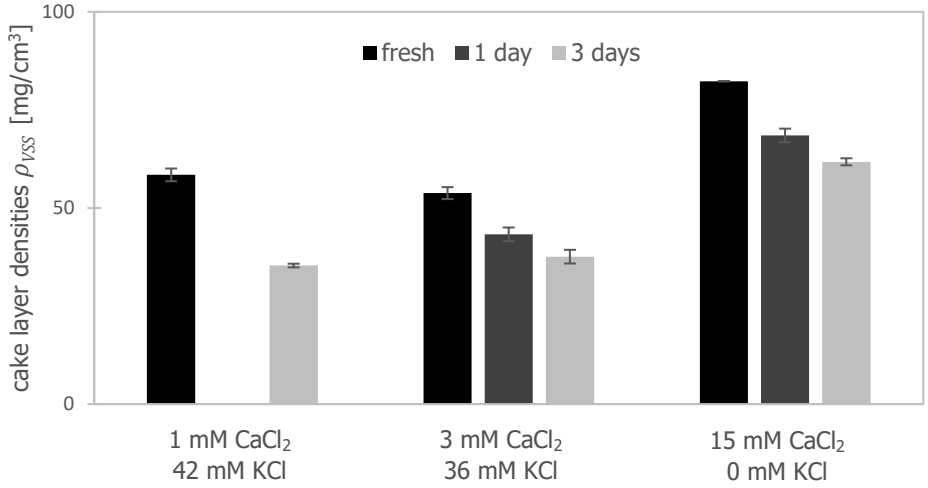

Figure 2-14: Densities of several ALE gel layers (60 mg/L ALE) produced with 45 mM ionic strength right after filtration and monitored over time. The error bars indicate the standard deviation between two samples of each concentration.

The molecular formula for ALE was not known, but its TOC content has been estimated to be between 40 wt% and 50 wt% (Kleikamp, 2017). Using this estimation, the observed 30 - 80 mg VSS/cm^3 corresponded to 15 - 40 g/L TOC content, about twice as much as found for the alginate gel layers. For lab-grown biofilms on membranes, values between 1 and 10 g/L TOC have been reported (Vrouwenvelder *et al.*, 2008; Dreszer *et al.*, 2013; Derlon *et al.*, 2016; Desmond *et al.*, 2018). Real installation biofilms are difficult to analyse for their density because they tend to grow in edges rather than on flat sheets (Vrouwenvelder *et al.*, 2010). Values for dense areas in biofilms have been reported as high as 60-130 g/L (Zhang and Bishop, 1994). The gel layers produced in this study were, therefore, found in a representative range of density for biofilms.

Since right after filtration OCT provided macroscopic uniform pictures, no direct information on porosity was available. For biofilms, a positive correlation between Ca^{2+} and porosity has been described (Safari *et al.*, 2014). On a microscopic scale, the same correlation might be valid for ALE as well. As mentioned before, the heterogeneity of the layers can have a

significant impact on the hydraulic resistance of membrane biofilms. In future research, it can be addressed with the addition of relatively big components such as bacterial cells.

Because the aim of this work was producing stable, uniform gel layers, the composition was adapted to 120 mg/L ALE and ionic strength of 24 mM. Gel layers produced with this new composition showed no filamentation in OCT for over 2 weeks, but the same swelling behaviour as described before (cf. Ch. 3). The ion accumulation was analysed based on those new gel layers. Like for alginate, an accumulation of Ca^{2+} and K^+ in the gel layers was observed. The values are reported in Table 2-8. Comparing the ratios between Ca^{2+} and K^+ in the feed solutions with those in the gels, it was concluded that again the accumulation was stronger for Ca^{2+} than for K^+.

Table 2-8: Inorganic composition of Ca^{2+}-ALE gels. Errors show the standard deviation over two samples.

Feed **elements in layers**	3 mM $CaCl_2$ 15 mM KCl	6 mM $CaCl_2$ 6 mM KCl
$[Ca^{2+}]$ (µmol/cm^3)	35.5 ± 2.0	40.9 ± 0.4
$[K^+]$ (µmol/cm^3)	33.5 ± 3.5	25.4 ± 7.6
ratio Ca^{2+}:K^+ (mol/mol)	1.05 ± 0.17	1.61 ± 0.49
Feed ratio Ca^{2+}:K^+	0.2	1

Comparison to Table 2-2 revealed that, although the VSS density in the ALE gel layers was higher than in the alginate gel layers, the ion concentration was lower for both, Ca^{2+} and K^+. This indicated a smaller ion binding disposition of the ALE extract compared to the alginate.
Using Equation 2-8, it was investigated whether a Donnan equilibrium between the ALE gel and the solution was established for the two ions. As before, the quotient of the two sides of this equation was calculated for the duplets of the two analysed compositions with 3 mM $CaCl_2$/15 mM KCl and 6 mM $CaCl_2$/6 mM KCl, resulting in values of 0.6 ± 0.1 and 1.8 ± 0.5, respectively. This shows a rather high variance, which was amongst others caused by the small number of samples. Nevertheless, the quotient is closer to 1 than in case of the alginate. With 378 ± 8 µmol/g and 505 ± 44 µmol/g bound Ca^{2+}/ALE (for feed solutions with 3 mM $CaCl_2$/15 mM KCl and 6 mM $CaCl_2$/6 mM KCl, respectively) the binding capacities were also found to be an order of magnitude smaller than for alginate. The observed high specificity of alginate for the binding of Ca^{2+} was not found for ALE. This was not surprising, having in mind the much more complex composition of ALE, containing many more types of molecules and thus many other functional groups next to carboxylic groups than the Ca^{2+}-binding-optimised commercial alginate (Felz, Neu, *et al.*, 2020). From the obtained data, it could not yet be decisively concluded if the ions in the ALE gel layers distributed according to a Donnan equilibrium or not, but it appeared possible. A more systematic approach to this topic could provide further valuable insight into the molecular interactions within ALE gel layers. With the experimental procedure applied in this work, it will be further possible to quantify this

relationship in terms of binding capacities. Extension of the experiments to other critical structural components of biofilm EPS, for example, proteins, will allow gaining knowledge about their binding behaviour as well.

In force spectroscopy measurements, 5 d old ALE gel layers with 60 mg/L ALE showed, despite their inhomogeneity, a much more linear elastic behaviour than the alginate gel layers, with only minimal differences between 0.5 µm, 1.0 µm and 1.5 µm indentation. A representative force-distance curve is shown in Figure 2-15.

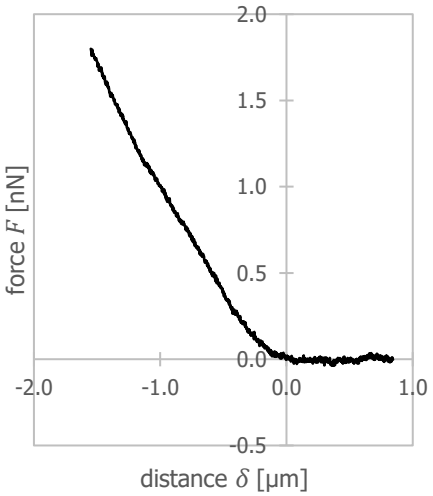

Figure 2-15: Force-distance curve measured on an ALE gel layer made with 60 mg/L ALE and 1 mM $CaCl_2$.

The rather constant slope of the curve (in contrast to Fig. 2-5) indicated that at least the top layers were homogenous. Young's moduli between 150 Pa and 500 Pa were measured for ALE gels with 1, 3 and 15 mM $CaCl_2$. With two gel layers of each composition and 17 force-distance measurements at different spots, no correlation with $CaCl_2$ concentration could be observed, but vast differences between samples with the same composition.

The magnitude of the observed Young's moduli was in good agreement with the values of an assumedly cell-free top EPS-layer detected by Safari *et al.*, 2014, and with those predicted by Laspidou *et al.*, 2014. It was therefore assumed that ALE gel layers provided a reasonable mechanical model for EPS. These experiments were not further continued because the ALE gel layers were not stable during these experiments, and over time still structural changes were observed. Before reliable mechanical measurements can be performed on these kinds of gel layers, firstly, the spatial homogeneity and the ripening process need to be investigated further. The ripening behaviour was an interesting aspect by itself and worth further investigation, including the question of what effect the addition of more components has on it. Once the ripening behaviour is understood, also for the ALE gel layers the compression and relaxation behaviour measured by LLCT can provide useful insights into the molecular interactions in deeper layers. Beyond such uniaxial compression measurements, the application

of shear stress and the interpretation of the gel layers' responses will complete the picture. Shear can, for example, be applied externally with the help of a rheometer (Patsios *et al.*, 2015) or, in a more natural environment, by a water flux (Picioreanu *et al.*, 2018).

2.4 Conclusions

By using a dead-end filtration setup, simple hydrogel gel layers with alginate and ALE were produced on membrane supports. In terms of thickness and density, they well resembled biofilms. The gel layers were a useful tool to study the binding capacity between the added components, i.e. the biopolymers and Ca^{2+} ions. For the studied systems, more available $CaCl_2$ correlated with more Ca^{2+} in the gel layers. Based on a Donnan equilibrium analysis, it was shown that specific interactions (i.e. other than electrostatic interactions) with Ca^{2+} were much less pronounced for the ALE than for alginate. More systematic experiments and the addition of further biofilm components are expected to provide new insights into the correlation between composition, structure and mechanical properties of biofilms.

Increasing the $CaCl_2$ concentration of the feed solution resulted in higher densities of the gel layers. Depending on this concentration, alginate aggregates could already form in the feed solution, resulting in a gel structure of not-so-well interconnected aggregates. Such gel layers were less representative for biofilms, structure-wise as well as concerning their relaxation (swelling) behaviour. The properties were shifted towards a more homogeneously crosslinked network with decreasing $CaCl_2$ concentrations. ALE gel layers, on the other hand, showed swelling and developed fibrous structures over time. This ripening process could be influenced by a change in the ionic composition. A more systematic approach can provide information on the role of ions and especially Ca^{2+} in the binding of ALE.

An important conclusion is the prominent role of the porosity of the gel layers in their hydrodynamic resistance. $CaCl_2$ appeared to increase the density of the gel layers, but in the case of the alginate gel layers at the same time also increased the porosity. In extreme cases, this meant a decrease in specific cake resistance of alginate gel layers, although the overall density increased. For the ALE layers, in contrast, a higher density hardly affected the specific cake layer resistance.

The alginate gel layers produced in this work were suitable for the determination of their Young's modulus using indentation on a microscale and compression on a macroscale. In principle, this also applied for the ALE gel layers, but mechanical measurements were yet impeded by the long-term ripening process of these layers.

Acknowledgements

We thank the Department of Biomedical Engineering at the UMCG and dr. P.K. Sharma for the provision of the instrument as well as their insights and useful suggestions concerning the LLCT. Royal HaskoningDHV and the Waterboard NoorderzijlvesT is thanked for supplying us with Nereda® sludge.

Chapter 3

Formation and ripening of alginate-like exopolymer cake layers during and after membrane filtration

Biofilms are formed by bacteria embedded in complex hydrogels. Their behaviour is determined by the multiple interactions between the constituents and with the surrounding environment. To identify the role of single components to biofilm properties, simplifications are necessary. In this work, the role of bacterial alginate-like exopolymers (ALEs) in the formation and ripening of gel layers were examined as a function of $CaCl_2$ and KCl concentration. Hereto ALE model gel layers were formed on membranes by dead-end filtration of ALE solutions containing the ions of interest. Accumulation of the cations Ca^{2+} and K^{+} in the gel layers could be well predicted by a Donnan equilibrium model based on the fixed negative charges in the ALE. This suggests that there was no specific binding of Ca^{2+} to the ALE and that on the time scale of the experiments, the Ca^{2+} ions could distribute freely over gels and surrounding solutions. From the Donnan equilibrium, the concentration of fixed negative charges in the ALE was estimated around 1 mmol/g VSS (volatile suspended solids, organic mass). Also accumulation of H^{+} was predicted. After initial fast relaxation from the pressure during filtration, a long term and slow increase in thickness were observed for the gel layers, depending on the $CaCl_2$ concentration of the supernatant. Gels with more $CaCl_2$ in the supernatant swelled less and bore a higher osmotic pressure than those with less $CaCl_2$, revealing the role of Ca^{2+} ions in the network crosslinking. It is hypothesised that this mechanism later transitions into a rearrangement of the ALE molecules, which eventually leads to a fibrous network structure with large voids.

3.1 Introduction

Biofilms have been a topic of investigation for almost half a century because of considerable negative industrial (Flemming, 2002; Meyer, 2003) and medical (Donlan, 2001; Bryers, 2008) impact. In reference to the adverse side effects of biofilms, the term 'biofouling' is used. The focus of investigations in this field is often on prevention or removal.
Regarding the structural elements of biofilms, one can distinguish between the bacteria, who produce and inhabit the film, and the polymeric matrix (Geesey, 1982; Flemming, 2016), often also referred to as extracellular polymeric substances (EPS). The latter has been found to consist of complex mixtures of biopolymers, such as polysaccharides and proteins, complemented by lipids, humic substances and eDNA (Lin *et al.*, 2014; Hobley *et al.*, 2015; Flemming, 2016).

The EPS matrix has been described as a physically crosslinked hydrogel (Mayer *et al.*, 1999; Seviour *et al.*, 2009; Wilking *et al.*, 2011; Galy *et al.*, 2012; Dreszer *et al.*, 2013; Lin, Sharma and van Loosdrecht, 2013), about its ability to incorporate up to 99 % water while providing a lasting polymeric network structure (Mayer *et al.*, 1999; Wingender and Flemming, 2004). In contrast to chemically crosslinked networks, the crosslinks in physically linked networks are provided by non-covalent interactions, in particular electrostatic interactions, hydrophobic interactions, H-bonding and van-der-Waals forces, and entanglement. As such, they are reversible. Essential parameters of hydrogels are their degree of crosslinking, their interaction with counter-ions, and their hydrophilicity (Ganji, Vasheghani-Farahani and Vasheghani-Farahani, 2010). The interplay of forces following from these parameters determines the state of swelling of the hydrogel under steady-state conditions (Bajpai, 2001) as well as their potential for water storage (Ganji, Vasheghani-Farahani and Vasheghani-Farahani, 2010). The swelling state has been identified as a crucial parameter with regards to adhesion, mechanical strength, permeability and degradation behaviour of hydrogels (Davidovich-Pinhas and Bianco-Peled, 2010). These properties have also been used to characterize biofilms: adhesion and mechanical strength have been correlated with fouling potential (Li and Elimelech, 2004; Lee and Elimelech, 2006; Villacorte *et al.*, 2017) and success of cleaning strategies (Ang, Lee and Elimelech, 2006; Möhle *et al.*, 2007; Powell *et al.*, 2013; Safari *et al.*, 2015). It strikes, therefore, that the number of studies about swelling of biofilms and EPS is minor so far. Changes in swelling behaviour of EPS have been described as a function of pH for EPS extracted from activated sludge (Frølund *et al.*, 1996), as well as for EPS extracted from different bacterial cultures (Dogsa *et al.*, 2005; Radchenkova *et al.*, 2018). Keiding concluded that the swelling properties of EPS depend significantly on the concentration and valence of ions in solution (Keiding, Wybrandt and Nielsen, 2001). For intact biofilms, an increase in NaCl has been found to decrease swelling, while pH only exerted a mellowing effect when it is rather

basic (Seviour *et al.*, 2009). Still, because of the high complexity of biofilms and EPS (Seviour *et al.*, 2019), there is so far no proper understanding of the interactions with ions.
A significant difference compared to the well-investigated artificial hydrogels is the high complexity of biofilms. Not only the chemical composition of the EPS varies depending on the producing bacteria, environmental conditions and maturity of the film, but also the physical structure of biofilms is very heterogeneous (Wimpenny, Manz and Szewzyk, 2000; Sutherland, 2001) and depending on external influences (van Loosdrecht, 1997). Because of the complex interrelations between composition, structure and function, it has been proposed to distinguish between structural molecules of the EPS, such as alginate-like exopolymers (ALE), and molecules with non-structural function (Felz *et al.*, 2016).

To understand the molecular interactions and allocate functions to molecules or functional groups, simplification of the EPS matrix is necessary. One material that has been used as a model for biofilm EPS is alginate extracted from brown algae (Wloka *et al.*, 2004; Ang, Lee and Elimelech, 2006; Katsoufidou, Yiantsios and Karabelas, 2007; Li, Xu and Pinnau, 2007; van den Brink *et al.*, 2009; Meng, Winters and Liu, 2015). Alginate is generally described as block copolymers of (1,4)-linked β-D-mannuronic and α-L-guluronic acid (Lee and Mooney, 2012). Characteristic is its crosslinking and gel formation in the presence of Ca^{2+} ions. Despite its apparent oversimplification of the biofilm system, alginate provides two benefits for biofilm researchers. Firstly, it is a common material to produce hydrogels, e.g., in medicine (Augst, Kong and Mooney, 2006; Lee and Mooney, 2012), and is therefore well-characterized (Davidovich-Pinhas and Bianco-Peled, 2010; Fu *et al.*, 2011; Hermansson *et al.*, 2016). Secondly, it shares some properties with alginate-like exopolymers (ALE), which have been identified as a crucial structural EPS component (Lin, Sharma and van Loosdrecht, 2013). One shared property of alginate and ALE is the observed gel-formation with Ca^{2+} (Lin *et al.*, 2008; Felz *et al.*, 2016), which was the focus this work. While a full chemical analysis of ALE is still pending, it was used as the linking intermediate between the very simplified alginate-model and the full complexity of a real biofilm.
This work aimed to use a system so simplified that conclusions concerning the molecular interactions between components could be drawn, yet a system as representative for biofilms as possible. Based on previous work (Ch. 2), model gel layers of Ca-ALE produced on membranes in dead-end filtration mode were chosen for this purpose. They were prepared in the presence of varying concentrations of $CaCl_2$ and KCl. From the swelling behaviour of the Ca-ALE layers, observed for 12 d, conclusions were drawn on the behaviour of ALE in the network-formation of EPS, with a particular focus on the interaction with Ca^{2+} and other ions. The composition (density, ions) and cake-layer resistances of the gel layers were correlated to the availability of Ca^{2+} and K^{+}, the ionic strength of the solutions. The results were analysed with a simple model based on the Donnan potential.

3.2 Materials and Methods

3.2.1 ALE extraction and characterisation

The alginate-like exopolymers used in this study were extracted from Nereda® sludge, which was collected from the wastewater treatment plant in Garmerwolde, the Netherlands (Pronk *et al.*, 2015). A combination of sodium carbonate, sonication and high temperature was used for extraction, following procedures described by Felz et al. (Felz *et al.*, 2016).
Granules were collected by decanting. About 150 g of the wet granules (20 g dry weight) were mixed with 1 L demineralised water and 10 g Na_2CO_3 (VWR, the Netherlands), to obtain a 1 % (m/v) carbonate solution. The mixture was homogenised with a Branson Sonifier 250 for 5 min at 70 % (of 200 W) in pulsed mode. Heating up of the solution was prevented using an ice bath. The mixture was then heated to 80 °C and vigorously stirred for 30 min. After centrifugation (Allegra X-12R Centrifuge, Beckman Coulter, 20 min, 3750 rpm), the supernatant was acidified with 1 M hydrochloric acid (Merck Millipore, Germany) to a final pH 2 - 2.5. The solution was centrifuged again (20 min, 3750 rpm), and the pellet was kept and stored at -80 °C until further use. It is henceforth referred to as ALE extract.

Directly after extraction, the ALE extract was tested for its gel-forming ability with $CaCl_2$ (Lin *et al.*, 2010). The acidic pellet was dissolved and neutralised with 1 M NaOH (Merck Millipore, Germany). Drops of the neutral ALE were then dripped into a 2.5 % (m/v) $CaCl_2$ solution. Gelling was considered successful if gel beads could be observed forming in the solution, rather than dissolving of the drops.
The dry mass (total suspended solids, TSS) and organic mass (represented by the volatile suspended solids, VSS) of the ALE extract were determined. In triplicate, samples were weighed out into dry porcelain crucibles (m_{sample}). Those were heated to 105 °C for 24 h. Afterwards, the dry sample weight was determined. Subsequently, the samples were heated to 550 °C for 2 h, and the mass of the remaining ash was measured (m_{ash}) Eventually, the water content (m_{water}) and the organic mass (VSS) were calculated according to

$$m_{water} = m_{sample} - TSS \quad (3\text{-}1)$$

$$VSS = TSS - m_{ash} \quad (3\text{-}2)$$

For elemental analyses, the ALE material was neutralised and converted into the (soluble) Na-ALE form using 1 M NaOH (Merck Millipore, Germany), and subsequently diluted with demineralized water to the required concentrations. Total carbon (TC), total organic carbon (TOC) and inorganic carbon (IC) were measured with a TOC analyser (Shimadzu TOC-L). Inductively coupled plasma optical emission spectroscopy (ICP-OES, Perkin Elmer, type Optima 5300 DV) was applied for identification of the ionic composition.

3.2.2 Model gel layer production

In previous experiments (Ch. 2) it has been found that 120 mg/L ALE in the feed solutions was a suitable concentration. This was used for all experiments in this work unless mentioned otherwise.

Because Ca^{2+} availability has been identified as an essential factor for biofilm stability (Körstgens *et al.*, 2001; Li and Elimelech, 2004; Wloka *et al.*, 2004) and has been shown to induce crosslinking of the chosen model component ALE (Lin *et al.*, 2010; Felz *et al.*, 2016), the effect of variations in its concentration was investigated in this study. Based on the behaviour that has been described for the structurally similar Ca-alginate gels caused by monovalent ions (Wang and Spencer, 1998) and ionic strength (van de Ven *et al.*, 2008; van den Brink *et al.*, 2009), KCl was chosen as a second ionic component. An overview of the tested combinations can be found in Table 3-1.

For a total volume of 2 L feed solution, 2.87 g of the frozen ALE (corresponding to a final VSS concentration around 120 mg/L) were neutralized with 0.1 M NaOH (Merck Millipore, Germany) and dissolved in ca. 1 L demineralized water by stirring and slight heating up to ca. 40 °C for 1 h. In a parallel vessel, the required amounts of $CaCl_2 \times 2H_2O$ (VWR, the Netherlands) and KCl (VWR, Belgium) were dissolved in ca. 500 mL demineralised water. The salt solution was added slowly and under stirring to the ALE solution, and the mixture was filled up to the final volume of 2 L. The ionic composition of the solution was determined with ion chromatography (IC, Metrohm Compact IC 761). Due to partially uneven distribution in the frozen ALE pellet, the final VSS concentration varied slightly. Additionally, 500 mL of storage solutions were prepared for each experiment, with the same composition of $CaCl_2$ and KCl as the corresponding feed solutions.

Gel layers were prepared by pressure-driven dead-end filtration of the feed solution through ultrafiltration membranes (UP150, polyethersulfone (PES), 150 kDa cut-off, Microdyn Nadir, Wiesbaden, Germany). Between experiments, the cells and tubing were cleaned with 1 % NaOCl and subsequently rinsed with demineralised water. The membranes were cut into circles with a diameter of 7.5 cm and immersed in demineralised water for 1 h. Afterwards, they were mounted at the bottom of 450 mL stainless steel dead-end filtration cells. To increase the feed volume capacity, the cells were by twos connected to a 10 L pressure vessel, by which the content of each vessel was split over two cells.

Initially, for all membranes, the clean water flux was determined by filtration of 750 mL of demineralised water at 1 bar. Then, 2 L of the ALE feed solution were added to the pressure vessel and filtered through the two membranes, until 600 mL were filtered through each cell. Filtration took between 18 and 20 h. The membranes with the model films were removed from the filtration cells and stored at 4 °C in Petri dishes with the corresponding storage solutions. During filtrations, the feed pressure was set to 1 ± 0.1 bar. To avoid inaccurate results based on fluctuations in the air pressure system, the actual pressure (p_a) was recorded alongside the

mass of the filtered solution (m_f). To allow uniform gel layer formation, no stirring was applied in the dead-end cells. All experiments were done at room temperature, which was found to be stable at 23.9 ± 0.7 °C. The density of water was approximated as ρ_{H2O} = 1 g/mL for the course of the experiments, to translate the logged data of filtered mass of water m_f at time t to the filtered volume of water V_f. The water flux J at time t through the active membrane area A_m (38.5 cm^2) was calculated using Equation 3-3.

$$J(t) = \frac{V_f(t + \Delta t) - V_f(t)}{A_m \cdot \Delta t} \qquad (3\text{-}3)$$

The time difference Δt was chosen depending on the flux. For the clean water flux, it was usually set to 10 s, for the later stages of the filtration it was increased to up to 5 min.

The transmembrane pressure (TMP) was approximated with the logged applied pressure p_a. The total filtration resistance R_f was calculated according to Equation 3-4, using the dynamic viscosity of water at 24 °C, 0.91 mPa·s (Paar, 2008) for η_{H2O}.

$$R_f(t) = \frac{p_a}{\eta_{H2O} \cdot J(t)} \qquad (3\text{-}4)$$

Subtraction of the so-obtained membrane resistance (calculated from the clean water flux) from the total filtration resistance resulted in the cake-layer resistance, R_{cl}:

$$R_{cl} = R_f - R_m \qquad (3\text{-}5)$$

To characterise the layers, the average resistance over the last hour before termination of the filtration was considered. In combination with the organic mass density (VSS/A_m, see 3.2.2), the specific cake resistance α_m (Ripperger *et al.*, 2013) was calculated as

$$\alpha_m = \frac{R_{cl}}{\left(\frac{VSS}{A_m}\right)}. \qquad (3\text{-}6)$$

3.2.3 Analysis of the ALE gel layers

The layers were visually inspected for accumulation of bacteria using an Olympus BX40 with a 40x magnification objective. A Ganymede SD-OCT (ThorLabs, Dachau, Germany) was used in combination with the ThorImage® Software to obtain information on the smoothness of the surface and to measure the thickness (h) of each gel layer. Because the gel layers consisted for more than 90 % of water and were immersed in the storage solutions during the measurements, the refractive index of water at 25 °C of 1.33 was used for the thickness determination. Gel layer thicknesses were observed over two weeks.

Eventually, excess water was removed from the gel layers by gently tapping it off the perpendicular membrane onto a paper towel. Subsequently, the membrane was put on the paper for 10 s. Next, the ALE gel layers were scratched from the membranes and weighed in

dry porcelain crucibles. Their dry mass (total suspended solids, TSS) and organic mass (volatile suspended solids, VSS) were determined according to the procedure described in 3.2. The organic mass was subsequently used to calculate the density ρ_{VSS}.

$$\rho_{VSS} = \frac{VSS}{h \cdot A_m} \qquad (3\text{-}7)$$

Here, h is the thickness of the gel layers observed by OCT, and A_m the effective membrane area. Accordingly, also the TSS density was calculated. The ash remaining after TSS determination was dissolved in 69 % HNO_3 (VWR, France), while heating up in a microwave oven (Ethos EASY Advanced Microwave Digestion System, Milestone, Sorisole, Italy) with 1500 mW to 200°C within 15 min, and then keeping at 200° C for another 15 min. The amounts of Ca^{2+} and K^+ in the gel layers (m_{ion}) were determined using ICP-OES. For the different ions, the molar concentration was calculated in reference to the original ALE gel layer volume, in the same manner as the VSS density.

$$c_{ion} = \frac{m_{ion}}{M_{ion} \cdot h \cdot A_m} \qquad (3\text{-}8)$$

M_{ion} is the molar mass of the ions. Eventually, the determined ion concentrations were related to the organic mass.

3.2.4 Experiments

For each ionic composition two feed solutions were produced, each split over two membranes. So, quadruplets of each of the gel layers described in Table 3-1 were observed for two weeks concerning their swelling behaviour while being stored at 4° C in their corresponding storage solutions with the same dissolved ion concentration as during preparation. If not stated otherwise, data in Tables is provided incl. the standard deviation over these quadruplets.

Table 3-1: Overview of ionic compositions tested in this work. The numbers indicate the ionic strength of the used feed solutions. The gel layers prepared using these different feed solutions have been analysed for their composition directly after preparation and after a swelling period of 12 d. The framed combinations were subsequently used for testing the reversibility of swelling.

$CaCl_2$ [mM] → ↓ KCl [mM]	**0**	**1**	**3**	**6**	**8**	**12**	**14**
24	24 mM			42 mM			
15			24 mM	33 mM			
6	6 mM		15 mM	24 mM	30 mM	42 mM	
0		3 mM	9 mM	18 mM	24 mM		42 mM

For the composition analysis, right after filtration another feed solution for each combination was prepared and filtered through two membranes. The ionic strength I was calculated with Equation 3-9. z_{ion} stands for the valence of the ions.

$$I = \frac{1}{2} \sum c_{ion} \cdot z_{ion}^2 \qquad (3\text{-}9)$$

Especially in case of the divalent Ca^{2+} ion a significant difference between the nominal concentration c_i and the effective activity a_i was expected. Applying the extended Debye-Hückel equation, the activity coefficients γ_i were determined as a function of the ionic strength I, the valence z_i and the hydrated radius r_i of the ions.

$$\log \gamma_i = \frac{-B \cdot z_i^2 \cdot \sqrt{I}}{1 + r_i \cdot C \cdot \sqrt{I}} \qquad (3\text{-}10)$$

In water at 25° C, the values for B and C are B = 0.51 $M^{-0.5}$ and C = 0.33 $M^{-0.5}Å^{-1}$ (Robinson and Stokes, 1959). The hydrated radii for the relevant ions were taken as 3 Å for K^+ and Cl^-, 6 Å for Ca^{2+}, and 9 Å for H^+ (Kielland, 1937). The activity coefficients calculated for the solutions of Table 3-1 can be found in the appendix, Tables 3-F.

The influence of the supernatant composition on the swelling state of the ALE gels during storage was further addressed with the combination of 6 mM KCl with either 3 mM or 12 mM $CaCl_2$. Three gel layers were prepared in parallel according to the procedure described in 3.3.2. A solution of 120 mg/L ALE, 3 mM $CaCl_2$ and 6 mM KCl was used. For observation of the swelling, one gel layer was directly transferred to a storage solution with 12 mM $CaCl_2$ and 6 mM KCl, the other two (a blank and the test gel layer) were observed for 2 d in the corresponding 3 mM $CaCl_2$ and 6 mM KCl storage solution. After 2 d, the test gel layer was also transferred to a storage solution with 12 mM $CaCl_2$ and 6 mM KCl, and the thicknesses of all gel layers were recorded for another 5 d.

3.3 Results

3.3.1 ALE characterisation

Complete chemical characterisation of ALE is still pending (Felz *et al.*, 2016; Seviour *et al.*, 2019) and was not part of this work. For practical purposes, the extracted ALE pellet was analysed for its organic and inorganic content. It contained 90.6 ± 0.6 % water. Organic mass (VSS) accounted for 89.3 ± 1.0 % of the dry mass. The dry mass of the gel layers once formed was stable during the experiments. Since the focus of this work was on the properties of the gel layers in relation to their composition, the VSS mass determined from the layers was used as a reference for further analyses. Table 3-2 shows the elements found in the ALE pellet, determined with ICP.

In solutions with 120 mg/L VSS, in addition to the investigated species, Ca^{2+} and K^+, only Na^+ was found in significant amounts. Including the NaOH added to neutralise the acidic ALE pellet, the Na^+ concentration in the solutions was approximately 0.4 mM. This was only a minor contribution to the ionic strengths of the filtration solutions used in the preparation of the gel

layers. During storage of the formed gel layers, this was further diluted. Na^+ was, therefore, not considered in further analysis.

Ion	c_{ion} [mmol/g VSS]
Sodium	2.37 ± 0.14
Potassium	0.71 ± 0.41
Cobalt	0.47 ± 0.07
Boron	0.39 ± 0.01
Sulphur	0.37 ± 0.02

Table 3-2: Cation composition of ALE pellet, incl. standard deviation over two samples.

Cake layer resistance

The development of cake-layer resistance in the course of the filtration is shown in Figure 3-1 for a representative experiment (with 6 mM $CaCl_2$ and 6 mM KCl in solution). The graphs looked very similar for all executed experiments with added $CaCl_2$.

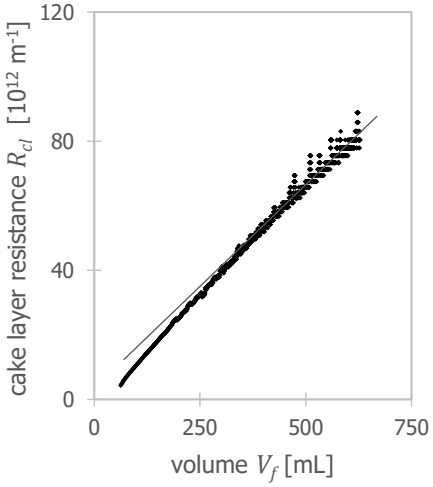

Figure 3-1: Development of cake layer resistance throughout filtration, including a trend line for the data above 400 mL. Data is shown for a representative experiment with 120 mg/L ALE, 6 mM $CaCl_2$ and 6 mM KCl, data points indicate the averaged resistance over 10 min.

Such shape of the development of the resistance has been observed before in fouling experiments (Listiarini *et al.*, 2009; van den Brink, 2014). A linear increase of the resistance in time would point to cake-layer formation without compression. The slight, continuous concave curvature suggested that the cake layers in this work were compressed during formation (Listiarini, Sun and Leckie, 2009).

The specific cake layer resistance, calculated (Eq. 3-8) using the organic mass (VSS) determined directly after the filtration, is shown in Figure 3-2. The differences in cake layer resistance among the tested ionic compositions were very small. Only with increasing $CaCl_2$ content, a slight increase in the specific cake layer resistance was observed. An effect of KCl was inconclusive.

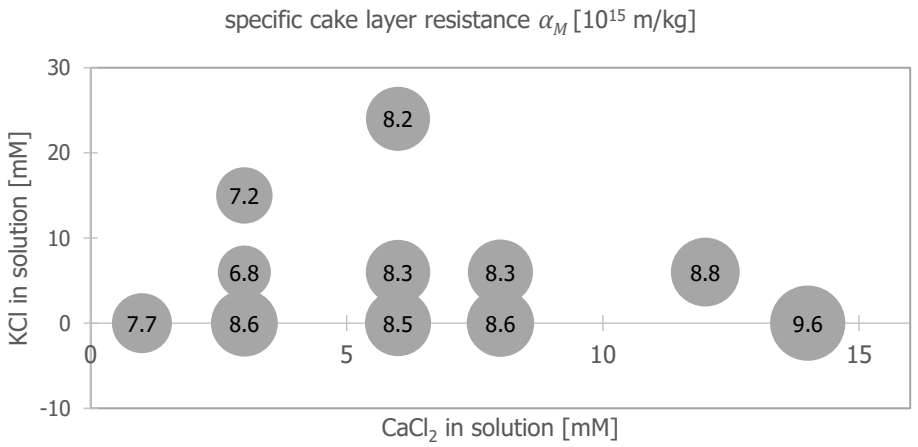

Figure 3-2: Bubble chart of the final specific cake layer resistance [10^{15} m/kg] of the ALE gel layers as a function of $CaCl_2$ and KCl concentrations of the solution. The bubble diameter indicates the specific cake layer resistance. Complete data, including standard deviations, are given in the Appendix, Table E.

3.3.2 Composition

3.3.2.1 Swelling behaviour after preparation

Comparison of gel layers analysed directly after production with those examined after 12 d showed no significant differences in VSS content. No bacterial accumulation was observed on the 12 d old gel layers. The amount of ALE was therefore considered constant during the observation period.

It was expected that after the formation of the gel layers by filtration, the gel layers would adjust to the removal of the applied pressure by swelling and eventually reach an equilibrium thickness with a balance between swelling and cohesion forces. This hydrogel-like behaviour has been observed for alginate gel layers under similar conditions (Ch. 2; Davidovich-Pinhas and Bianco Peled, 2010). The experiments described in section 3.3.3 were limited to 12 d because that was found to be the period over which all gel layers kept their macroscopic integrity, which was a requirement to calculate and compare the densities. In Figure 3-3 an example for the structural change of an ALE gel layer of the current study with 120 mg/L ALE, 6 mM $CaCl_2$ and 6 mM KCl is presented through OCT pictures.

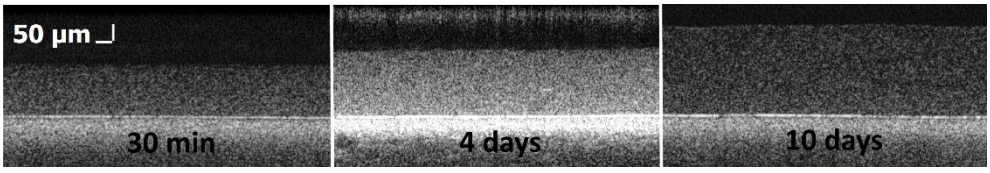

Figure 3-3: OCT pictures of an ALE gel layer made from a solution of 120 mg/L ALE and 6 mM $CaCl_2$/6 mM KCl after 30 min, 4 d and 10 d.

When stored for a more extended period, or with less optimised concentrations of ALE and $CaCl_2$, initially voids were observed in the gel layers and eventually a fibrous network developed (cf. Chapter 2, Fig. 2-13). The gel layers in this study stayed macroscopically homogeneous throughout the observation period, but swelling was still observed. For most samples, the observed height stabilised around the maximal observation period of 12 d. For all gel layers, an initially fast increase in thickness was observed. This was followed by a longer period of slow increase and final stabilisation (cf. Fig. 3-4).

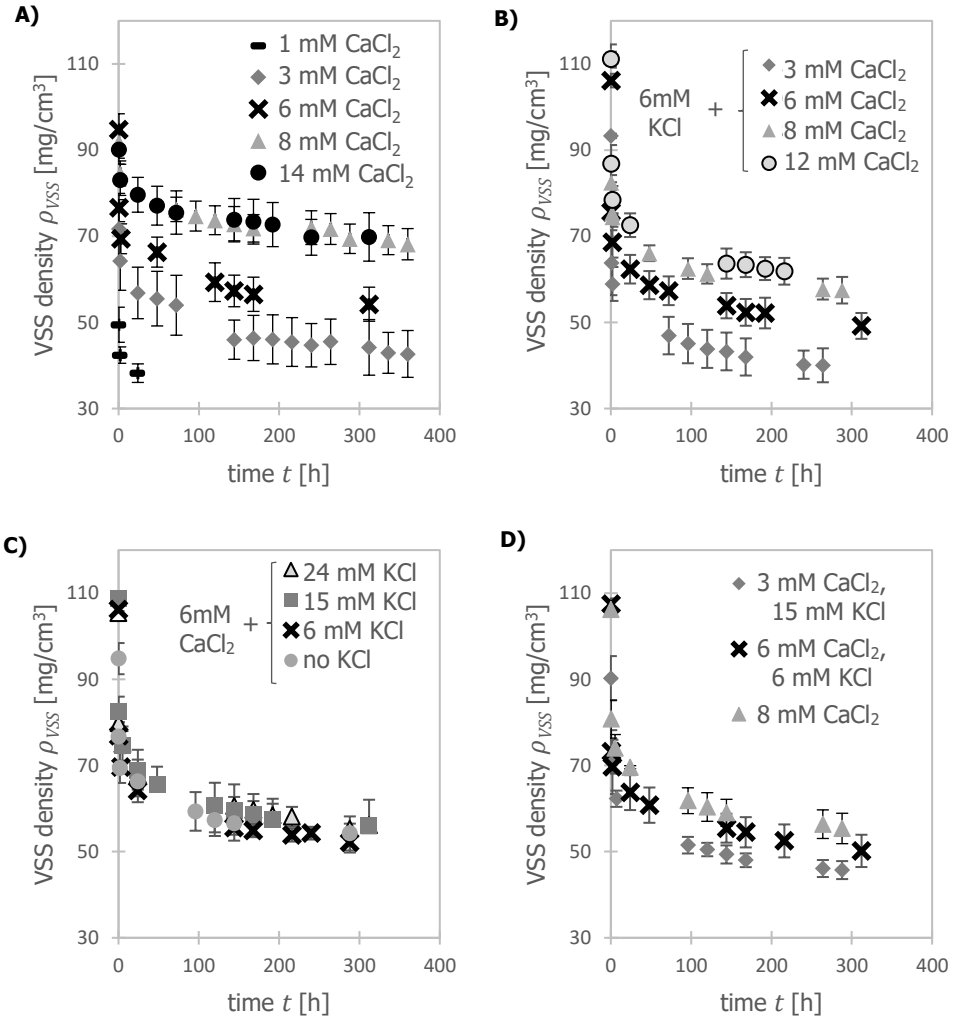

Figure 3-4: VSS density ρ_{VSS} as a function of time after the formation of ALE gel layers with A) only $CaCl_2$, B) constant KCl concentration, C) constant $CaCl_2$ concentration, and D) constant ionic strength. The error bars indicate standard deviations over four samples.

Using Equation 3-7, the thicknesses were converted into VSS density ρ_{VSS}. The development of ρ_{VSS} as a function of time is shown in Figure 3-4 for the different ionic compositions. The density of gel layers with constant $CaCl_2$ and varying KCl concentrations in the supernatant as the only variable showed fairly identical behaviour (Fig. 3-4C). In contrast, an increase in $CaCl_2$ concentration generally resulted in higher VSS densities (Fig. 3-4A, B and D), rather unaffected by the KCl concentration. Such behaviour was observed for alginate gels before (Ch. 2) and was attributed to more Ca^{2+} links between the ALE molecules, allowing less swelling. An exception from this observation was found at relatively high $CaCl_2$ concentrations: above 8 mM $CaCl_2$ in the solution the density and swelling behaviour did not depend on $CaCl_2$ concentration anymore (Fig. 3-4A) or only slightly (Fig. 3-4B). This suggested a saturation behaviour.

3.3.2.2 Distribution of K^+ and Ca^{2+} over gel layer and supernatant

In Figure 3-5, the Ca^{2+} and K^+ concentrations inside the gel layers are represented by the diameter of the bubbles as a function of $CaCl_2$ and KCl concentrations in the supernatant. As for the VSS densities, a decrease over time was observed (comparing the bubble sizes in the left and right figures), which was in accordance with the observed swelling.

Both Ca^{2+} and K^+ were more concentrated inside the gel layers than in the supernatant. The ionic distributions will be discussed in detail later. With more KCl in the supernatant, the amount of Ca^{2+} in the gel layers slightly decreased. The other way round, the $CaCl_2$ concentration in the supernatant had no apparent influence on the K^+ concentration in the gel layers. It was noted that for the K^+ concentrations the statistical variance was higher than for the Ca^{2+} concentrations (cf. Appendix Tables 3-A and 3-B). The reason for this was probably the lower mass of K^+ in the very diluted samples.

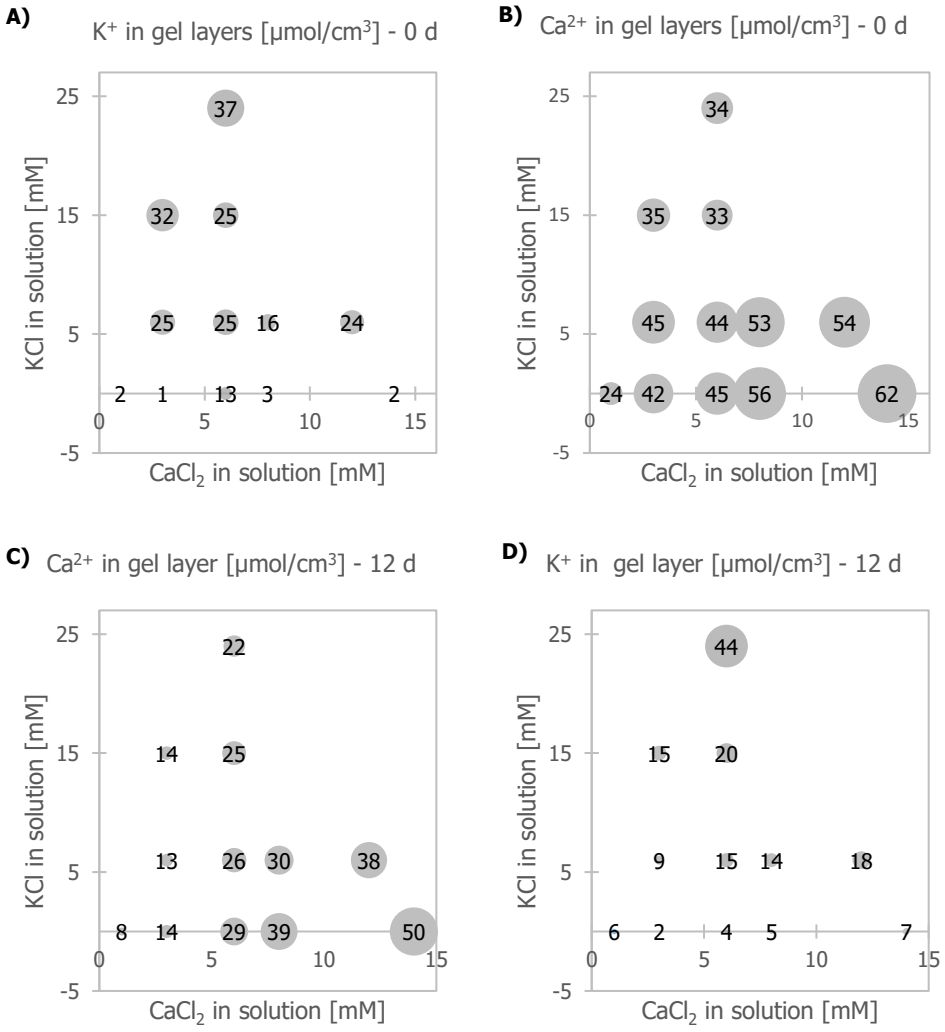

Figure 3-5: The Ca^{2+} (A and B) and K^{+} (C and D) concentrations in the ALE-gel layers as a function of KCl and $CaCl_2$ concentrations in the supernatant, visualised by bubble-diameter. A)+C) directly after filtration, B)+D) after 12 d. The complete data, including standard deviations, can be found in the Appendix in Tables A and B.

Figure 3-6 shows the amount of Ca^{2+} in the gel layers per gram of VSS as a function of KCl and $CaCl_2$ concentrations in the supernatant, again both directly after filtration and after 12 d storage (full data in the Appendix, Tables 3-C and 3-D). The observed Ca^{2+}-concentrations in the ALE gel layers were between 200 µmol/g VSS and 700 µmol/g VSS. Slightly higher binding capacities of ALE for Ca^{2+}, between 950 and 1300 µmol/g VSS, were determined in titration experiments without extra electrolyte (Kleikamp, 2017). Based on an estimation of 1.6 mmol/g VSS of negative charges in ALE (Felz, Kleikamp, *et al.*, 2020), and under the

assumption that one Ca^{2+} ion neutralises two negative charges, the higher values appeared to be close to the maximum.

As mentioned above, increasing the KCl concentration resulted in a slight decrease in the Ca^{2+} concentration in the gel layers. This effect was better visible in relation to VSS than as absolute concentration (see Figure 3-6). This could point to competition between Ca^{2+} and K^+ for accumulation in the ALE gel layers. Such competition has been described before for calcium-alginate gels (Wang and Spencer, 1998). We will come back to this phenomenon in the discussion. An interesting observation was that the values directly after filtration and after 12 d of storage were similar in the ranges with medium $CaCl_2$ and KCl concentrations, while the extremes tended to drift apart.

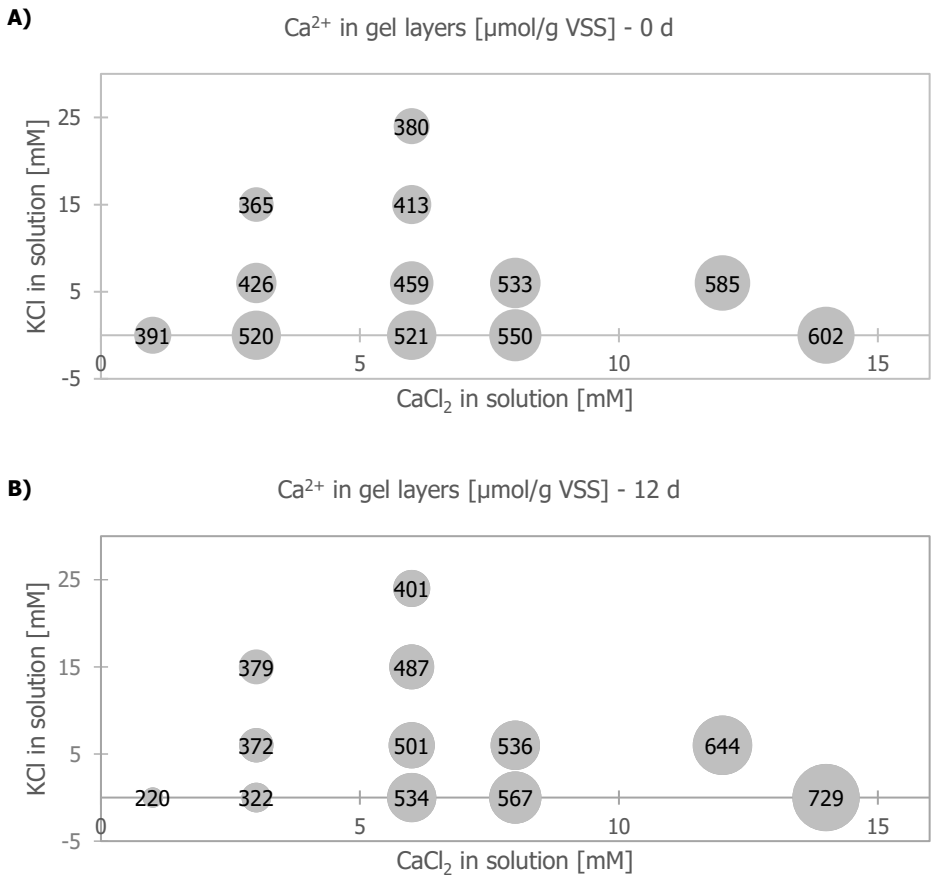

Figure 3-6: The Ca^{2+}:VSS ratio [µmol/g VSS] (illustrated as bubble-diameter) as a function of $CaCl_2$ and KCl concentrations in the supernatant, determined directly after filtration (A) and after 12 d of storage (B). The complete data, including standard deviations, can be found in the Appendix, Tables C and D.

3.3.3 Reversibility of swelling

3.3.3.1 Density

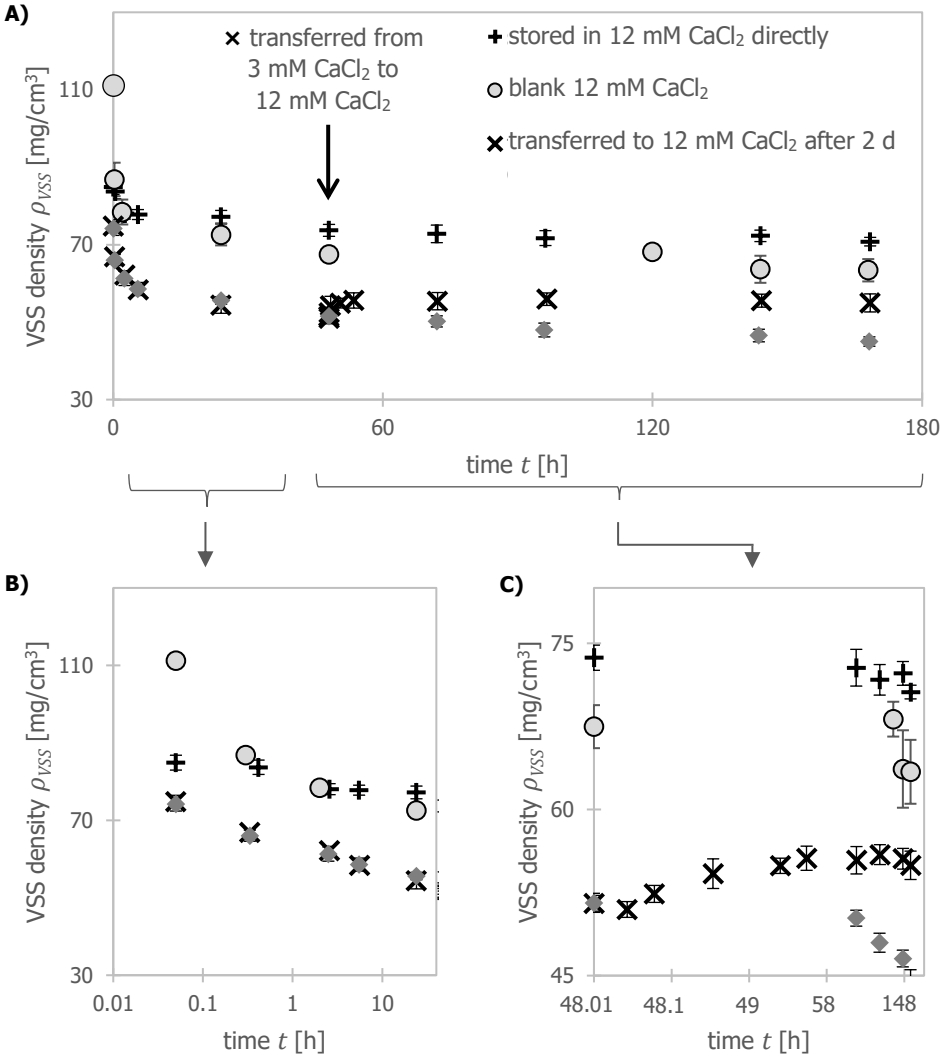

Figure 3-7: Comparison of the swelling behaviour of gel layers produced with 3 mM $CaCl_2$ and 6 mM KCl and subsequently stored in (+) 12 mM $CaCl_2$/6 mM KCl and (×) 3 mM $CaCl_2$/6 mM KCl for t2 d and then transferred to 12 mM $CaCl_2$/6 mM KCl. For comparison, blanks produced and stored with either high (circle) or low (diamond) $CaCl_2$ concentration are shown. A) shows the whole range of the experiment, B) zoomed in on the first 2 d and C) zoomed in on the swelling after transfer to the higher $CaCl_2$ concentration after 2 d. The error bars show the standard deviation over ten measurements on the same sample in case of the transferred gel layers, and the standard deviation of two samples for the blanks.

The experiments described in the previous section clearly showed the importance of the $CaCl_2$ concentration for ALE gel characteristics. To differentiate between the influence of $CaCl_2$ available during filtration and $CaCl_2$ available during the swelling, another experiment was performed. In this case, gel layers were produced with a rather low $CaCl_2$ concentration (3 mM $CaCl_2$, 6 mM KCl), and then transferred to storage solutions with a higher $CaCl_2$ concentration (12 mM $CaCl_2$, 6 mM KCl). The development of the VSS density in time of those gel layers is shown in Figure 3-7, compared to a blank that was kept in the storage solution with 3 mM $CaCl_2$, and to a blank produced and stored in 12 mM $CaCl_2$.
Already after 3 min, the gel layer that was directly transferred to the solution with 12 mM $CaCl_2$ had a higher density than those stored in the solutions with 3 mM $CaCl_2$, the concentration that was also used for production (Fig. 3-7B). The blank sample produced with 12 mM $CaCl_2$ was at this moment still much denser. After about 30 min, the density of the gel layer produced with 3 mM $CaCl_2$ but stored in 12 mM $CaCl_2$ equalled that of the 12 mM blank, and on a longer-term, it seemed even to keep a slightly higher density than this blank.

Also after the transfer of the gel layer stored for 2 d at 3 mM $CaCl_2$ to a solution with 12 mM $CaCl_2$, compaction of the ALE gel layer was observed within a few minutes (Fig. 3-7C). This process continued for about 6 h, and then an apparent steady-state was reached that lasted for the rest of the observation period (Fig. 3-7A). The density achieved by this compaction stayed below those of the gel layers that were stored directly after preparation in 12 mM $CaCl_2$. The swelling could, therefore, be described as partly, but not entirely reversible.

3.3.3.2 Ca^{2+} content

The Ca^{2+} concentrations in the gel layers used for the swelling experiments described above are shown in Figure 3-8. As expected, the Ca^{2+} content of the gel layers transferred to 12 mM $CaCl_2$ solutions after preparation at 3 mM $CaCl_2$ was significantly higher than of the blank produced and stored at 3 mM $CaCl_2$ (Fig. 3-8 A+B). However, the Ca^{2+}/VSS ratio of the gel layers produced and stored for 12 d with 12 mM $CaCl_2$/6 mM KCl (as described in section 3.4.3) was not reached.
Those blanks were stored for 12 d, while in this experiment, the observation period was only 7 d. There were two possible causes for the difference: 1) the effect of the lower concentration Ca^{2+} during preparation was not completely undone/reversed by directly storing the gel layer in 12 mM $CaCl_2$, or 2) after 7 d Ca^{2+} still accumulated in the gel layer. Considering the partial irreversibility of Ca^{2+} concentration influence observable in Fig. 3-7, and that between 7 d and 12 d the gel layers with high Ca^{2+} concentrations appeared rather stable (cf. Fig. 3-4), the first explanation appeared likeliest.

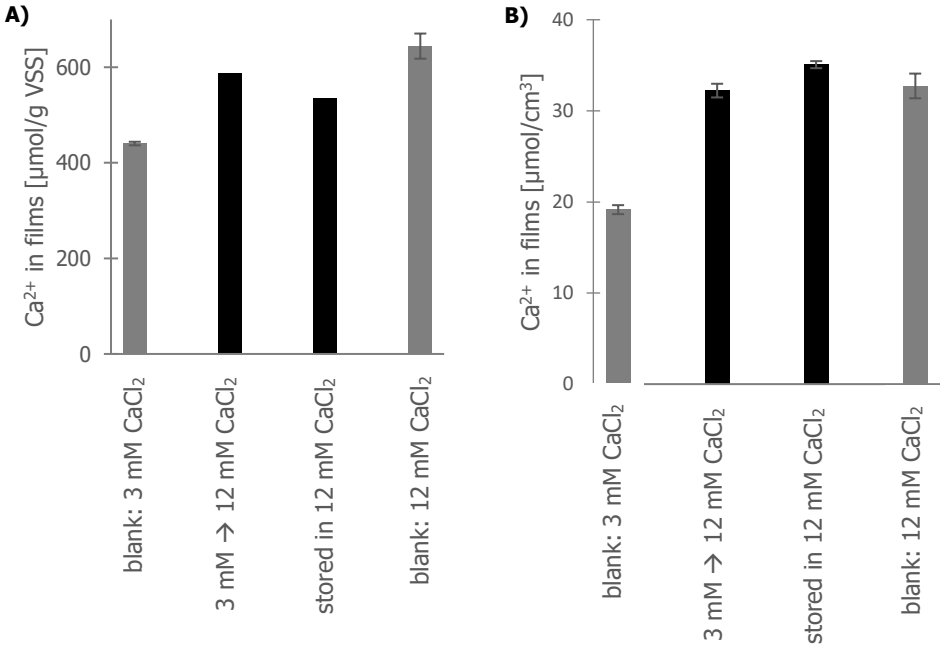

Figure 3-8: Ca^{2+} content of the gel layers produced with 3 mM $CaCl_2$ and 6 mM KCl and subsequently stored in a solution with higher $CaCl_2$ concentration (12 mM $CaCl_2$ and 6 mM KCl), analysed after 7 d in total. For comparison also the Ca^{2+} content of the blank, stored in 3 mM $CaCl_2$/6mM KCl for 7 d, and the results for gel layers produced and stored in 12 mM $CaCl_2$/6mM KCl (after 12 d) are shown. A) Ca^{2+}:VSS ratio, B) Ca^{2+} concentration. The error bars indicate the standard deviation over nine measurements on the same sample in case of the transferred gel layers, and the standard deviation of two samples for the blanks.

3.4 Discussion

In this work, the development of ALE gels after formation on ultrafiltration membranes by dead-end filtration in the presence of $CaCl_2$ and KCl was investigated. After removal of the filtration pressure, structural and compositional changes in the gels have been observed on a time scale of hours to several days up to more than a week. Using ALE as a simplified model compound of biofilms, the results offered hints towards the physical and chemical mechanisms involved in the formation and ripening of biofilms. The composition and appearance of the gel layers followed from the balances between electrostatic interactions in the gel, osmotic pressure differences between the gel and the outside solution, and the ability of the gel network to withstand swelling by water intake. These mechanisms will be discussed below.

3.4.1 Ionic distributions over gel layers and solutions

For the following discussion, the system was considered as two compartments: the gel (compartment 1) on the one hand and the supernatant solution (compartment 2) on the other

hand (see Fig. 3-9). The gel was fully penetrable for water and all ions contained in the system (Ca^{2+}, Cl^-, K^+, H^+, OH^-). Besides, the ALE gel contained fixed negative charges, of which the amount has been previously estimated as 1.6 mmol/g VSS, based on non-published work (Kleikamp, 2017).

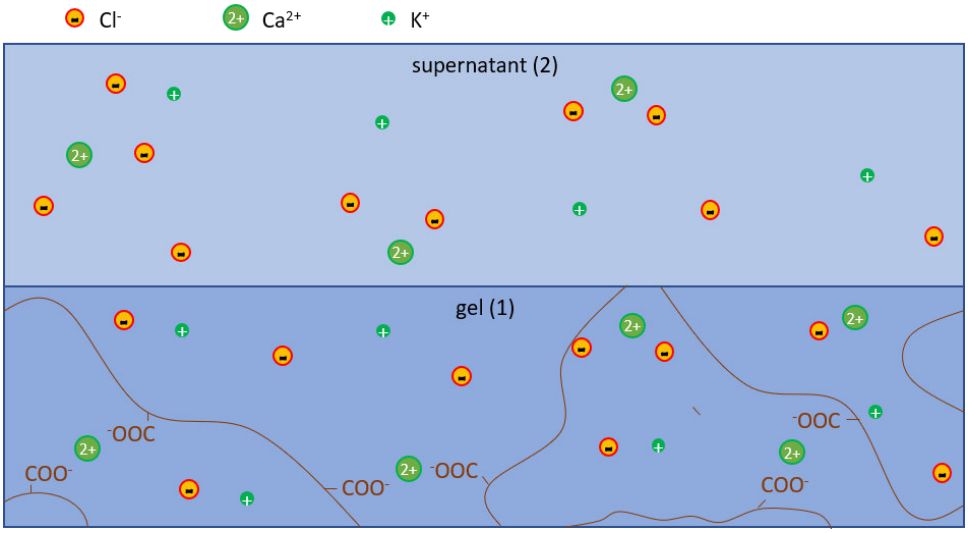

Figure 3-9: Schematic display of the two phases in the system: the ALE gel (1) and the supernatant (2). The ions need to balance the extra negative charges provided by the ALE.

Electroneutrality demanded that within each compartment, the charges were balanced. For the supernatant (compartment 2) this could be written as

$$\sum_i z_i \cdot c_{i,2} = 0. \qquad (3\text{-}11)$$

i are the ions specified above. In the experiments, the ionic composition in the supernatant was considered controlled and constant due to its substantial volumetric excess compared to the gel layers. The concentrations assumed were, therefore, those shown in Table 3-1, completed with a negligible concentration of 10^{-4} mM for both H^+ and OH^- (pH 7).

For the gel (compartment 1), the fixed negative charges of the ALE, illustrated in Figure 3-9 solely by carboxylic groups for the purpose of readability, needed to be considered in addition to the ions. Again, electroneutrality needed to be obeyed.

$$\sum_i z_i \cdot c_{i,1} - Z = 0 \qquad (3\text{-}12)$$

Z being the concentration of fixed negative charges in the gel. The pK_a values of the carboxylate groups of mannuronic and guluronic acid, the monomers building alginate, have been found at 3.38 and 3.65 (Draget, Skjåk Bræk and Smidsrød, 1994), so these groups all bore a negative charge at pH 7 and thus contributed to Z. The concentrations of Ca^{2+} and K^+

in the ALE gel layers were determined. Together with their known concentrations in the supernatants, it was possible to make an analysis based on the Donnan equilibrium, from which some important characteristics of the system could be derived as will be shown in the next sections.

3.4.2 Donnan equilibrium

Because of the presence of fixed negative charges in the ALE, a Donnan potential between the ALE gel and the supernatant was established. The Donnan potential describes the electrical potential difference between two compartments due to the uneven distribution of small ions over these two compartments as a result of the existence of fixed charges in one of them. It was derived using the electrochemical potentials $\tilde{\mu}_i$ of the small ions:

$$\tilde{\mu}_i = \mu_i^0 + RT \cdot ln(a_i) + z_i \cdot F \cdot \Psi \qquad (3\text{-}13)$$

The first two terms at the right-hand side of this equation describe the chemical potential, with μ_i^0 the standard chemical potential of the ion i, R the gas constant, T the absolute temperature, and a_i the activity of the ion in solution. The last term represents the electrostatic contribution to the molar Gibbs energy, with z_i the valency of the ion, F the Faraday constant and Ψ the local electrical potential. In equilibrium for each type of ion the electrochemical potentials in the two compartments 1 and 2 were equal:

$$\tilde{\mu}_{i,1} = \tilde{\mu}_{i,2} \qquad (3\text{-}14)$$

From this, an expression for the potential difference between the two compartments, which is defined as the Donnan potential E_{Donnan}, could be derived:

$$E_{Donnan} = \Psi_1 - \Psi_2 = \frac{RT}{z_i \cdot F} \cdot \ln\left(\frac{a_{i,2}}{a_{i,1}}\right) \qquad (3\text{-}15)$$

As before, compartment 1 represents the gel phase and 2 stands for the solution. So, all types of small ions, provided that they were not irreversibly bound to the gel on the timescale of the experiments, would distribute over the two compartments according to the Donnan potential. The z_i in the denominator in Equation 3-15 provided an electrochemical explanation for the apparent preference for the divalent Ca^{2+} over the monovalent K^+.

Whether the ions indeed distributed according to a Donnan equilibrium, was checked by comparing the Donnan potential values calculated from both the distributions of the Ca^{2+} ions and the K^+ ions (Tables 3-3 and 3-4). The values were in the range where passively established potentials in biological systems were expected (Sperelakis, 2012).
The activity coefficients of the ions at the different ionic strengths were calculated according to Equation 3-10. For evaluation of the overall ionic strength (Eq. 3-9), the Cl^- activity inside the gels was roughly estimated as $a_{Cl,1} = 0.5 \times a_{Cl,2}$. Comparison with the later calculated ionic activities (appendix, Tables 3-G) showed that this approximation was reasonable.

Table 3-3: Donnan potential [mV] between the ALE gel layers and the supernatant, as calculated by the experimentally determined Ca^{2+} concentrations, assuming electrochemical equilibrium. A) immediately after filtration, B) after 12 d.

A)

Ca^{2+} [mM] → K^+ [mM] ↓	**1**	**3**	**6**	**8**	**12**	**14**
24	-	-	-19.4 ± 0.1	-	-	-
15	-	-27.4 ± 0.6	-18.7 ± 0.3	-	-	-
6	-	-28.8 ± 1.1	-20.7 ± 1.5	-19.7 ± 0.6	-15.5 ± 0.4	-
0	-34.5 ± 0.3	-27.5 ± 0.6	-20.5 ± 0.4	-19.8 ± 0.1	-	-15.2 ± 0.5

B)

Ca^{2+} [mM] → K^+ [mM] ↓	**1**	**3**	**6**	**8**	**12**	**14**
24	-	-	-18.9 ± 1.0	-	-	-
15	-	-20.4 ± 0.2	-19.6 ± 1.3	-	-	-
6	-	-18.4 ± 1.7	-19.0 ± 0.9	-18.2 ± 0.2	-16.8 ± 0.2	-
0	-	-17.6 ± 1.4	-20.0 ± 1.1	-20.6 ± 0.8	-	-18.5 ± 0.9

Table 3-4: Donnan potential (mV) between the ALE gel layers and the supernatant, as calculated by the experimentally determined K^+ concentration, assuming electrochemical equilibrium. A) immediately after filtration, B) after 12 d.

A)

Ca^{2+} [mM] → K^+ [mM] ↓	**1**	**3**	**6**	**8**	**12**	**14**
24	-	-	-5.3 ± 0.4	-	-	-
15	-	-9.1 ± 1.9	-6.3 ± 1.7	-	-	-
6	-	-17.2 ± 0.9	-17.7 ± 3.8	-12.2 ± 1.5	-17.5 ± 3.7	-
0	-	-	-	-	-	-

B)

Ca^{2+} [mM] → K^+ [mM] ↓	**1**	**3**	**6**	**8**	**12**	**14**
24	-	-	-16.8 ± 5.9	-	-	-
15	-	-0.5 ± 0.9	-8.7 ± 8.8	-	-	-
6	-	-10.1 ± 3.3	-23.1 ± 3.7	-22.9 ± 4.8	-29.7 ± 8.4	-
0	-	-	-	-	-	-

The quite reasonable agreement between the Donnan potential values calculated from the distributions of Ca^{2+} and K^+ suggested that both types of ions could freely move between the two compartments on the timescale of the experiments. In contrast, for gel layers produced similarly from alginate in the presence of $CaCl_2$ and KCl (Ch. 2), values for the Donnan potential

calculated based on Ca^{2+} were systematically found twice as high as those derived from K^+ concentrations. While the high specificity and chelating nature of the Ca^{2+}-alginate bond are well known, the present results indicated that there was no specific (irreversible) binding of Ca^{2+} to ALE. This could be explained by the finding that a significant amount of the charged groups in ALE was sulfate rather than carboxylate (Felz, Neu, *et al.*, 2020). To identify possible specific binding reactions with other mono-, di- or trivalent ions, tests and analyses analogously to those above with those ions need to be done. Investigation of gel bead formation and stability hint at an interesting interaction with copper (Felz, Kleikamp, *et al.*, 2020).

Only in case of low Ca^{2+} concentrations, a clear difference was observed between the Donnan potentials calculated directly after filtration and after 12 d of storage. After releasing the filtration pressure used in the preparation, the gel layers started swelling, causing the concentration of fixed charges in the gel to decrease. Apparently, in case of the higher Ca^{2+} concentrations, the concentration change caused by the swelling was too small to be detected in these experiments. For the freshly prepared gel layers, the potential differences calculated from the Ca^{2+} distributions showed an explicit dependency on the $CaCl_2$ concentration in the supernatant. The standard deviations in the measurements of the K^+ concentrations were too large to see this trend.
After storage, the values of the Donnan potential were mostly in the same range between -15 mV and -20 mV, and seemed only slightly dependent on the supernatant ion concentrations. Since the $CaCl_2$ concentration had a strong impact on the ionic strength, it could not be decided if this was a dependence on Ca^{2+} concentration or the ionic strength.

It appeared that the Donnan equilibrium applied to the system. Assuming that there were no other specific interactions, this was true for all ions in the system. Equating Equation 3-15 for different ions $i = j$ and $i = k$ gives

$$\left(\frac{a_{j,2}}{a_{j,1}}\right)^{\frac{1}{z_j}} = \left(\frac{a_{k,2}}{a_{k,1}}\right)^{\frac{1}{z_k}}. \qquad (3\text{-}16)$$

From the known Ca^{2+} activities, in this way, it was possible to estimate the H^+ activities inside the gel layers, considering the supernatant H^+ activity was constant at $a_H = 10^{-4}$ mM (pH 7). The calculations predicted a slight decrease of pH inside the gel layers to pH 6.6 - 6.8. Protons were assumingly accumulated inside the ALE gel layers. Finally, based on the Donnan equilibrium and electroneutrality requirement, it was possible to estimate the concentration of fixed charges Z in the ALE according to Equation 3-12. The results are listed in Table 3-5.
For the calculations, it was assumed that the contribution of cations other than Ca^{2+} and K^+ to the neutralisation of Z was negligible and that Cl^- (calculated from the Donnan equilibrium according to Equation 3-16, see Appendix Tables 3-G) was the dominant anion in the system. The values of Z obtained in this way were, of course, dependent on the swelling state of the

gel layers. Divison by the corresponding VSS densities resulted in the number of fixed charges per g VSS, which should be constant. Indeed, the obtained values are rather constant, considering the assumptions and experimental errors, leading to the conclusion that the amount of fixed charges is approximately 1 mmol/g VSS, in line with the binding capacities between 950 and 1300 µmol/g VSS that were determined for ALE from different sources using dialysis experiments (Kleikamp, 2017).

Table 3-5: The estimated amount of fixed charged groups in the ALE (mmol/g VSS), based on Donnan equilibrium and electroneutrality condition. In the calculations, the Donnan potentials obtained from the Ca^{2+} distributions over gel layer and supernatant have been used. A) Immediately, B) After 12 d.

A)

Ca^{2+} [mM] → K^+ [mM] ↓	**1**	**3**	**6**	**8**	**12**	**14**
24	-	-	0.89 ± 0.02	-	-	-
15	-	1.13 ± 0.10	0.77 ± 0.05	-	-	-
6	-	1.29 ± 0.09	1.04 ± 0.09	1.07 ± 0.06	1.10 ± 0.09	-
0	0.80 ± 0.03	1.07 ± 0.10	1.09 ± 0.11	1.05 ± 0.02	-	1.06 ± 0.06

B)

Ca^{2+} [mM] → K^+ [mM] ↓	**1**	**3**	**6**	**8**	**12**	**14**
24	-	-	1.27 ± 0.24	-	-	-
15	-	0.74 ± 0.04	1.18 ± 0.29	-	-	-
6	-	0.74 ± 0.14	1.09 ± 0.12	1.11 ± 0.09	1.34 ± 0.15	-
0	-	0.63 ± 0.13	1.01 ± 0.16	1.10 ± 0.11	-	1.37 ± 0.19

3.4.3 Correlation between Ca^{2+} content and strength of the ALE gel layers

With increasing $CaCl_2$ concentration in the supernatant, the ALE gel layers as prepared in this work were found denser until a plateau was reached around 8 mM Ca^{2+} (Fig. 3-4). For bacterial EPS, Ca^{2+} availability has been directly linked to denser films (Körstgens *et al.*, 2001; Goode and Allen, 2011). It was assumed that the increase in density was caused by an increase in the number of crosslinks, where Ca^{2+} ions connect EPS molecules. In this section, the effect of Ca^{2+} on the strength of the ALE network is addressed.

As a consequence of the fixed negative charges in the ALE, an uneven ion distribution was established, as described above. In addition to the development of a Donnan potential, this caused an osmotic pressure difference between the gel layers and the supernatant. The osmotic pressure Π in each of the compartments could be calculated from the ionic concentrations using the van 't Hoff equation:

$$\Pi = RT \cdot \sum_i c_i \qquad (3\text{-}17)$$

Because of their very low molar concentrations, the ALE molecules as well as H^+ and OH^- hardly contributed to the osmotic pressure difference, so only Ca^{2+}, K^+ and Cl^- were considered. The resulting values for Π are shown in Table 3-6. After preparation of the gel layers, to minimise the osmotic pressure difference, water flew inside the gel layers and caused swelling. At some point, further swelling was prevented by the opposing elastic force of the ALE network. In a balanced system, the osmotic pressure difference was, therefore, an indicator for the network strength.

Table 3-6: Estimation of osmotic pressure difference [Pa] between the ALE gel layers and the supernatant concentration after 12 d of storage, as calculated by the experimentally determined concentrations of Ca^{2+} and K^+.

Ca^{2+} [mM] → K^+ [mM] ↓	**1**	**3**	**6**	**8**	**12**	**14**
24	-	-	43.2 ± 25.5	-	-	-
15	-	0.3 ± 1.4	25.0 ± 18.6	-	-	-
6	-	18.4 ± 5.4	47.3 ± 7.1	48.9 ± 6.8	59.1 ± 14.7	-
0	29.3 ± 6.8	23.8 ± 4.0	51.4 ± 6.4	67.2 ± 7.0	-	72.7 ± 14.4

Assuming that the ALE gel layers after 12 d of storage were in equilibrium with the supernatant, the data in Table 3-6 shows that with increasing $CaCl_2$ concentration in the supernatant, the network strength slightly increased. This indicated that Ca^{2+} was involved in crosslinking of the gel layers. Another contribution to the strengthening of the network might be shielding of negative charges inside the gel layers from each other, allowing denser packing. The final density of the gel layers (Fig. 3-5) was dependent on the ion concentrations in the supernatant and the network strength. While the ionic composition of the supernatant defined the ion concentration inside the gels (given the fixed amount of charges of the ALE per g VSS) and thus the osmotic pressure difference, the network strength determined the maximum amount of water that could be taken up to reduce the osmotic pressure difference.

3.4.4 Hydraulic resistance of ALE gel layers

A positive correlation between EPS density and hydraulic resistance of biofilms has been postulated several times before (Vrouwenvelder *et al.*, 2016; Desmond *et al.*, 2018; Jafari *et al.*, 2018). Also, the Ca^{2+} concentration in films has been correlated to flux decline in membrane filtration (Herzberg, Kang and Elimelech, 2009). This went along with the finding that the specific cake-layer resistance of the ALE gel layers in this work slightly increased with supernatant $CaCl_2$ concentration (Fig. 3-2). In this context, it attracted attention that while the VSS density reached a maximum around 110 mg/cm^3, the specific resistance still slightly increased (e.g. between 8 mM $CaCl_2$ and 14 mM $CaCl_2$, cf. Fig. 3-2). The differences in relation to the experimental errors (cf. Appendix, Table 3-E) were so small, though, that no further conclusions could be drawn from these data.

3.4.5 Compressibility, relaxation and ripening

The slightly concave shape observed in all experiments during the build-up of the cake-layer resistance (as illustrated by the example in Fig. 3-1) indicated that cake layers were formed and at the same time were slightly compressed during the filtration (cf. Roorda and van der Graaf, 2001). Compressibility is a feature of biofilms that has been investigated for several years (Laspidou and Aravas, 2007; Desmond, Morgenroth and Derlon, 2018; Jafari *et al.*, 2018), and that has also been used as an indication for the viscoelastic behaviour of biofilms (Körstgens *et al.*, 2001; Safari *et al.*, 2015). Based on this, relaxation was expected as soon as the filtration pressure was released. Due to experimental restrictions, the changes in the thickness of the ALE gel layers in this study were only recorded from ca. 3 min after pressure release. The relaxation of biofilms has often been described with the help of Maxwell springs (Jones *et al.*, 2011; Peterson *et al.*, 2012; Safari *et al.*, 2015), with by approximation exponential behaviour. Missing the first 3 min of the process, a quantitative analysis of the collected data is deemed unreliable. For accurate collection and analysis of relaxation data to extract characteristic viscoelastic data, systems with controllable compression and instantaneous observation of the stress and strain are needed.

An interesting observation in this study was the long continuation of the swelling (Fig. 3-3 and 3-4). For alginate gels produced under similar conditions, such equilibration took only about 2 h (cf. Fig. 2-4). While in the current study the composition was chosen in a way that the gel layers kept macroscopic homogeneity over the observation period, previous work suggested a ripening process that slowly causes the development of a fibrous network (see Fig. 2-13) by internal rearrangements of the polymer network. The slow molecular rearrangement was suspected to already happen on the microscale not observable by OCT so that it was probably involved in the long swelling process observed in this study.
Upon transfer of a gel layer to a higher $CaCl_2$ concentration than the one used during production directly after the release of the filtration pressure, the same high densities as for gel layers produced with these high concentrations were reached (Fig. 3-7B). Yet, if gel layers were allowed to swell for 2 d in solutions with less $CaCl_2$, transfer to a solution with more $CaCl_2$ did not lead to the same high densities (Fig. 3-7C). Apparently, immediately after the filtration pressure was released, swelling by water intake started as well as the slow rearrangement of the ALE molecules into microfibres. The latter caused the development of initially microscopic voids in the structure (cf. (Laspidou *et al.*, 2014; Jafari *et al.*, 2018), which could not be fully reversed, even when the gel layer was later transferred to a solution with a higher $CaCl_2$ concentration. This assumption was supported by non-reversible differences in the Ca^{2+} content of the gel layers (Fig. 3-8).

Table 3-7 presents the osmotic pressures calculated for these gel layers according to Equation 3-17. For gel layers prepared and stored at 3 mM $CaCl_2$, there was a decrease in the osmotic pressure difference between gel layer and supernatant between 7 d and 12 d. Less

pronounced, similar behaviour was expected for the 12 mM $CaCl_2$/6 mM KCl blank, in parallel with the observed slow reduction in density (Fig. 3-4). Keeping the assumption of electrochemical equilibrium between the gel layer and supernatant, this was a sign for the slow rearrangement of the ALE molecules inside the gels, resulting in the formation and growth of voids that weakened the network structure. Fibrous structures and a decrease in density over longer time scales (between 7 and 12 d) were especially found in the gel layers that were prepared with and stored at lower $CaCl_2$ concentrations (1 and 3 mM).

Table 3-7: Estimation of osmotic pressure [Pa] in the ALE gel layers transferred after production to supernatant with higher $CaCl_2$ concentration. Analysis after 7 d. As a reference, the data for the gel layers after 12 d is shown as well. Note that other than the quadruplets performed for 12 d, the 7-d experiments were only performed as singlets (3 mM $CaCl_2$/6 mM KCl blank as duplet). The stated standard deviations concern the average over nine measurements at different locations of the gel layers.

storage time	blank: 3 mM $CaCl_2$ 6 mM KCl	produced: 3 mM $CaCl_2$ 6 mM KCl after 2 d: 12 mM $CaCl_2$ 6 mM KCl	produced: 3 mM $CaCl_2$ 6 mM KCl stored: 12 mM $CaCl_2$ 6 mM KCl	blank: 12 mM $CaCl_2$ 6 mM KCl
7 d	33.1 ± 1.0	46.6 ± 0.2	65.8 ± 0.1	-
12 d	18.4 ± 5.4	-	-	59.1 ± 14.7

A clear hierarchy in network strength was found, increasing from the blank with 3 mM $CaCl_2$ via the one transferred to 12 mM $CaCl_2$ after 2 d to the one directly stored in 12 mM $CaCl_2$. Assumingly, water was expelled from the later transferred gel layer as a consequence of the new ion distribution. However, since the network had already started to be weakened by microscopic voids, the density and strength of gel layers directly stored in the higher $CaCl_2$ concentration could not be reached. It was concluded that the internal rearrangement was delayed the more Ca^{2+} crosslinks were in the network, but once microscopic voids have been formed, the process could not be reversed by adding Ca^{2+} in a later stage.

According to Desmond, Morgenroth and Derlon, 2018, compression caused by filtration pressure is reversible for structurally homogeneous biofilms and irreversible for films with a heterogeneous structure. This finding was supported by this work in such a way that it was shown that networks with voids, which can structurally be considered more heterogeneous than networks without voids, were weaker than more homogenous networks without voids.

It was shown in this work that Ca^{2+} played a role in the formation and strength of the ALE network. In contrast to alginate, however, the Ca^{2+} binding was dynamic and nonspecific, so that Ca^{2+} ions distributed over gel and solution according to a Donnan equilibrium. Therefore, they could be easily removed, for example, by dilution, or replaced by other ions. Based on the results of this study, other divalent cations should also be able to fulfil the crosslinking

role. Formation of stable gels with comparable elastic properties has indeed been confirmed with a whole range of divalent cations (Felz, Kleikamp, *et al.*, 2020). In this context, it was also observed that unlike Ca-alginate beads, Ca-ALE beads stayed intact when treated with EDTA. This observation, in combination with the found ripening of the gel layers discussed in this study, opens the doors to speculations about the role of Ca^{2+} or other divalent cations beyond gel formation. If, for example, the fibrous structures (Fig. 3-3) were still mainly crosslinked by Ca^{2+}, or if other mechanisms such as hydrogen bonds, hydrophobic interactions, H-bonds, van-der-Waals forces and entanglement became more important at this stage, will be a topic for future research.

3.4.6 Outlook

This work provided valuable insight into the interaction between ALE and Ca^{2+} in the presence of K^+ and Cl^-. As a next step, the influence of Ca^{2+} content of ALE gels on their mechanical properties such as modulus, strength and adhesion can be investigated. While a closer look on the swelling behaviour can be a start (e.g. with observation in the filtration cell during filtration, possibly also under application of different pressures), direct determination of the viscoelastic properties of the gels by rheological measurements will provide more quantitative data, making it possible to link the composition to mechanical properties of the gel layers (Weiss and Freeman, 1997).

The system of ALE and specific ions still represented a simplified model for biofilms. The model can be extended by adding other kinds of molecules, such as peptides, humic acids and eDNA, to eventually get close to the complexity of real biofilms (Lin *et al.*, 2014; Hobley *et al.*, 2015; Flemming, 2016). It was hypothesized that after Ca-ALE gel layers were formed, interactions beyond electrostatic attraction, such as hydrogen bonds, hydrophobic interactions, H-bonds, and van-der-Waals forces, became more important and were probably involved in the modification into the observed fibrous structure. Evaluating the interactions within the ALE network with added compounds, also based on better chemical characterization of ALE and EPS (Seviour *et al.*, 2019; Felz, Neu, *et al.*, 2020), can lead the path towards further understanding of these cohesive forces of biofilms. Understanding of the effect on the network strength and the mechanical properties is an important step towards tailored cleaning strategies.

3.5 Conclusions

By filtration of solutions containing bacterial alginate-like exopolymers extracted from granular biofilms and $CaCl_2$, ALE-layers with a thickness between 100 µm and 200 µm were prepared on ultrafiltration membranes. Once the filtration pressure was released, these gel layers showed viscoelastic relaxation behaviour similar to biofilms. Subsequently, slow structural

rearrangements in the gel caused further swelling, and would eventually result in the development of a fibrous ALE network.

The negative charges contained in the ALE caused accumulation of counter-ions inside the gel layers and the establishment of a negative Donnan potential between the gel layers and the supernatants. It was shown that the ionic distributions in the system followed the Donnan equilibrium. This observation allowed the conclusion that Ca^{2+} ions did not specifically bind to ALE in a way as shown for alginate, but that they could move freely in and out of the ALE gel on the timescale of the experiments, just like K^{+}. Yet, the more Ca^{2+} was contained in a gel layer, the stronger (withstanding a higher osmotic pressure) was the gel network. This indicated that Ca^{2+} played an important role in the crosslinking of the network. Since there was no apparent specific binding of Ca^{2+} to the ALE, crosslinking by Ca^{2+} would be purely electrostatic. Therefore, other divalent cations should also be able to take this role, which is worth further investigation.

The maximum accumulation of Ca^{2+} in ALE under the tested conditions was around 700 µmol/g VSS (solid organic matter), which was reached for Ca^{2+} concentrations of 8 mM and higher. From the Donnan equilibrium analyses, it followed that the amount of fixed negative charges on the used ALE polymers was about 1 mmol/ g VSS. These values were in line with the available literature data on the maximum Ca^{2+} binding capacity of ALE.

The density of the gel layers showed a clear dependence on the $CaCl_2$ concentration of the supernatant, but not on the KCl concentration nor on the ionic strength. Ca^{2+} delayed swelling of the network and the slow rearrangement of the ALE polymers resulting in a heterogeneous open structure. In the range of the experimental conditions, only little effect of the $CaCl_2$ concentration on the specific cake-layer resistance was observed. Specifically, the density played a smaller role than expected, while the influence of the feed solutions' composition appeared more prominent.

Undoubtedly, more factors affect the system than could be addressed in this study. For further insight into the ripening mechanism, the development of the network structure of the gel layers could be investigated using techniques with higher resolutions than OCT. To find rational ways to control biofouling based on the experimental approach used here, the next steps could be the determination of the mechanical and adhesion properties of the gel layers and relation of these to their composition. Once this is possible, the complexity of the system can be step by step increased to identify the roles of different constituents.

Appendix

Tables 3-A: Ion concentrations measured in gel layers [mM] directly after filtration has finished.

Ca^{2+}

Ca^{2+} [mM]→ K^+ [mM] ↓	**1**	**3**	**6**	**8**	**12**	**14**
24	-	-	33.8 ± 0.2	-	-	-
15	-	35.5 ± 1.4	32.8 ± 0.7	-	-	-
6	-	45.5 ± 3.1	43.8 ± 4.2	53.2 ± 2.0	54.1 ± 1.4	-
0	24.3 ± 0.5	42.1 ± 1.8	45.0 ± 1.1	56.0 ± 0.4	-	62.4 ± 1.7

K^+

Ca^{2+} [mM]→ K^+ [mM] ↓	**1**	**3**	**6**	**8**	**12**	**14**
24	-	-	36.9 ± 1.2	-	-	-
15	-	32.2 ± 4.8	25.4 ± 3.3	-	-	-
6	-	25.0 ± 1.8	25.4 ± 7.6	16.2 ± 1.9	23.9 ± 6.8	-
0	1.6 ± 0.5	1.0 ± 0.4	13.0 ± 7.0	2.5 ± 0.5	-	1.7 ± 0.1

Tables 3-B: Ion concentrations measured in gel layers after 12 d of storage [mM].

Ca^{2+}

Ca^{2+} [mM]→ K^+ [mM] ↓	**1**	**3**	**6**	**8**	**12**	**14**
24	-	-	22.3 ± 1.7	-	-	-
15	-	14.2 ± 0.2	25.0 ± 2.6	-	-	-
6	-	13.3 ± 1.8	25.6 ± 1.9	30.4 ± 0.5	37.9 ± 0.6	-
0	8.4 ± 1.1	13.7 ± 1.5	29.2 ± 2.4	38.6 ± 2.5	-	50.5 ± 3.6

K^+

Ca^{2+} [mM]→ K^+ [mM] ↓	**1**	**3**	**6**	**8**	**12**	**14**
24	-	-	43.8 ± 10.2	-	-	-
15	-	15.1 ± 0.5	20.4 ± 7.0	-	-	-
6	-	9.1 ± 1.2	14.6 ± 2.1	14.3 ± 2.7	18.1 ± 5.9	-
0	5.6 ± 2.5	1.8 ± 0.7	3.8 ± 1.0	5.0 ± 1.2	-	6.9 ± 4.6

Tables 3-C: Ion concentrations measured in gel layers [µmol/g VSS] directly after filtration has finished.

Ca^{2+}

Ca^{2+} [mM]→ K^+ [mM] ↓	**1**	**3**	**6**	**8**	**12**	**14**
24	-	-	380 ± 3	-	-	-
15	-	365 ± 15	413 ± 16	-	-	-
6	-	426 ± 34	459 ± 29	533 ± 16	585 ± 5	-
0	391 ± 4	520 ± 6	521 ± 1	550 ± 1	-	602 ± 3

K^+

Ca^{2+} [mM]→ K^+ [mM] ↓	**1**	**3**	**6**	**8**	**12**	**14**
24	-	-	415 ± 13	-	-	-
15	-	332 ± 50	317 ± 23	-	-	-
6	-	234 ± 19	299 ± 109	166 ± 17	261 ± 79	-
0	26.5 ± 7.1	18.8 ± 6.1	152 ± 84	24.8 ± 4.8	-	16.6 ± 1.4

Tables 3-D: Ion concentrations measured in gel layers [µmol/g VSS] after 12 d of storage.

Ca^{2+}

Ca^{2+} [mM]→ K^+ [mM] ↓	**1**	**3**	**6**	**8**	**12**	**14**
24	-	-	401 ± 33	-	-	-
15	-	379 ± 8	487 ± 28	-	-	-
6	-	369 ± 50	496 ± 49	536 ± 22	644 ± 26	-
0	220 ± 22	322 ± 10	534 ± 8	566 ± 17	-	729 ± 37

K^+

Ca^{2+} [mM]→ K^+ [mM] ↓	**1**	**3**	**6**	**8**	**12**	**14**
24	-	-	785 ± 171	-	-	-
15	-	403 ± 1	400 ± 136	-	-	-
6	-	237 ± 41	283 ± 44	252 ± 54	305 ± 95	-
0	146 ± 64	41.7 ± 17.1	71.0 ± 21.0	74.9 ± 22.0	-	101 ± 68

Table 3-E: Specific cake layer resistance at the end of filtration [10^{15} m/kg]

Ca^{2+} [mM]→ K^+ [mM] ↓	**1**	**3**	**6**	**8**	**12**	**14**
24	-	-	8.21 ± 0.76	-	-	-
15	-	7.23 ± 0.49	7.34 ± 0.32	-	-	-
6	-	6.25 ± 0.28	8.25 ± 0.40	8.34 ± 0.76	8.82 ± 1.06	-
0	7.68 ± 0.24	8.56 ± 0.42	8.26 ± 0.40	8.63 ± 0.89	-	9.64 ± 0.45

Tables 3-F: Activity coefficients [-] of the original filtration solutions.

Ca^{2+}

Ca^{2+} [mM]→ K^+ [mM] ↓	**1**	**3**	**6**	**8**	**12**	**14**
24	-	-	0.50	-	-	-
15	-	0.57	0.53	-	-	-
6	-	0.63	0.57	0.55	0.50	-
0	0.79	0.69	0.61	0.57	-	0.50

K^+/Cl^-

Ca^{2+} [mM]→ K^+ [mM] ↓	**1**	**3**	**6**	**8**	**12**	**14**
24	-	-	0.81	-	-	-
15	-	0.85	0.83	-	-	-
6	-	0.88	0.85	0.84	0.82	-
0	0.94	0.90	0.87	0.85	-	0.82

H^+

Ca^{2+} [mM]→ K^+ [mM] ↓	**1**	**3**	**6**	**8**	**12**	**14**
24	-	-	0.86	-	-	-
15	-	0.87	0.87	-	-	-
6	-	0.90	0.88	0.87	0.86	-
0	0.95	0.92	0.89	0.88	-	0.86

Tables 3-G: Cl^- activities [mM] in the ALE gel layers calculated from Ca^{2+} concentrations.

immediately

Ca^{2+} [mM]→ K^+ [mM] ↓	**1**	**3**	**6**	**8**	**12**	**14**
24	-	-	13.8 ± 0.1	-	-	-
15	-	6.2 ± 0.1	10.9 ± 0.1	-	-	-
6	-	3.4 ± 0.1	6.8 ± 0.4	8.6 ± 0.2	13.4 ± 0.2	-
0	0.5 ± 0.0	1.9 ± 0.0	4.7 ± 0.1	6.3 ± 0.0	-	12.7 ± 0.2

After 12 d of storage

Ca^{2+} [mM]→ K^+ [mM] ↓	**1**	**3**	**6**	**8**	**12**	**14**
24	-	-	14.1 ± 0.5	-	-	-
15	-	8.1 ± 0.1	10.5 ± 0.5	-	-	-
6	-	5.1 ± 0.3	7.3 ± 0.3	9.1 ± 0.1	12.7 ± 0.1	-
0	0.7 ± 0.0	2.7 ± 0.1	4.8 ± 0.2	6.1 ± 0.2	-	11.1 ± 0.4

Chapter 4

Rheological characterization of alginate-like exopolymer gels crosslinked with calcium

Internally gelled bacterial alginate-like exopolymers (ALE) gels were used in this work as a model for the extracellular polymeric matrix of biofilms, to gain insight into the complex cohesive molecular interactions that make biofilms as persistent to cleaning as they are. Mechanical properties of the gels as a function of $CaCO_3$ concentration were investigated using dynamic and static rheology. Gels with relatively low $CaCO_3$ concentrations, between 100 µmol and 300 µmol per g ALE, were found to exhibit similar viscoelastic behaviour as real biofilms, with elastic moduli between 50 Pa and 100 Pa and dissipation factors between 0.2 and 0.3. Increasing $CaCO_3$ concentrations in combination with a successive increase of non-ALE VSS involved an increase of the elastic modulus up to 250 Pa, accompanied by an increase in brittleness. At a $CaCO_3$ ion concentration of 1250 µmol per g ALE, this trend stopped, probably due to disturbance of the continuous ALE network by calcium salt precipitation. This disturbance can be an approach for future removal of biofouling using overdosing of salts. All gels exhibited permanent strain hardening under medium strain, and their mechanical properties showed dependency on their strain history. Even after application of an oscillatory strain with 200 % amplitude that caused the gel structure to collapse, the gels recovered 65 % to 90 % of their original shear modulus, for the major part within about 20 s. Recovery was slightly less for gels with high $CaCO_3$ content. In creep tests fitted with a Burgers model with multiple Kelvin elements at least three different interactions in the ALE gels could be distinguished with characteristic retardation times in the range of 10 s, 100 s and 1000 s. Further identification of the mechanisms underlying the gel mechanics will allow the development of targeted strategies to undermine the mechanical strength of biofouling, and aid their removal.

4.1 Introduction

Biofouling is the term commonly used for the unfavourable attachment and biofilm formation of bacterial communities on wetted surfaces such as ship hulls, pipelines, membranes or implants. Because of the negative impact exerted on industrial membrane processes (Flemming, 2002; Herzberg, Kang and Elimelech, 2009), water distribution systems (Bachmann and Edyvean, 2005) and in the medical field (Donlan, 2001; Bryers, 2008), biofouling has been a topic of investigation for several decades. While the complete chemical composition of biofilms is as diverse as the bacterial communities and in most cases not easy to determine, there is a distinction between two main components: the bacteria and the matrix of extracellular polymeric substances (EPS) (Geesey, 1982; Christensen, 1989; Donlan, 2002; Flemming, 2020). The latter can make up to 90% of the biofilms' organic matter (Wingender, Neu and Flemming, 1999). Polysaccharides, proteins, lipids, humic substances and eDNA (Lin *et al.*, 2014; Hobley *et al.*, 2015; Seviour *et al.*, 2019) have been identified as major components of the EPS. Together they provide a physically crosslinked 3D molecular network with the ability to incorporate, in addition to the bacterial cells, high amounts of water. As such, biofilms can be treated as complex hydrogels (Mayer *et al.*, 1999; Körstgens *et al.*, 2001; Galy *et al.*, 2012; Dreszer *et al.*, 2013; Lin, Sharma and van Loosdrecht, 2013).

The EPS matrix acts as a protective shield for the bacteria against biological, chemical and mechanical influences as well as desiccation (Flemming and Wingender, 2010). It has been shown to considerably reduce the effectivity of biocides (Smalley, Hansen and Baselski, 1983; Gristina *et al.*, 1987; LeChevallier, Cawthon and Lee, 1988; Donlan, 2001). On top of that, it is responsible for the mechanical strength and integrity of biofilms (Mayer *et al.*, 1999; Flemming and Wingender, 2001).

The mechanical properties of biofilms have been found to stay mostly intact even if the bacterial cells are killed (Flemming *et al.*, 1997; Chen and Stewart, 2000; Davison, Pitts and Stewart, 2010; Jones *et al.*, 2011; Zrelli *et al.*, 2013). Therefore, the EPS matrix and its mechanical strength have become a crucial topic when it comes to cleaning strategies against biofouling (Ang, Lee and Elimelech, 2006; Möhle *et al.*, 2007; Powell *et al.*, 2013; Safari *et al.*, 2015). In its definition as the biofilms' ability to resist physical forces, like the shear stress from water flowing over it, the mechanical strength involves two aspects: the adhesion to the surface on the one hand, and the internal cohesion, often described by the viscoelasticity (Galy *et al.*, 2012; Safari *et al.*, 2015; Ferrando Chavez, Nejidat and Herzberg, 2016), on the other hand. Biofilms show the typical viscoelastic behaviour of crosslinked polymer networks (Stoodley *et al.*, 2001; Lieleg *et al.*, 2011). In contrast to covalently bound networks, the crosslinks in biofilms have for the most part been identified as physical interactions such as van-der-Waals forces, hydrogen bonds, electrostatic interactions including ion bridges, and entanglements (Mayer *et al.*, 1999). The viscoelastic properties of biofilms have also been

directly linked to the persistence of bacteria in medical infections (Peterson *et al.*, 2015; Gloag *et al.*, 2018). Therefore, their investigation is attractive from several perspectives.

Cohesion and adhesion are closely related and follow from the molecular interactions within the EPS and with the environment. Especially for thin films, like many biofilms are, both properties can hardly be separated (Safari *et al.*, 2015). It stays a relevant question in biofouling research if mechanical removal of biofilms from the substrate on which they were formed, which is often practised for investigation, does not alter the actual characteristics that are meant to be investigated (Guelon, Mathias and Stoodley, 2011).

To overcome adhesion and cohesion of a biofilm, the most successful cleaning strategies are expected to be a combination of a weakening of the structure (by attacking or disturbing the molecular interactions) and mechanical removal (Meyer, 2003; Bereschenko *et al.*, 2011; Brindle, Miller and Stewart, 2011). In many cases, the practical application of cleaning agents today is based on experiences, following a trial-and-error approach (e.g. (Chen and Stewart, 2000; Simões, Pereira and Vieira, 2005; Ang, Lee and Elimelech, 2006; Brindle, Miller and Stewart, 2011)). Understanding how a chemical treatment works on a molecular basis and what effects it has on the mechanical removability would allow for a more rational search for optimal cleaning agents and doses (Ang, Lee and Elimelech, 2006).

'Alginate-like exopolymers' (ALEs) have been identified as a representative group of bacterial exopolymers. Because ALEs were found providing structural integrity to granular sludge (Lin *et al.*, 2008) and biofilms (Lin, Sharma and van Loosdrecht, 2013), they were chosen in this study as a model for the EPS matrix to investigate the mechanical properties of biofilms. Like its eponymous, well-characterized algal equivalent alginate, this mixture of exopolymers can form gels with the calcium ion Ca^{2+} (Lin *et al.*, 2008; Felz *et al.*, 2016). As such, ALE provides an interim stage between the often used biofilm model component algal alginate (Wloka *et al.*, 2004; Katsoufidou, Yiantsios and Karabelas, 2007; van de Ven *et al.*, 2009; van den Brink, 2014), and the complex, real-world biofilm EPS. This work focused on the cohesive strength of ALE gels as a function of Ca^{2+} content by measuring their viscoelastic properties. The cohesion was chosen over the adhesion to address the molecular interactions within the gels. To minimize the impact of adhesion, thick gel structures were produced, and maximum adhesion (no slip) between the samples and the rheometer was ensured. Ca^{2+} is important for adhesion and strength of many biofilms (Herzberg, Kang and Elimelech, 2009; Goode and Allen, 2011; Safari *et al.*, 2014). Therefore, it was used as the simplest chemical variable in the applied setup to gain knowledge on the intermolecular interactions within the ALE samples.

4.2 Materials and Methods

4.2.1 ALE extraction

Because of the high ALE content of granular sludge, the material was extracted from Nereda® sludge collected from the wastewater treatment plant in Garmerwolde, the Netherlands (Pronk

et al., 2015). The extraction was done in alkaline conditions, followed by acid precipitation, based on a protocol by Felz et al. (Felz *et al.*, 2016).

The granules were collected by decantation. In 1 L demineralised water ca. 150 g of the wet granules (20 g dry weight) were mixed with 10 g sodium carbonate (VWR, the Netherlands) and homogenised by pulsed sonication (Branson Sonifier 250, 5 min at 70 %, max output 200 W). In the course of the sonication, the mixture was cooled on an ice bath to prevent overheating. Subsequently, the alkaline extraction step was performed by heating the mixture to 80 °C for 30 min under vigorous stirring. The pellet was discarded after centrifugation (Allegra X-12R Centrifuge, Beckman Coulter, 20 min, 3750 rpm). The supernatant was dialysed in 4-6 steps using a Spectra/Por® Dialysis Membrane with a cut-off of 3.5 kDa, each against 20 L demineralised water until the conductivity in the dialysis solution was below 50 µS/cm. Subsequently, the extract was acidified with 1 M hydrochloric acid (Merck Millipore, Germany) to pH 2 – 2.5. After another centrifugation (Allegra X-12R Centrifuge, Beckman Coulter, 20 min, 3,750 rpm) the pellet was collected, lyophilised (ALPHA 2-4 LDplus, Christ, Germany) and stored at room temperature until further use. It is henceforth referred to as ALE.

ALE has been found to have similar behaviour to brown algal alginate (Lin *et al.*, 2010). Therefore, the gelling test proposed for alginate was adapted for the ALE extract (Felz *et al.*, 2016). Before lyophilising, the material was dissolved and neutralised with 1 M NaOH (Merck Millipore, Germany). The solution then was added dropwise to a 2.5 wt% $CaCl_2$ solution. Gelling was successful if the droplets visually formed beads in the solution rather than dissolving.

4.2.2 Sample preparation

Gels were produced by internal gelation (Draget, Østgaard and Smidsrød, 1989; Davidovich-Pinhas and Bianco-Peled, 2010), using $CaCO_3$ as a Ca^{2+} source, slowly released by glucono-δ-lactone (GdL). In contrast to the fast gelling with $CaCl_2$, this procedure promised the slow production of homogeneous gels. Based on the concentrations found in ALE films formed on membranes (between 4 wt% and 5 wt% ALE content after swelling, with 300-500 µmol Ca^{2+}/g ALE, cf. Ch. 3), the final concentrations were set to 40 g/L ALE and 5, 12.5, 25, 50 and 100 mM $CaCO_3$ (see Table 4-1). A molar ratio of 2:1 was applied between GdL and $CaCO_3$.

Table 4-1: Nominal concentrations of the ALE gels of this study.

	$CaCO_3$ [mmol]	**ALE [g/L]**	**Ca^{2+}: ALE [µmol/g]**
A	5	40	125
B	12.5	40	312.5
C	25	40	625
D	50	40	1250
E	100	40	2500

The lyophilised ALE was dissolved in 1 M NaOH (Merck Millipore, Germany), and diluted with demineralised water to a final concentration of 50 g/L. The resulting solution was neutralized using a little more NaOH. 10 times concentrated stock suspensions of $CaCO_3$ (anhydrous, reagent grade, VWR, the Netherlands) were prepared by adding the necessary amount of $CaCO_3$ to demineralised water and putting them in an ultrasonic bath (Bandelin, Sonorex Technik) for 10 min. GdL solutions were prepared, also ten times more concentrated than the final one, by dissolving the necessary amount of glucono-δ-lactone (Sigma-Aldrich, France) in demineralised water. The three stock solutions of ALE, $CaCO_3$, and freshly prepared GdL were mixed in a volume ratio of 8:1:1. Portions of 1.5 mL were immediately pipetted into moulds (see Fig. 4-1A). Gelling took place in sandpaper (grit size P180, waterproof, Sencys, the Netherlands) lined disposable rheometer dishes (Anton Paar, 56 mm). The gel dimensions were determined by stencils of 30 mm in diameter. The samples were left for crosslinking at room temperature in a sealed plastic box partly filled with water, providing 100 % humidity for 36 h. Before starting the mechanical measurements, the stencils were removed, and the surfaces and heights of the gels were equalised by cutting them to 1 mm height using a 1 mm frame of the same size as the stencils, and a razor blade. By using the lowest layers, the effect of possible draining was minimised.

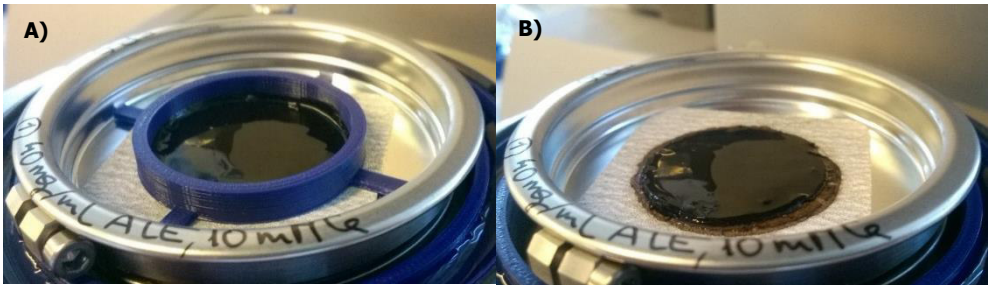

Figure 4-1: ALE-gels were prepared in sandpaper lined disposable rheometer dishes. (A) including the stencil, (B) after removing the stencil.

4.2.3 Chemical characterisation

Crosslinked ALE-gel samples were scratched and weighed into dry porcelain crucibles (m_{sample}). After heating to 105 °C for 24 h, the dry mass (total suspended solids, TSS) was determined. The samples were then burnt at 550 °C for 2 h to remove the organic matter (volatile suspended solids, VSS). The dry mass, the water content and the organic mass VSS were calculated according to the following equations.

$$m_{water} = m_{sample} - TSS \quad (4\text{-}1)$$

$$VSS = TSS - m_{ash} \quad (4\text{-}2)$$

m_{ash} represents the mass after heating to 550 °C. The VSS amount was interpreted as ALE, while the ash was interpreted as the inorganic content of the material. The VSS density ρ_{VSS} was calculated as VSS per V_{water}, under the assumption that for water 1 g ≙ 1 mL.

4.2.4 Rheological measurements

Rheological characterisation of the samples was performed using an MCR 102 Rheometer (Anton Paar) with a 25 mm plate-plate geometry.

Before the start of every measurement, the upper plate was provided with clean sandpaper, and the zero-height and measurement system inertia were recalibrated. The sample surface was approached by lowering the upper plate until a normal force of 0.15 N was observed for the first time. Corresponding to ca. 300 Pa this was in the range of the expected moduli already, to make sure it was really the sample surface detected. Subsequently, the samples were trimmed and left equilibrating until the normal force remained below 0.05 N. Tests in the linear viscoelastic region (LVER), applying several of these approaching procedures with the sequence of slight compression and equilibration, resulted in identical measurements. The procedure had apparently no impact on the results. A 3D-printed liquid trap was used to avoid evaporation of water during the measurements.

4.2.4.1 Amplitude sweeps

Oscillating measurements were performed in triplicates at an angular frequency ω of 10 rad/s with exponentially increasing amplitudes between 0.01 % and 250 % shear strain (ε). The strain was defined as the displacement in relation to the sample thickness. From the resulting torque, measured by the instrument, the corresponding average shear stress σ on the sample was extracted. The ratio between shear stress σ and shear strain ε is defined as the complex modulus G^*.

$$G^* = \frac{\sigma}{\varepsilon} \qquad (4\text{-}3)$$

Combined with the phase shift δ, the complex modulus G^* was subsequently split into the real component G', representing the storage modulus, and the imaginary component G'', representing the loss modulus. For a given strain, these moduli signified how much of the applied stress was stored elastically, and how much was lost by dissipation. The ratio between storage modulus G' and loss modulus G'', $\tan\delta$, is also referred to as the dissipation factor.

$$\tan\delta = \frac{G''}{G'} \qquad (4\text{-}4)$$

A representative example of an amplitude sweep is shown in Figure 4-2. It can be seen that at lower strains, up to ca 10 %, the moduli were independent of the applied strain and stress. This region, in which this independence is valid, is referred to as the linear viscoelastic region

(LVER), where no permanent damage is done to the structure of the sample. It was defined as the region where the modulus values did not differ more than 5 % from the average. The storage and loss moduli in the LVER were determined for each sample.

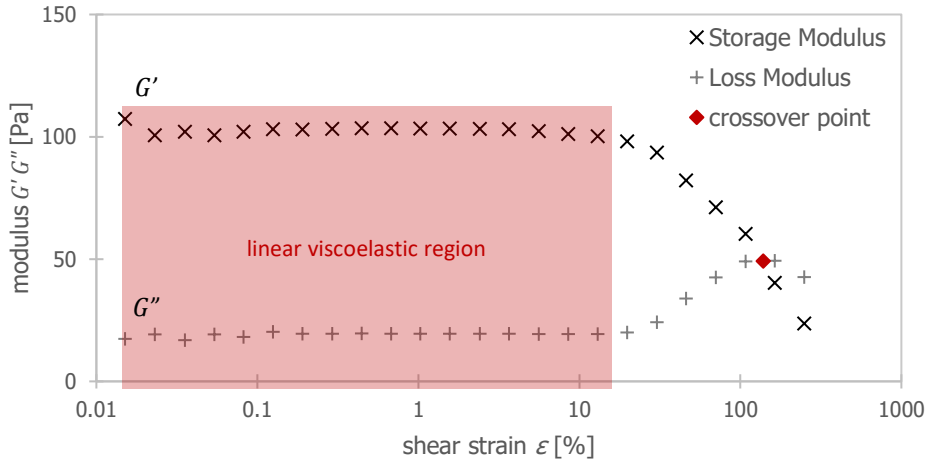

Figure 4-2: Typical amplitude sweep for a 40 g/L ALE, 12.5 mM $CaCO_3$ gel. The linear viscoelastic region and the crossover point are highlighted.

Within the viscoelastic region in Figure 4-2, G' was much higher than G'', meaning that the material's behaviour was predominantly elastic ($\tan \delta < 1$). Towards higher strains, G' and G'' approached each other and finally crossed. Eventually, G'' dominated the material's behaviour. In this case, the material was considered 'flowing'. The so-called crossover point ($G' = G''$) therefore was a practical indicator for the force necessary to move the material. It meant that the network structure was broken. The strains and stresses at the crossover points were also determined as a function of the $CaCO_3$ concentration. Note that beyond the LVER regime, the material response was not necessarily linear anymore so that the crossover point could depend on specifics of the protocol (e.g. the number of oscillations used per data point).

4.2.4.2 Frequency sweeps

After determination of the LVER during the amplitude sweeps, frequency sweeps were performed for some gels at 0.3 % strain (inside the LVER) with angular frequencies ω between 100 and 1 rad/s. Like in the amplitude sweeps, the resulting torque was translated into a complex modulus by the internal software, which eventually determined the storage modulus G' and loss modulus G''.

4.2.4.3 Recovery after oscillatory strain

The recovery capacity of the gels was investigated by observing the storage and loss moduli during application of different oscillatory strains (10 rad/s). Again, all experiments were performed in triplicate. As reference and baseline, a strain amplitude of 0.3 % was used, which

was well within the LVER. Strain amplitudes of 10 %, 30 % and 200 % were applied for 120 s each, followed by 400 s recovery at 0.3 % strain.

4.2.4.4 Creep-recovery tests

To investigate the response of the gels to continuous stresses, creep-recovery tests were performed in triplicate. A constant shear stress σ of 10 Pa, found to be inside the LVER for all samples, was applied for 300 s and the strain ε was monitored. Subsequently, the stress was removed, and the strain was monitored for another 600 s. A representative measurement is shown in Figure 4-3.

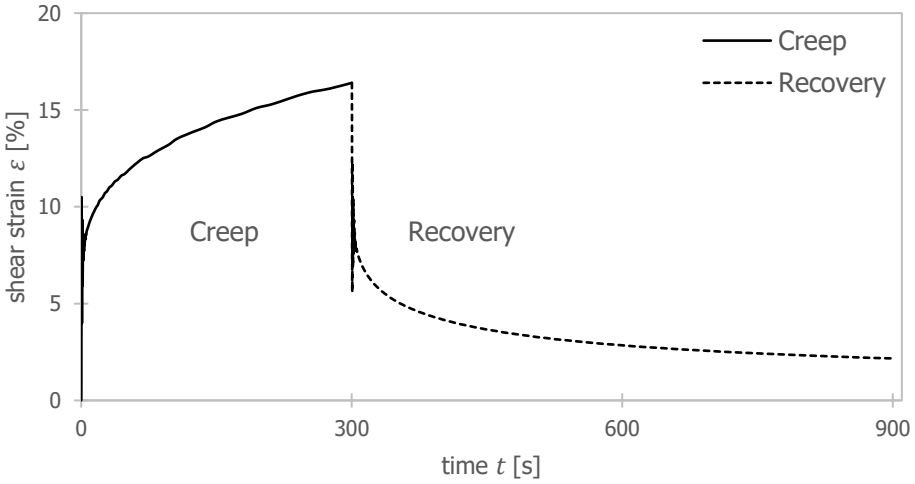

Figure 4-3: Overview of a creep-recovery experiment on a 25 mM $CaCO_3$ ALE gel. Monitored is the shear strain ε during application of a constant stress σ of 10 Pa, and subsequent removal of this stress.

Because of creep ringing (the initial 'overshooting' visible in Figure 4-3 at the first application of the stress), the first 5 s of each step were not included in the analysis. The creep was interpreted using the Burgers model, which has been successfully applied to describe the viscoelastic behaviour of biofilms (Vinogradov *et al.*, 2004; Jones *et al.*, 2011).

An indefinite number of Kelvin elements was allowed for the Burgers fit (Cooper, 2002). The ALE gels were described as a series of a Maxwell element, consisting of a spring (describing the elastic jump at the beginning of the curve), and a dashpot (describing the viscous response, represented by the linear increase at the end of the creep curve), and an indefinite number of Kelvin elements, consisting of parallel spring-dashpot pairs (see Fig. 4-4 and Eq. 4-5).

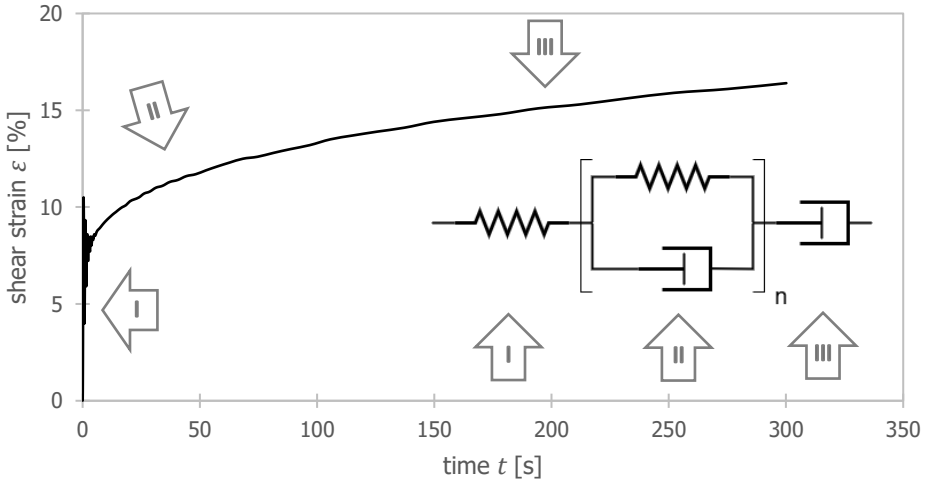

Figure 4-4: Analysis of a creep step. The mechanical analogy to the ALE's behaviour according to the Burgers model with multiple Kelvin elements is shown: the initial jump upon application of the stress is depicted by an elastic spring (I), while the steady incline towards the end is described by a dashpot (III). The intermediate curvature can be described by n pairs of parallel springs and dashpots (II).

$$\varepsilon_{creep}(t) = \frac{\sigma}{G_0} + \sum_n \frac{\sigma}{G_{K,n}} \cdot \left(1 - \exp\left(-t \cdot \frac{G_{K,n}}{\eta_{K,n}}\right)\right) + \frac{\sigma}{\eta_0} \cdot t \qquad (4\text{-}5)$$

ε_{creep} was the shear strain measured over time t under application of a constant shear stress σ. G_0 was the initial elastic modulus, η_0 the viscosity, and $G_{K,n}$ and $\eta_{K,n}$ the elastic moduli and viscosities of each Kelvin element n.

The retardation time τ was a measure for the delay in the material's full elastic response to applied stress, caused by its viscous elements. The characteristic retardation time τ of each Kelvin element was represented by the ratio between the viscosity and the elastic modulus. It depicted the time after which 63 % of the maximum strain of the element was reached:

$$\tau_{K,n} = \frac{\eta_{K,n}}{G_{K,n}} \qquad (4\text{-}6)$$

Similarly, for a simple Maxwell liquid, the characteristic relaxation time was given by

$$\tau_M = \frac{\eta_0}{G_0} \qquad (4\text{-}7)$$

Also for materials with a more complicated stress relaxation, like the investigated case, this equation was a reasonable estimate, with τ_M representing the longest retardation time in the system.

4.3 Results and Discussion

4.3.1 Swelling state and syneresis

The ALE gels were prepared with equal amounts of ALE, but different amounts of $CaCO_3$ and glucono-δ-lactone (GdL). GdL hydrolysed in water forming gluconic acid, which added to the final *VSS*. Estimating a constant amount of water of 1000 g/L and a stable amount of other salts of 1.64 mg/L, Table 4-2 shows the composition of the samples at the beginning of the gelling process.

Table 4-2: ALE, Ca^{2+} and gluconic acid content, calculated for the gels from the initial sample compositions.

	ALE		**Ca^{2+}**		**Gluconic acid**	
	[g/L]	[wt%]	[g/L]	[wt%]	[g/L]	[wt%]
5 mM $CaCO_3$	40	3.83	0.20	0.02	2.0	0.19
12.5 mM $CaCO_3$	40	3.82	0.50	0.05	4.9	0.47
25 mM $CaCO_3$	40	3.80	1.00	0.10	9.8	0.93
50 mM $CaCO_3$	40	3.76	2.00	0.19	19.6	1.84
100 mM $CaCO_3$	40	3.69	4.00	0.37	39.2	3.61

The ALE gels were left for gelling in a 100 % humidity environment to avoid evaporation. It can be observed in Figure 4-5 that the final gel composition of *VSS* and water differed from the original sample composition. Salts have been neglected in this observation because they provide only 0.5 wt% (cf. Table 4-2).

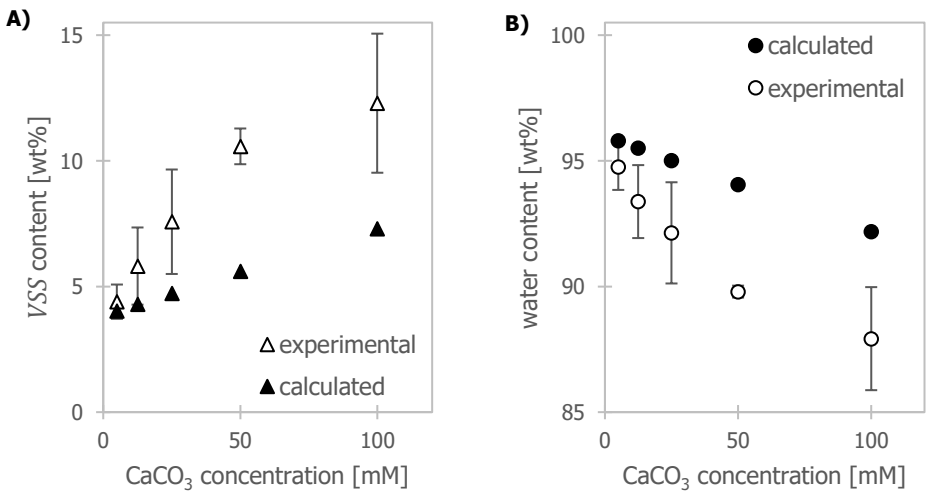

Figure 4-5: (A) VSS and (B) water content of the different ALE gels as a function of $CaCO_3$ concentration, after 36 h gelation in 100 % humidity. The empty markers depict the measured data, the full markers the calculated initial compositions of the samples. The error bars show the standard deviation over the performed triplicates.

Only at 5 mM $CaCO_3$, the original composition was almost maintained. With increasing Ca^{2+}:ALE ratio, the ratio between VSS and water shifted towards the VSS. At first sight, this phenomenon might appear like an artefact following from evaporation of CO_2 as a decay product of $CaCO_3$. However, the contribution of theoretically evaporable CO_2 to the weight distribution was in the same range as that of Ca^{2+} (cf. Table 4-2), which was too little to explain the differences. Apparently, during and/or after the gelation water was expelled from the samples. This phenomenon is known as syneresis and has been described for several hydrogel systems, including Ca-alginate (Draget *et al.*, 2001; Kuo and Ma, 2001). It comes down to the contraction of the hydrogel network resulting from the molecular interactions inside (Bajpai, 2001). In physically crosslinked networks such as Ca-alginate, these interactions are mainly electrostatic like H-bonding and salt (ion) bridges, and entanglements.

As observed for the ALE gels in this work, syneresis in alginate gels increased with increasing $CaCO_3$ concentration (Davidovich-Pinhas and Bianco-Peled, 2010), indicating that the ALE network was getting more compact. The molecular mechanisms behind this are not yet fully understood. Possible explanations are a higher number of crosslinks (Grant *et al.*, 1973; Wang and Spencer, 1998; Kuo and Ma, 2001) or lateral association of the present crosslinks (Draget *et al.*, 2001; Hermansson *et al.*, 2016). Since the phenomenon was also observed above the assumed neutralization of negative charges in ALE around 20 mM Ca^{2+}, internal restructuring processes like the lateral association of crosslinks should be further considered with this regard. The result was a denser gel upon the addition of more $CaCO_3$, as illustrated in Figure 4-6. In this regard, ALE gels (see also Fig. 3-4) behaved similarly to alginate gels as well as to biofilms (Goode and Allen, 2011).

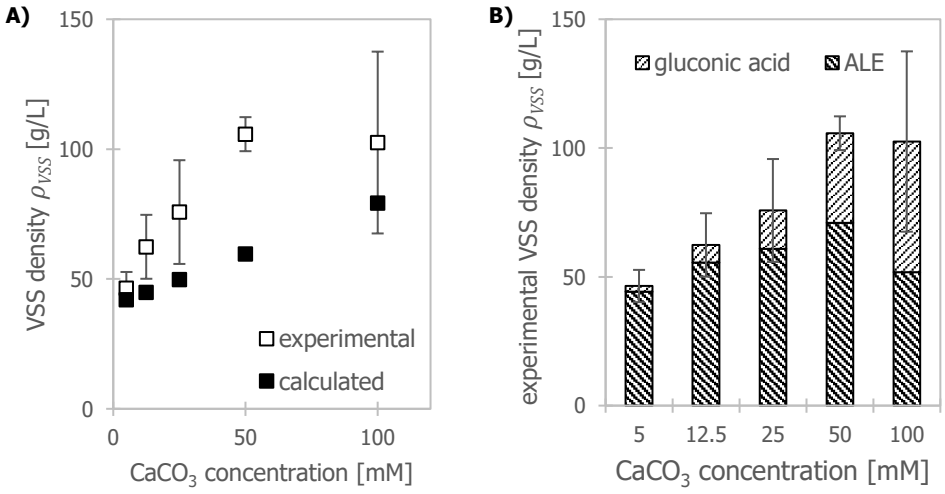

Figure 4-6: VSS density (A) inside the ALE gels and (B) split into the contribution from ALE and gluconic acid. The error bars depict the statistical error in the VSS content over the triplicates.

It has been observed for ALE films with varying $CaCl_2$ content prepared by dead-end filtration that the density reached a maximum around 550 µmol/g Ca^{2+}/ALE ratio (Ch. 3). The amount of Ca^{2+} in that system corresponded fairly well to 25 mM $CaCO_3$ in this study (625 µmol/g) and to the above-mentioned neutralization of negative ALE charges around 20 mM Ca^{2+}. In the current work, the VSS density increased further with the $CaCO_3$ content, up to 50 mM $CaCO_3$, and then levelled. For an analysis of this behaviour, the shift in the composition of the *VSS* needed to be taken into account. The fraction of gluconic acid increased parallel with increasing $CaCO_3$ concentration, as shown in Table 4-2. At the maximum, it reached almost 50 % of the *VSS*. Considering the density of the Ca-ALE network particularly, in this study a maximum was reached around 50 mM Ca^{2+} (Figure 4-6B). Reasons for the shift towards higher Ca^{2+} concentrations were probably the very different experimental systems.

Concerning the gluconic acid, it could be assumed that as a monomeric sugar it did not form a network by itself, but rather dissolved in the water phase, including the water that fills the pores in the ALE network. To what extent there were direct interactions with the ALE network was beyond the scope of this work. At neutral pH it is known to form weak, mononuclear complexes with Ca^{2+} (Pallagi *et al.*, 2010). As mentioned above, in the current experiments, the solubility product for calcium gluconate of 35 g^3/L^3 was only reached in ALE gels with 100 mM $CaCO_3$. It was, therefore, possible that precipitation of calcium gluconate caused inhomogeneity in addition to calcium carbonate precipitation, which could explain the decreasing density of the ALE network at very high concentrations. At the same time, the Ca-gluconate could be assumed to be denser, so that overall, both processes cancelled each other. For future research, the potential weakening of biofilms with the help of calcium precipitates (Kuo and Ma, 2001) appears to be an interesting aspect for cleaning studies. Another aspect to consider in this regard is that the presence of inorganic precipitates has furthermore been observed to reduce the hydraulic resistance of membrane biofilms (Chomiak *et al.*, 2014).

The ALE densities between 45 g/L and 70 g/L found for the gels in the present study agreed with those found for the ALE gel layers produced in dead-end filtration (Ch. 3).
The swelling state of hydrogels has been found to impact mechanical strength, adhesion, permeability and degradation (Davidovich-Pinhas and Bianco-Peled, 2010). Inversely, the viscoelastic properties in combination with gel size and permeability have been found responsible for syneresis (Scherer, 1989). Spontaneous syneresis as a reaction to increasing salt concentrations in the supernatant (due to screening of charges in the gel network) has been described as a possibly important mechanism of biofilm survival during desiccation (Decho, 2016). In this work, it was shown that gels made from bacterial ALE exhibited syneresis as a function of the Ca^{2+} content. As important influencing factors, the actual degree of crosslinking, the interaction with ions and the hydrophilicity of the material have been reported (Ganji, Vasheghani-Farahani and Vasheghani-Farahani, 2010). Research with a focus

on these topics appears interesting, also for better understanding the effect of adding other important ingredients of biofilms to ALE to mimic real biofilms.

4.3.2 Viscoelastic behaviour

For all samples, a linear viscoelastic region (LVER) was identified at lower strains (cf. Fig. 4-2) and the storage and loss moduli were determined. This was typical behaviour for polymers and has been observed for biofilms, too (Vinogradov *et al.*, 2004; Lieleg *et al.*, 2011; Patsios *et al.*, 2015). For all compositions, the storage modulus was the predominant factor in the LVER. This indicated that for all gels, at low strains, the elastic behaviour was more pronounced than the viscous one. In Figure 4-7 the storage moduli and dissipation factors in the linear elastic region are plotted as a function of the $CaCO_3$ concentration.

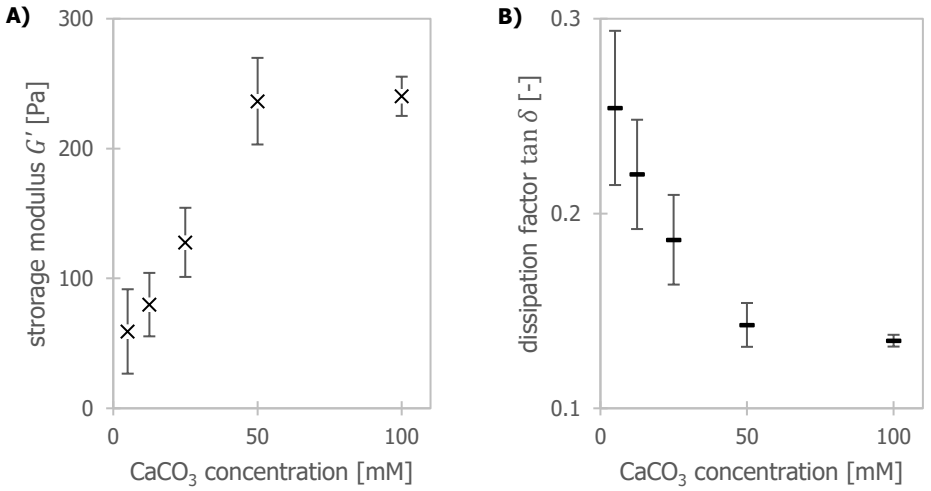

Figure 4-7: Storage moduli and dissipation factors extracted from amplitude sweeps of ALE gels as a function of $CaCO_3$ concentration. Error bars show the standard deviation over the performed triplicates.

The course of the storage modulus G' was fairly similar to that of the VSS density (cf. Fig. 4-6A). It increased with the $CaCO_3$ concentration until 50 mM, corresponding to a ratio of 1.25 mmol Ca^{2+} per g ALE. Above this concentration, a further increase in $CaCO_3$ did not result in an additional increase in the storage modulus. This could be explained by the conclusions drawn above for the binding of Ca^{2+} in the gels: While the maximum amount of bound negative charges was assumingly reached around 20 mM Ca^{2+}, above this concentration, the surplus Ca^{2+} seemed initially involved in further densification of the network, e.g. through the lateral association of the crosslinks. In this way, the number of crosslinks per volume further increased, so that the modulus increased. Depending on the phase and shape of the Ca^{2+}-gluconate compounds, it was also imaginable that they exerted a strengthening composite

effect on the gels. At 100 mM $CaCO_3$, though, the disturbing effect on the ALE network predominated, as can be seen by the decreasing ALE density (Fig. 4-6B).
The maximum storage modulus for 40 g/L ALE gels was found around 250 Pa. Preparation of Ca-ALE gel layers on membranes by dead-end filtration resulted in a maximum ratio of 550 µmol Ca^{2+}/g ALE (Ch. 3). A possible explanation for this difference (1.25 mmol Ca^{2+}/g ALE vs 500 µmol Ca^{2+}/g ALE) might be that in the filtration experiments Ca^{2+} that was not bound tight enough to the ALE was washed away. Besides, additional binding of Ca^{2+} to the chelating gluconic acid may play a role as well (Ramachandran *et al.*, 2006; Pallagi *et al.*, 2010). The generally positive correlation of the elastic modulus with $CaCO_3$ concentration corresponded with the expectation. Similar behaviour has been observed for alginate gels (Kuo and Ma, 2001; Kaklamani *et al.*, 2014) and biofilms (Körstgens *et al.*, 2001).

The dissipation factor was found between 0.3 and 0.2. It showed a trend analogous to the storage modulus: with increasing Ca^{2+} content, the domination of the elastic energy storage increased, but this trend flattened out above 50 mM $CaCO_3$. As mentioned before, it was assumed that the reason for this apparent limit was the saturation of the gels with Ca^{2+} and precipitation of calcium salts in the samples with 100 mM $CaCO_3$.
These observations were in agreement with earlier experiences, which indicate that gels with a dissipation factor less than 0.2-0.3 are more likely to exhibit syneresis (Mezger, 2014). The same interactions that caused an increase of the elastic modulus (e.g. an increasing number of crosslinks) also resulted in a contraction of the network, causing the liquid to be pressed out (Scherer, 1989). In the current work, syneresis was less pronounced at low (5-10 mM) $CaCO_3$ concentrations with dissipation factors above 0.2. The viscoelastic data obtained for these gels corresponded well with the few rheological experiments on intact biofilms. Shear storage moduli were found to be around 100 Pa for biofilms grown for 7 d on membranes in a membrane bioreactor (Patsios *et al.*, 2015), 100-400 Pa for different *P. aeruginosa* films grown in culture on membrane filters (Wloka *et al.*, 2005), and between 80 Pa and 200 Pa for biofilms of *S. mutans* grown in a rotating disk reactor (Vinogradov *et al.*, 2004). Also, the dissipation factors agreed with around 0.25 found for the MBR biofilms (Patsios *et al.*, 2015) and 0.27 (Powell *et al.*, 2013) found in *P. aeruginosa* films grown on media. For scraped biofilm material, storage moduli were in the same range as for biofilms from a wastewater treatment facility (Safari *et al.*, 2015). Others determined values an order of magnitude higher for biofilms grown on nanofiltration membranes in drinking water treatment (Houari *et al.*, 2011) and for *Pseudomonas aeruginosa* biofilms grown on culture media in the lab (Lieleg *et al.*, 2011). It appeared that the mechanical properties of the ALE gels in this work, especially at low Ca^{2+} concentrations, were representative for biofilms.

The composition (Ca^{2+}:ALE ratio and water content) of the gels in the current work with relatively low $CaCO_3$ concentration was in the range of the values achieved in the thin ALE gel layers created in dead-end filtration experiments (Ch. 3). It was, therefore, suggested that this

is the 'natural' composition that ALE induces under the given conditions. It may be noticed that also this composition was in a range with only little syneresis.

4.3.2.1 Time dependency

For additional insight into the ALE gel structure, frequency sweeps were performed. During this dynamic measurement, the effect of time on the viscoelastic behaviour of samples was investigated. Low frequencies represented slow motion and revealed long relaxation times. In contrast, high frequencies represented fast motion and revealed short relaxation times. Theories defining biofilms as viscoelastic fluids suggest that at long time scales (i.e. low frequencies) biofilms behave fluid-like (Klapper *et al.*, 2002; Vinogradov *et al.*, 2004; Wilking *et al.*, 2011). A representative measurement of our ALE gels is shown in Figure 4-8. The lowest frequency tested in the current work was 0.1 rad/s, corresponding to relaxation time-scales around 1 min. The absence of a cross-over point in this range implied that the ALE gels were crosslinked networks that were not broken at this timescale and the applied strains (all well within the LVER), meaning that the gels behaved mainly elastically.

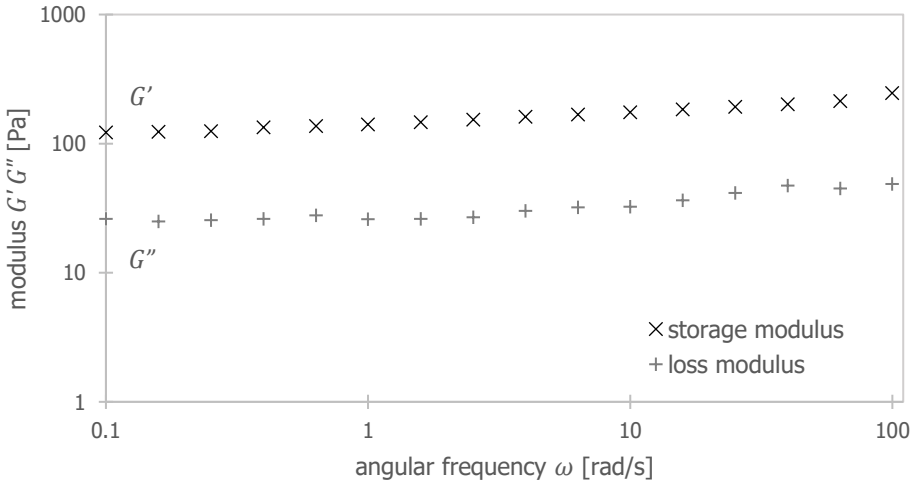

Figure 4-8: Storage and loss moduli over a frequency sweep, performed at 0.3% strain on a gel with 40 g/L ALE and 10 mM Ca^{2+}.

While the tests in oscillation mode were used to characterise the intact structure of the ALE gels, in most applications biofilms are exposed to continuous forces, for example to shear forces exerted by the water flow over a membrane. For further investigation of the long-time behaviour, creep-tests with continuous application of 10 Pa shear stress for 300 s were performed. The resulting strain was monitored. All recorded curves followed the concave shape presented in Figure 4-4, indicating viscoelasticity and the absence of ruptures.

The creep strain data over time was fitted according to Equation 4-5. The use of two Kelvin elements (n = 2 in Eq. 4-5) was found to be sufficient to fit all measurements. In Figure 4-9 a representative creep experiment with the corresponding Burgers fit is shown. While all data points were plotted, only those above 5 s were considered for the fit to avoid disturbance by creep ringing. Datasets containing the Maxwell elastic modulus (G_0) and viscosity (η_0) as well as the elastic moduli ($G_{K,1}$, $G_{K,2}$) and viscosities ($\eta_{K,1}$, $\eta_{K,2}$) of the Kelvin elements were derived (cf. Eq. 4-5). The latter ones were combined into the characteristic retardation times according to Equations 4-6 and 4-7.

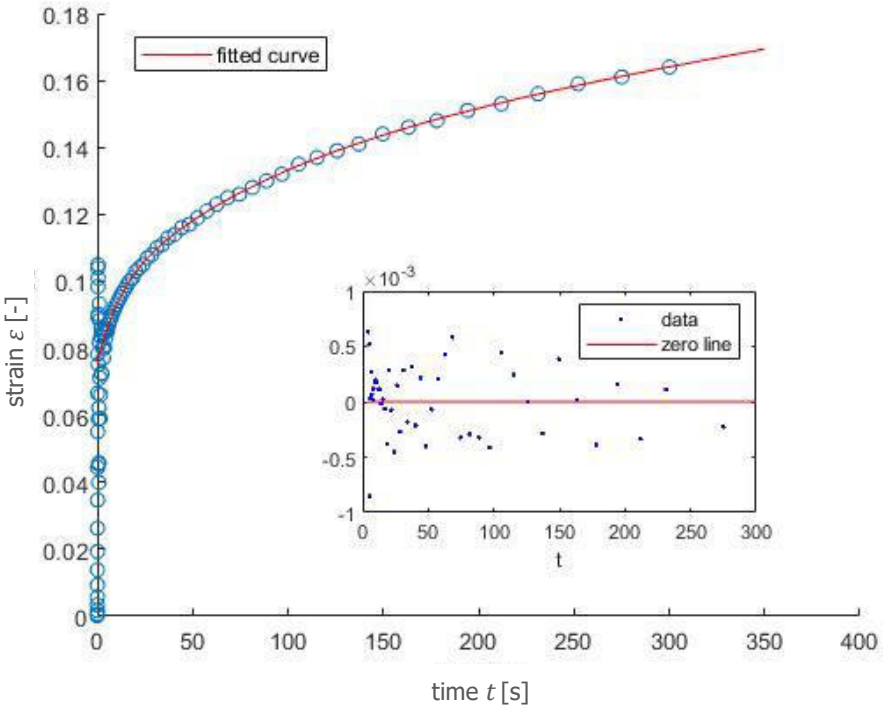

Figure 4-9: Experimental creep data and Burgers fit with multiple Kelvin elements allowed of an ALE gel containing 25 mM Ca^{2+}. The included graph shows the deviation of the data from the fit.

The Maxwell elastic moduli (Fig. 4-10A) were found in good agreement with the storage moduli from the amplitude sweeps (Figure 4-7). The viscosity was found following the same trend, increasing with calcium concentration (Fig. 4-10B).

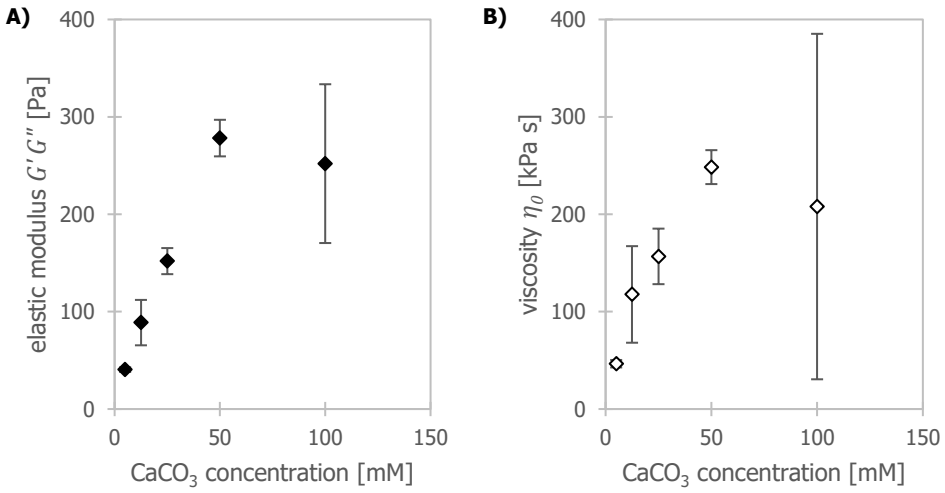

Figure 4-10: Elastic modulus (A) and viscosity (B) of the ALE gels, as derived from the generalised Kelvin model. Notice the linear increase in modulus for small $CaCO_3$ concentrations. The error bars show the standard deviation over the performed triplicates.

In Table 4-3, the characteristic retardation times extracted for the two Kelvin elements are shown as well as the estimated Maxwell retardation time. They were found all to be rather unaffected by changes in the Ca^{2+} concentration, and in the order of 10, 100 and 1000 s, respectively. Rather than depending on the Ca^{2+} concentration or strain, these characteristic times were only dependent on the type of interactions involved (Ehret and Böl, 2013).

Table 4-3: Characteristic retardation times of the different ALE gels, derived from creep experiments. Errors are the standard deviation over the triplicates.

	$\tau_{k,1}$ [s]	$\tau_{k,2}$ [s]	τ_M [s]
5 mM $CaCO_3$	12.3 ± 0.6	82.3 ± 4.1	1144 ± 22
12.5 mM $CaCO_3$	11.2 ± 0.7	85.2 ± 6.2	1203 ± 292
25 mM $CaCO_3$	12.2 ± 1.0	74.2 ± 11.7	950 ± 116
50 mM $CaCO_3$	10.8 ± 0.3	77.3 ± 3.2	901 ± 123
100 mM $CaCO_3$	6.3 ± 5.1	65.2 ± 19.3	741 ± 321

In Figure 4-11, it can be observed that after 5 min of creep the elastic deformation was still the dominating contribution to the strain (> 50 %). The two Kelvin elements together only contributed around 25 %. At this point, the maximum extension of the Kelvin elements could be considered to be reached, so that for longer timescales only the viscous contribution was expected to grow. On shorter timescales, the ratio shifted further towards domination of the elastic modulus G_0 (cf. Fig. 4-11B).

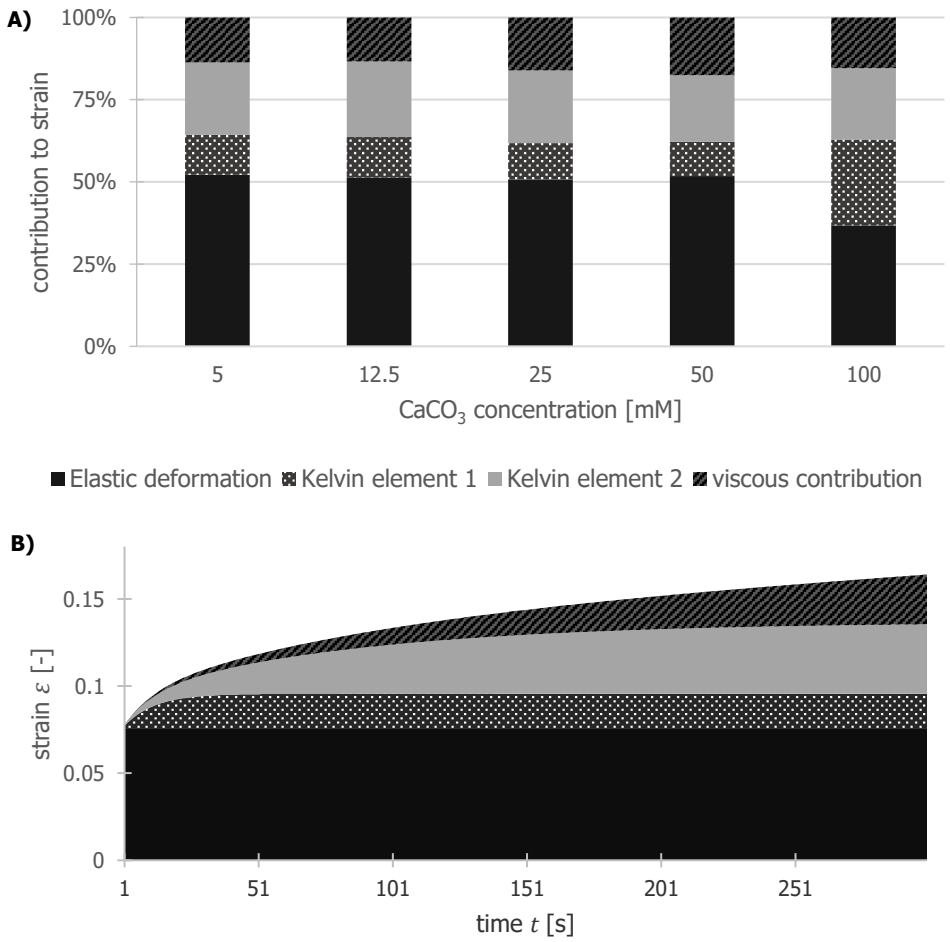

Figure 4-11: Contribution of the different elements to the final strain after the application of 10 Pa shear stress for 5 min. A) after 5 min for the different Ca^{2+} concentrations, B) for a 25 mM Ca^{2+} gel over time.

In Figure 4-12, the change in strain over time is compared for the creep and recovery steps of ALE gels with 5 mM Ca^{2+} (A) and with 25 mM Ca^{2+} (B). It can clearly be observed that with the same stress, a much larger strain was obtained in the gels with lower Ca^{2+} content. Also, differences in the recovery of the strain are visible. While in the 5 mM experiment the recovery strain graph differed from the creep graph from the beginning, in case of the 25 mM experiment they are identical up to ca. 30 s.

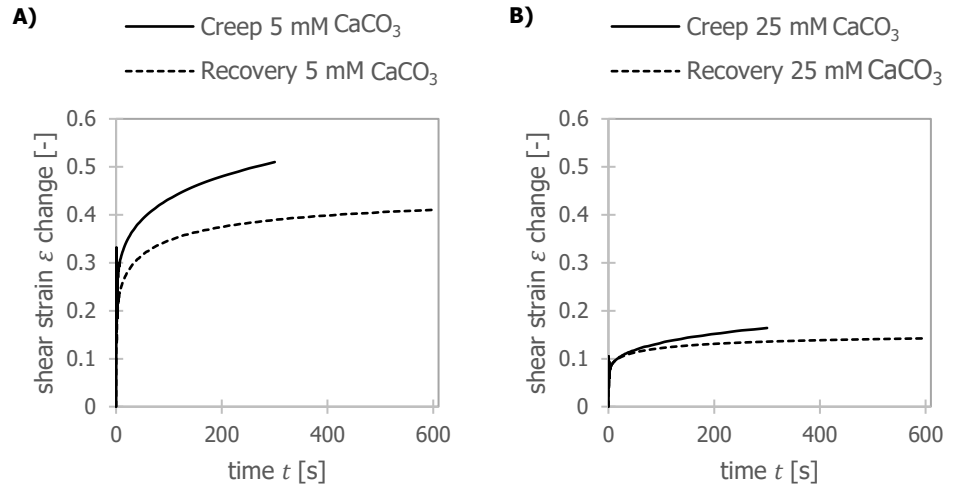

Figure 4-12: Comparison of the creep (straight line) and recovery (dashed line) steps of ALE gels with 5 mM Ca^{2+} (A) and 25 mM Ca^{2+} (B). Absolute values of the change in strain are presented (the changes are positive during creep and negative during recovery steps).

The final recovery of the strain was found between 80 % and 90 % (cf. Table 4-4). This was in line with the results of the Burgers fits of the creep data, showing that the viscous contribution to the deformation, i.e. the non-recoverable part, was around 15 % (between 13 % and 18 %).

Table 4-4: Strain recovered after the creep experiments, incl. the standard deviation of the triplicates.

$CaCO_3$ [mM]	5 mM	12.5 mM	25 mM	50 mM	100 mM
Strain recovery [%]	82.5 ± 2.7	84.0 ± 4.6	90.2 ± 3.1	90.1 ± 1.4	85.1 ± 2.0

The molecular interpretation of these findings could be based on considering the gels as a polymeric network, reversibly interlinked via physical interactions, in particular van-der-Waals forces, hydrogen bonds, electrostatic interactions and entanglements (Mayer *et al.*, 1999; Seviour *et al.*, 2009; Wilking *et al.*, 2011; Galy *et al.*, 2012; Dreszer *et al.*, 2013; Lin, Sharma and van Loosdrecht, 2013). The property of behaving like a liquid on a longer time scale has been attributed to a limited life-span of all of these interactions in a network exposed to stress or strain (Körstgens *et al.*, 2001; Klapper *et al.*, 2002; Ehret and Böl, 2013). This means that a particular bond in the gel might stay intact during short exposure to stress, but broke and potentially rearranged in another place when the exposure continued over a longer period.

In the case of the ALE gels tested in this work, four different regimes could be distinguished (cf. Fig. 4-11):

- The immediate (in the case of this experiment defined up to 5 s) jump as soon as stress was applied (Fig. 4-4, I).
- Two different cushioned increases with retardation times of ca. 12 s and ca. 80 s (Table 4-3).
- A further viscous increase of strain (Fig. 4-4, III).

It was hypothesized that the initial, immediate jump in strain involved stretching of the chain fragments of the ALE polymers between crosslinks, such as entanglements and ion (Ca^{2+}) bonds. Since the elastic modulus of polymer networks was proportional to the number density of crosslinks, the increase of the initial modulus with Ca^{2+} concentration (Fig. 4-7 and 4-10) showed that this ion played an important role in the network formation. The viscous behaviour at the end of the experiment could be interpreted as a balance between breaking and formation of bonds – the whole gel slowly flowed. The flow was slower when more Ca^{2+} was available (comparing the slopes of the creep curves in Fig. 4-12) since the density was higher and more crosslinks needed to be broken with increasing strain. The retardation time estimated from these two (Maxwell) processes was in the range of 1000 s, in correspondence with earlier findings: for biofilm EPS networks with Ca^{2+} crosslink lifespans of 20 – 30 min have been found (Shaw *et al.*, 2004; Ehret and Böl, 2013). It could be related to the disentanglement of the ALE (EPS) polymers, which occurs over time scales longer than breaking single crosslink bonds like Ca^{2+} bridges.
The two Kelvin elements described interactions with a life-span of 12 s and 80 s, respectively. An assignment to specific interactions was complicated because of the not yet full characterization of ALE. The independence of the importance of the elements on Ca^{2+} concentration (Fig. 4-11A) was remarkable, though. While the modulus increased with increasing Ca^{2+} concentration (Fig. 4-7 and 4-10), the relative contribution of the different elements to the final strain stayed stable over a wide range of $CaCO_3$ concentrations. This means that either Ca^{2+} had the same impact on all the elements, or none on any. The general hypothesis about gel formation of ALE with Ca^{2+} is that Ca^{2+}-ions crosslink ALE molecules (Lin *et al.*, 2010), in analogy to Ca-alginate gels of algaeal (Grant *et al.*, 1973) or bacterial origin (Wloka *et al.*, 2004). More Ca^{2+} was correlated with a higher number of crosslinks (Körstgens *et al.*, 2001), causing a higher modulus, which was in line with the findings of the present study. An increase in the number of one kind of crosslinks would be expected to increase its relative importance. Therefore, the current data indicated that there were at least two more relevant kinds of crosslinks, which both include Ca^{2+}. Possible candidates for these interactions are between Ca^{2+} and guluronic acid resp. mannuronic acid in ALE (Lin, Sharma and van Loosdrecht, 2013), or between Ca^{2+} and sulfated groups in ALE (Felz, Neu, *et al.*, 2020).

In Chapter 3, it was noted that maturing of ALE films led to a filamentous network with voids that grew over time. This process probably started already on the microscale in freshly prepared ALE gels, which caused local inhomogeneity and presumably also changes in the rheological behaviour. This aspect was not followed up on in the current work.

4.3.3 Structure breakdown and recovery

Most cleaning strategies against biofouling involve the application of external stress to remove the biofilms. Therefore, information about the recovery as soon as the stress is removed is addressed in the following section.

The crossover point found in the amplitude sweep experiments (Fig. 4-2) showed the point when the energy dissipation became more important for the materials' behaviour than the energy storage: the whole material started behaving like a fluid. For the ALE gels tested, the crossover point shifted towards higher stresses and lower strains with increasing calcium concentration, as can be seen in Figure 4-13. Gels with less Ca^{2+} could deform up to 200 % before the structure broke, while the gels with higher Ca^{2+} content already broke at 100 % strain.

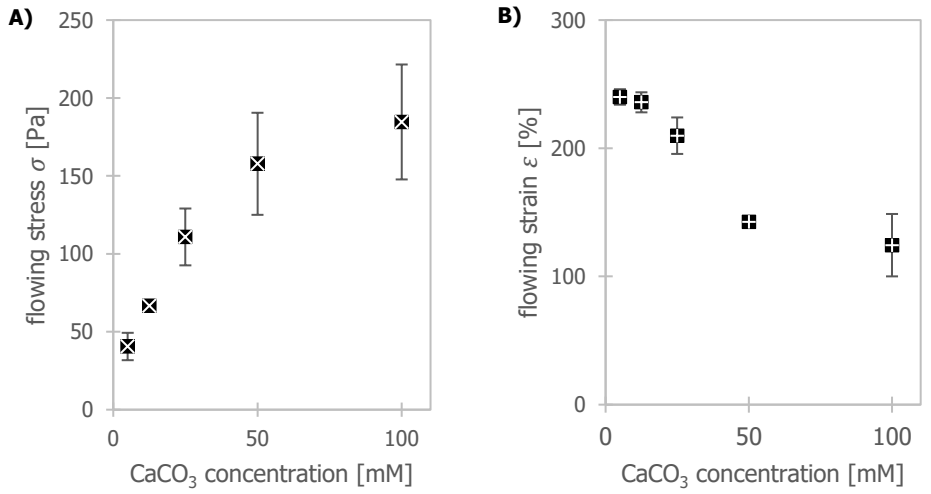

Figure 4-13: (A) Shear stress and (B) strain at the crossover points found from the amplitude sweep experiments as a function of $CaCO_3$ concentrations. The error bars show the standard deviation over the performed triplicates.

A special feature was visible at the upper limit of the LVER for the different $CaCO_3$ concentrations (Fig. 4-14): a slight strain stiffening occurred before the breakdown of the structure, indicated by the presence of a maximum in storage modulus, which became more prominent with increasing Ca^{2+} concentrations. Strain stiffening is a property commonly found in soft biological tissue (Storm *et al.*, 2005; Weisel and Litvinov, 2013), and is occasionally reported for biofilms (Wilking *et al.*, 2011; Böl *et al.*, 2013). It has also been described as a

characteristic behaviour of physically crosslinked polymer networks (Erk, Henderson and Shull, 2010; Bharadwaj, Schweizer and Ewoldt, 2017).

At this point, it was not possible to differentiate between stiffening due to strain or due to strain rate. The latter could at least partly be explained by an increase of the contribution of short lifetime bonds (e.g. hydrogen bonds, entanglement) (Ehret and Böl, 2013). In this case, extra power would be necessary to break bonds which at lower strain rates would break by themselves. The decrease of the phenomenon with decreasing Ca^{2+} concentration is probably related to the decreasing ALE density (cf. Fig. 4-5). The simplest explanation for the real strain stiffening would be an accumulation of stretching but not breaking junctions. When the structure eventually broke, the slope was steeper the more $CaCO_3$ was contained in the samples (Fig. 4-14). Steeper slopes are associated with higher brittleness. Brittle materials are more likely to break into inhomogeneous chunks, while the slighter slope at low $CaCO_3$ concentrations described rather ductile deformation (cf. Fig. 4-13).

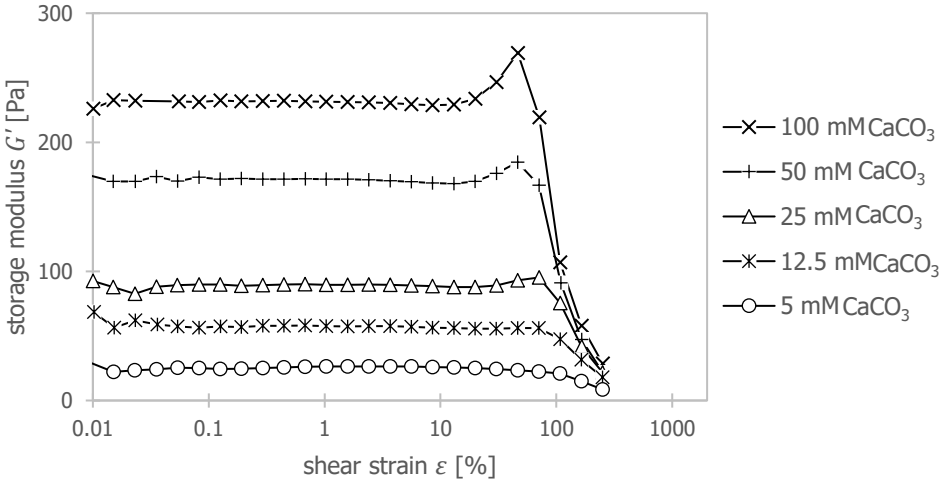

Figure 4-14: Set of storage moduli of ALE gels with different $CaCO_3$ concentrations as a function of strain during amplitude sweeps (10 rad/s).

For a better understanding of the observed strain hardening and eventual breaking of the structure, strain steps were performed, applying 10 %, 30 % and 200 % strain for 120 s, while in between these steps the relaxing behaviour at 0.3 % strain was observed for 400 s. In Figure 4-15, the storage modulus G', loss modulus G'' and dissipation factor $\tan\delta$ throughout a representative oscillation recovery experiment are presented. The data shown was measured on an ALE gel sample containing 25 mM $CaCO_3$. A comparison of the behaviour of the storage moduli of the gels with different $CaCO_3$ concentrations is shown in Figure 4-16. Figure 4-17 depicts the corresponding dissipation factors.

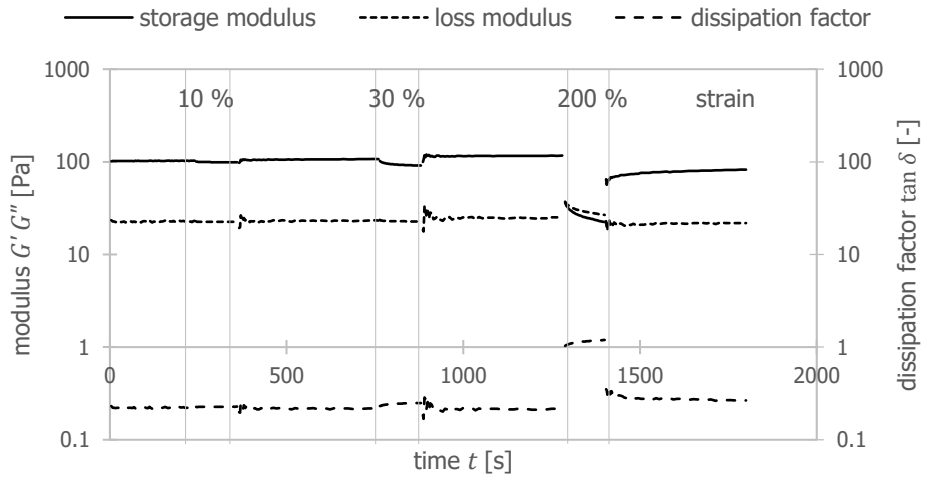

Figure 4-15: Typical behaviour of the storage modulus G', loss modulus G" and dissipation factor $\tan\delta$ *in oscillation experiments applying 10 %, 30 % and 200 % strain. The baseline and recovery are recorded in the linear viscoelastic region at 0.3 % strain. The results depicted are for 40 g/L ALE, 25 mM* $CaCO_3$.

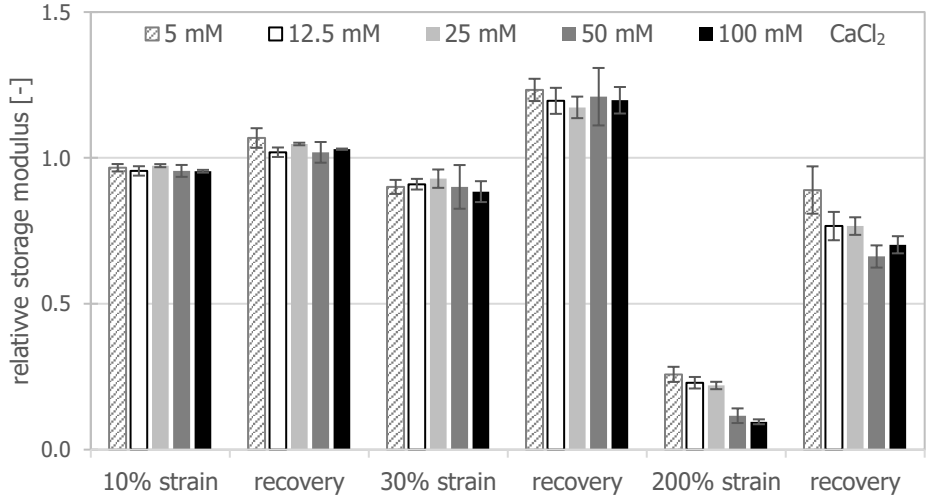

Figure 4-16: Change and recovery of the storage moduli (relative to the original storage modulus at 0.3 %) during the oscillation recovery experiments of ALE gels as a function of $CaCO_3$ *concentration. The error bars show the standard deviation over the performed triplicates.*

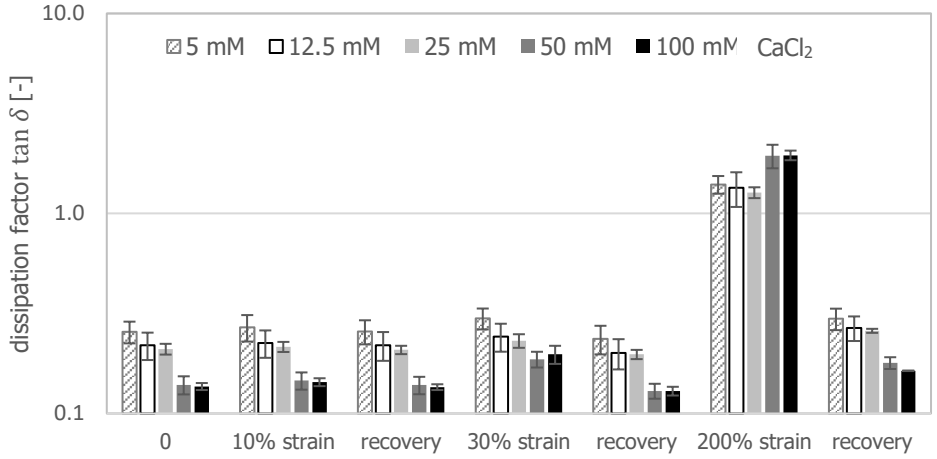

Figure 4-17: Dissipation factors during the oscillation recovery experiments. The error bars show the standard deviation over the performed triplicates.

The response of the storage modulus G' to the application of the different strains was very similar for all $CaCO_3$ concentrations. At 10 % strain, only a small decrease compared to the baseline was observed, followed by full recovery. The dissipation factor hardly varied. At 30 % strain, the storage modulus decreased a bit more than during the 10 % strain. The loss modulus increased in some cases, causing the dissipation factor to slightly rise, especially for the ALE gels with 50 mM and 100 mM $CaCO_3$. Still, all gels kept their predominantly solid behaviour, indicated by the dissipation factor staying well below 0.5.

A remarkable observation was that the storage moduli during the recovery phase after 30 % strain increased to about 120 % of their original values. This suggested that changes in the gels' structure, which were irreversible on the time scale of the measurements, were underlying the strain hardening observed in the ALE gels. A possible molecular explanation for this behaviour is that the originally randomly coiled ALE molecules got stretched and aligned under shear (cf. Ehret and Böl, 2013), while at the same time crosslinks with lower life-times broke and bound again, fixing to some extent the new alignment (Erk, Henderson and Shull, 2010). When subsequently a lower shear force was applied, the ALE molecules were already stretched somewhat, and breaking of the weaker bonds did not allow as much stretching as initially so that the ALE gel appeared stiffer than originally. Whether or not this explanation of the strain hardening applied, it was clear that the elastic modulus of the gels depended on the strain history. This memory effect is an important factor considering the common practice of scratching biofilms for investigation.

At 200 % strain, eventually, the dissipation factor passed the storage modulus, and the gels predominantly behaved like liquids (Fig. 4-15 and 4-17). As apparent in Figure 4-15, the predominantly solid behaviour was restored quickly when the strain was reduced again. Between 60 % and 90 % of the original storage moduli were recovered within the observation

time of 400 s. The full original storage modulus could not be reached, which hints at permanent destruction of parts of the network. A possible explanation is that ALE molecules were broken during the treatment. The average binding enthalpy of a C-O bond as it is found in the glycosidic linkages of guluronic and mannuronic acid in alginate is 360 kJ/mol (Atkins and Paula, 2006). The maximum shear stress applied during 200 % strain was between 50 Pa for ALE gels with 5 mM $CaCO_3$ and towards 200 Pa for 50 and 100 mM $CaCO_3$. With the sample area, defined by the plate radius of 125 mm, and the maximum strain of 200 % of 1 mm, the corresponding average transmitted energy on the gels as a whole could be roughly estimated as between 50 µJ and 200 µJ. It was not possible to determine which part of this energy was actually available to break the bonds. However, the energy is in a range where breaking of C-O bonds is possible. A slight trend was observed that the gels with high $CaCO_3$ recovered less than those with less $CaCO_3$ (Fig. 4-16). This was in agreement with the earlier observed higher brittleness of the gels with high $CaCO_3$. The chunks produced upon breaking were more inhomogeneous and therefore recombined less strong than the more flexible structure of the gels with less $CaCO_3$.

The course of the recovery after 200 % oscillatory strain was very similar for all tested $CaCO_3$ concentrations. An example is given in Figure 4-18. After an initial jump to around 60 % recovery there was a fast increase within the first 15-20 s to ca. 80 %, followed by a slower further recovery.

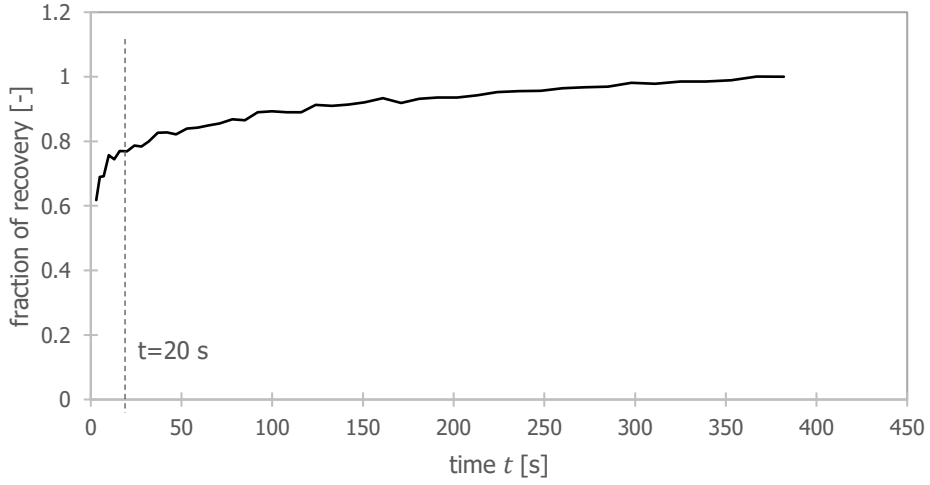

Figure 4-18: Recovery step after 200 % strain for a 25 mM $CaCO_3$ ALE gel, showing the accomplished recovery as part of the final value over time.

It is hypothesized that the rather quick recovery in the beginning depicted the elastic response of what was still intact of the network, and the rebuilding of the physical interactions (like electrostatic bonds that were built after slight rearrangement, e.g. by moving of Ca^{2+} ions).

The subsequent slow further recovery of the original modulus could have several mechanisms, including further syneresis, which were not further investigated in this work.
The period of the initial, fast recovery of the ALE gels' storage moduli was in accordance with the recovery of *P. aeruginosa* biofilms, which were found to fully recover within 20 s after 12.5 % strain yielding (Lieleg *et al.*, 2011). This fast and thorough recovery, even after complete break-down of the structure, emphasized one of the big challenges in biofouling removal. It has been proposed before that mechanical removal of biofilms should be preceded by a weakening of the chemical structure. This was supported by this work: as well as mere chemical treatment could not remove biofouling, neither could simple force, even if it was strong enough to overcome the cohesion of the films initially.

Focus on cohesion meant that the biofilm structure collapsed. For cleaning, this has the disadvantage of a probably strongly attached base-layer (Möhle *et al.*, 2007), that makes regrowth very easy. Further research should, therefore, also focus on increasing cohesion and decreasing adhesion. Furthermore, a full chemical characterization of ALE will be useful for the assignment of molecular interactions to observed behaviour. Such work could further support the existence of at least two distinguishable interactions with Ca^{2+} involved in the cohesion of Ca-ALE gels. A potential candidate are the already mentioned sulfate groups that have been identified in ALE (Felz, Neu, *et al.*, 2020).

4.4 Conclusion

In this work, the mechanical response of Ca-ALE gels to shear was investigated as a function of the $CaCO_3$ concentration. The mechanical properties of gels with relatively low $CaCO_3$ concentrations (100-300 µmol/g ALE) were in good correspondence with those of real biofilms, making the Ca-ALE system a suitable starting model for studying biofilm properties to develop biofouling cleaning methods. It can be extended by adding more ingredients encountered in real biofilms, such as proteins, DNA and (micro) particles. While this work focused on understanding the cohesion of ALE gels as a model for biofilms, an additional important field for research for cleaning purposes is the adhesion of biofilms to surfaces.

$CaCO_3$ induced syneresis was observed and showed the large impact that Ca^{2+} had in crosslinking ALE and beyond. With more $CaCO_3$, ALE gels initially became stronger and less ductile, even when the nominal binding capacity of ca. 1 mmol/g VSS was twofold exceeded. A further overload of $CaCO_3$ caused the weakening of the structure, probably by precipitation and heterogenization of the ALE network. The gels with more than 1 mmol $CaCO_3$ per g VSS showed slightly less recoverability after application of 200 % shear strain.

There was an optimum Ca^{2+} concentration found for biofilm models, providing suitable mechanical strength without overdosing. The upper limit found in this work was between 1.25 and 2.5 mol/g VSS. While the limitation of ions, using e.g. chelating agents, is already common

practice in countering biofouling (Ang, Lee and Elimelech, 2006; Lieleg *et al.*, 2011), this work suggested that also overdosing can be an approach, making the films more brittle and thus easier removable.

Creep tests in combination with a Burgers model fit with unlimited Kelvin elements provided insight into the molecular cohesion of the ALE gels. At least three different kinds of crosslinks seemed to be present, with retardation times in the order of 10, 100 and 1000 s. Attributing them to specific molecular interactions in future work can be the basis for a thorough understanding of the molecular network of biofilms.
Strain hardening was observed, also lasting when a mid-level strain was applied for a short period and subsequently removed. A possible explanation is an alignment of ALE molecules under strain, combined with breaking and forming of new crosslink. This process caused a dependency of the mechanical properties of biofilm samples on their strain history. As a conclusion, it needs to be questioned how much the analysis of scratched biofilms can tell about the properties of natural biofilms. Even after applying strains that caused the ALE gels to behave fluid-like, they showed fast and under most conditions complete recovery as soon as the shear force was stopped, emphasizing the physical and thus easily recoverable nature of the crosslinks. For successful cleaning, therefore, these physical interactions need to be permanently broken, and the applied force may not be stopped too soon. This work provides a first approach to identify the significant interactions so that in future applications, they can be specifically attacked to facilitate subsequent mechanical removal of biofouling.

Acknowledgements

Special thanks to dr. J.A. Dijksman and the PCC group of Wageningen University for an introduction into the world of rheology as well as help and advice whenever it was necessary for the interpretation of the data.

Chapter 5

Biofilms as composite materials: the effect of bacteria-sized micro-beads on the viscoelastic properties of alginate hydrogels

Biofilms can be considered as reinforced composites, consisting of a polymer matrix stabilised by bacteria. For a first insight into the potential contribution of bacteria to the viscoelastic characteristics of biofilms, simple model systems of weak Ca^{2+}-alginate gels with 1 µm diameter polystyrene spheres with different surface properties were investigated by rheological methods. The particle concentration used (2.3×10^{10} mL^{-1}) was in the rather low range but in the same order as the typical concentration of bacteria in biofilms. The impact of carboxy-functionalised particles on the viscoelasticity of the gels was too small to be observed in the current work. In contrast, sulfate-functionalised particles appeared to enhance the elastic modulus, and particles with amino surface groups seemed to weaken the network. Apart from the observed electrostatic interactions with the alginate matrix, the volume fraction and geometry of the particles were concluded to be important factors. Based on composite models, it is expected that a tenfold increase of the particle concentration in combination with a change in geometry to aspect ratios of 5:1 will show a more significant impact. Since bacteria generally have a larger volume than the particles used in this study and often have a rod-like shape, it was concluded that their presence could contribute significantly to the strength and stiffness of biofilms.

5.1 Introduction

Biofilms are formed when bacteria attach to a surface and produce a protective polymer matrix. This process is ubiquitous in nature. Sometimes it interferes with human interests, like causing problems with membrane filtration (Flemming *et al.*, 1997; Vrouwenvelder *et al.*, 2008) or threatening human health (Donlan, 2001; Bryers, 2008; Wingender and Flemming, 2011). In such cases, the biofilms are called biofouling.

One aspect of biofouling research is the mechanical stability of biofilms (Hall-Stoodley, Costerton and Stoodley, 2004; Möhle *et al.*, 2007; Guelon, Mathias and Stoodley, 2011), which has been proposed to be determined by the polymer matrix (Flemming *et al.*, 1997; Mayer *et al.*, 1999; Lin *et al.*, 2014; Hobley *et al.*, 2015). The extracellular polymeric substances (EPS) provide up to 90 % of biofilms' organic matter (Wingender, Neu and Flemming, 1999) and include biopolymers such as polysaccharides and proteins, complemented by lipids, humic substances and eDNA (Lin *et al.*, 2014; Flemming, Neu and Wingender, 2016). Recently, it has been proven that additionally also more complex biomolecules with manifold functionalisation are contained (Seviour *et al.*, 2019; Felz, Neu, *et al.*, 2020). Due to its ability to incorporate large amounts of water, the EPS matrix is considered a complex hydrogel (Mayer *et al.*, 1999; Körstgens *et al.*, 2001; Lin *et al.*, 2010; Galy *et al.*, 2012). To fully understand the mechanical properties of biofilms on a molecular basis is, therefore, a complex challenge.

It has been experimentally shown that for the mechanical stability of biofilms it is not essential if bacteria are dead or alive (Flemming *et al.*, 1997; Chen and Stewart, 2000; Davison, Pitts and Stewart, 2010; Zrelli *et al.*, 2013). However, below a shallow, assumingly bacteria-free surface layer, biofilms were found to be significantly stiffer based on compression tests (Safari *et al.*, 2015). This indicates that from a physical point of view, bacteria may be important for the mechanical stability of biofilms. One theory to explain this contribution is to consider the biofilm as a composite material of softer EPS and more rigid bacterial cells (Laspidou *et al.*, 2014; Safari *et al.*, 2014; Boudarel *et al.*, 2018).

In this work, the effect of rigid particles on the mechanical properties of a simplified biofilm model was investigated. The EPS matrix was mimicked by a hydrogel of alginate extracted from brown seaweed. Consisting of linear 1,4-linked chains of β-D-mannuronic acid and α-L-guluronic acid (Fischer and Dörfel, 1955; Haug and Larsen, 1966), it was known for its stable hydrogel formation with divalent cations (Haug *et al.*, 1965; Smidsrød *et al.*, 1965; Lee and Mooney, 2012). Alginate is regularly used as a model for biofilms (Wloka *et al.*, 2004; Katsoufidou, Yiantsios and Karabelas, 2007; van de Ven *et al.*, 2008; van den Brink, 2014) because it is chemically similar to some critical structural elements of biofilms (Lin *et al.*, 2008). It is commercially available and well characterised. Polystyrene beads of 1 µm diameter and with different surface functionalities (carboxylic groups, amino groups and sulfate groups) were used to represent bacterial cells. This diameter was representative for the size of bacteria.

Because of the simple spherical shape, with about 0.5 µm^3, the volume was on the small range of bacterial cells with 0.4 – 3 µm^3 (Levin and Angert, 2015).

5.2 Materials and Methods

5.2.1 Gels

Gels with 2 wt% alginate and 10 mM Ca^{2+} were produced using internal gelation (Draget, Østgaard and Smidsrød, 1989), a commonly applied method to obtain homogeneous gels. In preliminary experiments, this composition was found to result in gels with an elastic shear modulus in the range of a few hundred Pa, similar to biofilms (Vinogradov *et al.*, 2004; Wloka *et al.*, 2005; Patsios *et al.*, 2015). Particles with different functional groups (see below) were added to a final concentration of 2.275×10^{10} mL^{-1}. An overview of the gels' compositions is presented in Table 5-1.

Table 5-1: Compositions of the investigated alginate gels. GdL abbreviates glucono-δ-lactone.

Particles functionalized with …-groups	**Alginate [mg/mL]**	**Ca^{2+} [mM]**	**GdL [mM]**	**Particles [1/mL]**
blank (no particles)	20	10	20	0
amino				2.275×10^{10}
carboxylic				
sulfate				

Alginic acid sodium salt (Sigma Aldrich) was dissolved in demineralised water to an initial concentration of 50 g/L by stirring and heating to ca. 40 °C for 1 h. The pH was set to 7, using 0.2 M NaOH (Merck Millipore, Germany). Calcium, as $CaCO_3$ (anhydrous, reagent grade, VWR, the Netherlands), was prepared as 200 mM suspension. For fine dispersion, the suspension was treated in an ultrasonic bath for 10 min before further use. Both the alginate solution and $CaCO_3$ suspension were used as stock for preparation of all gels, while 400 mM solutions of glucono-δ-lactone (GdL) were prepared freshly for each batch. After mixing all ingredients, the samples directly were pipetted onto sand-paper (grit size P180, waterproof, Sencys, the Netherlands) lined disposable rheometer dishes (Anton Paar, 56 mm). Per sample, a volume of 1.7 mL was pipetted into circular stencils of 30 mm diameter. The samples were left for crosslinking at room temperature in 100 % humidity for 36 h.

Before the mechanical measurements, the stencils were removed. The thickness of the gels was equalised by cutting them to 1 mm height with a razor blade, using a 1 mm frame of the same size as the stencils.

Two gels of each composition were weighed into dry porcelain crucibles and heated to 105 °C for 24 h to determine the dry mass (total suspended solids, TSS). The so defined sample composition was compared to the composition as described above (Table 5-1) to determine the degree of syneresis (expulsion of water) during the gelation process.

5.2.2 Particles

The particles used in this work were Polybead® functionalised microspheres obtained from Polysciences Europe (Germany). They consisted of polystyrene (PS) with a nominal diameter of 1 µm, covered with either carboxylic (-COO^-), amino (-NH_3^+) or sulfate (-OSO_3^-) groups (charges expected at pH 7). The carboxylic and sulfate groups were, according to the manufacturer, directly bound to the particles' surfaces, while the amino groups were 11 to 12 carbon atoms away. They were delivered as a 4.55×10^{10} particles/mL solution, corresponding to a weight concentration of 2.5 % w/v. Before use, the particle solutions were adjusted to pH 7 using 0.2 M NaOH (Merck Millipore, Germany) or 0.1 M HCl (Merck Millipore, Germany). With a final concentration of 2.275×10^{10} particles/mL, they contributed about 1.2 % to the total gel volume, and provided a surface area of 715 cm^2/mL particle solution.

Also, micron-sized polystyrene particles with carboxylate surface groups were synthesised in-house according to a protocol from Appel *et al.*, 2013, and characterised for their surface charge density. Another batch of such particles, labelled with the fluorescent dye Cyanine 5.5 was obtained from dr. Stan Willems (Willems *et al.*, 2019). This batch was used to produce a particle-containing alginate gel. Using CLSM (excitation: 675 nm, emission: 694 nm) the distribution of the particles in the gel was determined.

Synthesis of the polystyrene particles with carboxylate surface groups was carried out as follows: 25 g styrene (Sigma-Aldrich) and 0.5 g itaconic acid (Sigma-Aldrich) were mixed with 120 g demineralised water in a one neck round-bottom flask. The neck was closed with a rubber septum, and the reaction mixture was flushed with nitrogen while stirring for 15 min. The flask was then placed in an oil bath of 85 °C and stirred at 500 rpm for another 15 min. In the meantime, 0.25 g of the initiator, 4,4-azobis(4-cyanovaleric acid) (ACVA, Sigma Aldrich), was dissolved in 5 mL 0.2 M sodium hydroxide solution. The initiator was injected into the reaction mixture and stirring at 85 °C was continued for 12 h. After filtration (Whatman™ filter paper, Grade 2) the particles were washed three times with demineralised water, using centrifugation (Allegra X-12R Centrifuge, Beckman Coulter, 30 min, 3750 rpm) for their separation. Particle size and number were analysed using by laser obscuration time (DIPA 2000 Particle Analyzer). Due to a rather broad particle size distribution and differences in the determined particle concentration of more than one order of magnitude, the in-house synthesized particles were not used for the rheological experiments. Instead, the commercial particles, as described above, were utilized.

The carboxylic groups surface coverage of the synthesised particles was addressed in duplet by conductometric titration (Hen, 1974). For this, 20 mL of the particle solution was initially alkalified with 0.8 mL 10 mM NaOH. During titration with 2 mM HCl in steps of 80 µL, the conductivity of the solution was measured. In the resulting graph of conductivity as a function of titrated HCl (V_{HCl}, Fig. 5-1), three stages with different constant slopes could be distinguished. In the first stage, the excess base was neutralised. Subsequently, the carboxylic

groups on the particles became re-protonated, and eventually excess acid was added. The intercepts of the regression lines marked the start- and endpoint of protonating the carboxylic groups. The obtained amount of HCl $n_{eq,HCl}$ was equivalent to the amount of carboxylic n_{COOH} groups neutralised.

$$n_{COOH} = V_{eq,HCl} \cdot c_{HCl} \qquad (5\text{-}1)$$

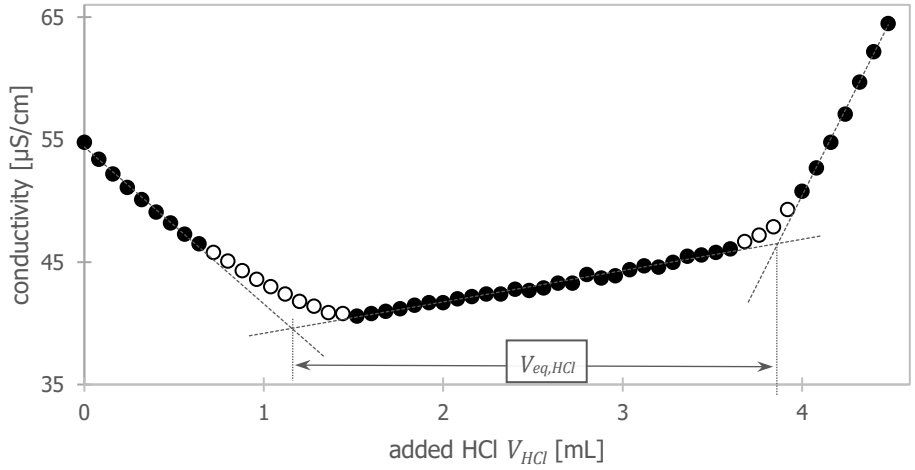

Figure 5-1: Conductometric titration of 20 mL 1.2 × 10^{10} mL^{-1} synthesized particle solution. The filled circles indicate the data points used for linear regression of the three stages of titration (see text). The dotted lines present the respective regression lines.

In combination with $c_{particles}$ and the size (average surface area S) of the particles, the number of carboxylic groups per area and per particle was estimated. The averaged diameter of the synthesised particles obtained by laser obscuration time from 6 measurements was 1.13 µm ± 0.15 µm, comparable to that of the commercially obtained particles. This corresponded to a particle surface area of 5.2 μm^2 ± 1.4 μm^2. (Apparent deviations between diameter and area were a consequence of the size distribution.) The particle concentration was found to be around 1.2 ± 0.3 × 10^{13} L^{-1}. Based on this value, the coverage with carboxylic groups was estimated as 3.3 ± 0.6 nm^{-2} with conductometric titration. This means that every particle contained in the order of ten million carboxylic groups. These were very rough values, and especially in case of the further functionalized particles probably not representative for the commercially obtained particles with functionalized surfaces. Therefore, the in-house synthesised particles were only used for the preliminary test below, while the systematic measurements were conducted with the commercial particles.

5.2.3 Viscoelastic analysis using rheology measurements

For rheology measurements, an MCR 102 rheometer (Anton Paar) with a 25 mm plate-plate geometry was used. As mentioned above, the lower plate was replaced by disposable plates

containing the sample. To enhance the friction between the samples and the plates, the latter were covered with sandpaper (grit size P180, waterproof, Sencys, the Netherlands). A 3D-printed liquid trap was applied, to minimise evaporation of water during measurements. The measurement setup (before trimming and application of the liquid trap) is shown in Figure 5-2.

Figure 5-2: A particle containing Ca-alginate gel in the rheometer, with the bottom part of the liquid trap.

Before each measurement, the upper plate sand-paper was renewed, the new zero-height was determined, and the respective system inertia was recalibrated. To approach the sample surface, the upper plate was lowered with 50 µm/s until a normal force of 0.15 N was detected. This corresponded with ca. 300 Pa, which was in the range of the expected moduli, so it could be assumed that the sample surface was reached. The samples were trimmed and left equilibrating until the normal force remained below 0.05 N. Data collection and conversion (e.g. from torque to shear stress σ) was done with the inbuilt RheoCompass™ software.

5.2.3.1 Dynamic measurements

Firstly, measurements in oscillation mode were performed at a constant angular frequency ω of 10 rad/s, raising the amplitude exponentially from 0.01 % up to 250 % shear strain (ε). The purpose of these amplitude sweeps was the identification of the linear viscoelastic regime (LVER) as well as quantification of the storage modulus G' and the loss modulus G'' within the LVER.

The RheoCompass™ software calculated the average shear stress σ on the samples from the measured torque. The ratio between shear stress σ and shear strain ε gave the complex modulus G^*:

$$G^* = \frac{\sigma}{\varepsilon} \qquad (5\text{-}2)$$

G^* could be split into the real component G', representing the storage modulus, and the imaginary component G'', representing the loss modulus. These moduli were measures for the parts of the applied stress stored elastically and lost by dissipation, respectively. Their ratio, $\tan\delta$, is referred to as the dissipation factor.

$$\tan \delta = \frac{G''}{G'} \qquad (5\text{-}3)$$

$\sigma, \varepsilon, G', G''$ and $\tan \delta$ were all outputs from the RheoCompass™ software. The LVER, where G' and G'' were rather stable and independent of the shear strain ε, was identified as the amplitude range where the deviation from the average was less than 5 %. In this region, it was assumed that no damage was done to the structure of the gel. Therefore, further measurements like frequency sweeps and creep tests were done in an amplitude range that was amply within the LVER for all considered samples.
The storage and loss moduli G' and G'' in the LVER were determined for all samples. Also, the behaviour of the gels above the LVER was qualitatively investigated.

Frequency sweeps were conducted to gain more insight into the gels' behaviour at rest and dependent on the time frame. In this case, the amplitude was kept constant at 1 % strain while the angular frequency ω was varied from 500 rad/s to 0.1 rad/s. For each composition, two gels were examined. The measurement output included, again, the storage modulus G' and the loss modulus G'' as a function of the angular frequency ω. The values for ω = 10 rad/s were combined with the values from the LVER determined in the amplitude sweeps to calculate the average values of G', G'' and $\tan \delta$.

5.2.3.2 Creep-recovery tests

For the investigation of the gels' behaviour during and after the application of constant stress, creep-recovery tests were performed on two gels of each composition. For 5 min, constant shear stress of 5 Pa was applied, which in the amplitude sweeps had been found to be inside the LVER. The strain ε was recorded as a function of the time t from the initial application of the stress until 15 min after stress release.
The results were interpreted using the Burgers model. This is a mechanical model in which the viscoelastic behaviour of materials is described by a combination of model springs and dashpots. The springs represent elastic contributions, while the dashpots account for the mechanical consequences of dissipation. In case of the Burgers model, a viscoelastic material is described as a series of a Maxwell element, consisting of a spring (describing the elastic jump at the beginning of the creep curve), and a dashpot (describing the viscous response, represented by the linear part of the curve at longer time scales), and a Kelvin element, consisting of parallel spring-dashpot pairs. The model has been found to successfully describe the viscoelastic behaviour of biofilms (Vinogradov *et al.*, 2004; Jones *et al.*, 2011). To allow the description of higher complexity, an indefinite number of Kelvin elements was allowed (cf. 4.2.4). For the description of the behaviour of the (composite) alginate gels in this study, one Kelvin element was found sufficient (Fig. 5-3). The strain ε_{creep} that the gels experienced during the creep tests was expressed as a function of the time t, the applied stress σ, the Maxwell modulus G_0, the Maxwell viscosity η_0, the Kelvin modulus G_K and the Kelvin viscosity η_K.

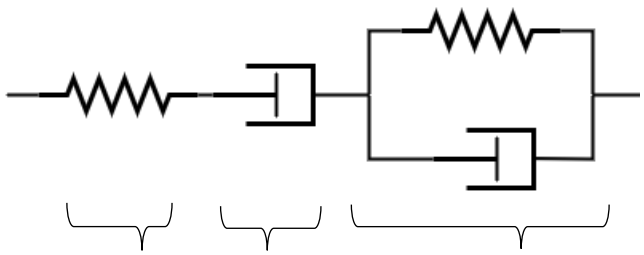

$$\varepsilon_{creep} = \frac{\sigma}{G_0} + \frac{\sigma}{\eta_0} \cdot t + \frac{\sigma}{G_K} \cdot \left(1 - \exp\left(-\frac{G_K}{\eta_K} \cdot t\right)\right) \quad (5\text{-}4)$$

Figure 5-3: Combination of springs and dashpots that represent a Burgers solid. The corresponding terms of the creep function are indicated below the drawing.

Eventually, the characteristic retardation times were calculated as the ratio between viscosity and elastic modulus.

$$\tau_K = \frac{\eta_K}{G_K} \quad (5\text{-}5)$$

$$\tau_M = \frac{\eta_0}{G_0} \quad (5\text{-}6)$$

5.3 Results

5.3.1 Particle distribution in gels

With a particle batch produced under addition of Cy5.5, gels were produced and analysed with the CLSM concerning the distribution of the particles. In Figure 5-4, scans from the top and the bottom of a Cy5.5 dyed gel are compared. The particles appeared evenly distributed in the gels.

The maximum particle concentration obtained in the systematic measurements was 2.3×10^{10}/mL of the mixture before gelling. This was a bit lower than, but in the same order of magnitude as the bacterial concentration of around 7-8 $\times 10^{10}$ cells/cm^3 that was for example found in biofilms in drinking water installations (Dreszer *et al.*, 2013).

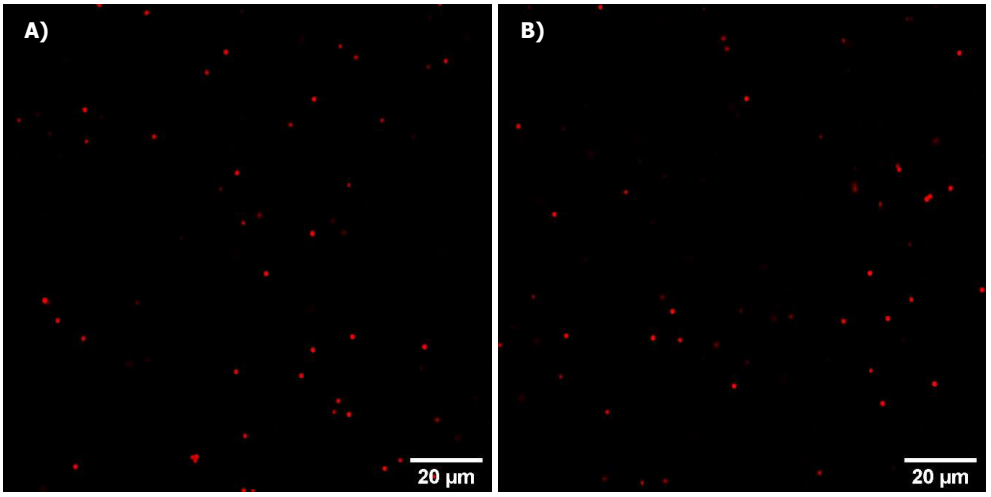

Figure 5-4: CLSM pictures (contrast and brightness are 40 % enhanced) 7 µm from the top (A) and the bottom (B) of the same gel, containing the synthesised particles with the dye Cy5.5.

5.3.2 Composition

The measured dry masses (*TSS*) for the four types of gels are presented in Figure 5-5. Based on the known ratios between alginate, glucono-δ-lactone (GdL) and calcium (cf. Table 5-1), also the mass distribution is depicted. For comparison, the original compositions of the mixtures before gelling are shown as well.

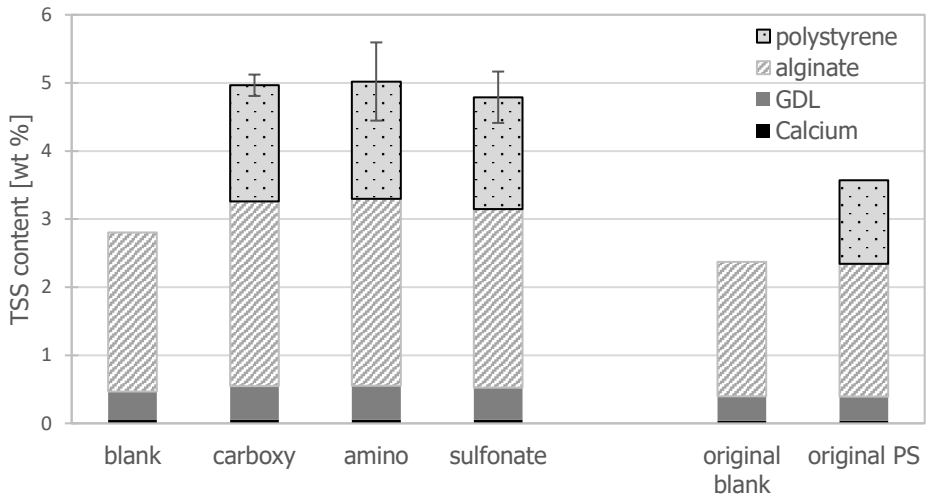

Figure 5-5: TSS content of the analysed gels and assumed composition. The errors indicate the standard deviation over two gels, each. GDL is glucono-δ-lactone. PS denotes the polystyrene particle solutions.

It was apparent that especially for the particle-containing gels, the final dry mass was higher than in the original mixture. The humidity in the gelation chamber was approximately 100 %, and all the gels were stored in the same chamber. (Mere) evaporation could, therefore, not be the cause. The changes in composition during gelation indicated that all gels underwent syneresis (Scherer, 1989) and that this effect was more substantial for the particle-containing gels. As a result, not only the TSS density but also the alginate density in the particle-containing gels was higher than in the blank without particles.

For systems containing calcium and alginate, syneresis is a known phenomenon that occurs more strongly with increasing calcium concentrations (Kuo and Ma, 2001; Davidovich-Pinhas and Bianco-Peled, 2010). It has also been observed for gels made with an extract of alginate-like extracellular polymeric substances and Ca^{2+} (Ch. 4). Often this syneresis effect has been associated with an increasing elastic modulus and has been explained by an assumed increase in crosslinks or lateral association of crosslinks (Draget *et al.*, 2001).

5.3.3 Viscoelastic behaviour of the gels

In Figure 5-6 the storage moduli G' and the dissipation factors $\tan\delta$ obtained from amplitude sweeps on the four different kinds of gels are presented. The storage modulus G' of all gels was in the range of 130 - 280 Pa and the dissipation factor around 7 %. The rather low dissipation factors were in accordance with the observed syneresis (Fig. 5-5). Materials with dissipation factors below ca. 20 % are considered to be more prone for syneresis (Mezger, 2014). For comparison, biofilms in non-extreme conditions have been found to have dissipation factors above 20 % (Powell *et al.*, 2013; Patsios *et al.*, 2015).

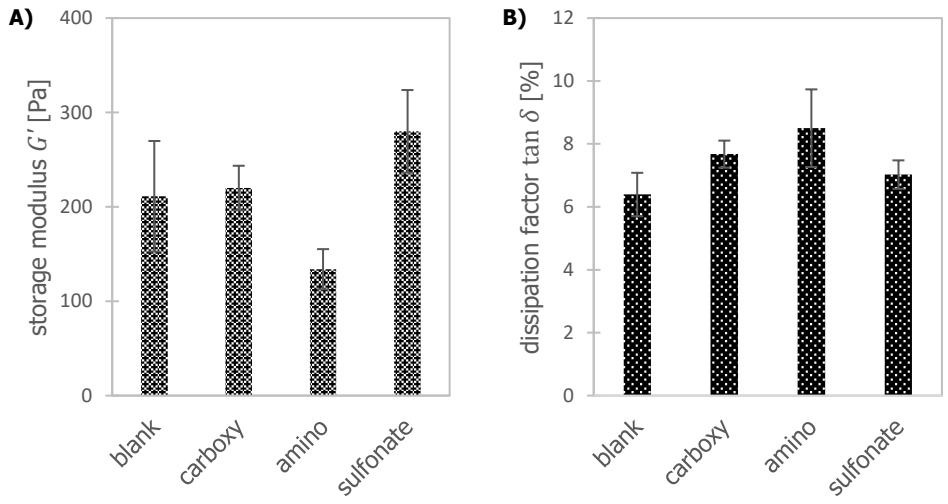

Figure 5-6: Storage moduli G' (Pa) and dissipation factors tan δ *(%) of the four different gels, obtained from amplitude sweeps. The indicated errors show the standard deviation over four gels.*

In Figure 5-7, an example of the storage and loss moduli throughout a typical amplitude sweep is shown. Up to ca. 10 % strain the LVER could be identified by quite stable values of G' and G''. The storage modulus G' in this region was significantly higher than the loss modulus G'' ($\tan\delta < 1$), indicating dimensional stability at rest (Mezger, 2014). The gels were predominantly elastic. At higher strains, in all gels, a slight increase of G' was observed, indicating strain hardening (Erk, Henderson and Shull, 2010; Bharadwaj, Schweizer and Ewoldt, 2017). For crosslinked alginate gels, this behaviour has been explained with the pre-breaking deformation of crosslinks (Zhang, Daubert and Foegeding, 2007). The resulting G' maxima were followed by a steep decrease, accompanied by an increase of G''. Such a steep reduction was associated with a brittle material, breaking inhomogeneously into chunks. In Figure 5-7B, indeed a single crack through the gel can be observed. The gels were destroyed at amplitudes above 100 %. This brittle destruction was a significant difference to similar gels prepared with bacterial alginate (Ch. 4). The presence of particles did not show any measurable influence on this behaviour.

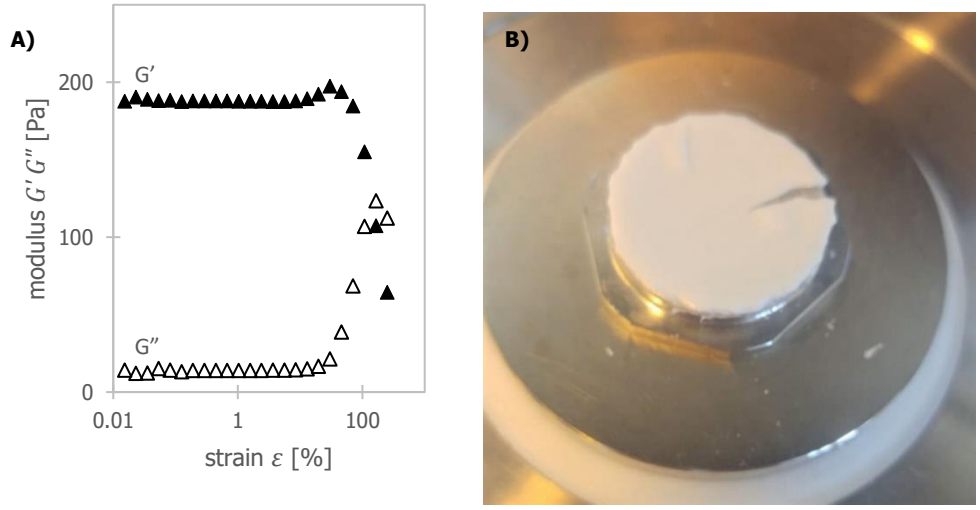

Figure 5-7: Example of a typical amplitude sweep. A) The storage modulus G' and the loss modulus G" of an alginate gel containing polystyrene beads covered with carboxylic groups over an amplitude range between 0.01 % and 250 % strain. B) The gel is shown right after the measurement: it is broken.

Similar conclusions were drawn from the comparison of frequency sweeps on the four different gels; examples of each are presented in Figure 5-8. As in the amplitude sweep results, a lower storage modulus G' was found for the gels containing amino-functionalized particles as compared to the other gels. The particles did not change the behaviour towards different frequencies.

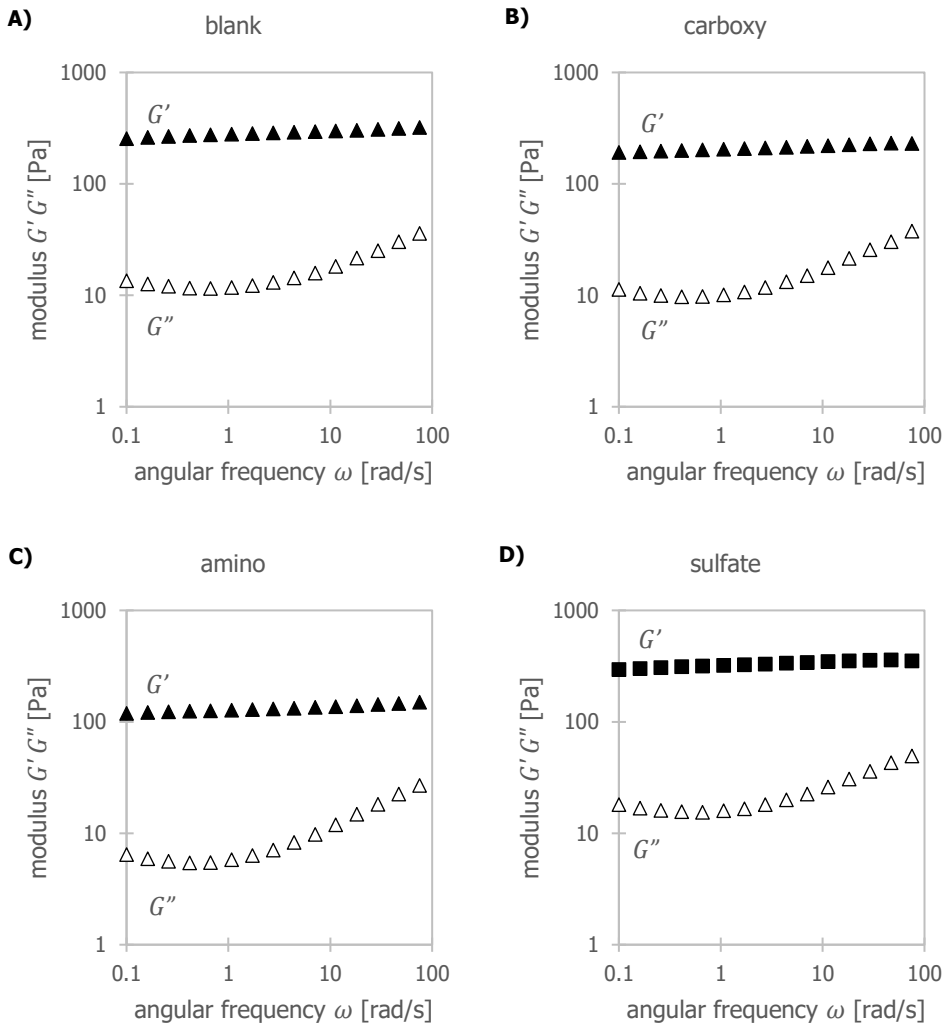

Figure 5-8: Example frequency sweeps in the LVER on alginate gels with the addition of different functionalized particles. While increasing the angular frequency ω from 0.1 rad/s to 500 rad/s, the shear strain was kept constant at 1 %.

Over the major part of the tested angular frequency, the storage modulus G' and loss modulus G'' were rather stable and G' was dominating. This again confirmed the presence of a 3D network within the gels. Towards lower frequencies, G' was only slightly decreasing, while G'' increased somewhat.

A measurement down to a frequency of 0.01 rad/s is presented in Figure 5-9, showing that a crossover point was not expected even at frequencies one or two decades lower. The gels could be expected to be stable at least in the range of tens of minutes to an hour. The long-term stability of the network could be attributed to interactions between alginate and Ca^{2+} (Augst, Kong and Mooney, 2006; Davidovich-Pinhas and Bianco-Peled, 2010; Kaklamani *et al.*, 2014). Towards the high end of the angular frequency range measured, an increase of G" was found. This could be a sign that at even higher frequencies, the end of the so-called rubbery plateau was reached (Mezger, 2006).

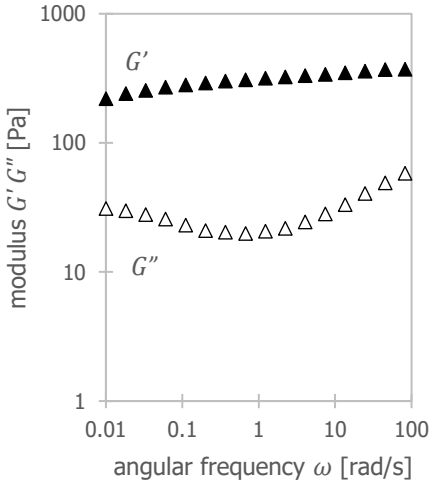

Figure 5-9: Frequency sweep of an alginate gel with carboxylated PS particles, extended to 0.01 rad/s in the lower frequency range.

In contrast to the dynamic measurements, the creep-recovery tests illustrated the reaction of the samples towards steady stress. In Figure 5-10A, a typical creep-recovery experiment is shown. In the first step (creep), constant shear stress of 5 Pa was applied for 5 min. After removal of the shear stress, the strain was observed for another 15 min (recovery). At the beginning of each step, an initial overshoot could be seen. This phenomenon is known as creep ringing. It was assigned to interactions between the rheometer's inertia and the elasticity of the sample (Ewoldt and Mckinley, 2007). Further analysis would go beyond the scope of this work. Instead, the parts of the curves showing this kind of damped oscillation were excluded from further analysis.

Characteristic behaviour of viscoelastic materials can be observed in Figure 5-10A: an immediate change in the strain followed application and removal of the shear stress, which was associated with the elastic behaviour of a Maxwell solid (cf. Figure 5-3, Maxwell spring). At the end of the recovery step, the strain was not entirely back to 0 %, meaning that a part of the shear energy was dissipated during the experiment.

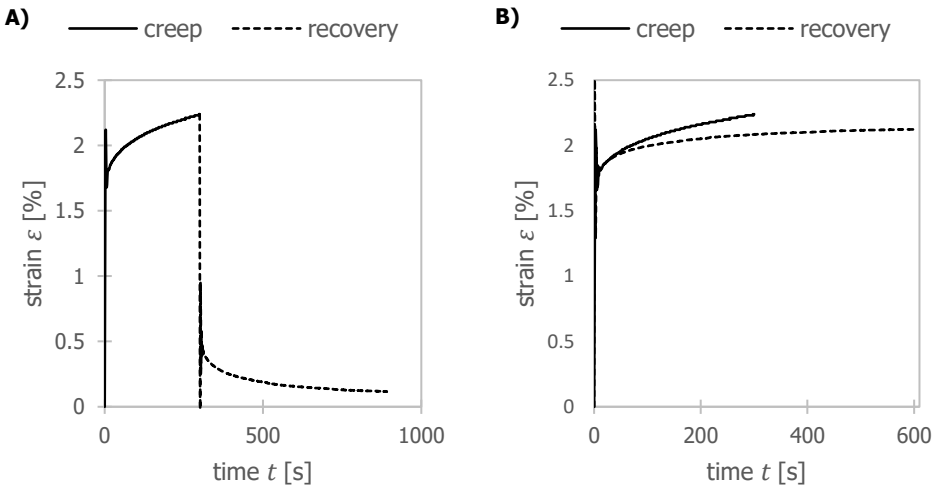

Figure 5-10: Strain as a function of time throughout a creep-recovery experiment (A). The data shown are for an alginate gel containing polystyrene beads with sulfate groups. In the first 300 s, a shear stress of 5 Pa was applied. For better comparison, in (B) the curves for creep and recovery are superposed.

The dissipation over time was well visible by direct comparison of creep and recovery in Figure 5-10B. In the Burgers model, the dissipated energy was accounted for by the viscous part of the Maxwell solid in the form of a dashpot. Viscous behaviour was accounted for by the approximately constant slope of the curve towards the end of the creep step. The middle part of the creep curve was described in the Burgers model by a parallel pair of dashpot and spring. While the spring defined the maximum expansion of this Kelvin element, the dashpot delayed its attainment. All gels could sufficiently be fitted with the Burgers model. An example is shown in Figure 5-11. Because of the creep ringing, no evaluation could be made about the behaviour below ca. 10 s.

Although the Burgers model is relatively simple, it described the creep-recovery behaviour of the alginate gels well. The Maxwell moduli and viscosities, as well as the characteristic retardation times determined using the Burgers model, are summarised in Table 5-2. The immediate elastic responses described by the Maxwell modulus were in good agreement with the results from the amplitude sweeps (Figure 5-6). The long-term (Maxwell) retardation time was in line with the conclusion from the frequency sweeps that the gels could be expected to be stable at least in the range of tens of minutes to an hour. The Kelvin element described damped elastic interactions with a characteristic lifetime of about 60 s.

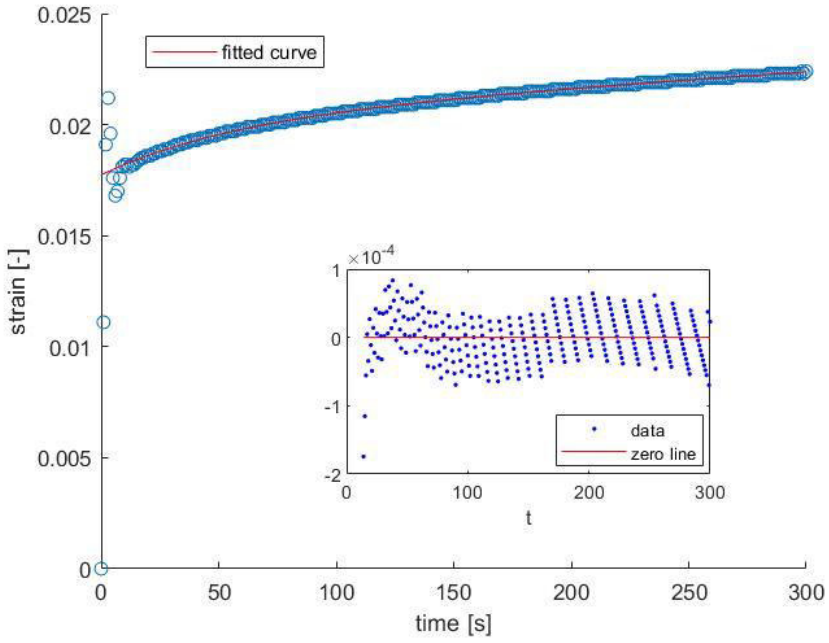

Figure 5-11: Example of a Burgers fit of the data for an alginate gel containing particles with sulfate groups. The inset shows the residuals of the fit, omitting the ringing at the start of the curve. The small graph shows the deviation of the fit from the single data points.

Table 5-2: Variables determined for alginate gels analysing creep-test data with the Burgers model. The indicated variances refer to the standard deviation of two analysed gels, each.

Particles functionalized with ...-groups	**Maxwell modulus [Pa]**	**Maxwell viscosity [10^5 Pas]**	**Maxwell retardation time [min]**	**Kelvin retardation time [s]**
blank (no particles)	181 ± 58	7.5 ± 2.5	68 ± 1	71 ± 1
carboxylic	215 ± 20	5.3 ± 0.3	41 ± 1	52 ± 10
amino	101 ± 17	3.9 ± 1.1	63 ± 8	68 ± 11
sulfate	293 ± 12	9.2 ± 2.1	52 ± 10	71 ± 11

The different regimes were interpreted as follows. The initial jump in the strain in response to the application of shear stress was attributed to the stretching of alginate chain fragments in between the Ca^{2+} crosslinks with blocks of guluronic acids. It has been shown that the guluronic acid residues, especially in homopolymeric chain form, are mainly responsible for the stable binding in Ca-alginate gels (Grant *et al.*, 1973; Morris, Rees and Thom, 1973; Smidsrød, 1974). The complete recovery of the elastic jump as soon as the stress was relieved (cf. Fig. 5-10B) showed that these interactions stayed intact over the range of the experiment. The dampened elastic response to the strain described by the Kelvin element was ascribed to the breaking and less specific formation of Ca^{2+} bonds with chains containing mannuronic acid

residues. While the stable crosslinking of alginate by Ca^{2+} is usually ascribed to poly-G-blocks, weaker interactions between Ca^{2+} and blocks of mannuronic acids have been observed as well (Meng, Winters and Liu, 2015). To date, they are, to the author's knowledge, not further characterized yet. The interactions observed had an apparent lifetime of about 60 s and might be dampened by further stretching of the chain fragments. Finally, the long-time viscous or plastic response was related to the disentanglement of the alginate polymers, which was a slower process than breaking single crosslink bonds.

Reviewing the results of the three different rheology experiments with a focus on the impact of the added particles, it was systematically found that the carboxy-functionalised particles did not affect the storage modulus of the gels enough to be detected within the accuracy of the experiments. The stabilizing interactions between Ca^{2+} and guluronic acid residues seemed unaffected by the addition of particle-bound carboxy groups. Interestingly, though, the carboxy particles were the only ones showing a significant influence on the characteristic retardation times (see Table 5-2). The sulfated particles seemed to enhance the strength of the network. The amino particles gave rise to a lower elastic modulus than measured for the blank.

In principle, the particles with COO^- and SO_3^- surface groups could participate in the alginate network through Ca^{2+}. It seemed that the net effect of adding carboxylated particles was neither a weaker nor a stronger guluronic acid network, but the lifetime of other, less specific interactions was shortened. A possible explanation is a competition for ionic combination with Ca^{2+}. Sulfate particles, on the other hand, made the guluronic network stronger. It was noted that in a previous study on the effect of Ca^{2+} concentration on the properties of ALE gels (Ch. 3 and 4) it was found that the sulfate groups in ALE also interacted with Ca^{2+}. However, this interaction was found to be much less specific than the interaction between the carboxylic groups in alginate and Ca^{2+} and therefore is likely predominantly electrostatic in nature. Amino groups, positively charged at neutral pH, could not bind to Ca^{2+}. There could be an electrostatic attraction between particles and alginate though. The result might be that the alginate polymers tended to adsorb onto the particles, causing a weaker network. In other measurements, not discussed here, with slightly stronger alginate gels as a consequence of a lower temperature during gelation, the results for the sulfated particles exhibited the same trend, while the amino particles showed, like the carboxy particles, no effect on the elastic modulus. Therefore, the role of electrostatic interactions between charged particles and the Ca^{2+}-alginate network requires further investigation. One approach could be varying these interactions by changing the pH, allowing deprotonation of NH_3^+ or protonation of COO^-.

5.3.4 Composites

In general, one of the reasons to add particles to materials is to enhance their hardness and strength. Composites like concrete show a significant enhancement of material properties

compared to mere cement: adding granules (gravel, sand) to cement increases the elastic modulus by a factor of 1.5 to 2 (Aulia and Deutschmann, 1999). The same approach has been applied to hydrogels, opening a wide range of application for enhanced biomaterials (Shapiro and Oyen, 2013; Dannert, Stokke and Dias, 2019). The stability of polymer gels like alginate showed significant enhancement after addition of fibrous (Khavari *et al.*, 2016; Aarstad *et al.*, 2017) or particulate co-materials (Han *et al.*, 2013; Zlopasa *et al.*, 2016; Choe *et al.*, 2019).

An important factor determining the effect of particles on the elastic modulus of alginate gels is the volume fraction of the particles φ_p used. In this work, a volume fraction as small as 1.2 % was used. As mentioned before, the applied particle concentration was in the lower range of the concentration of bacteria in biofilms, and the particle diameter on the small side of bacterial size. Still, using the general rule of mixtures (Safari *et al.*, 2014; Fan and Njuguna, 2016),

$$G'_{comp,up} = G'_{PS} \cdot \nu_f + G'_{alginate} \cdot \left(1 - \varphi_p\right) \quad (5\text{-}7)$$

$$G'_{comp,low} = \frac{G'_{PS} \cdot G'_{alginate}}{G'_{PS} \cdot \left(1 - \nu_f\right) + G'_{alginate} \cdot \varphi_p} \quad (5\text{-}8)$$

the upper limit for the elastic modulus of a 200 Pa alginate gel reinforced with 1.2 vol% polystyrene particles with an assumed elastic modulus of 1 GPa (Bangs Laboratories) would be around 12 000 Pa (using Eq. 5-7). It should be noted however that the upper limit can only be reached in case of solid composites like ceramics and concrete, in which the elastic moduli of matrix and granules are not so extremely different as in our case so that the isostrain condition holds. The lower limit for the elastic modulus of the same mixture was 202.4 Pa (calculated with Eq. 5-8). It became clear that based on the so estimated lower and upper limits of G' it was difficult to judge whether the particle volume fraction used in this work was sufficient to contribute to the viscoelastic properties of the composite gels. The Einstein equation (5-9) can be used as a simple alternative to estimate the change of the storage modulus upon addition of spherical particles to a matrix (Smallwood, 1944; Bourkas *et al.*, 2010).

$$G'_{comp} = G'_{alginate} \cdot \left(1 + 2.5 \cdot \varphi_p\right) \quad (5\text{-}9)$$

From this equation, the estimated storage modulus $G'_{alginate}$ of 200 Pa would only be increased to 206 Pa, which was too small to determine from the current experiments.

In addition to the volume fraction, another critical factor is the geometry of the potentially reinforcing particles. The spherical particles had a minimal area-to-volume ratio, implying that interactions with the polymer network were minimised. While locally the particles had their own, much higher elastic moduli, they were apparently not connected, so that in the shear experiments performed in this work deformation came from the Ca-alginate matrix, while the

particles inside moved along with the alginate network, or even 'slid' through. With more expanded forms of the added particles, like rods or even fibres, this would change, and the added particles could get more impact on the shear behaviour, for example by alignment according to the shear. Bacteria can have various shapes, from more or less spherical to rod-like to spiral or filamentous (Weiss *et al.*, 1995; Bergmans *et al.*, 2005). As such, their physical impact on mechanical biofilm properties could be as varied as their appearance. An advancement of the Einstein equation by Guth (Guth, 1945; Fan and Njuguna, 2016), considers the aspect ratio α (which was 1 for the used spherical particles).

$$G'_{comp} = G'_{alginate} \cdot \left(1 + 0.67 \cdot \alpha \cdot \varphi_p + 1.62 \cdot \alpha^2 \cdot \varphi_p^2\right) \qquad (5\text{-}10)$$

This equation predicted that at an aspect ratio of ca. 50:1 the elastic modulus would double when the concentration stayed the same. With four times the used concentration, approaching the bacterial concentration of 7-8 × 10^{10} cells/cm^3 found by Dreszer in drinking water biofilms (Dreszer et al., 2013), the doubling would already be reached with an aspect ratio of 13:1. With the 10-fold of the used concentration, an aspect ratio of 5:1 already would be predicted to have the same effect (as presented in Figure 5-12). This latter aspect ratio is not uncommon for rod-like bacteria like *Escherichia coli* or *Myxococcus xanthus* (Adams et al., 1992; Starruß et al., 2007; Ojkic, Serbanescu and Banerjee, 2019). Therefore, it was concluded that the mechanical impact of bacteria, even if they are not alive anymore, in the biofilm matrix may not be neglected. Especially when it comes to filamentous bacteria, they can exhibit a strong mechanical impact.

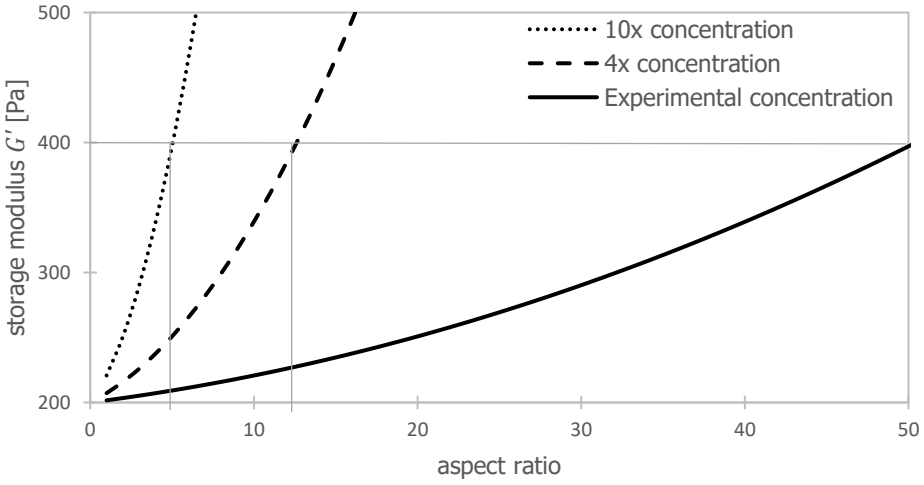

Figure 5-12: Predicted storage moduli as a function of aspect ratios for different concentrations, as calculated with Equation 10. The guides depict the aspect ratios needed to reach a predicted storage modulus of 400 Pa, which is considered to be significant in the current experiments.

While, as discussed, volume fraction and geometry played a crucial role in composite enhancement, the interactions between the particles and the matrix were at least as important. Especially at relatively low concentrations, when direct interactions between the particles were unlikely, like in this work, an effect would be dependent on the interaction between particles and polymeric network. Because the carboxy-functionalised particles were expected to interact with the alginate matrix through Ca^{2+}, it was anticipated to see such an effect. However, within experimental error, gels containing these particles exhibited the same rheological behaviour as the blank (gel without particles). Potential small effects as predicted by the Einstein equation (5-9) were hidden in the experimental error. On the other hand, the sulfate-functionalised particles seemed to enhance the elastic modulus of the gel to some extent. Unexpectedly, the addition of amino-functionalised particles appeared to decrease the storage modulus of the alginate gel, despite the electrostatic attraction between particles and gel matrix. As stated before, the role of electrostatic interactions between particles and the Ca^{2+}-alginate network needs further investigation.

5.4 Conclusions

As a first step to unravel the contribution of the presence of bacteria to the mechanical strength of biofilms, in this work, the effects of functionalised polystyrene beads on the mechanical properties of Ca^{2+}-alginate gels were investigated. The addition of these particles caused a small increase in syneresis in all gels, showing a densifying effect on the network. The effects of the various particles' surface functionalities on the gels' rheological behaviour were limited but different. While influences of carboxylic acid groups on the elastic modulus were too small to be detected, the gel appeared slightly strengthened by sulfated particles and weakened by particles carrying amino groups. Probably, electrostatic interactions and the ability of the particles to participate in the Ca^{2+}-alginate network were responsible for the observed effects. Further research is required to verify and characterize these interactions.

Considering the relatively low particle concentration used (2.3×10^{10} mL^{-1} corresponding to 1.2 vol%) and their spherical geometry, simple composite models predicted only minor effects on the elastic behaviour of the gels, within the experimental error of the measurements performed here. However, with a tenfold increase in particle concentration, which is still in the range for concentrations of bacteria observed in biofilms, and a particle aspect ratio of about 5:1, a more significant impact on the mechanical properties would be expected. Such impact can manifest beyond the modulus in changes of the brittleness and fracture persistence of films or in the recovery behaviour of films after application of shear stress. In addition to the experiments of this study, time step experiments as described in Chapter 4 (4.3.3) can be a useful tool for further insight, especially in the recovery behaviour. On top, complementary compression and relaxation experiments can provide further information on the behaviour of particles with different shapes, e.g. whether they align when the network is deformed. By choosing higher particle concentrations and different geometries in the range where their

impact is expected to be clearly visible in rheological experiments, a better assessment of the effect of functional groups will be possible. Manipulation of the charge of the functional groups by changing the pH can further reveal the importance of electrostatic interactions.
Both the current work and composite theory suggest a mechanical impact of bacteria, dead or alive, on the physical properties of biofilms. Especially for filamentous bacteria, a strong impact is expected. Therefore, to understand the mechanical properties of biofilms, the bacteria, i.e. their concentration, morphology and interactions with the EPS network, should be included in the analysis.

Chapter 6

Conclusions and Outlook

Biofilms are a ubiquitous phenomenon with both serious implications on human health and technology and a promising potential for useful applications. In either case, a thorough understanding of the formation, stabilization and disintegration of biofilms on a molecular level seems necessary. Especially, a better understanding of the gel matrix of the biofilm, or the extracellular polymeric matrix, is the key to better control on biofilm systems. Caused by the enormous complexity of biofilms and the extracellular polymers, such understanding can, yet, not be extracted from complete systems. Instead, simplified models are used to gain insights on specific aspects.

The objective of this work was the correlation of strength and structure to the chemical composition of membrane biofilms. The strength is defined by the molecular interactions between the different components, resulting in the cohesion of biofilms and determining their response to externally applied stress. Understanding these interactions will allow the targeted strengthening or weakening of structures, easing biofouling removal or promoting the stability of useful biofilm material. The chosen model materials, mimicking extracellular polymeric substances (EPS) in biofilms, were commercial alginate as a fully characterized but only slightly representative component, and alginate-like exopolymers (ALE) as a less characterized but crucial structural component of EPS, actually detected in biofilms. Both components were known to form hydrogels in the presence of Ca^{2+} ions. Thus they were considered suitable as physical-chemical models for EPS with the aim to gain insight into the intermolecular interactions.

6.1 Gelling and binding behaviour of alginate-like exopolymers as a model for biofilms

Although named after alginate, based on the gel formation with Ca^{2+} (Lin *et al.*, 2010), the higher compositional complexity of ALE was meanwhile proven (Felz, Neu, *et al.*, 2020). Results of this work clearly illustrate this higher complexity. Gels with Ca^{2+}, prepared and examined in creep tests under comparable conditions, exhibited more complex viscoelastic properties when ALE was used (Ch. 4) than when alginate was used (Ch 5). The description of the creep behaviour of the ALE gels using the mechanical Burgers model required an extra Kelvin element, indicating that more different molecular interactions were involved in the gels' response to stress. The further identification of these interactions, resp. the interpretation of such data, is still a quite new field and will be discussed below.

Just like alginate, ALE formed hydrogels with Ca^{2+}. This work shows that the binding mechanism is substantially different from the 'egg-box model' postulated for alginate. In Chapter 3 (cf. 3.4.2) it is shown that the distribution of Ca^{2+}, K^+ and likely also H^+ between supernatant and gels was determined by the Donnan potential established by the fixed negative charges of the ALE molecules. This implies that the binding of Ca^{2+} and other cations to ALE is electrostatic and reversible on the timescale of the experiments. As a comparison,

the same calculations on the distribution of Ca^{2+} between alginate and supernatant (see 2.3.1) showed that in this case Ca^{2+} is more irreversibly bound to alginate than to ALE. This is in accordance with the known highly specific interaction between Ca^{2+} and alginate. The application of such calculations on biofilms is usually complicated because of the high complexity of ALE. This example shows, however, that under the right (simplified) conditions, valuable insight can be obtained from basic physical chemistry principles. Application of the Donnan equilibrium allowed, for example, an estimation of the concentration of fixed negative charges contained in the ALE. The non-specificity and reversibility of the Ca^{2+}-ALE bonds have further implications. In combination with observations concerning the stability of Ca^{2+}-ALE and Ca^{2+}-alginate gels in the presence of a chelator such as EDTA (Felz, Kleikamp, *et al.*, 2020), it was concluded that although necessary for gel formation, Ca^{2+} may not be necessary for preserving the structure but can be replaced by other ions and interactions.

ALE was, of course, just a simplified model for the real biofilm EPS. Still, these findings provide a first glimpse of how the EPS structure is bound together – and why EDTA as a cleaning agent is sometimes not as effective as one would expect. For future research, these findings open several interesting directions. Firstly, the gelation mechanism appears interesting for further investigation. Based on this the findings in Chapter 3, it appears that gelling occurred when ALE molecules were brought close together with Ca^{2+} ions (or other multivalent cations (Felz, Kleikamp, *et al.*, 2020)) that formed bridges between the negatively charged functional groups. Without these ions, no ALE gels were formed. In addition to common strategies like nutrient limitation, for some applications the strict regulation of such ions could, therefore, be an option to prevent gelling in the first place. However, after the formation of the gel network, there seemed room for rearrangement of the structure, resulting in a more fibrous network. Its stability might stem from other interactions, such as H-bonds, Van-der-Waals and/or hydrophobic interactions, and no longer depend as crucially on the presence of Ca^{2+}. Such maturing of the gels and the shift in the importance of the binding mechanisms were observed in this work (Ch. 2 and 3), and the nature of the underlying interactions is a second direction for further research. To clarify the role of Ca^{2+} in later stages and gain more insight into the mechanism and chronology of crosslinking, the experiment for the reversibility of swelling (3.4.4) could be reversed, so that gel layers originally crosslinked with a high amount of Ca^{2+} are later transferred to storing solutions with lower amounts of Ca^{2+}. As stated before, an understanding of the molecular interactions deems necessary for successful control and manipulation of biofilms. Last but not least, ALE gel has been proven to be an interesting model to investigate the molecular interactions in biofilms. After understanding the molecular interactions in sheer ALE, the next step can be the extension of the model by adding, step-by-step, further biofilm-characteristic components and analyze the resulting shifts, strengthening or weakening of molecular interactions. One example for such an extension can be adding small particles as bacterial cell surrogates, as described in Chapter 5.

6.2 Strength of model gel layers

The viscoelastic properties of ALE gels with bound Ca^{2+} in the range of 100-300 µmol/g showed good agreement with real biofilms. For the purpose of this work, ALE was considered a suitable model component. From calculations of the osmotic pressure based on the ionic distributions over gel and supernatant, it was concluded that the more Ca^{2+} was present during and after gelation, the stronger was the resistance of the gel network against swelling (Ch. 3). But what happened when an external force is applied? Under the application of shear stress (Ch. 4), the trend was confirmed: gels with more Ca^{2+} had a higher elastic modulus, related to stronger molecular interactions. Besides, the measurements of viscoelastic properties revealed that multiple interactions with different lifespans played a role in the strength of the gel network. Although the involvement of different types of interactions like H-bonding or van-der-Waals forces is usually assumed, it was, also in this work, mostly the electrostatic interactions that got most of the attention. Acknowledging the contribution of each interaction with its typical lifetime can help the interpretation of, for example, the complex creep behaviour of ALE gels. What can be learned from this study is, therefore, that in some cases interactions can be between the same components but of a different nature. Further insight in this topic can be gained with experiments where the electrostatic interactions are manipulated, for example, by decreasing the pH until all carboxylic groups in the ALE can be assumed protonated.

Yet another aspect of 'strength' when it comes to biofouling is its ability to withstand cleaning attempts, e.g. by shear due to fluid flow over the biofilm. In Chapter 4, a possible explanation for this is presented. It was shown that the elastic modulus of the investigated ALE gels could recover for a large part even after application of fierce shear stress, which was explained by the non-covalent interactions that simply re-arranged after being broken. Even worse for purely mechanical cleaning attempts is the observation that permanent strain hardening occurred after application of stresses too weak to destroy the network structure. Practically, these findings underline two points of attention for the cleaning of biofouling. An initial weakening of the structure by chemicals is desirable, and flushing should not be stopped before the material is fully removed. Scientifically, this finding raised the question on the reliability of research on biofilm material that has been scratched from their origin, since it implied the dependency of viscoelastic properties on the strain history. Methods that can determine biofilm properties directly on the substrate on which they were formed (as discussed for example by Galy *et al.*, 2012 or Picioreanu *et al.*, 2018) can minimize such problems. In the meanwhile, it should be noted that the proposed underlying molecular mechanisms for both the recovery of the elastic modulus and the strain hardening were only educated guesses so far. Certainty about the involved mechanisms will ease biofouling control. For clarification of the impact of the different suspected interaction partners, an approach would be going one step back and repeating the rheology experiments with defined macromolecules holding carboxylic and/or sulfated groups, so that both interactions can be investigated individually as

well as together. Alginate can be discarded as a model material in this case, since the specific egg-box binding appears to be an artefact when it comes to biofouling. With progressing characterization (Felz, Kleikamp, *et al.*, 2020; Felz, Neu, *et al.*, 2020), ALE provides a much more representative material for studying the impact of adding more and more complexity to the system.

Although the target of this work was biofilm EPS, the importance of bacteria as a mechanical constituent of biofilms kept appearing. In Chapter 2, it was concluded that their presence could contribute to the inhomogeneity and the porosity of biofilms, which both can have a crucial impact on the hydraulic resistance a membrane biofilm exhibits. In Chapter 5, the contribution of spherical particles in the size range of bacteria to the viscoelastic properties of alginate gels was examined. The impact observed experimentally was rather small. By reference to composite models, with aspect ratios different from 1 and concentrations in the range of 10^{11} particles/mL, both representative values for bacterial biofilms, a significant contribution to the elastic modulus can be expected. The experimental confirmation of this expectation still needs to be conveyed. Other than for the analysis of chemical interactions, for this kind of mechanical impact study, Ca-alginate provides a suitable, simple model.

6.3 Importance of selecting the appropriate models

An important lesson that could be learned from this work was the significance of choosing appropriate models for the scope of the respective research question. Dead-end filtration (Ch. 2 and 3) provided valuable insights into the binding and gelling behaviour of the model components and the structure arising from that. It allowed the production of gel layers with a similar shape as actual biofilms, and could also be used for an estimation of their impact on membrane filtration. Mechanical measurements, however, appeared complicated on the produced thin gel layers. For this purpose, further abstraction proved to be a good solution. Although their form did not resemble biofilms very much, the gels investigated in Chapters 3 and 4 allowed an analysis of the viscoelastic properties as a function of composition, without having to take into account the adhesion to the membrane. This provided valuable insights for further biofilm research. While there is still a lot more to learn concerning the cohesion of biofilms, it must be added here that for actual biofilm removal also the adhesion between biofilms and the surface is of importance.

As mentioned before, ALE is a complex substance of which the composition is not yet fully revealed. How suitable is it then, after all, as a simplified model in biofilm research? Would not alginate be the better option, because it is fully defined? For some questions, where very few things are known beforehand, the answer would be yes: alginate is a very good first model when it is the only known variable in the experiment. That is the reason why it was used in Chapter 5 for a first approach on the impact of bacterial cell surrogates on the viscoelastic properties of a hydrogel, and in Chapter 2 for the development of the experimental set-up. For

the intermolecular forces within biofilms, however, alginate is not considered the best option anymore. The main reason for this evaluation is its characteristic specific binding with Ca^{2+}. As has been shown, this specifity is not the case for the structural EPS extract called ALE (Ch. 3) – and probably not for biofilms, as well. Polymers or polymer blends with less selective interactions are, therefore, the better solution. But how about ALE, which is slowly revealing its full complexity? In the scope of this work, it has proven to be a suitable model. In addition to the requirement of forming hydrogels at all, it allowed consistent calculations (Ch. 3) and conclusions (Ch. 4) on the molecular interactions. With further revealing of its chemical composition in the future, the now collected data may be re-evaluated and further interpreted, but already today the results are conclusive. ALE might not be representative for each and every biofilm, but it is a decent model to start understanding what chemically/physically happens inside the biofilm matrix.

A last important point in this concluding chapter is the application of abstract viscoelastic-mechanical models, like the Burgers model, for the interpretation of rheological data, and their interpretation. Because of the discrete output data, it appears tempting to allocate discrete molecular interactions to, for example, extracted relaxation times (Ch. 2). This is, however, a tricky task. A finite abstract model needs to comply with the indefinite reality. Figuring out which of the various kinds of interactions and components is reflected in the output of the model needs to be done with care. The availability of data for comparison is small at the moment and consequently, the main use of such data at this moment is the comparison of experiments within one study. As soon as further research provides more data in this area (this would be a good application for alginate, thanks to its good characterization), it can, however, become a powerful tool for the identification of intermolecular interactions – not only in biofouling research.

References

Aarstad, O., Heggset, E. B., Pedersen, I. S., Bjørnøy, S. H., Syverud, K. and Strand, B. L. (2017) 'Mechanical properties of composite hydrogels of alginate and cellulose nanofibrils', *Polymers*. doi: 10.3390/polym9080378.

Adams, A. J., Wennerstrom, D. E., Mayhue, M., Mrak, R. E. and Hinson, W. G. (1992) 'Bacteria: rods of continuously variable aspect ratio', *Aerosol Science and Technology*. Taylor & Francis Group, 16(3), pp. 198–204. doi: 10.1080/02786829208959548.

Ahmed, E. M. (2015) 'Hydrogel: Preparation, characterization, and applications: A review', *Journal of Advanced Research*, 6(2), pp. 105–121. doi: 10.1016/j.jare.2013.07.006.

Ang, W. S., Lee, S. and Elimelech, M. (2006) 'Chemical and physical aspects of cleaning of organic-fouled reverse osmosis membranes', *Journal of Membrane Science*, 272(1–2), pp. 198–210. doi: 10.1016/j.memsci.2005.07.035.

Appel, J., Akerboom, S., Fokkink, R. G. and Sprakel, J. (2013) 'Facile one-step synthesis of monodisperse micron-sized latex particles with highly carboxylated surfaces', *Macromolecular Rapid Communications*, 34(16), pp. 1284–1288. doi: 10.1002/marc.201300422.

Arciola, C. R., Campoccia, D. and Montanaro, L. (2018) 'Implant infections: Adhesion, biofilm formation and immune evasion', *Nature Reviews Microbiology*. doi: 10.1038/s41579-018-0019-y.

Ashton, N. N. and Williams, D. L. (2019) 'Targeting Biofilms in Translational Research', in Williams, D. L. (ed.) *Targeting Biofilms in Translational Research, Device Development, and Industrial Sectors*. Springer International Publishing, pp. 131–155. doi: 10.1007/978-3-030-30667-0_9.

Aslam, S. (2008) 'Effect of antibacterials on biofilms.', *American Journal of Infection Control*, 36(10), p. S175.e9-11. doi: 10.1016/j.ajic.2008.10.002.

Atkins, P. W. and Paula, J. de (2006) 'Appendix 4 - Tables', in *Physikalische Chemie*. 4th editio. Weinheim: Wiley-VCH Verlag GmbH & Co. KGaA, pp. 1099–1138.

Augst, A. D., Kong, H. J. and Mooney, D. J. (2006) 'Alginate Hydrogels as Biomaterials', *Macromolecular Bioscience*. WILEY-VCH Verlag, 6(8), pp. 623–633. doi: 10.1002/mabi.200600069.

Aulia, T. B. and Deutschmann, K. (1999) 'Effect of mechanical properties of aggregate on the ductility of high performance concrete', *Leipzig Annual Civil Engineering Report*, 4, pp. 133–148. Available at: https://www.researchgate.net/publication/285631807_Effect_of_mechanical_properties_of_aggregate_on_the_ductility_of_high_performance_concrete (Accessed: 29 February 2020).

Bachmann, R. T. and Edyvean, R. G. J. (2005) 'Biofouling: an historic and contemporary review of its causes, consequences and control in drinking water distribution systems', *Biofilms*. Cambridge University Press, 2(3), pp. 197–227. doi: 10.1017/S1479050506001979.

Bajpai, S. K. (2001) 'Swelling studies on hydrogel networks - A review', *Journal of Scientific and Industrial Research*, 60(6), pp. 451–462. Available at: http://nopr.niscair.res.in/handle/123456789/26500.

Bangs Laboratories (no date) *Material Properties of Polystyrene and Poly(methylmethacrylate) (PMMA) Microspheres*, *Tech Support Doc 0021*. Available at: https://www.bangslabs.com/material-properties-polystyrene-and-polymethyl-methacrylate-pmma-microspheres (Accessed: 12 March 2020).

Bereschenko, L. A., Prummel, H., Euverink, G. J. W., Stams, A. J. M. and van Loosdrecht, M. C. M. (2011) 'Effect of conventional chemical treatment on the microbial population in a biofouling layer of reverse osmosis systems.', *Water Research*, 45(2), pp. 405–16. doi: 10.1016/j.watres.2010.07.058.

Bergmans, L., Moisiadis, P., Van Meerbeek, B., Quirynen, M. and Lambrechts, P. (2005) 'Microscopic observation of bacteria: Review highlighting the use of environmental SEM', *International Endodontic Journal*. John Wiley & Sons, Ltd, pp. 775–788. doi: 10.1111/j.1365-2591.2005.00999.x.

Bharadwaj, N. A., Schweizer, K. S. and Ewoldt, R. H. (2017) 'A strain stiffening theory for transient polymer networks under asymptotically nonlinear oscillatory shear', *Journal of Rheology*. Society of Rheology , 61(4), pp. 643–665. doi: 10.1122/1.4979368.

Blandino, A., Macias, M. and Cantero, D. (1999) 'Formation of calcium alginate gel capsules: Influence of sodium alginate and CaCl2 concentration on gelation kinetics', *Journal of Bioscience and Bioengineering*, 88(6), pp. 686–689. doi: 10.1016/S1389-1723(00)87103-0.

Böl, M., Ehret, A. E., Bolea Albero, A., Hellriegel, J. and Krull, R. (2013) 'Recent advances in mechanical characterisation of biofilm and their significance for material modelling.', *Critical Reviews in Biotechnology*. Informa Healthcare New York, 33(2), pp. 145–71. doi: 10.3109/07388551.2012.679250.

Boudarel, H., Mathias, J.-D., Blaysat, B. and Grédiac, M. (2018) 'Towards standardized mechanical characterization of microbial biofilms: analysis and critical review', *npj Biofilms and Microbiomes*. Nature Publishing Group, 4(1), p. 17. doi: 10.1038/s41522-018-0062-5.

Bourkas, G., Prassianakis, I., Kytopoulos, V., Sideridis, E. and Younis, C. (2010) 'Estimation of Elastic Moduli of Particulate Composites by New Models and Comparison with Moduli Measured by Tension, Dynamic, and Ultrasonic Tests', *Advances in Materials Science and Engineering*. Hindawi, 2010, pp. 1–13. doi: 10.1155/2010/891824.

Branda, S. S., Vik, S., Friedman, L. and Kolter, R. (2005) 'Biofilms: the matrix revisited.', *Trends in Microbiology*, 13(1), pp. 20–6. doi: 10.1016/j.tim.2004.11.006.

Brindle, E. R., Miller, D. A. and Stewart, P. S. (2011) 'Hydrodynamic deformation and removal of Staphylococcus epidermidis biofilms treated with urea, chlorhexidine, iron chloride, or DispersinB.', *Biotechnology and Bioengineering*, 108(12), pp. 2968–77. doi: 10.1002/bit.23245.

van den Brink, P., Zwijnenburg, A., Smith, G., Temmink, H. and van Loosdrecht, M. (2009) 'Effect of free calcium concentration and ionic strength on alginate fouling in cross-flow membrane filtration', *Journal of Membrane Science*, 345(1–2), pp. 207–216. doi: 10.1016/j.memsci.2009.08.046.

van den Brink, P. (2014) *Gel layer formation on membranes increases particle retention and fouling*, *Gel Layer Formation on membranes in Membrane Bioreactors*. Dissertation, TU Delft. Available at: https://doi.org/10.4233/uuid:9766fdc7-fe74-47a4-86e5-e17e1f4ee911.

Bryers, J. D. (2008) 'Medical biofilms', *Biotechnology and Bioengineering*, 100(1), pp. 1–18. doi: 10.1002/bit.21838.

Cai, S., Hu, Y., Zhao, X. and Suo, Z. (2010) 'Poroelasticity of a covalently crosslinked alginate hydrogel under compression', *Journal of Applied Physics*. American Institute of Physics, 108(11), p. 113514. doi: 10.1063/1.3517146.

Callow, M. E. and Callow, J. A. (2002) 'Mariṅe biofouling: A sticky problem', *Biologist*, 49(1), pp. 10–14. PMID: 11852279.

Candiello, J., Singh, S. S., Task, K., Kumta, P. N. and Banerjee, I. (2013) 'Early differentiation patterning of mouse embryonic stem cells in response to variations in alginate substrate stiffness', *Journal of Biological Engineering*. doi: 10.1186/1754-1611-7-9.

Chen, X. and Stewart, P. S. (2000) 'Biofilm removal caused by chemical treatments', *Water Research*, 34(17), pp. 4229–4233. doi: 10.1016/S0043-1354(00)00187-1.

Chimileski, S., Franklin, M. J. and Papke, R. T. (2014) 'Biofilms formed by the archaeon Haloferax volcaniiexhibit cellular differentiation and social motility, and facilitate horizontal gene transfer', *BMC Biology*. BioMed Central Ltd., 12(1), p. 65. doi: 10.1186/s12915-014-0065-5.

Choe, G., Oh, S., Seok, J. M., Park, S. A. and Lee, J. Y. (2019) 'Graphene oxide/alginate composites as novel bioinks for three-dimensional mesenchymal stem cell printing and bone regeneration applications', *Nanoscale*. Royal Society of Chemistry, 11(48), pp. 23275–23285. doi: 10.1039/c9nr07643c.

Chomiak, A., Sinnet, B., Derlon, N. and Morgenroth, E. (2014) 'Inorganic particles increase biofilm heterogeneity and enhance permeate flux', *Water Research*. Elsevier Ltd, 64, pp. 177–186. doi: 10.1016/j.watres.2014.06.045.

Christensen, B. E. (1989) 'The role of extracellular polysaccharides in biofilms', *Journal of Biotechnology*. Elsevier, 10(3–4), pp. 181–202. doi: 10.1016/0168-1656(89)90064-3.

Cooper, R. F. (2002) 'Seismic wave attenuation: Energy dissipation in viscoelastic crystalline solids', in *Reviews in Mineralogy and Geochemistry*, pp. 1–42. doi: 10.2138/gsrmg.51.1.253.

Dannert, C., Stokke, B. T. and Dias, R. S. (2019) 'Nanoparticle-hydrogel composites: From molecular interactions to macroscopic behavior', *Polymers*. MDPI AG. doi: 10.3390/polym11020275.

Davidovich-Pinhas, M. and Bianco-Peled, H. (2010) 'A quantitative analysis of alginate swelling', *Carbohydrate Polymers*. Elsevier, 79(4), pp. 1020–1027. doi: 10.1016/J.CARBPOL.2009.10.036.

Davies, D. (2003) 'Understanding biofilm resistance to antibacterial agents', *Nature Reviews Drug Discovery*. Nature Publishing Group, pp. 114–122. doi: 10.1038/nrd1008.

Davison, W. M., Pitts, B. and Stewart, P. S. (2010) 'Spatial and temporal patterns of biocide action against Staphylococcus epidermidis biofilms', *Antimicrobial Agents and Chemotherapy*. doi: 10.1128/AAC.01734-09.

Decho, A. W. (2016) 'Unique and baffling aspects of the matrix: EPS syneresis and glass formation during desication', in Flemming, H., Neu, D. T. R., and Wingender, D. J. (eds) *The Perfect Slime: Microbial Extracellular Polymeric Substances (EPS)*. London: IWA Publishing, pp. 207–226.

Decho, A. W. and Gutierrez, T. (2017) 'Microbial extracellular polymeric substances (EPSs) in ocean systems', *Frontiers in Microbiology*, 8(MAY). doi: 10.3389/fmicb.2017.00922.

Derlon, N., Grütter, A., Brandenberger, F., Sutter, A., Kuhlicke, U., Neu, T. R. and Morgenroth, E. (2016) 'The composition and compression of biofilms developed on ultrafiltration membranes determine hydraulic biofilm resistance', *Water Research*, 102, pp. 63–72. doi: 10.1016/j.watres.2016.06.019.

Desmond, P., Best, J. P., Morgenroth, E. and Derlon, N. (2018) 'Linking composition of extracellular polymeric substances (EPS) to the physical structure and hydraulic resistance of membrane biofilms', *Water Research*. Pergamon, 132, pp. 211–221. doi: 10.1016/j.watres.2017.12.058.

Desmond, P., Morgenroth, E. and Derlon, N. (2018) 'Physical structure determines compression of membrane biofilms during Gravity Driven Membrane (GDM) ultrafiltration', *Water Research*, 143, pp. 539–549. doi: 10.1016/j.watres.2018.07.008.

Dimitriadis, E. K., Horkay, F., Maresca, J., Kachar, B. and Chadwick, R. S. (2002) 'Determination of elastic moduli of thin layers of soft material using the atomic force microscope.', *Biophysical journal*, 82(5), pp. 2798–810. doi: 10.1016/S0006-3495(02)75620-8.

Dogsa, I., Kriechbaum, M., Stopar, D. and Laggner, P. (2005) 'Structure of bacterial extracellular polymeric substances at different pH values as determined by SAXS', *Biophysical Journal*, 89(4), pp. 2711–2720. doi: 10.1529/biophysj.105.061648.

Donlan, R. M. (2001) 'Biofilms and device-associated infections', in *Emerging Infectious Diseases*, pp. 277–281. doi: 10.3201/eid0702.010226.

Donlan, R. M. (2002) 'Biofilms: Microbial life on surfaces', *Emerging Infectious Diseases*, 8(9), pp. 881–890. doi: 10.3201/eid0809.020063.

Draget, K. I., Østgaard, K. and Smidsrød, O. (1989) 'Alginate-based solid media for plant tissue culture', *Applied Microbiology and Biotechnology*, 31(1), pp. 79–83. doi: 10.1007/BF00252532.

Draget, K. I., Skjåk Bræk, G. and Smidsrød, O. (1994) 'Alginic acid gels: the effect of alginate chemical composition and molecular weight', *Carbohydrate Polymers*. Elsevier, 25(1), pp. 31–38. doi: 10.1016/0144-8617(94)90159-7.

Draget, K. I., Gåserød, O., Aunea, I., Andersen, P. O., Storbakken, B., Stokke, B. T. and Smidsrød, O. (2001) 'Effects of molecular weight and elastic segment flexibility on syneresis in Ca-alginate gels', *Food Hydrocolloids*, 15(4–6), pp. 485–490. doi: 10.1016/S0268-005X(01)00046-7.

Dreszer, C., Vrouwenvelder, J. S., Paulitsch-Fuchs, A. H., Zwijnenburg, A., Kruithof, J. C. and Flemming, H.-C. (2013) 'Hydraulic resistance of biofilms', *Journal of Membrane Science*, 429, pp. 436–447. doi: 10.1016/j.memsci.2012.11.030.

Dreszer, C., Wexler, A. D., Drusová, S., Overdijk, T., Zwijnenburg, A., Flemming, H.-C., Kruithof, J. C. and Vrouwenvelder, J. S. (2014) 'In-situ biofilm characterization in membrane systems using Optical Coherence Tomography: Formation, structure, detachment and impact of flux change', *Water Research*. Pergamon, 67, pp. 243–254. doi: 10.1016/j.watres.2014.09.006.

Ehret, A. E. and Böl, M. (2013) 'Modelling mechanical characteristics of microbial biofilms by network theory', *Journal of the Royal Society Interface*. The Royal Society, 10(78), pp. 1–12. doi: 10.1098/rsif.2012.0676.

Erk, K. A., Henderson, K. J. and Shull, K. R. (2010) 'Strain stiffening in synthetic and biopolymer networks', *Biomacromolecules*, 11(5), pp. 1358–1363. doi: 10.1021/bm100136y.

Ewoldt, R. H. and Mckinley, G. H. (2007) 'Creep Ringing in Rheometry or How to Deal with oft-discarded Data in Step Stress Tests', *Rheology Bulletin*. Available at: http://web.mit.edu/nnf/publications/GHM103.pdf (Accessed: 23. November 2019).

Fan, J. and Njuguna, J. (2016) 'An Introduction to Lightweight Composite Materials and Their Use in Transport Structures', in *Lightweight Composite Structures in Transport: Design, Manufacturing, Analysis and Performance*. Woodhead Publishing, pp. 3–34. doi: 10.1016/B978-1-78242-325-6.00001-3.

Felz, S., Al-Zuhairy, S., Aarstad, O. A., van Loosdrecht, M. C. M. and Lin, Y. M. (2016) 'Extraction of Structural Extracellular Polymeric Substances from Aerobic Granular Sludge', *Journal of Visualized Experiments*, (115), pp. e54534–e54534. doi: 10.3791/54534.

Felz, S., Neu, T. R., van Loosdrecht, M. C. M. and Lin, Y. (2020) 'Aerobic granular sludge contains Hyaluronic acid-like and sulfated glycosaminoglycans-like polymers', *Water Research*, 169. doi: 10.1016/j.watres.2019.115291.

Felz, S., Kleikamp, H., Zlopasa, J., van Loosdrecht, M. C. M. and Lin, Y. (2020) 'Impact of metal ions on structural EPS hydrogels from aerobic granular sludge', *Biofilm*, 2. doi: 10.1016/j.bioflm.2019.100011.

Feng, L., Li, X., Song, P., Du, G. and Chen, J. (2014) 'Physicochemical properties and membrane biofouling of extra-cellular polysaccharide produced by a Micrococcus luteus strain.', *World Journal of Microbiology & Biotechnology*, 30(7), pp. 2025–31. doi: 10.1007/s11274-014-1627-y.

Ferrando Chavez, D. L., Nejidat, A. and Herzberg, M. (2016) 'Viscoelastic properties of extracellular polymeric substances can strongly affect their washing efficiency from reverse osmosis membranes', *Environmental Science and Technology*, 50(17), pp. 9206–9213. doi: 10.1021/acs.est.6b01458.

Fischer, F. G. and Dörfel, H. (1955) 'Die Polyuronsäuren der Braunalgen (Kohlenhydrate der Algen I)', *Hoppe-Seyler's Zeitschrift fur Physiologische Chemie*, 302(1–2), pp. 186–203. doi: 10.1515/bchm2.1955.302.1-2.186.

Flemming, H.-C., Schaule, G., Griebe, T., Schmitt, J. and Tamachkiarowa, A. (1997) 'Biofouling—the Achilles heel of membrane processes', *Desalination*, 113(2–3), pp. 215–225. doi: 10.1016/S0011-9164(97)00132-X.

Flemming, H.-C. (2000) 'Membranes and Microorganisms - Love at First Sight and the Consequences', in Hillis, P. (ed.) *Membrane Technology in Water and Wastewater Treatment*. Lancaster University, pp. 139–149. doi: 10.1039/9781847551351-00139.

Flemming, H.-C. and Wingender, J. (2001) 'Relevance of microbial extracellular polymeric substances (EPSs)--Part I: Structural and ecological aspects.', *Water science and technology : a journal of the International Association on Water Pollution Research*, 43(6), pp. 1–8. Available at: http://www.ncbi.nlm.nih.gov/pubmed/11381954 (Accessed: 26 September 2019).

Flemming, H.-C. (2002) 'Biofouling in water systems - Cases, causes and countermeasures', *Applied Microbiology and Biotechnology*, 59(6), pp. 629–640. doi: 10.1007/s00253-002-1066-9.

Flemming, H.-C. and Wingender, J. (2010) 'The biofilm matrix.', *Nature Reviews Microbiology*. Nature Publishing Group, 8(9), pp. 623–33. doi: 10.1038/nrmicro2415.

Flemming, H.-C. (2011) 'The perfect slime', *Colloids and Surfaces B: Biointerfaces*, pp. 251–259. doi: 10.1016/j.colsurfb.2011.04.025.

Flemming, H.-C., Wingender, J., Szewzyk, U., Steinberg, P., Rice, S. A. and Kjelleberg, S. (2016) 'Biofilms: An emergent form of bacterial life', *Nature Reviews Microbiology*, 14(9), pp. 563–575. doi: 10.1038/nrmicro.2016.94.

Flemming, H.-C. (2016) 'EPS—Then and Now', *Microorganisms*, 4(4), p. 41. doi: 10.3390/microorganisms4040041.

Flemming, H.-C., Neu, T. R. and Wingender, J. (2016) 'The Perfect Slime: Microbial Extracellular Polymeric Substances (EPS)', in *Water Intelligence Online*, pp. 9781780407425–9781780407425. doi: 10.2166/9781780407425.

Flemming, H.-C. (2020) 'Biofouling and me: My Stockholm syndrome with biofilms', *Water Research*, 173, p. 115576. doi: 10.1016/j.watres.2020.115576.

Frølund, B., Palmgren, R., Keiding, K. and Nielsen, P. H. (1996) 'Extraction of extracellular polymers from activated sludge using a cation exchange resin', *Water Research*, 30(8), pp. 1749–1758. doi: 10.1016/0043-1354(95)00323-1.

Fu, S., Thacker, A., Sperger, D. M., Boni, R. L., Buckner, I. S., Velankar, S., Munson, E. J. and Block, L. H. (2011) 'Relevance of Rheological Properties of Sodium Alginate in Solution to Calcium Alginate Gel Properties', *AAPS PharmSciTech*. Springer, 12(2), pp. 453–460. doi: 10.1208/s12249-011-9587-0.

Gagliano, M. C., Neu, T. R., Kuhlicke, U., Sudmalis, D., Temmink, H. and Plugge, C. M. (2018) 'EPS Glycoconjugate Profiles Shift as Adaptive Response in Anaerobic Microbial Granulation at High Salinity', *Frontiers in Microbiology*. Frontiers Media S.A., 9(JUL), p. 1423. doi: 10.3389/fmicb.2018.01423.

Gagliano, M. C., Sudmalis, D., Temmink, H. and Plugge, C. M. (2020) 'Calcium effect on microbial activity and biomass aggregation during anaerobic digestion at high salinity', *New Biotechnology*. Elsevier B.V., 56, pp. 114–122. doi: 10.1016/j.nbt.2020.01.001.

Galy, O., Latour-Lambert, P., Zrelli, K., Ghigo, J.-M. M., Beloin, C. and Henry, N. (2012) 'Mapping of bacterial biofilm local mechanics by magnetic microparticle actuation.', *Biophysical Journal*. Biophysical Society, 103(6), pp. 1400–1408. doi: 10.1016/j.bpj.2012.07.001.

Ganji, F., Vasheghani-Farahani, S. and Vasheghani-Farahani, E. (2010) 'Theoretical Description of Hydrogel Swelling: A Review', *Irymer Journalanian Pol*, 19(5), pp. 375–398. doi: 10.1007/s12303-009-0004-6.

Geesey, G. G. (1982) 'Microbial exopolymers: ecological and economic considerations', *American Society for Microbiology News*, 48(1), pp. 9–14. Available at: https://ci.nii.ac.jp/naid/10017164720/en/.

Gloag, E. S., German, G. K., Stoodley, P. and Wozniak, D. J. (2018) 'Viscoelastic properties of Pseudomonas aeruginosa variant biofilms', *Scientific Reports*. Nature Publishing Group, 8(1). doi: 10.1038/s41598-018-28009-5.

Gloag, E. S., Fabbri, S., Wozniak, D. J. and Stoodley, P. (2020) 'Biofilm mechanics: Implications in infection and survival', *Biofilm*. Elsevier BV, 2, p. 100017. doi: 10.1016/j.bioflm.2019.100017.

Gomes, I. B., Simões, M. and Simões, L. C. (2014) 'An overview on the reactors to study drinking water biofilms.', *Water Research*, 62, pp. 63–87. doi: 10.1016/j.watres.2014.05.039.

Goode, C. and Allen, D. G. (2011) 'Effect of Calcium on Moving-Bed Biofilm Reactor Biofilms', *Water Environment Research*, 83(3), pp. 220–232. doi: 10.2175/106143010x12780288628255.

Gorret, N., Renard, C. M. G. ., Famelart, M. ., Maubois, J. . and Doublier, J. . (2003) 'Rheological characterization of the EPS produced by P. acidi-propionici on milk microfiltrate', *Carbohydrate Polymers*, 51(2), pp. 149–158. doi: 10.1016/S0144-8617(02)00141-8.

de Graaff, D. R., Felz, S., Neu, T. R., Pronk, M., van Loosdrecht, M. C. M. and Lin, Y. (2019) 'Sialic acids in the extracellular polymeric substances of seawater-adapted aerobic granular sludge', *Water Research*. Elsevier Ltd, 155, pp. 343–351. doi: 10.1016/j.watres.2019.02.040.

Grant, G. T., Morris, E. R., Rees, D. A., Smith, P. J. C. and Thom, D. (1973) 'Biological interactions between polysaccharides and divalent cations: The egg-box model', *FEBS Letters*, 32(1), pp. 195–198. doi: 10.1016/0014-5793(73)80770-7.

Gristina, A. G., Hobgood, C. D., Webb, L. X. and Myrvik, Q. N. (1987) 'Adhesive colonization of biomaterials and antibiotic resistance', *Biomaterials*, 8(6), pp. 423–426. doi: 10.1016/0142-9612(87)90077-9.

Guan, D., Dai, J., Ahmar Siddiqui, M. and Chen, G. (2018) 'Comparison of different chemical cleaning reagents on fouling recovery in a Self-Forming dynamic membrane bioreactor (SFDMBR)', *Separation and Purification Technology*. Elsevier B.V., 206, pp. 158–165. doi: 10.1016/j.seppur.2018.05.059.

Guelon, T., Mathias, J. D. and Stoodley, P. (2011) 'Advances in Biofilm Mechanics', in *Biofilm Highlights*, pp. 111–139. doi: 10.1007/978-3-642-19940-0.

Guth, E. (1945) 'Theory of filler reinforcement', *Journal of Applied Physics*. American Institute of Physics, 16(1), pp. 20–25. doi: 10.1063/1.1707495.

Hall-Stoodley, L., Costerton, J. W. and Stoodley, P. (2004) 'Bacterial biofilms: From the natural environment to infectious diseases', *Nature Reviews Microbiology*, 2(2), pp. 95–108. doi: 10.1038/nrmicro821.

Han, Y., Zeng, Q., Li, H. and Chang, J. (2013) 'The calcium silicate/alginate composite: Preparation and evaluation of its behavior as bioactive injectable hydrogels', *Acta Biomaterialia*. Elsevier, 9(11), pp. 9107–9117. doi: 10.1016/j.actbio.2013.06.022.

Haug, A., Smidsrød, O., Larsen, B., Gronowitz, S., Hoffman, R. A. and Westerdahl, A. (1965) 'The Effect of Divalent Metals on the Properties of Alginate Solutions. II. Comparison of Different Metal Ions.', *Acta Chemica Scandinavica*. doi: 10.3891/acta.chem.scand.19-0341.

Haug, A. and Larsen, B. (1966) 'A Study on the Constitution of Alginic Acid by Partial Acid Hydrolysis', in *Proceedings of the Fifth International Seaweed Symposium, Halifax, August 25–28, 1965*. Elsevier, pp. 271–277. doi: 10.1016/b978-0-08-011841-3.50043-4.

Hen, J. (1974) 'Determination of surface carboxyl groups in styrene/itaconic acid copolymer latexes', *Journal of Colloid and Interface Science*, 49(3), pp. 425–432. doi: 10.1016/0021-9797(74)90388-9.

Hermansson, E., Schuster, E., Lindgren, L., Altskär, A. and Ström, A. (2016) 'Impact of solvent quality on the network strength and structure of alginate gels', *Carbohydrate Polymers*, 144, pp. 289–296. doi: 10.1016/j.carbpol.2016.02.069.

Hertz, H. (1882) 'Ueber die Berührung fester elastischer Körper', *Journal fur die Reine und Angewandte Mathematik*. doi: 10.1515/crll.1882.92.156.

Herzberg, M., Kang, S. and Elimelech, M. (2009) 'Role of Extracellular Polymeric Substances (EPS) in Biofouling of Reverse Osmosis Membranes', *Environmental Science & Technology*. American Chemical Society, 43(12), pp. 4393–4398. doi: 10.1021/es900087j.

Hobley, L., Harkins, C., MacPhee, C. E. and Stanley-Wall, N. R. (2015) 'Giving structure to the biofilm matrix: An overview of individual strategies and emerging common themes', *FEMS Microbiology Reviews*, pp. 649–669. doi: 10.1093/femsre/fuv015.

Høiby, N., Bjarnsholt, T., Givskov, M., Molin, S. and Ciofu, O. (2010) 'Antibiotic resistance of bacterial biofilms', *International Journal of Antimicrobial Agents*, 35(4), pp. 322–332. doi: 10.1016/j.ijantimicag.2009.12.011.

Houari, A., Picard, J., Habarou, H., Galas, L., Vaudry, H., Heim, V. and Martino, P. Di (2011) 'Rheology of biofilms formed at the surface of NF membranes in a drinking water production unit', *Biofouling*. Taylor & Francis. doi: 10.1080/08927010802023764.

Hu, Y. and Suo, Z. (2012) 'Viscoelasticity and poroelasticity in elastomeric gels', *Acta Mechanica Solida Sinica*. Elsevier, 25(5), pp. 441–458. doi: 10.1016/S0894-9166(12)60039-1.

Huang, H., Yu, Q., Ren, H., Geng, J., Xu, K., Zhang, Y. and Ding, L. (2018) 'Towards physicochemical and biological effects on detachment and activity recovery of aging biofilm by enzyme and surfactant treatments', *Bioresource Technology*. Elsevier Ltd, 247, pp. 319–326. doi: 10.1016/j.biortech.2017.09.082.

Huang, J. and Pinder, K. L. (1995) 'Effects of calcium on development of anaerobic acidogenic biofilms', *Biotechnology and Bioengineering*. John Wiley & Sons, Ltd, 45(3), pp. 212–218. doi: 10.1002/bit.260450305.

Ikuma, K., Decho, A. W. and Lau, B. L. T. (2013) *The Extracellular Bastions of Bacteria — A Biofilm Way of Life*, *Nature Education Knowledge*. Available at: https://www.nature.com/scitable/knowledge/library/the-extracellular-bastions-of-bacteria-nbsp-a-100450088/.

International Labour Organization (2009) *Calcium Gluconate*. Available at: http://www.ilo.org/dyn/icsc/showcard.display?p_version=2&p_card_id=1736 (Accessed: 12 February 2020).

International Labour Organization (2012) *Calcium Carbonate*. Available at: http://www.ilo.org/dyn/icsc/showcard.display?p_lang=en&p_card_id=1193&p_version=2 (Accessed: 12 February 2020).

Jafari, M., Desmond, P., van Loosdrecht, M. C. M., Derlon, N., Morgenroth, E. and Picioreanu, C. (2018) 'Effect of biofilm structural deformation on hydraulic resistance during ultrafiltration: A numerical and experimental study', *Water Research*, 145, pp. 375–387. doi: 10.1016/j.watres.2018.08.036.

Jamal, M. *et al.* (2018) 'Bacterial biofilm and associated infections', *Journal of the Chinese Medical Association*, 81(1), p. 2018. doi: 10.1016/j.jcma.2017.07.012.

Jones, W. L., Sutton, M. P., McKittrick, L. and Stewart, P. S. (2011) 'Chemical and antimicrobial treatments change the viscoelastic properties of bacterial biofilms.', *Biofouling*. Taylor & Francis, 27(2), pp. 207–215. doi: 10.1080/08927014.2011.554977.

Kaklamani, G., Cheneler, D., Grover, L. M., Adams, M. J. and Bowen, J. (2014) 'Mechanical properties of alginate hydrogels manufactured using external gelation', *Journal of the Mechanical Behavior of Biomedical Materials*, 36, pp. 135–142. doi: 10.1016/j.jmbbm.2014.04.013.

Katsoufidou, K., Yiantsios, S. G. and Karabelas, A. J. (2007) 'Experimental study of ultrafiltration membrane fouling by sodium alginate and flux recovery by backwashing', *Journal of Membrane Science*, 300(1–2), pp. 137–146. doi: 10.1016/j.memsci.2007.05.017.

Keiding, K., Wybrandt, L. and Nielsen, P. H. (2001) 'Remember the water - A comment on EPS colligative properties', *Water Science and Technology*, 43(6), pp. 17–23. doi: 10.2166/wst.2001.0330.

Khavari, A., Nydén, M., Weitz, D. A. and Ehrlicher, A. J. (2016) 'Composite alginate gels for tunable cellular microenvironment mechanics', *Scientific Reports*. Nature Publishing Group, 6(1), pp. 1–11. doi: 10.1038/srep30854.

Kielland, J. (1937) 'Individual Activity Coefficients of Ions in Aqueous Solutions', *Journal of the American Chemical Society*. American Chemical Society, 59(9), pp. 1675–1678. doi: 10.1021/ja01288a032.

Klapper, I., Rupp, C. J., Cargo, R., Purvedorj, B. and Stoodley, P. (2002) 'Viscoelastic fluid description of bacterial biofilm material properties', *Biotechnology and Bioengineering*. John Wiley & Sons, Ltd, 80(3), pp. 289–296. doi: 10.1002/bit.10376.

Kleikamp, H. (2017) *Metal Sorption and Mechanical Stiffness of Metal-Cross-linked Hydrogels of ALE from Aerobic Granular Sludge and Anammox Granules*. Master Thesis, TU Delft.

Koo, H., Allan, R. N., Howlin, R. P., Stoodley, P. and Hall-Stoodley, L. (2017) 'Targeting microbial biofilms: Current and prospective therapeutic strategies', *Nature Reviews Microbiology*. doi: 10.1038/nrmicro.2017.99.

Körstgens, V., Flemming, H.-C., Wingender, J. and Borchard, W. (2001) 'Influence of calcium ions on the mechanical properties of a model biofilm of mucoid Pseudomonas aeruginosa', *Water Science and Technology*, 43(6), pp. 49–57. doi: 10.1371/journal.pone.0091935.

Krzeminski, P., Leverette, L., Malamis, S. and Katsou, E. (2017) 'Membrane bioreactors – A review on recent developments in energy reduction, fouling control, novel configurations, LCA and market prospects', *Journal of Membrane Science*. Elsevier B.V., pp. 207–227. doi: 10.1016/j.memsci.2016.12.010.

Kühn, P. T., Rozenbaum, R. T., Perrels, E., Sharma, P. K. and van Rijn, P. (2017) 'Anti-microbial biopolymer hydrogel scaffolds for stem cell encapsulation', *Polymers*, 9(4), p. 149. doi: 10.3390/polym9040149.

Kuo, C. K. and Ma, P. X. (2001) 'Ionically crosslinked alginate hydrogels as scaffolds for tissue engineering: Part 1. Structure, gelation rate and mechanical properties', *Biomaterials*, 22(6), pp. 511–521. doi: 10.1016/S0142-9612(00)00201-5.

Laspidou, C. S. and Rittmann, B. E. (2004) 'Evaluating trends in biofilm density using the UMCCA model', *Water Research*, 38(14–15), pp. 3362–3372. doi: 10.1016/j.watres.2004.04.051.

Laspidou, C. S. and Aravas, N. (2007) 'Variation in the mechanical properties of a porous multi-phase biofilm under compression due to void closure', *Water Science and Technology*, 55(8–9), pp. 447–453. doi: 10.2166/wst.2007.289.

Laspidou, C. S., Spyrou, L. A., Aravas, N. and Rittmann, B. E. (2014) 'Material modeling of biofilm mechanical properties', *Mathematical Biosciences*, 251(1), pp. 11–15. doi: 10.1016/j.mbs.2014.02.007.

Lau, P. C. Y., Dutcher, J. R., Beveridge, T. J. and Lam, J. S. (2009) 'Absolute Quantitation of Bacterial Biofilm Adhesion and Viscoelasticity by Microbead Force Spectroscopy', *Biophysical Journal*, 96(7), pp. 2935–2948. doi: 10.1016/j.bpj.2008.12.3943.

LeChevallier, M. W., Cawthon, C. D. and Lee, R. G. (1988) 'Inactivation of biofilm bacteria.', *Applied and environmental microbiology*. American Society for Microbiology (ASM), 54(10), pp. 2492–9. Available at: http://www.ncbi.nlm.nih.gov/pubmed/2849380 (Accessed: 26 September 2019).

Lee, K. Y. and Mooney, D. J. (2012) 'Alginate: properties and biomedical applications.', *Progress in Polymer Science*. NIH Public Access, 37(1), pp. 106–126. doi: 10.1016/j.progpolymsci.2011.06.003.

Lee, S. and Elimelech, M. (2006) 'Relating Organic Fouling of Reverse Osmosis Membranes to Intermolecular Adhesion Forces', *Environmental Science & Technology*. American Chemical Society, 40(3), pp. 980–987. doi: 10.1021/es051825h.

Levin, P. A. and Angert, E. R. (2015) 'Small but mighty: Cell size and bacteria', *Cold Spring Harbor Perspectives in Biology*, 7(7), pp. 1–11. doi: 10.1101/cshperspect.a019216.

Li, Q. and Elimelech, M. (2004) 'Organic Fouling and Chemical Cleaning of Nanofiltration Membranes: Measurements and Mechanisms', *Environmental Science & Technology*. American Chemical Society, 38(17), pp. 4683–4693. doi: 10.1021/es0354162.

Li, Q., Xu, Z. and Pinnau, I. (2007) 'Fouling of reverse osmosis membranes by biopolymers in wastewater secondary effluent: Role of membrane surface properties and initial permeate flux', *Journal of Membrane Science*, 290(1–2), pp. 173–181. doi: 10.1016/j.memsci.2006.12.027.

Lieleg, O., Caldara, M., Baumgärtel, R. and Ribbeck, K. (2011) 'Mechanical robustness of Pseudomonas aeruginosa biofilms', *Soft Matter*, 7, pp. 3307–3314. doi: 10.1039/c0sm01467b.

Lin, H., Zhang, M., Wang, F., Meng, F., Liao, B. Q., Hong, H., Chen, J. and Gao, W. (2014) 'A critical review of extracellular polymeric substances (EPSs) in membrane bioreactors: Characteristics, roles in membrane fouling and control strategies', *Journal of Membrane Science*. Elsevier, 460, pp. 110–125. doi: 10.1016/j.memsci.2014.02.034.

Lin, Y. M., Wang, L., Chi, Z. M. and Liu, X. Y. (2008) 'Bacterial Alginate Role in Aerobic Granular Bio-particles Formation and Settleability Improvement', *Separation Science and Technology*. Taylor & Francis Group, 43(7), pp. 1642–1652. doi: 10.1080/01496390801973805.

Lin, Y. M., de Kreuk, M., van Loosdrecht, M. C. M. and Adin, A. (2010) 'Characterization of alginate-like exopolysaccharides isolated from aerobic granular sludge in pilot-plant.', *Water Research*, 44(11), pp. 3355–3364. doi: 10.1016/j.watres.2010.03.019.

Lin, Y. M., Sharma, P. K. and van Loosdrecht, M. C. M. (2013) 'The chemical and mechanical differences between alginate-like exopolysaccharides isolated from aerobic flocculent sludge and aerobic granular sludge', *Water Research*, 47(1), pp. 57–65. doi: 10.1016/j.watres.2012.09.017.

Lin, Y. M., Nierop, K. G. J., Girbal-Neuhauser, E., Adriaanse, M. and van Loosdrecht, M. C. M. (2015) 'Sustainable polysaccharide-based biomaterial recovered from waste aerobic granular sludge as a surface coating material', *Sustainable Materials and Technologies*, 4, pp. 24–29. doi: 10.1016/j.susmat.2015.06.002.

Lin, Y. M., Reino, C., Carrera, J., Pérez, J. and van Loosdrecht, M. C. M. (2018) 'Glycosylated amyloid-like proteins in the structural extracellular polymers of aerobic granular sludge enriched with ammonium-oxidizing bacteria', *MicrobiologyOpen*, 7(6). doi: 10.1002/mbo3.616.

Listiarini, K., Chun, W., Sun, D. D. and Leckie, J. O. (2009) 'Fouling mechanism and resistance analyses of systems containing sodium alginate, calcium, alum and their combination in dead-end fouling of nanofiltration membranes', *Journal of Membrane Science*. doi: 10.1016/j.memsci.2009.08.010.

Listiarini, K., Sun, D. D. and Leckie, J. O. (2009) 'Organic fouling of nanofiltration membranes: Evaluating the effects of humic acid, calcium, alum coagulant and their combinations on the specific cake resistance', *Journal of Membrane Science*, 332(1–2), pp. 56–62. doi: 10.1016/j.memsci.2009.01.037.

Liu, L., Huang, Q. and Qin, B. (2018) 'Characteristics and roles of *Microcystis* extracellular polymeric substances (EPS) in cyanobacterial blooms: a short review', *Journal of Freshwater Ecology*. Taylor and Francis Inc., 33(1), pp. 183–193. doi: 10.1080/02705060.2017.1391722.

van Loosdrecht, M., Eikelboom, D., Gjaltema, A., Mulder, A., Tijhuis, L. and Heijnen, J. (1995) 'Biofilm structures', *Water Science and Technology*, 32(8), pp. 35–43. doi: 10.1016/0273-1223(96)00005-4.

van Loosdrecht, M. (1997) 'A more unifying hypothesis for biofilm structures', *FEMS Microbiology Ecology*, 24(2), pp. 181–183. doi: 10.1016/S0168-6496(97)00064-0.

Ma, J., Wang, Z., Li, H., Park, H.-D. and Wu, Z. (2016) 'Metagenomes reveal microbial structures, functional potentials, and biofouling-related genes in a membrane bioreactor.', *Applied Microbiology and Biotechnology*. doi: 10.1007/s00253-016-7312-3.

Malone, M. *et al.* (2017) 'The prevalence of biofilms in chronic wounds: A systematic review and meta-analysis of published data', *Journal of Wound Care*, 26(1), pp. 20–25. doi: 10.12968/jowc.2017.26.1.20.

Mancini, M., Moresi, M. and Rancini, R. (1999) 'Mechanical properties of alginate gels: empirical characterisation', *Journal of Food Engineering*. Elsevier, 39(4), pp. 369–378. doi: 10.1016/S0260-8774(99)00022-9.

Massol-Deyá, A. A., Whallon, J., Hickey, R. F. and Tiedje, J. M. (1995) 'Channel structures in aerobic biofilms of fixed-film reactors treating contaminated groundwater.', *Applied and Environmental Microbiology*, 61(2), pp. 769–77. doi: 10.1128/AEM.61.2.769-777.1995.

Mayer, C., Moritz, R., Kirschner, C., Borchard, W., Maibaum, R., Wingender, J. and Flemming, H. C. (1999) 'The role of intermolecular interactions: Studies on model systems for bacterial biofilms', *International Journal of Biological Macromolecules*, 26(1), pp. 3–16. doi: 10.1016/S0141-8130(99)00057-4.

McCrate, O. a, Zhou, X., Reichhardt, C. and Cegelski, L. (2013) 'Sum of the parts: composition and architecture of the bacterial extracellular matrix.', *Journal of Molecular Biology*. Elsevier Ltd, 425(22), pp. 4286–94. doi: 10.1016/j.jmb.2013.06.022.

Meng, S., Winters, H. and Liu, Y. (2015) 'Ultrafiltration behaviors of alginate blocks at various calcium concentrations.', *Water Research*, 83, pp. 248–257. doi: 10.1016/j.watres.2015.06.008.

Meyer, B. (2003) 'Approaches to prevention, removal and killing of biofilms', *International Biodeterioration & Biodegradation*, 51(4), pp. 249–253. doi: 10.1016/S0964-8305(03)00047-7.

Mezger, T. G. (2006) *The Rheology Handbook: For Users of Rotational and Oscillatory Rheometers*. 2nd revise, *The Rheology Handbook*. 2nd revise. Hannover: Vincentz Network GmbH & Co KG.

Mezger, T. G. (2014) '16. Frequency sweeps', in *Applied Rheology*. Anton Paar, pp. 113–122.

Möhle, R. B., Langemann, T., Haesner, M., Augustin, W., Scholl, S., Neu, T. R., Hempel, D. C. and Horn, H. (2007) 'Structure and shear strength of microbial biofilms as determined with confocal laser scanning microscopy and fluid dynamic gauging using a novel rotating disc biofilm reactor.', *Biotechnology and Bioengineering*, 98(4), pp. 747–755. doi: 10.1002/bit.21448.

More, T. T., Yadav, J. S. S., Yan, S., Tyagi, R. D. and Surampalli, R. Y. (2014) 'Extracellular polymeric substances of bacteria and their potential environmental applications', *Journal of Environmental Management*. Academic Press, 144, pp. 1–25. doi: 10.1016/J.JENVMAN.2014.05.010.

Moresi, M., Bruno, M. and Parente, E. (2004) 'Viscoelastic properties of microbial alginate gels by oscillatory dynamic tests', *Journal of Food Engineering*. Elsevier, 64(2), pp. 179–186. doi: 10.1016/j.jfoodeng.2003.09.030.

Morris, E. R., Rees, D. A. and Thom, D. (1973) 'Characterization of polysaccharide structure and interactions by circular dichroism: Order-disorder transition in the calcium alginate system', *Journal of the Chemical Society, Chemical Communications*, (7), pp. 245–246. doi: 10.1039/C39730000245.

Müller-Steinhagen, H., Malayeri, M. R. and Watkinson, A. P. (2011) 'Heat exchanger fouling: Mitigation and cleaning strategies', *Heat Transfer Engineering*. Taylor & Francis Group , 32(3–4), pp. 189–196. doi: 10.1080/01457632.2010.503108.

Ojkic, N., Serbanescu, D. and Banerjee, S. (2019) 'Universal surface-to-volume scaling and aspect ratio homeostasis in rod-shaped bacteria', *eLife*. Cold Spring Harbor Laboratory, 8, p. e47033. doi: 10.7554/eLife.47033.

Paar, A. (2008) *Viscosity Table - Measurement data*, *Viscosity of Water*. Available at: https://wiki.anton-paar.com/en/water/ (Accessed: 11 June 2019).

Pallagi, A., Sebk, P., Forgó, P., Jakusch, T., Pálinkó, I. and Sipos, P. (2010) 'Multinuclear NMR and molecular modelling investigations on the structure and equilibria of complexes that form in aqueous solutions of Ca2+ and gluconate', *Carbohydrate Research*. doi: 10.1016/j.carres.2010.05.009.

Paramonova, E., Kalmykowa, O. J., Van Der Mei, H. C., Busscher, H. J. and Sharma, P. K. (2009) 'Impact of hydrodynamics on oral biofilm strength', *Journal of Dental Research*, 88(10), pp. 922–926. doi: 10.1177/0022034509344569.

Patsios, S. I. I., Goudoulas, T. B. B., Kastrinakis, E. G. G., Nychas, S. G. G. and Karabelas, A. J. J. (2015) 'A novel method for rheological characterization of biofouling layers developing in Membrane Bioreactors (MBR)', *Journal of Membrane Science*, 482, pp. 13–24. doi: 10.1016/j.memsci.2015.02.016.

Pellicer-Nàcher, C. and Smets, B. F. (2014) 'Structure, composition, and strength of nitrifying membrane-aerated biofilms.', *Water research*, 57, pp. 151–61. doi: 10.1016/j.watres.2014.03.026.

Peterson, B. W., Busscher, H. J., Sharma, P. K. and van der Mei, H. C. (2012) 'Environmental and centrifugal factors influencing the visco-elastic properties of oral biofilms in vitro', *Biofouling*, 28(9), pp. 913–920. doi: 10.1080/08927014.2012.721515.

Peterson, B. W., van der Mei, H. C., Sjollema, J., Busscher, H. J. and Sharma, P. K. (2013) 'A distinguishable role of eDNA in the viscoelastic relaxation of biofilms', *mBio*, 4(5). doi: 10.1128/mBio.00497-13.

Peterson, B. W. *et al.* (2015) 'Viscoelasticity of biofilms and their recalcitrance to mechanical and chemical challenges', *FEMS Microbiology Reviews*, pp. 234–245. doi: 10.1093/femsre/fuu008.

Picioreanu, C., Blauert, F., Horn, H. and Wagner, M. (2018) 'Determination of mechanical properties of biofilms by modelling the deformation measured using optical coherence tomography', *Water Research*, 145, pp. 588–598. doi: 10.1016/j.watres.2018.08.070.

Powell, L. C., Sowedan, A., Khan, S., Wright, C. J., Hawkins, K., Onsøyen, E., Myrvold, R., Hill, K. E. and Thomas, D. W. (2013) 'The effect of alginate oligosaccharides on the mechanical properties of Gram-negative biofilms.', *Biofouling*. Routledge, 29(4), pp. 413–421. doi: 10.1080/08927014.2013.777954.

Pronk, M., de Kreuk, M. K., de Bruin, B., Kamminga, P., Kleerebezem, R. and van Loosdrecht, M. C. M. (2015) 'Full scale performance of the aerobic granular sludge process for sewage treatment', *Water Research*. Pergamon, 84, pp. 207–217. doi: 10.1016/j.watres.2015.07.011.

Radchenkova, N. *et al.* (2018) 'Extracellular polymer substance synthesized by a halophilic bacterium Chromohalobacter canadensis 28', *Applied Microbiology and Biotechnology*, 102(11), pp. 4937–4949. doi: 10.1007/s00253-018-8901-0.

Ramachandran, S., Fontanille, P., Pandey, A. and Larroche, C. (2006) 'Gluconic acid: Properties, applications and microbial production', *Food Technology and Biotechnology*, pp. 185–195. Available at: http://ir.niist.res.in:8080/jspui/handle/123456789/2172.

Rao, T. S., Kora, A. J., Chandramohan, P., Panigrahi, B. S. and Narasimhan, S. V. (2009) 'Biofouling and microbial corrosion problem in the thermo-fluid heat exchanger and cooling water system of a nuclear test reactor', *Biofouling*, 25(7), pp. 581–591. doi: 10.1080/08927010903016543.

Remminghorst, U. and Rehm, B. H. A. (2006) 'Bacterial alginates: From biosynthesis to applications', *Biotechnology Letters*, pp. 1701–1712. doi: 10.1007/s10529-006-9156-x.

Rezakazemi, M., Khajeh, A. and Mesbah, M. (2018) 'Membrane filtration of wastewater from gas and oil production', *Environmental Chemistry Letters*. Springer Verlag, pp. 367–388. doi: 10.1007/s10311-017-0693-4.

Ripperger, S., Gösele, W., Alt, C. and Loewe, T. (2013) 'Filtration, 1. Fundamentals', in *Ullmann's Encyclopedia of Industrial Chemistry*, pp. 1–38. doi: 10.1002/14356007.b02_10.pub3.

Rittmann, B. E. (2018) 'Biofilms, active substrata, and me', *Water Research*. Elsevier Ltd, pp. 135–145. doi: 10.1016/j.watres.2017.12.043.

Robinson, R. A. and Stokes, R. H. (1959) 'Appendix 7', in *Electrolyte Solutions (2nd Revised Edition)*. Dover Publications, p. 468. Available at: https://app.knovel.com/hotlink/pdf/id:kt00B6RCD3/electrolyte-solutions/appendix-7 (Accessed: 22 April 2020).

Rochex, A., Godon, J.-J., Bernet, N. and Escudié, R. (2008) 'Role of shear stress on composition, diversity and dynamics of biofilm bacterial communities.', *Water Research*, 42(20), pp. 4915–22. doi: 10.1016/j.watres.2008.09.015.

Romero, D., Aguilar, C., Losick, R. and Kolter, R. (2010) 'Amyloid fibers provide structural integrity to Bacillus subtilis biofilms', *Proceedings of the National Academy of Sciences*, 107(5), pp. 2230–2234. doi: 10.1073/pnas.0910560107.

Roorda, J. H. and van der Graaf, J. H. J. M. (2001) 'New parameter for monitoring fouling during ultrafiltration of WWTP effluent', *Water Science and Technology*, 43(10), pp. 241–248. doi: https://doi.org/10.2166/wst.2001.0631.

Safari, A., Habimana, O., Allen, A. and Casey, E. (2014) 'The significance of calcium ions on Pseudomonas fluorescens biofilms - a structural and mechanical study', *Biofouling*, 30(7), pp. 859–869. doi: 10.1080/08927014.2014.938648.

Safari, A., Tukovic, Z., Walter, M., Casey, E. and Ivankovic, A. (2015) 'Mechanical properties of a mature biofilm from a wastewater system: from microscale to macroscale level', *Biofouling*, 31(8), pp. 651–664. doi: 10.1080/08927014.2015.1075981.

Scherer, G. W. (1989) 'Mechanics of syneresis I. Theory', *Journal of Non-Crystalline Solids*. North-Holland, 108(1), pp. 18–27. doi: 10.1016/0022-3093(89)90328-1.

Schippers, J. C. and Verdouw, J. (1980) 'The modified fouling index, a method of determining the fouling characteristics of water', *Desalination*. Elsevier, 32(C), pp. 137–148. doi: 10.1016/S0011-9164(00)86014-2.

Schultz, M. P., Bendick, J. A., Holm, E. R. and Hertel, W. M. (2011) 'Economic impact of biofouling on a naval surface ship', *Biofouling*, 27(1), pp. 87–98. doi: 10.1080/08927014.2010.542809.

Seviour, T., Pijuan, M., Nicholson, T., Keller, J. and Yuan, Z. (2009) 'Understanding the properties of aerobic sludge granules as hydrogels', *Biotechnology and Bioengineering*, 102(5), pp. 1483–1493. doi: 10.1002/bit.22164.

Seviour, T. *et al.* (2019) 'Extracellular polymeric substances of biofilms: suffering from an identity crisis', *Water Research*. Pergamon, 151, pp. 1–7. doi: 10.1016/j.watres.2018.11.020.

Shannon, M. A., Bohn, P. W., Elimelech, M., Georgiadis, J. G., Marĩas, B. J. and Mayes, A. M. (2008) 'Science and technology for water purification in the coming decades', *Nature*. Nature Publishing Group, pp. 301–310. doi: 10.1038/nature06599.

Shapiro, J. M. and Oyen, M. L. (2013) 'Hydrogel composite materials for tissue engineering scaffolds', *JOM*. Springer, 65(4), pp. 505–516. doi: 10.1007/s11837-013-0575-6.

Sharma, P. K., Busscher, H. J., Terwee, T., Koopmans, S. A. and van Kooten, T. G. (2011) 'A comparative study on the viscoelastic properties of human and animal lenses', *Experimental Eye Research*, 93(5), pp. 681–688. doi: 10.1016/j.exer.2011.08.009.

Shaw, T., Winston, M., Rupp, C. J., Klapper, I. and Stoodley, P. (2004) 'Commonality of elastic relaxation times in biofilms', *Physical Review Letters*. American Physical Society, 93(9), p. 098102. doi: 10.1103/PhysRevLett.93.098102.

Simões, M., Pereira, M. O. and Vieira, M. J. (2005) 'Effect of mechanical stress on biofilms challenged by different chemicals.', *Water Research*, 39(20), pp. 5142–52. doi: 10.1016/j.watres.2005.09.028.

Singh, R. (2015) 'Water and Membrane Treatment', in *Membrane Technology and Engineering for Water Purification*. 2nd edn. Elsevier, pp. 81–178. doi: 10.1016/b978-0-444-63362-0.00002-1.

Sioutopoulos, D. C. and Karabelas, A. J. (2012) 'Correlation of organic fouling resistances in RO and UF membrane filtration under constant flux and constant pressure', *Journal of Membrane Science*. Elsevier, 407–408, pp. 34–46. doi: 10.1016/j.memsci.2012.03.036.

Sitterly, G. (2008) *Poly-L-Lysine Cell Attachment Protocol*, *BioFiles*. Available at: https://www.sigmaaldrich.com/technical-documents/articles/biofiles/poly-lysine-product.html (Accessed: 22 April 2020).

Siviello, C., Greco, F. and Larobina, D. (2015) 'Analysis of linear viscoelastic behaviour of alginate gels: Effects of inner relaxation, water diffusion, and syneresis', *Soft Matter*. Royal Society of Chemistry, 11(30), pp. 6045–6054. doi: 10.1039/c5sm01244a.

Skjk-Bræk, G., Grasdalen, H. and Larsen, B. (1986) 'Monomer sequence and acetylation pattern in some bacterial alginates', *Carbohydrate Research*, 154(1), pp. 239–250. doi: 10.1016/S0008-6215(00)90036-3.

Smalley, D. L., Hansen, V. R. and Baselski, V. S. (1983) 'Susceptibility of Pseudomonas paucimobilis to 24 antimicrobial agents.', *Antimicrobial agents and chemotherapy*. American Society for Microbiology (ASM), 23(1), pp. 161–2. doi: 10.1128/aac.23.1.161.

Smallwood, H. M. (1944) 'Limiting law of the reinforcement of rubber', *Journal of Applied Physics*. American Institute of Physics, 15(11), pp. 758–766. doi: 10.1063/1.1707385.

Smidsrød, O., Haug, A., Larsen, B., Gronowitz, S., Hoffman, R. A. and Westerdahl, A. (1965) 'The Effect of Divalent Metals on the Properties of Alginate Solutions. I. Calcium Ions.', *Acta Chemica Scandinavica*. doi: 10.3891/acta.chem.scand.19-0329.

Smidsrød, O. (1974) 'Molecular basis for some physical properties of alginates in the gel state', *Faraday Discussions of the Chemical Society*. The Royal Society of Chemistry, 57(0), pp. 263–274. doi: 10.1039/DC9745700263.

Song, J. L., Au, K. H., Huynh, K. T. and Packman, A. I. (2014) 'Biofilm responses to smooth flow fields and chemical gradients in novel microfluidic flow cells.', *Biotechnology and bioengineering*, 111(3), pp. 597–607. doi: 10.1002/bit.25107.

Sperelakis, N. (2012) 'Chapter 10 - Gibbs-donnan equilibrium potentials', in *Cell Physiology Source Book*. 4th edn. Elsevier BV, pp. 147–151. doi: 10.1016/B978-0-12-387738-3.00010-X.

Starruß, J., Peruani, F., Bär, M. and Deutsch, A. (2007) 'Bacterial swarming driven by rod shape', in *Modeling and Simulation in Science, Engineering and Technology*. Springer Basel, pp. 163–174. doi: 10.1007/978-0-8176-4558-8_14.

Stoodley, P., Wilson, S., Cargo, R., Piscitteli, C. and Rupp, C. J. (2001) 'Detachment and other dynamic processes in bacterial biofilms', in *Surfaces in Biomaterials 2001 Symposium Proceedings*. Surfaces in Biomaterials Foundation, pp. 189–192. Available at: https://eprints.soton.ac.uk/157633/ (Accessed: 24 October 2014).

Storm, C., Pastore, J. J., MacKintosh, F. C., Lubensky, T. C. and Janmey, P. A. (2005) 'Nonlinear elasticity in biological gels', *Nature*, 435(7039), pp. 191–194. doi: 10.1038/nature03521.

Strogatz, S. H. (2018) *Nonlinear Dynamics and Chaos: With Applications to Physics, Biology, Chemistry, and Engineering*. 2nd edn. Boca Raton: CRC Press. doi: 10.1201/9780429492563.

Sutherland, I. (2001) 'The biofilm matrix – an immobilized but dynamic microbial environment', *Trends in Microbiology*, 9(5), pp. 222–227. doi: 10.1016/S0966-842X(01)02012-1.

van de Ven, W. J. C., Sant, K. van t., Pünt, I. G. M., Zwijnenburg, A., Kemperman, A. J. B., van der Meer, W. G. J. and Wessling, M. (2008) 'Hollow fiber dead-end ultrafiltration: Influence of ionic environment on filtration of alginates', *Journal of Membrane Science*. Elsevier, 308(1–2), pp. 218–229. doi: 10.1016/j.memsci.2007.09.062.

van de Ven, W., Pünt, I., Kemperman, A. and Wessling, M. (2009) 'Unraveling ultrafiltration of polysaccharides with flow field flow fractionation', *Journal of Membrane Science*, 338(1–2), pp. 67–74. doi: 10.1016/j.memsci.2009.04.008.

Villacorte, L. O., Ekowati, Y., Calix-Ponce, H. N., Kisielius, V., Kleijn, J. M., Vrouwenvelder, J. S., Schippers, J. C. and Kennedy, M. D. (2017) 'Biofouling in capillary and spiral wound membranes facilitated by marine algal bloom', *Desalination*, 424, pp. 74–84. doi: 10.1016/j.desal.2017.09.035.

Vinogradov, A. M., Winston, M., Rupp, C. J. and Stoodley, P. (2004) 'Rheology of biofilms formed from the dental plaque pathogen Streptococcus mutans', *Biofilms*, 1, pp. 49–56. doi: 10.1017/s1479050503001078.

Vrouwenvelder, H., Dreszer, C., Linares, R. V., Kruithof, J. C., Mayer, C. hristia. and Flemming, H.-C. (2016) 'Why and how biofilms cause biofouling–the "hair-in-sink"-effect', in *The Perfect Slime: Microbial extracellular polymeric substances*. Heidelberg, New York: IWA Publishing, pp. 193–206.

Vrouwenvelder, J. S., Manolarakis, S. A., van der Hoek, J. P., van Paassen, J. A. M., van der Meer, W. G. J., van Agtmaal, J. M. C., Prummel, H. D. M., Kruithof, J. C. and van Loosdrecht, M. C. M. (2008) 'Quantitative biofouling diagnosis in full scale nanofiltration and reverse osmosis installations.', *Water Research*, 42(19), pp. 4856–68. doi: 10.1016/j.watres.2008.09.002.

Vrouwenvelder, J. S., Buiter, J., Riviere, M., van der Meer, W. G. J., van Loosdrecht, M. C. M. and Kruithof, J. C. (2010) 'Impact of flow regime on pressure drop increase and biomass accumulation and morphology in membrane systems.', *Water Research*, 44(3), pp. 689–702. doi: 10.1016/j.watres.2009.09.054.

Wang, L. L. *et al.* (2012) 'PH dependence of structure and surface properties of microbial EPS', *Environmental Science and Technology*, 46(2), pp. 737–744. doi: 10.1021/es203540w.

Wang, X. and Spencer, H. G. (1998) 'Calcium alginate gels: Formation and stability in the presence of an inert electrolyte', *Polymer*, 39(13), pp. 2759–2764. doi: 10.1016/S0032-3861(97)00597-1.

Wang, Z. W., Liu, Y. and Tay, J. H. (2007) 'Biodegradability of extracellular polymeric substances produced by aerobic granules', *Applied Microbiology and Biotechnology*. Springer, 74(2), pp. 462–466. doi: 10.1007/s00253-006-0686-x.

Weisel, J. W. and Litvinov, R. I. (2013) 'Adaptation of fibrous biopolymers to recurring increasing strains', *Proceedings of the National Academy of Sciences*. National Academy of Sciences, 110(30), pp. 12164–12165. doi: 10.1073/pnas.1310351110.

Weiss, T. F. and Freeman, D. M. (1997) 'Equilibrium behavior of an isotropic polyelectrolyte gel model of the tectorial membrane: The role of fixed charges', *Auditory Neurosicences*, 3(4), pp. 351–361. doi: 10.1016/S0378-5955(97)00096-8.

Weiss, T. H., Mills, A. L., Hornberger, G. M. and Herman, J. S. (1995) 'Effect of Bacterial Cell Shape on Transport of Bacteria in Porous Media', *Environmental Science and Technology*. American Chemical Society, 29(7), pp. 1737–1740. doi: 10.1021/es00007a007.

Whitman, W. B., Coleman, D. C. and Wiebe, W. J. (1998) 'Prokaryotes: The unseen majority', *Proceedings of the National Academy of Sciences*. National Academy of Sciences, 95(12), pp. 6578–6583. doi: 10.1073/PNAS.95.12.6578.

Wilking, J. N., Angelini, T. E., Seminara, A., Brenner, M. P. and Weitz, D. A. (2011) 'Biofilms as complex fluids', *MRS Bulletin*. Cambridge University Press, 36(05), pp. 385–391. doi: 10.1557/mrs.2011.71.

Willems, S. B. J., Bunschoten, A., Wagterveld, R. M., Van Leeuwen, F. W. B. and Velders, A. H. (2019) 'On-Flow Immobilization of Polystyrene Microspheres on β-Cyclodextrin-Patterned Silica Surfaces through Supramolecular Host-Guest Interactions', *ACS Applied Materials and Interfaces*. American Chemical Society, 11(39), pp. 36221–36231. doi: 10.1021/acsami.9b11069.

Wimpenny, J., Manz, W. and Szewzyk, U. (2000) 'Heterogeneity in biofilms', *FEMS Microbiology Reviews*, 24(5), pp. 661–671. doi: 10.1111/j.1574-6976.2000.tb00565.x.

Wingender, J., Neu, T. R. and Flemming, H.-C. (1999) 'What are Bacterial Extracellular Polymeric Substances?', in *Microbial Extracellular Polymeric Substances*. 1st edn. Berlin: Springer, pp. 1–19. doi: 10.1007/978-3-642-60147-7_1.

Wingender, J. and Flemming, H. C. (2004) 'Contamination potential of drinking water distribution network biofilms', *Water Science and Technology*, 49(11–12), pp. 277–286. doi: 10.2166/wst.2004.0861.

Wingender, J. and Flemming, H.-C. (2011) 'Biofilms in drinking water and their role as reservoir for pathogens', *International Journal of Hygiene and Environmental Health*, 214(6), pp. 417–423. doi: 10.1016/j.ijheh.2011.05.009.

Wloka, M., Rehage, H., Flemming, H.-C. and Wingender, J. (2004) 'Rheological properties of viscoelastic biofilm extracellular polymeric substances and comparison to the behavior of calcium alginate gels', *Colloid and Polymer Science*, 282(10), pp. 1067–1076. doi: 10.1007/s00396-003-1033-8.

Wloka, M., Rehage, H., Flemming, H.-C. and Wingender, J. (2005) 'Structure and rheological behaviour of the extracellular polymeric substance network of mucoid Pseudomonas aeruginosa biofilms', *Biofilms*. Cambridge University Press, 2(04), p. 275. doi: 10.1017/S1479050506002031.

Yadav, M. K., Vidal, J. E. and Song, J.-J. (2020) 'Microbial biofilms on medical indwelling devices', in *New and Future Developments in Microbial Biotechnology and Bioengineering: Microbial Biofilms*. Elsevier, pp. 15–28. doi: 10.1016/b978-0-444-64279-0.00002-5.

Yue, Z. B., Li, Q., Li, C. chuan, Chen, T. hu and Wang, J. (2015) 'Component analysis and heavy metal adsorption ability of extracellular polymeric substances (EPS) from sulfate reducing bacteria', *Bioresource Technology*. Elsevier Ltd, 194, pp. 399–402. doi: 10.1016/j.biortech.2015.07.042.

Zhang, J., Daubert, C. R. and Foegeding, E. A. (2007) 'A proposed strain-hardening mechanism for alginate gels', *Journal of Food Engineering*. Elsevier, 80(1), pp. 157–165. doi: 10.1016/j.jfoodeng.2006.04.057.

Zhang, L., Han, J., Wang, H., Car, R. and Weinan, E. (2018) 'Deep Potential Molecular Dynamics: A Scalable Model with the Accuracy of Quantum Mechanics', *Physical Review Letters*. doi: 10.1103/PhysRevLett.120.143001.

Zhang, T. C. and Bishop, P. L. (1994) 'Density, porosity, and pore structure of biofilms', *Water Research*. Pergamon, 28(11), pp. 2267–2277. doi: 10.1016/0043-1354(94)90042-6.

Zhang, X. and Bishop, P. L. (2003) 'Biodegradability of biofilm extracellular polymeric substances', *Chemosphere*. Pergamon, 50(1), pp. 63–69. doi: 10.1016/S0045-6535(02)00319-3.

Zhu, L., Qi, H. Y., Lv, M. Le, Kong, Y., Yu, Y. W. and Xu, X. Y. (2012) 'Component analysis of extracellular polymeric substances (EPS) during aerobic sludge granulation using FTIR and 3D-EEM technologies', *Bioresource Technology*. Elsevier, 124, pp. 455–459. doi: 10.1016/j.biortech.2012.08.059.

Zlopasa, J., Norder, B., Koenders, E. A. B. and Picken, S. J. (2016) 'Rheological investigation of specific interactions in Na Alginate and Na MMT suspension', *Carbohydrate Polymers*, 151, pp. 144–149. doi: 10.1016/j.carbpol.2016.05.055.

Zrelli, K., Galy, O., Latour-Lambert, P., Kirwan, L., Ghigo, J. M., Beloin, C. and Henry, N. (2013) 'Bacterial biofilm mechanical properties persist upon antibiotic treatment and survive cell death', *New Journal of Physics*. IOP Publishing, 15(12), p. 125026. doi: 10.1088/1367-2630/15/12/125026.

Acknowledgements

This work has been written with sweat, blood and chocolate. That not many tears are contained is the merit of several people making my PhD journey a challenging and valuable time. So, clear the stage, honour where honour is due:

First of all, thanks to Mark, my promotor, who created and enabled the project in the first place, and during the, alas, rare meetings never failed to (re)share his enthusiasm and innovative ideas with me. In some cases it took me some years to pick them up, but every time I travelled back from Delft I felt full of motivation and confidence. Related to that, my thank goes to Mieke, my copromotor, who managed to lead this motivation into realistic, scientific experiments. Especially when it came to explaining my results with applicable models the discussions and your guidance were of major value! Closing the cycle of supervisors, I am not sure if I would be able to write these lines without Antoine's featured trust in my ability to finish this project. Stepping in as a supervisor when I was (at least time-wise) already half-way into my PhD, you never seemed to consider failure an option – and so, here we are! I am very happy that, eventually, you can be on stage with me during the defence as a copromotor, as well.
Before continuing with people directly helping me with my PhD, I also want to dearly thank Bruno Bastos Sales and Annemiek ter Heijnen, my supervisors at Wetsus and WUR during my master thesis. You were responsible that I ever considered doing a PhD!

Genuine support throughout my project I have always found in the "biofilms" theme of Wetsus. Thanks (posthumously) to Arie, for planning the project from the Wetsus side, and to Paula, for standing in as my first supervisor and helping me with the first steps within biofilms, setup planning and becoming an independent researcher. Thanks to the company members under the lead of Hilde, for your patience and interest in my work, when also in the third or fourth theme meeting in a row I told you about what awesome thigs I was planning rather than tangible results. A special thanks to Bastiaan, providing me with first insight into what membrane filtration actually is, and to Caroline and Rik for the introduction and constant reminder what microbiology is capable of.

None of the research would have been possible without the lab facilities and assistance that I could approach in Wetsus and Wageningen. Therefore, my gratitude goes to the analytical and technical team of Wetsus, as well as to everybody involved in choosing, buying and installing the rheometer up here in Leeuwarden. Concerning the latter, I'd like to dearly thank Joshua for sharing his knowledge on rheology and the WUR rheometers with me. Moreover, thanks to Elmar, who gave me the right hints how to approach this issue, and to Gerrit and Janneke, for vanquishing the final order and installation with me. Also, big thanks to Yuemei and Simon from TU Delft, who helped me out whenever I asked for more information about ALE.

Moreover, I'd like to express my gratitude towards "my" students, Alperen, Yifei, Thomas, Dovydas and Elena. Not only can you find the outcomes of your work spread over this thesis, I value the experience of the collaboration with you at least as much as the "hard" results. As such, you are representative for the unique place that Wetsus is – not only for its technical facilities, but for the people it hosts: You can always find scientific support on mostly any topic raised, but there is a lot beyond that, and I am very grateful that I could be part of this for more than six years by now (still counting, because thanks to social networks and alumni events you never really leave). From mountain biking, wind surfing, survival running (We are Vikings!), archery, mud walking, via all kinds of board games and countless nights and lunches out to an awesome trip to Mexico – many activities I tried during my time I would probably have never done alone, and if so, they would for sure not have been the same. Mentioning all the people involved would break the mould of this (alone for the more than 20 people I have shared offices with, and who all have in one way or another a special place in my memory), so I hope nobody feels offended when I cannot name every single one.

Fabian, who has always been there during my PhD journey, the initiator of a Wetsus-cover band during my wedding, who gave some of my family at home a rough idea of why I loved my work: Thanks for the countless discussions, more often than not accompanied by a drink or two, for listening to my complaints when stuff didn't go as I planned as well as to my enthusiasm when things finally worked out – and for reminding me once in a while that there are things that I am not responsible for and that I just cannot change! And Paulina, for reminding me of the value of a good hug, for introducing me to Mexican food and eventually to Mexico (in collaboration with Hector), and for all the adventures still to come! When I left the building long after the sun went down, I could rely on you still sitting in your office and being in for a late chat.

A huge thanks also to Marianne, for the motivation to do sports even in the cold winter days, and being my partner in crime during several (mostly crazy) sports events. Your help with my Dutch summary not to forget! Thanks to Raquel and Karine for the most awesome and unexpected Bachelorette party. Thanks to Joeri, for being the kind and positive person that I tried to take as a role model, and to Victor for keeping telling me that I already am "good" until I almost believed it. Thanks to Hakan for constantly challenging me to play chess, for the "kidnaps" and for taking good care of my beloved flat. Coming back still feels a bit like coming home! A big hug for Lisette, João and your growing family: We had some unforgettable windsurfing days and I still enjoy dropping by whenever I'm in the area! Thanks to Terica and Prashanth, my buddies in making our way through that MBA…. Christina, you were my first friend at Wetsus, and somehow we managed to keep the connection far beyond.

Thanks to all the people appreciating a good hug just because (Gosia, Steffen, Swarupa). For the shared cultural experiences (Carlo, Casper, Diego, Kaustub, Olivier, Philipp, Shuyana, Zexin), for the parties, no matter if in the karaoke bar or making food (Caspar, Jan, Michele, Ragne, Roel, Ruizhe, Sandra, Wokke) and for the deep conversations when they were least

expected (Sam, Jordi, Sébastian). Yang, your hotpots are the best! I had some beguiling times in Leeuwarden. Thanks to Gerwin, Jaap, Janneke D., Maarten, Pau, Philipp W., Rebeca, for being part of this journey!
Summing up this part, I most sincerely thank Cees, Johannes and Bert for enabling Wetsus. Many thanks also to Gerben, always helping with some food and a smile, to Jannie, listening to my early morning attempts of Dutch, and to everybody else who keeps Wetsus running! And to everybody in Wetsus, caring for your colleagues. Keep that up, please!

Last but not least, thanks to Mike for the support and for the shelter when I had to run away for a weekend from non-working experiments or unfinished reports. Having this safe haven always made the challenges I was facing in Leeuwarden look a bit smaller and more doable.
Also thanks to my family and friends back in Germany, who never failed to ask when I will finally be back.

And, to whom it may concern: Thanks to everybody I have eventually forgotten!

Curriculum Vitae

Natascha-Monique Pfaff (née Dietrich) was born on January 23rd 1988 in Hann Münden, Germany. After obtaining her university entrance diploma from Fridrichsgymnasium in Kassel in 2007, she started her studies in Chemistry at the Georg-August University in Göttingen.

With the bachelor finished in 2011, during a 2-month internship at Koç-University in Istanbul, Turkey, she made and enjoyed her first international steps in the electro-chemical lab, supervised by Assistant. Prof. Dr. Uğur Ünal. Subsequently, she joined the Master programme 'Molecular Life Science' at Wageningen University, choosing 'Environmental chemistry' for specialization. After insights into various biotechnological topics, for the finishing projects of the master she focused on renewable energies. Her master thesis took place at 'Wetsus, European centre of excellence for sustainable water technology' in Leeuwarden, approaching the optimization of electrodes for energy generation from salt water gradients. Following this, she did another 5-months internship at the Fraunhofer Institute for Wind Energy and Energy system technology (IWES, nowadays split into IWES and IEE), working at a biogas plant and on a technology for storage of sustainable energy in the form of hydrogen or methane. She obtained her master degree in 2013.

One year later, she came back to Leeuwarden for a PhD in collaboration with TU Delft. Supervised by Mark van Loosdrecht, Mieke Kleijn (WUR) and Antoine Kemperman (UTwente) she worked on the physico-chemical characterization of biofilm models.

Since 2020 she is currently working at AFOTEK in Bad Hersfeld, Germany, on the development of a biological way to clean the exhaust air released during painting and coating processes.

List of publications

Conference contributions

- Membranes in Drinking and Industrial Water Production (MDIW) conference, Leeuwarden, 2017. **Pfaff, N.M.**, van den Brink, P., Kleijn, J.M., van Loosdrecht, M.C.M.. *Combining force measurements to relate composition and strength of (artificial) biofilms.* Oral presentation.
- WUR Rheology workshop, Wageningen, 2017. **Pfaff, N.M.**, van Loosdrecht, M.C.M., Kleijn, J.M., van den Brink, P.. *Challenges in the application of rheology on biofilms*. Oral presentation.
- EURObiofilms, Amsterdam, 2017. **Pfaff, N.M.**, Kemperman, A.J.B., van Loosdrecht, M.C.M., Kleijn, J.M.. *Challenges in the application of rheology on biofilms.* Poster presentation.
- Wetsus Internal Congress, Leeuwarden, 2018. **Pfaff, N.M.**, Kemperman, A.J.B., van Loosdrecht, M.C.M., Kleijn, J.M.. *Lifting the lid on biofilm mechanics - Theory & Practice.* Oral presentation.